

Optimization of Metrological Characterization of Machining Distortions

By

DESTINY R. GARCIA
DISSERTATION

Submitted in partial satisfaction of the requirements for the degree of

DOCTOR OF PHILOSOPHY

in

Mechanical and Aerospace Engineering

in the

OFFICE OF GRADUATE STUDIES

of the

UNIVERSITY OF CALIFORNIA

DAVIS

Approved:

Barbara S. Linke, Chair

Rida T. Farouki

Jörg Seewig

Committee in Charge

2020

ProQuest Number:27667737

All rights reserved

INFORMATION TO ALL USERS

The quality of this reproduction is dependent on the quality of the copy submitted.

In the unlikely event that the author did not send a complete manuscript and there are missing pages, these will be noted. Also, if material had to be removed, a note will indicate the deletion.



ProQuest 27667737

Published by ProQuest LLC (2020). Copyright of the Dissertation is held by the Author.

All Rights Reserved.

This work is protected against unauthorized copying under Title 17, United States Code
Microform Edition © ProQuest LLC.

ProQuest LLC
789 East Eisenhower Parkway
P.O. Box 1346
Ann Arbor, MI 48106 - 1346

ACKNOWLEDGMENTS

There are too many people that I need to thank for helping me achieve my academic goals. It has taken an entire village to get me to where I am today. Thank you to my early foster parents for helping me when my parents couldn't. Thank you to every great teacher in my life that told me I could, and every other teacher who told me I couldn't – both were needed to fuel me and motivate me to transcend all types of barriers. Thank you to all my coaches that helped prepare me mentally for such a challenging endeavor. To every mentor at UC Davis who cheered me on during both my undergrad and graduate school journey – thank you! To all my friends, I couldn't have done this without you all! From undergrad to grad school – you all made higher education so much better!

Thank you to every student support program made for students like me – from Educational Talent Search (ETS), Upward bound, Summer Transitional Enrichment Program (STEP '09), SSS TRiO, Equal Opportunity Program (EOP), Student Academic Success Center (SASC), McNair Scholars, California Alliance for Minority Participation (CAMP), Center for Biophotonics Science and technology (CBST), Guardian Scholars Program (GSP), Guardians Professional Program (GPP), Chicano and Latino Engineering and Scientist Society (CALESS), Chicana Latina Foundation (CLF), Society of Hispanic Engineers (SHPE), Mexican American Engineers and Scientists (MAES), The National GEM Consortium – they all work, and have supported me to get to where I am today!

Thank you to my PhD qualifying examination committee – Dr. VanderGheynst, Dr. Schaaf, Dr. Soshi, Dr. Farouki and Dr. La Saponara. The QE exam is one I will never forget – I am grateful to have had a team of experts and mentors, ready to help guide and direct my research proposal to the fullest. I would also like to thank and acknowledge my dissertation committee members, Dr. Linke, Dr. Farouki and Dr. Seewig – thank you for guiding me during the last stretch of the PhD and the writing process.

Thank you for all your genuine advice and feedback to help improve my final dissertation draft.

Thank you, to all the co-authors and collaborators throughout my research career. Thank you, Dr. Aurich, Dr. Hill, Dr. Urbassek, Dr. Zhang, Dr. Farouki, and Dr. Linke for research guidance and direction on experiments and writing. Also, my research could not have been conducted without the help and support from the Department of Mechanical and Aerospace Engineering (MAE), the Engineering Student Design Center (ESDC), the International Research Training Group (IRTG 2057), the FBK Institute at the Technical University of Kaiserslautern (TUK) Germany, and joint collaboration between the National Science Foundation (NSF) and the German Research Foundation (DFG) Distortion Project. I want to thank and acknowledge some funds for this research came from the NSF/DFG Award No. 1663341, and NSF Award No. 1505080.

An enormous thanks to the Manufacturing and Sustainable Technologies Research (MASTeR) Lab for being a huge support during my graduate school journey! From members who have already graduated, current masters and PhD students, and all the undergraduates who have helped me with my PhD research – thank you! Helen Smith, Dr. Jayanti Das, Gurpreet Kaur, Susana Ramirez, Kyle Howser, Nicholas Maharaj, Jieh Meinhold, Mae Underwood, Yasmine Salame, Francois Torner, Ian Garretson, Akshay Kamath, and Felicia Fashanu, Maja Beltz, Sebastian Quaisser, Anthony Goldstone, Karim Natafji, Jongchan Lee – I'm grateful for all your camaraderie and research support!

A special thanks to the Material Performance Lab at UC Davis, for involving me and welcoming me into the lab. Thank you to all the lab members for supporting me and helping me throughout my PhD – Dr. Minh Tran, Dr. Mitch Olson, Dr. Renan Ribeiro, Daniel Goldin, Christopher Chighizola, Christopher D'Elia, Nicholas Bachus – I am thankful for every supportive interaction and collaboration!

Thank you for Dr. Michael Hill – you first sparked my interest in material fracture and failure analysis while I was still an undergraduate taking EME 150A, *Mechanical Design*. Thank you for teaching me

and mentoring me throughout my PhD journey, I couldn't have done this without you. You helped shape and formulate my PhD research topic on machining distortion. Thank you for sharing your research lab and machines with me to advance further in this field. Thank you for always being there for me!

A big thank you to Dr. Farouki for expanding my knowledge and curiosity on manufacturing and design. Thank you for sharing your expertise in surface fitting and Gaussian curvature to direct and shape my PhD research dissertation. From taking your courses ENG 102 Dynamics and EME150B Mechanical Design as an undergraduate student, to having you as the chair of my qualifying exam committee, you have been a great support and mentor for me throughout these years. Thank you for all your research, teaching service and commitment to education!

To my research PI, Dr. Linke, I cannot thank you enough for all your continued support throughout my PhD journey! You taught me how to be a great researcher, ask questions, be patient, and to not be so hard on myself. You especially taught me that even though diamonds form under pressure – we can always ask for help! You are a great mentor and I could not have completed this PhD journey without your consistent guidance and support as my research advisor. Danke, Doktormutter!

I am so grateful to my family. To my parents, who had to struggle and lose us, just to realize their entire world was right in front of them. Thank you, mom, for always trying your absolute best to raise each and every one of us – I love you mom. All my siblings – Jessica, Letty, Alfredo, Vicente, Bianca and Alexio – this was our journey, we did it! Thank you all for pushing me and motivating me – the sky is the limit! To Ray's family – thank you for being an extension of Ray and supporting me through love, encouragement, and shelter. I am so very grateful to have two Garcia families!

A special thank you to my dog, Nana! Adopting you from the shelter right after the preliminary exams, was the best decision I ever made in graduate school. You are a once in a lifetime dog – I am so lucky to have you! Thank you for all your love and kisses throughout these grad school years!

And finally, to my partner and best friend, Ray. Thank you, Raymond Garcia, for everything you do for me. Thank you for loving me, supporting me, and being so patient with me – especially throughout my graduate school career. From my bachelors to my PhD – and everywhere in between – I couldn't have done this without you. I can't even express in words how much you mean to me. I am so thankful to have you in my life. On to our next journey together – we did it! I love you!

DECLARATION OF CO-AUTHORSHIP AND PREVIOUS PUBLICATION

I hereby declare that this dissertation incorporates material that are the result of previous research conducted under the guidance and collaboration of Dr. Barbara Linke (Ch. 3, Ch. 4, Ch. 5, and Ch. 6) and in collaboration with other researchers including Dr. Michael Hill (Ch. 3), Dr. Jan Aurich (Ch. 3), Dr. Rida Farouki (Ch. 4), Dr. Herbert M. Urbassek (Ch. 5), and Dr. Zhibo Zhang (Ch. 5). I declare that this dissertation includes original papers that have been previously published/under publication review/will be submitted for publication in a peer reviewed journal, and that the published journal and/or conference proceedings are the original source. I certify that I have properly acknowledged the contributions of the other researchers to my dissertation.

ABSTRACT

Manufacturing methods and procedures are advancing through research and development, to optimize machine tools, machining strategies, and the overall manufacturing system, where higher quality products have higher tolerances. In all industries part distortion occurs. In the aerospace industry, machining distortion, or the deviation of part shape from the original intent after being machined and released from a fixture, occur, reducing productivity and increasing costs, waste and scrap materials. Although machining distortion has been a challenge in the aerospace industry for many years, several of the current approaches to this problem provide point solutions for specific circumstances while relying on empirical trials at excessive cost. Modern analysis and computing resources as well as synergistic approaches from multiple disciplines are needed to tackle this problem.

In the distortion literature, basic information is missing about how distortion is practically characterized and therefore the results of experiments or modeling approaches are not easy to transfer. To fully understand part and machining distortion, a transparent way to quantify distortion data collection and analysis is needed and will enhance the transferability of experimental and analytical results. This research therefore aims at bridging the gap of part and machining distortion data collection and analysis to understand how workpiece deformations can be characterized, and manufacturing parameters optimized to reduce overall part distortion for a more economical and sustainable manufacturing method.

The presented research focuses on a detailed investigation of machining distortion characterization techniques that are used to create a uniform method for analyzing machining distortion data used in the aerospace industry. The research objectives of this study are divided into three specific objectives including: understand measurement machine capabilities and data collection methods for machining distortion, develop a clear methodology for analyzing distortion data, develop an algorithm for

distortion data collection and analysis, and characterize part and machining distortion for specific manufacturing operations and geometries. The final results of this dissertation include a state of the art review on machining distortion, an initial machining distortion characterization method using pre and post z-height deviation for overall distortion, an updated 3D characterization tool incorporating Gaussian surface curvature via Bernstein basis function surface fitting and analysis, an initial case study of micro-scale distortion in a molecular dynamics simulations of a single grain pure Al in a vice structure for nanomanufacturing applications, a case study on a process planning tool that regards part quality for sustainability research and teaching, and an overall conclusion and future work.

TABLE OF CONTENTS

Declaration of Co-Authorship and Previous Publication.....	vi
Abstract.....	vii
Nomenclature.....	xii
List of Figures.....	xiv
List of Tables.....	xxii
Chapter 1 State of the Art.....	1
1.1 Introduction.....	1
1.2 Quality and Manufacturing.....	2
1.3 Residual Stresses.....	6
1.4 Machining Distortion Modeling and Simulations.....	12
1.5 Machining Distortion Measurement Methods.....	14
1.6 Metrological Advancements.....	21
1.7 Conclusion.....	25
Chapter 2 Research Objectives.....	27
Chapter 3 Initial Routine of Machining Distortion Characterization.....	31
3.1 Methods.....	31
3.1.1 Material and Experimental Setup.....	31
3.1.2 Initial Distortion Characterization Tool.....	36
3.2 Results and Discussion.....	39
3.2.1 International Collaboration Distortion Data.....	45
3.2.2 Machining Distortion Data collection.....	50
3.3 Conclusion.....	50

Chapter 4	Optimized Routine of Machining Distortion Characterization Featuring Gaussian Surface Curvature	53
4.1	Methods	54
4.1.1	Sample Workpiece.....	54
4.1.2	Initial CMM Selection and Parameters.....	55
4.1.3	Leveling Distortion Data.....	62
4.1.3.1	Least-Squares Surface Fit Using the Bernstein Basis Functions	64
4.1.3.2	Surface Curvature Analysis.....	67
4.2	Results and Discussion	69
4.3	Conclusion	72
Chapter 5	Case Study: Molecular Dynamics Simulations of Single Grain Pure Aluminum in a Vice Fixture for Nanomanufacturing Applications	74
5.1	Background.....	74
5.1.1	Nanomachining.....	74
5.1.2	Machining Fixtures.....	75
5.2	Methods	77
5.3	Results and Discussion	81
5.4	Conclusion	89
Chapter 6	Case Study: Process Planning Tool for Sustainability Research and Teaching with emphasis on Scrap Reduction	91
6.1	Introduction.....	91
6.1.1	Process Planning	92
6.1.2	Process Chain Model	95
6.1.3	Engineering Education	96
6.1.4	Educational Water Table Study.....	96

6.2	Process Chain Steps	97
6.3	Case study	105
6.3.1	Part-Specific and Site-Specific Data.....	105
6.3.2	Unit Manufacturing Process (UMP) Data and Unit Auxiliary Process (AP) Data	106
6.3.3	Generation of Alternative Process Chains	108
6.4	Results and Discussion	110
6.5	Conclusion	122
Chapter 7	Conclusion and Future Work.....	125
7.1	Overall Summary of Contributions	125
7.2	Future Research.....	128
Appendix.....		131
Publications.....		170
References.....		171

NOMENCLATURE

a_e	Depth of cut in mm
AP	Auxiliary process
a_p	Width of cut in mm
C	Costs in \$
$C_{\text{electricity}}$	Electricity Costs in \$/kWh
$C_{\text{electricity_batch}}$	Electricity costs per batch in \$/kWh
C_{labor}	Worker costs per hour in \$/h
C_{machine}	Machine costs per hour in \$/h
C_{material}	Material Costs per kg in \$/kg
CO2PE	Cooperative Effort on Process Emissions in Manufacturing
CMM	Coordinate Measuring Machine
C_{rework}	Rework costs in \$
C_{scrap}	Scrap Costs in \$
C_{tool}	Tool costs per part in \$
$C_{\text{total_batch}}$	Total costs per batch in \$
$C_{\text{total_part}}$	Total costs for the complete process chain in \$
DF	Degrees of fulfilment
DOE	Design of Experiments
E	Energy in J
$E_{\text{total_batch}}$	Total energy per batch in J
$E_{\text{total_part}}$	Total energy per part in J
KPI	Key performance indicators
l_c	Length to be cut in mm
MD	Molecular Dynamics
m_{aux}	Auxiliary material waste in kg
MCA	Measurement Capability Analysis
MSA	Measurement Systems Analysis
$m_{\text{scrap_part}}$	Scrap material mass in kg
$m_{\text{w_raw}}$	Mass of workpiece material in kg
N	Parts per batch
N_t	Number of passes
P_{basic}	Basic power in W

P_{idle}	Idle power in W
$P_{process}$	Process power in W
QA	Quality Assurance
ρ	Material Density in g/cm ³
RS	Residual Stress
S	Scrap
Scrap_rate	Total accumulating scrap rates in % scrap
S_i	Scrap rate in % scrap
SI	Sustainability Indicator
SMIR	Sustainable Manufacturing Indicators Repository
S_{scrap_batch}	Scrap parts for the complete chain
S_{scrap_part}	Total scrap per part
t	Time in min
t_{idle}	Idle time in min
$t_{process}$	Processing time in min
t_{setup}	Set-up time in min
t_{total_batch}	Total time per batch in min
t_{total_part}	Total time per part for the complete process chain in min
UMP	Unit Manufacturing Process
UPLCI	Unit Process Life Cycle Inventory
v_f	Feed rate
V_w	Material volume of the finished part in mm ³
V_{w_raw}	Material Volume of the raw part in mm ³
$V_{w_removal}$	Material volume removed in mm ³
$V_{w_removal}$	Material volume removed in mm ³
WF	Weight factor

LIST OF FIGURES

Figure 1 Four geometric attributes of features are considered to define the geometry: (a) orientation, (b) form, (c) size and (d) location [Budynas et al., 2011].....	3
Figure 2 Examples of external loads including compression, tension, bending, torsion, shear, and no force [photo created by UC Davis undergraduate student Jongchan Lee]	4
Figure 3 Example of manufacturing processes that create residual stresses [Schajer et al., 2013]	7
Figure 4 Summary of different residual stress measurement techniques [Fitzpatrick, Open University, UK, Schajer et. al, 2013].	9
Figure 5 Residual stress profile for a rolled aluminum 7050 T74 plate in the cross- section [Prime et al., 2001].....	11
Figure 6 Distortion as a 2D line measurement along the central line [Ma et al., 2015].....	16
Figure 7 Distortion as multiple line plot measurements [Zhang et al., 2014]	16
Figure 8 Distortion presented as a 3D measurement [Jayanti et al., 2013].....	17
Figure 9 Distortion as a 2D measurement [Huang et al., 2015]	17
Figure 10 Distortion measured as a grid measurement [Gulpak et al., 2013].....	18
Figure 11 Distortion as a 2D line measurement [Bi et al., 2009].....	19
Figure 12 Maximum distortion at varying plate thickness example [Sim et al., 2011]	19
Figure 13 Distortion measured along the longitudinal axis in the centre of the specimen [Madariaga et al., 2018]	20
Figure 14 Measured distortion of thin walled part using mathematical model [Yang et al., 2018]	20
Figure 15 Measured distortion using uniform measurement CMM scheme [Li et al., 2015].....	21
Figure 16 Schematic of the combined research objectives with overall goal of producing a distortion tool used for various manufacturing distortion data	30
Figure 17 Residual stress profile in the aluminum bar [Hill et al., 2014]	32

Figure 18 Schematic of the material division	33
Figure 19 Clamping fixture with labeled components	34
Figure 20 U-shape geometry	35
Figure 21 U-shape locations in the initial sample	35
Figure 22 Distortion data was measured using a Taylor Hobson Talyscan 250 CMM at the University of California Davis	37
Figure 23 Algorithmic steps in characterizing distortion	38
Figure 24 Analysis steps depicted in distortion characterization tool [Garcia et al., 2017].....	39
Figure 25 Distortion visualization of z-deviation of top, middle and bottom blank displayed together from left to right respectively	40
Figure 26 Representation of bending and torsion each blank experience along the y- axis.....	40
Figure 27 Line plots at the midline of each distortion sample combined together in both x and y directions	41
Figure 28 UC Davis top sample distortion presented along with central line plots in both x and y directions	42
Figure 29 UC Davis middle sample distortion presented along with central line plots in both x and y directions	43
Figure 30 UC Davis bottom sample distortion presented along with central line plots in both x and y directions	43
Figure 31 Shifted line plots at midline of each distortion sample	44
Figure 32 Tactile probe of the Micro-Hite DCC 3D CMM measuring a distortion sample at TUK with measurement fixture for repeat measurements	45
Figure 33 Similar milling experiments were conducted at TUK using a DMU 70 eVolution Deckel Maho advance CNC.....	46
Figure 34 Distortion visualization of z-deviation of top, middle and bottom blanks from TUK displayed together from left to right respectively.....	47
Figure 35 Top sample distortion shown for TUK experiment 1	48

Figure 36 Middle sample distortion shown for TUK experiment 1	48
Figure 37 Bottom sample distortion shown for TUK experiment 1	49
Figure 38 Coordinate data from the Top sample experiment 1 pre (left) and post (right), obtained from the Micro-Hite DCC 3D CMM had poor data quality.....	49
Figure 39 Distortion sample of machined pockets with 60-degree stiffener wall [NSF/DFG Award No. 1663341], [Ribeiro and Hill, 2016].....	54
Figure 40 Three coordinate measuring machines are introduced from left to right as the Mitutoyo Bright BRT 504 CMM (left), Faro Arm Edge and Scan Arm HD CMM (middle), and the Taylor Hobson Talyscan 250 CMM (right).....	56
Figure 41 Distortion coordinate data of the same part 60 degree part sample, from 3 different CMMs (FaroArm, Talyscan, and Mitutoyo) are shown.....	57
Figure 42 Contour distortion 3D representation using a 5 x 5 mm coordinate spacing scheme.....	59
Figure 43 Contour distortion 3D representation using a 2 x 2 mm coordinate spacing scheme.....	59
Figure 44 Contour distortion 3D representation using a 1 x 1 mm coordinate spacing scheme.....	60
Figure 45 Contour distortion 3D representation using a 0.5 x 0.5 mm coordinate spacing scheme.....	60
Figure 46 Illustration of the coordinate distortion data leveling analysis with raw data fitted to a plane (top), and the distortion data minus the fitted data (bottom).....	63
Figure 47 Algorithmic steps in the optimized routine of machining distortion characterization.....	64
Figure 48 The leveled distortion data for the 60-degree sample with midline plots for both horizontal and vertical directions.....	69
Figure 49 Left: the height variations of the least-squares surface fit (magnified 120x about the mean height) for the surface of degrees, $d = 4$ (top), $d = 6$ (center), and $d = 8$ (bottom). Right: corresponding surface regions that have negative (red) and positive (blue) Gaussian curvature.	70
Figure 50 Left: the height variations of the least-squares surface fit (magnified 120x about the mean height) for the surface of degrees, $d = 4$ (top), $d = 6$ (center), and $d = 8$ (bottom). Right: corresponding surface regions that have $K > 0.1 z_{rms2}$ (red), $-0.1 z_{rms2} \leq K \leq 0.1 z_{rms2}$ (green), and $K < -0.1 z_{rms2}$ (blue)	71

Figure 51 Depiction of the characterization process from leveled data to Gaussian curvature distribution.....	72
Figure 52 The two vices clamp the bottom half of the aluminum bar. Heights (A, B, C) and lengths (D, E, F) are shown for result references [Garcia et al., 2018]	79
Figure 53 The initial bar undergoes three simple setups in the simulation: 1. Bar, clamp, hold, release. 2. Bar, clamp, hold, L-shape, hold, release. 3. Bar, clamp, hold, U-shape, hold, release.	80
Figure 54 The stress distribution (in the frontal x-z plane) of the bar sample after each vice moved into the bar by 2 nm.	82
Figure 55 The stress distribution of the bar sample after being held in the vice for 2×10^{-10} second. The bottom image describes the dislocation found in the top left corner box.	82
Figure 56 The stress distribution in the mid-plane cross section (y-z plane) after the bar sample was held in the vice for 2×10^{-10} second.....	83
Figure 57 The stress distribution of the bar sample after being released from the vice fixture.	84
Figure 58 The distortion as percentages (%) for each sample (Bar, U-shape, and L-shape) and their respective locations (A, B, C, D, E, and F) are plotted.....	85
Figure 59 The stress distribution (in the frontal plane) of the U-shaped sample in the fixture after being held in the vice for 2×10^{-10} second.....	86
Figure 60 The stress distribution (in the frontal plane) of the U-shape sample after it was released from the vice fixture.....	87
Figure 61 The stress distribution (in the frontal plane) of the L-shaped sample in the fixture after being held in the vice for 2×10^{-10} second.....	88
Figure 62 The stress distribution of the L-shape sample after it was released from the vice fixture.....	88
Figure 63 Visualizing process chains including unit processes and non-value adding steps (left: process map with triangles representing inventory [Anderson et al., 2013], right: example from [Linke et al., 2016])	94
Figure 64 Visualizing unit processes (left: UMP method [ASTM E3012-16], right: generic description)	94
Figure 65 An example of a generic electric power and time profile for a grinding process [Linke and Overcash, 2017].....	99

Figure 66 Process chain with specific UMPs and non-value adding steps (auxiliary processes) [Linke et al., 2016].....	101
Figure 67 Diamond model of the milled and water jetted models [Linke et al., 2017 NAMRC 45].....	106
Figure 68 A generic process chain is shown for the diamond model.....	109
Figure 69 Matlab process chain model presented as a flowchart.....	110
Figure 70 The complete steps of each process chains A, B and C	111
Figure 71 The overall metric comparison including time, energy, scrap and cost for the complete process chains A, B and C	114
Figure 72 Times for process chains A, B, and C	116
Figure 73 Energy for process chains A, B, and C.....	117
Figure 74 Scrap percentage for process chains A, B, and C	118
Figure 75 Costs for process chains A, B and C	119
Figure 76 The total Sustainability Indicator versus weight factors for process chains A, B, and C, see schemes in table 5	121
Figure 77 Schematic of dissertation objectives and outcomes	126
Figure 78 Top sample distortion shown for TUK experiment 2.....	131
Figure 79 Middle sample distortion shown for TUK experiment 2	132
Figure 80 Bottom sample distortion shown for TUK experiment 2.....	132
Figure 81 Reference surface datum from the pre (left) and post (right) for the top sample of TUK experiment 1.....	133
Figure 82 Reference surface datum from the pre (left) and post (right) for the middle sample of TUK experiment 1.....	133
Figure 83 Reference surface datum from the pre (left) and post (right) for the bottom sample of TUK experiment 1.....	134
Figure 84 Reference surface datum from the pre (left) and post (right) for the top sample of TUK experiment 2.....	134

Figure 85 Reference surface datum from the pre (left) and post (right) for the middle sample of TUK experiment 2.....	135
Figure 86 Reference surface datum from the pre (left) and post (right) for the bottom sample of TUK experiment 2.....	135
Figure 87 TUK Experiment 3 top sample distortion results.....	136
Figure 88 TUK Experiment 3 middle sample distortion results.....	137
Figure 89 TUK Experiment 3 middle sample distortion results.....	137
Figure 90 TUK Experiment 4 top sample distortion results.....	138
Figure 91 TUK Experiment 4 middle sample distortion results.....	138
Figure 92 TUK Experiment 4 bottom sample distortion results.....	139
Figure 93 A dial indicator is used to measure deflection of thin walled aerospace workpieces in between milling passes at designated constant incremental locations.....	141
Figure 94 A front view of a dial indicator is used to measure deflection of thin walled aerospace workpieces.....	141
Figure 95 Height deviation collected via dial indicator for sample #9.....	142
Figure 96 Height deviation collected via dial indicator for sample #24.....	142
Figure 97 Distortion data collected at 3 different midline locations (lines 1, 2, and 3).....	143
Figure 98 Three central distortion lines taken along the length of the sample for pass 0.....	143
Figure 99 Three central distortion lines taken along the length of the sample for pass 1.....	144
Figure 100 Three central distortion lines taken along the length of the sample for pass 2.....	144
Figure 101 Three central distortion lines taken along the length of the sample for pass 3.....	145
Figure 102 Three central distortion lines taken along the length of the sample for pass 4.....	145
Figure 103 Three central distortion lines taken along the length of the sample for pass 5.....	146

Figure 104 Three central distortion lines taken along the length of the sample for pass 6	146
Figure 105 Three central distortion lines taken along the length of the sample for pass 7	147
Figure 106 Probe feature from the Faro Arm Edge calculated the deviation between scan and CAD.....	148
Figure 107 Probe features from the Faro Arm Edge display the deviation from scanned surface and CAD model	149
Figure 108 Standard Caliper tool features from the Faro Arm Edge provided displacement values of the surface to the CMM table	150
Figure 109 Distortion values from the CMM table plane are calculated using Create Surface Comparison Points on the Faro Arm Edge CMM	150
Figure 110 Display of the sample grid used to measure deviations from the CAD surface	151
Figure 111 Selected points and their respective deviation value from the CAD model using a Faro Arm Edge CMM Software.....	152
Figure 112 A screenshot of the comparison point table created from the Faro Arm Edge software.....	153
Figure 113 Al 7050 samples with induced bending, twisting, and combined bending and twisting distortions.....	154
Figure 114 A Dake Hydraulic Press is displayed exerting force on a distortion sample	155
Figure 115 A craftsman torque wrench is displayed exerting torsion onto a distortion sample.....	156
Figure 116 All three samples are displayed after applying bending and torsion forces with top, middle, and bottom samples as 14, 10, and 22 respectively	157
Figure 117 Distortion analysis and visuals for sample 10 torsion	158
Figure 118 Distortion analysis and visuals for sample 14 bending	159
Figure 119 Distortion analysis and visuals for sample 22 combined bending and torsion	160
Figure 120 The distortion measurement survey collected individual responses of how they would measure a feature for distortion or deviations	161

Figure 121 UMP for a quality assurance step – a coordinate measuring machine (CMM)	163
Figure 122 The distortion sample machined geometry (0, 90, and 60-degree)	165
Figure 123 0-degree sample measured on the Mitutoyo CMM	165
Figure 124 0-degree sample measured on the FaroArm CMM	166
Figure 125 0-degree sample measured on the Talyscan CMM	166
Figure 126 90-degree sample measured on the Mitutoyo CMM	167
Figure 127 90-degree sample measured on the FaroArm CMM	167
Figure 128 90-degree sample measured on the Talyscan CMM	168
Figure 129 Gaussian curvature analysis for the 0 (top) and 90-degree (bottom) stiffener samples	169

LIST OF TABLES

Table 1 Distortion research examples from the literature often show a vague description of the data collection and analysis methods used [Ma et al., 2015], [Zhang et al., 2014], [Jayanti et al., 2013], Huang et al., 2015], [Gulpak et al., 2013], [Bi et al., 2009].....	15
Table 2 Machining Parameters of distortion sample.....	36
Table 3 Maximum distortion in z-deviation.....	45
Table 4 Specifications for the different CMM machines.....	56
Table 5 Mitutoyo BRT Bright 504 distortion measurement parameters.....	61
Table 6 Scoring Tool, after [Linke et al., 2013].....	104
Table 7 Part-specific and site-specific data.....	105
Table 8 UMP and AP data for the case study.....	108
Table 9 Results from process chains A, B and C.....	114
Table 10 Total SI values for different weighing schemes.....	121
Table 11 Purposely induced distortion sample summary.....	155
Table 12 Induced distortion results.....	157
Table 13 Distortion survey collection for perceived distortion data collection methods for various parts.....	162
Table 14 Accuracy measurements (20 measurements) from the Faro Arm Edge CMM.....	164

CHAPTER 1 STATE OF THE ART

1.1 Introduction

In the aerospace and manufacturing industries, billions of dollars are attributed to costs from reworking, remanufacturing, and/or rejecting components that are defective due to machining distortions [Thoben et al., 2002, Bowden et al., 2001]. Manufacturing methods and procedures are advancing through research and development, to optimize machine tools, machining strategies, and the overall manufacturing system, where higher quality products have higher tolerances. In all industries part distortion occurs. In the aerospace industry, machining distortion has been an expensive problem for many decades. In the aerospace industry, machining distortions, or the deviation of part shape from the original intent after being released from a fixture, occur, reducing productivity [Chantzis et al., 2013]. Residual stresses locked into the workpiece are a primary factor contributing to machining distortions. The residual stresses are induced by prior material processing steps such as rolling, forging, heat treating, etc., which are needed in the aerospace industry for high strength.

Although machining distortion has been a challenge in the aerospace industry for many years, several of the current approaches to this problem provide point solutions for specific circumstances while relying on empirical trials at excessive cost. Modern analysis and computing resources as well as synergistic approaches from multiple disciplines are needed to tackle this problem. In the distortion literature, basic information is missing about how distortion is practically characterized and therefore the results of experiments or modeling approaches are not easy to transfer. To fully understand part and machining distortion, a transparent way to quantify distortion data collection and analysis is needed and will enhance the transferability of experimental and analytical results.

In the distortion literature, basic information is missing about how distortion is practically characterized and therefore the results are not easily transferred. Examples from the literature show an inconsistent methodology for effectively collecting and analyzing distortion data.

To fully understand part and machining distortion, a transparent way to quantify distortion data collection and analysis are needed to enhance the transferability of experimental and analytical results. This dissertation focuses on the methodology of characterizing distortions including data collection and analysis to understand how workpiece deformations can be categorized, and manufacturing parameters optimized to reduce overall part distortions for a more economical and sustainable manufacturing method.

1.2 Quality and Manufacturing

Manufacturing methods and procedures are advancing through research and development to optimize machine tools, manufacturing strategies, and process control. Quality, as defined as the degree of excellence, is a distinguishing attribute [Merriam-Webster], and is an important aspect of manufacturing. In process planning, quality is one of the metrics and contributes to the optimization problem to find the best process sequence and parameters [Linke et al., 2016]. Process planning is an optimization problem with the associated process parameters at a minimum cost [Deshpande et al., 2004]. Common metrics for studying and optimizing sustainability in manufacturing include: energy, material efficiency, emissions, waste, costs, productivity, investment, impacts on society, safety, health, etc. [Sakar et al., 2011].

Quality can be further described as the degree to which a set of inherent characteristics of an object fulfills requirements [ISO 9000, 1992]. To understand part quality, we need information about the requirements of the manufactured part (as designed), as well as the actual characteristics of the manufactured part. In other words, we need information extracted from the product design such as a

technical drawing, and characteristics of the part measured using some form of metrology, or measurement equipment.

The manufacturing industry has been trying to solve the obstacle of inevitable machining distortion for over 50 years. Modern analysis and computing resources as well as synergistic approaches from multiple disciplines are needed to tackle this problem. Reducing scrapped and reworked parts related to distortion will be a huge improvement for sustainable manufacturing. Defective parts accrue additional labor and material expenses. For any items that must be scrapped, all the labor, material, and resource expenses of producing them is wasted [Nicholas, 2010]. This research simultaneously promotes key insight to reducing machining distortions in various industries, as well as improving sustainability related to overall scrapped and reworked parts that can become waste.

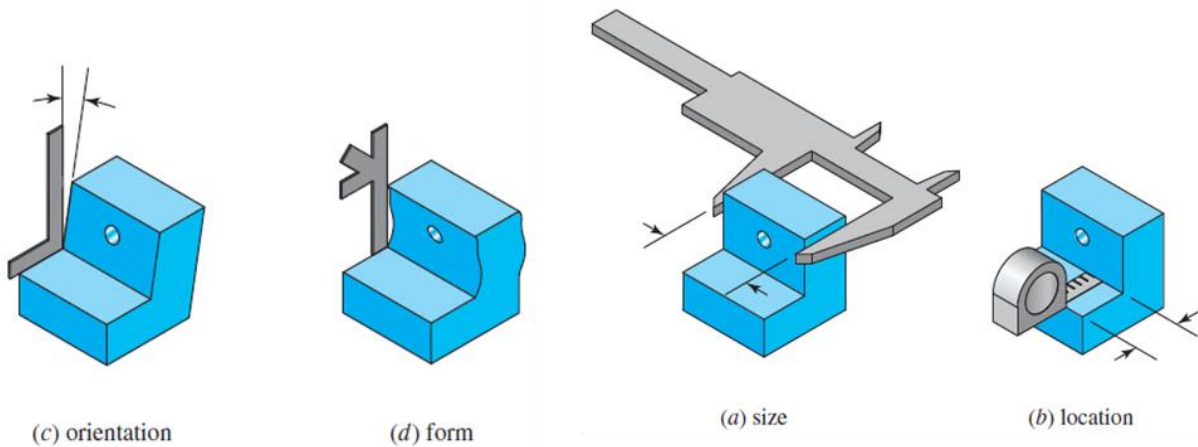


Figure 1 Four geometric attributes of features are considered to define the geometry: (a) orientation, (b) form, (c) size and (d) location [Budynas et al., 2011]

In manufacturing industries, the manufacturer will optimize for the most efficient and inexpensive operations allowable [Budynas et al., 2011]. Part specification in turn defines the overall part quality since in fact, traditional dimensioning and tolerancing systems in manufacturing can never achieve perfect manufactured orientation, form, size and location as seen in Figure 1 [Budynas et al., 2011].

The overarching problem is that every dimension may be within its tolerance, but the part may not be usable for its application owing to one or more imperfections [Budynas et al., 2011]. Some examples of imperfections can include, but are not limited to geometry, material, regulations, etc. A more challenging problem is that it is not clear how to measure some attributes defining quality based on multiple factors including precision size tolerances, measurement equipment, measurement technology, measurement resolution, etc. Furthermore, it is a challenge to uniquely and transferably measure the characteristics that define machining distortion, or the deviation of a part dimension from the original intent, after being released from a fixture [Chantzis et al., 2013] – at a uniform level. Distortion can also be defined as the act of twisting or altering something out of its true, natural, or original state [Merriam-Webster] as depicted in a cartoon illustration in Figure 2.

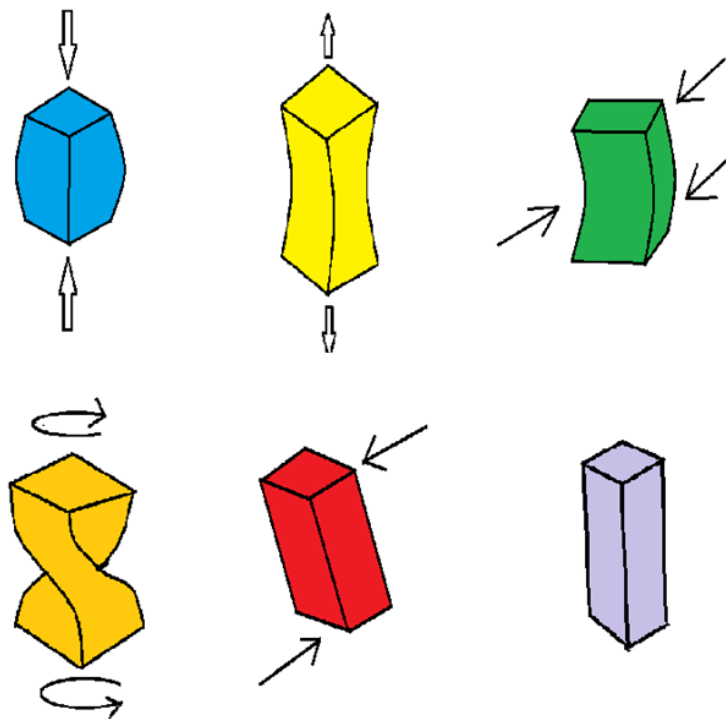


Figure 2 Examples of external loads including compression, tension, bending, torsion, shear, and no force [photo created by UC Davis undergraduate student Jongchan Lee]

Machining distortion is a critical issue in the design, manufacturing, and assembly process of aerospace structures [Jayanti et al., 2013], and remains a leading unsolved problem in the industry. Machining distortion is not caused by dimensional inaccuracies, machining intolerances, and or over or under machining [Chantzis et al., 2013]. Every year, the aerospace industry experiences significant loss in profits from part distortion [Sim et al., 2010].

As technologies are advancing, manufacturing methods and procedures are changing to achieve more sustainable and efficient products. In the aerospace industry, there is a high demand for an improved fleet of aircraft, which are lighter, stronger, and more fuel efficient [Denkena et al., 2013]. In achieving these objectives, modern aircraft are designed such that the component rigidity is maximized, and the material thickness is minimized [Denkena et al., 2013]. Machining of monolithic aerospace components is one way to harness the advantages of high-performance designs, with respect to a high overall strength-to-weight ratio, and improved fatigue life [Jayanti et al., 2013]. In machining monolithic aerospace components, up to 90% of the initial material can be machined away for a start-to-finish weight ratio of about 10:1 [Yang et al., 2014]. Although the machining of monolithic components results in a low weight structure to maximize energy and efficiency, machining distortions challenge reliable production.

Machining distortions are caused by many different sources that require interdisciplinary research efforts from many experts. Through the research efforts of multiple scientific backgrounds, key areas related to machining distortion are investigated such as residual stresses, part clamping mechanisms, machining parameters, materials processing, temperature affects, geometrical parameters, etc. Several approaches have been investigated to minimize part distortion [Li and Wang, 2016].

With efforts to understand causes of distortion, capabilities for better prediction and simulations are developing related to manufacturing operations that are prone to causing distortion such as milling,

additive manufacturing or AM processes, and arc welding [Li and Wang, 2016],[Santana et al., 2017], [Ma et al., 2017]. Current industrial solutions to reducing machining distortion include machining incrementally in small symmetrical steps until the part is obtained within tolerances and desired dimensions [Schajer et al., 2013]. However, this practice is slow, costly, and intolerant to variations in the bulk residual stress state of inbound materials. New knowledge to allow distortion control is still needed to solve this ongoing manufacturing problem.

Although machining distortion has been a challenge in the aerospace industry for many years, many of the current approaches to this problem provide point-solutions for specific circumstances while relying on empirical trials at excessive costs. Modern analysis and computing resources as well as synergistic approaches from multiple disciplines are needed to tackle this problem.

1.3 Residual Stresses

The effects of residual stresses have proven to be of primary concern for machining distortions and deformations [Wang et al., 2005]. Residual stresses are defined as the “locked-in” stresses that exist in materials and structures, independent of the presence of external loads [Totten et al., 2002]. Residual stresses are known to cause poor surface integrity in manufacturing [Shet et al., 2003]. Almost all manufacturing processes create residual stresses, including forging, rolling, bending, extruding, machining, grinding, plating, peening, welding, casting, quenching, hardening, etc. as seen in Figure 3 [Schajer et al., 2013]. Residual stresses are a function of the materials processing and machining history and can enhance or impair functional part behavior [Brinksmeier et al., 1982].

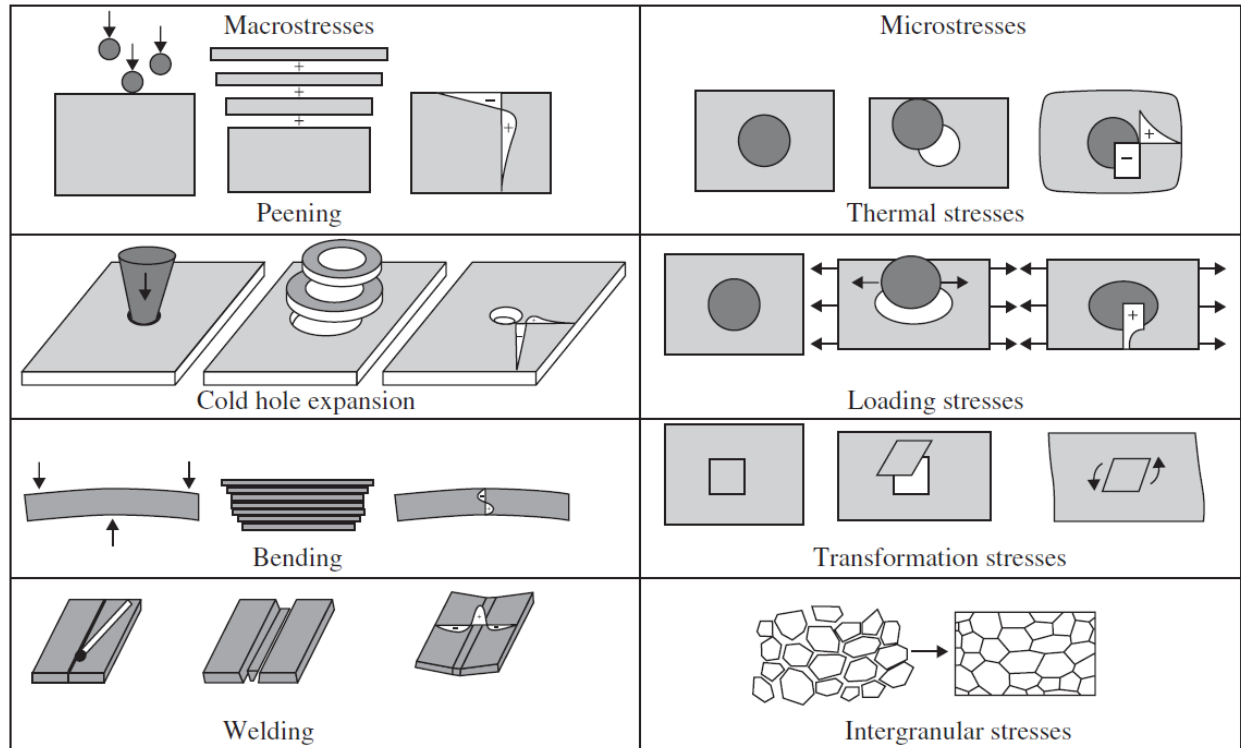


Figure 3 Example of manufacturing processes that create residual stresses [Schajer et al., 2013]

Residual stress develops from three main mechanisms: non-uniform plastic deformation, surface modification, and material phase and/or density changes [Brinksmeier et al., 1982],[Ma et al., 2015]. These mechanisms occur in most manufacturing processes [Ma et al., 2015]. After processing, the residual stresses can cause deformation due to the re-equilibration of the tensile and compressive stresses to arrive at mechanical equilibrium within the whole volume of material [Brinksmeier et al., 1982], [Husson et al., 2012]. The re-equilibration, causes the workpieces to distort (i.e. bend and twist). Machining distortion can be seen as the result of a “distortion potential”, in which the distortion is stored into the material all throughout the processes by residual stresses [Husson et al., 2012]. Each manufacturing step can be viewed as contributing to the overall distortion potential which is physically related to the deformation [Husson et al., 2012].

Residual stresses can be advantageous or dangerous based on product application, stress locations, and type of stresses [Brinksmeier et al., 1982]. Compressive residual stresses in the surface layer of aerospace materials can be beneficial in resisting against fatigue [Schajer et al., 2013]. In contrast, residual stresses can be detrimental when they accelerate failure phenomena, as tensile residual stresses are known to do for corrosion and fatigue [Schajer et al., 2013], [Lu 1996]. In manufacturing, bulk residual stresses can drive part deformation when removal of residual stresses in material removed by cutting causes a redistribution of residual stresses in the material remaining, to attain mechanical equilibrium, and the redistribution causes an analogous deformation [Schajer et al., 2013], [Gulpak et al., 2013].

Measurements and causes of residual stresses in machining processes has been the main effort of research in this particular field of manufacturing [Brinksmeier et al., 1982]. Due to the “locked-in” physical characteristic of residual stresses, their measurements are complex and challenging. Except for a few exceptions, residual stress measurement methods are classified into two categories: mechanical relaxation and diffraction methods [Schajer et al., 2013], [Brinksmeier et al., 1982].

Relaxation techniques rely on measurement of deformation caused by residual stress release induced by material removal (cutting), and therefore identify residual stresses indirectly [Schajer et al., 2013]. In general, relaxation techniques require residual stresses to be determined analytically (or with the aid of finite element method (FEM)) from measured deformation [Schajer 2001], [DeWald et al., 2009]. Examples of relaxation techniques include splitting, sectioning, layer removal, hole-drilling, ring-core, deep-hole, slitting, and contour method [Schajer et al., 2013], [Brinksmeier et al., 1982].

In comparison, diffraction techniques interrogate the interatomic lattice spacing of material, which can be correlated to residual stress. Some examples of diffraction techniques include: XRD (X-ray diffraction), Synchrotron X-ray, and Neutron diffraction, where electromagnetic radiation and

precision instrumentation is used to measure diffraction angles, determine the interatomic spacing using Bragg's Law, and relate the spacing to the stress state in the material [Schajer et al., 2013].

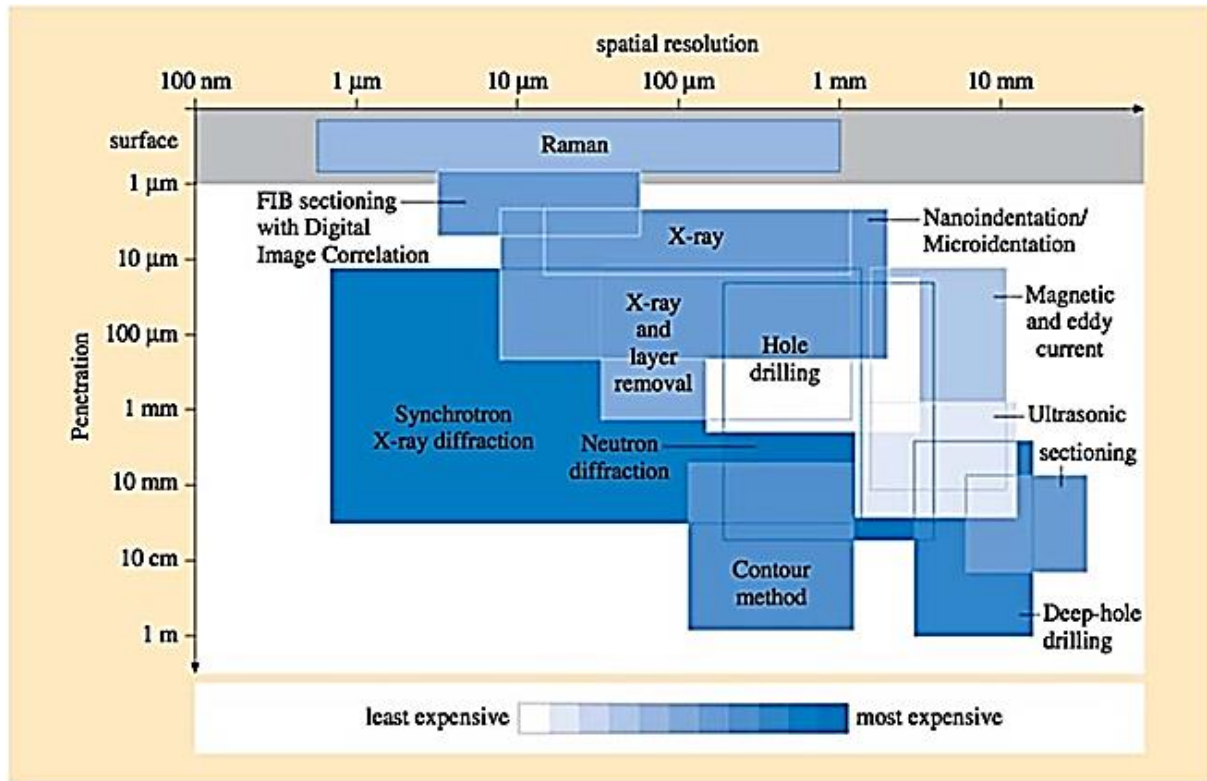


Figure 4 Summary of different residual stress measurement techniques [Fitzpatrick, Open University, UK, Schajer et. al, 2013].

Figure 4 displays a summary of the different techniques related to spatial resolution and penetration capabilities [Schajer et al., 2013]. A problem in residual stress measurements is that variation in measurement method leads to differences in the stress determined, which does not allow for precise inter-method comparison [Li and Wang, 2016]. Careful consideration should be given in technique selection, so that measurement results are fit to purpose. There are several factors to consider in choosing a suitable method to measure residual stresses, with major factors being: measurement objectives, specimen damage, specimen shape, specimen dimensions, measurement environment,

equipment availability, nature of residual stresses, specimen material, accuracy and spatial resolution, cost and duration, and safety concerns [Schajer et al., 2013], [Schajer et al., 2006].

Residual stresses related to machining distortion are commonly categorized into two main classifications: bulk and machining induced. Bulk residual stresses, or inherent residual stresses come from former manufacturing processes [Teng et al., 2003]. Bulk residual stresses often result from complex process combinations that include heat transfer, inelastic mechanical deformation, and metallurgical changes [Chantzis et al., 2013]. Residual stresses caused from materials processing usually follow process specific symmetrical shape profiles. The profiles are related directly to the process symmetry and workpiece geometry [Sim et al., 2011], [Prime et al., 2001]. For example, through thickness residual stress profiles for a quenched rolled aluminum plate can exhibit an “M” shape, as in Figure 5 [Prime et al., 2002]. When large thermal gradients exist, and strength is high, large bulk residual stresses can arise [Yang et al., 2013], [Navalho et al., 2012]. Material processing with extreme thermal and mechanical conditions produces greater residual stresses. In certain workpiece configurations, the bulk residual stresses, induced by prior processing, can account for the majority of distortion [Huang et al., 2014].

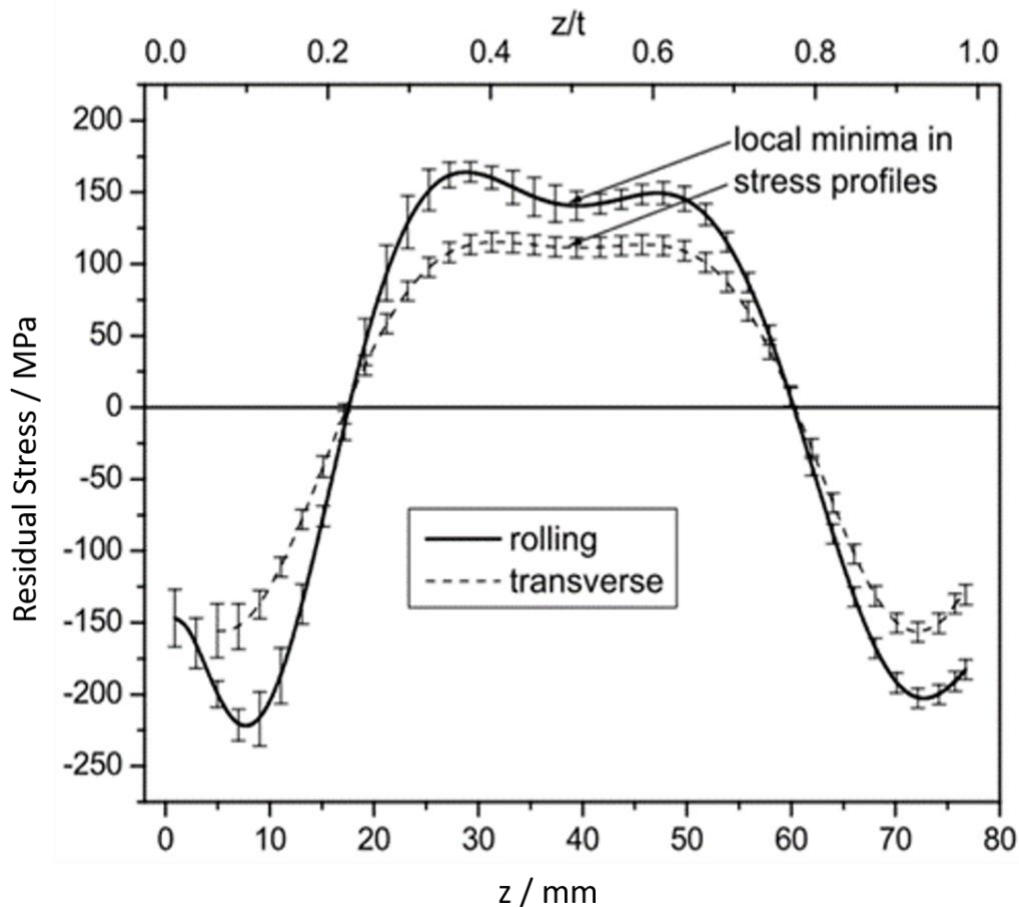


Figure 5 Residual stress profile for a rolled aluminum 7050 T74 plate in the cross-section [Prime et al., 2001]

Machining induced residual stresses are mainly related to a shallow depth at the machined surface of the workpiece [Li and Wang, 2016], [Jawahir et al., 2011]. Machining induced residual stresses are caused by forces and heat applied by the cutting tool, and are a combined result of plastic deformation, thermal strain, phase transformation, and their combined effects [Han et al., 2007], [Serruys et al., 1988]. Many research studies related to machining induced residual stress have focused on the effects of cutting parameters and tool geometry [Li and Wang, 2016]. Commonly, mechanical loads produce compressive residual stresses close to the surface, and thermal loads produce tensile residual stresses related to machining induced residual stresses [Wyatt et al., 2006]. Compressive residual stresses

generated from cutting forces are the dominant effect [Rao et al., 2001]. Residual stresses induced by machining have been closely related to distortion of thin-walled parts [Masoudi et al., 2014].

In order to understand the total distortion caused by machining, which includes the effects of bulk residual stress (throughout the workpiece) and machining induced residual stresses (in a shallow surface layer), it may be important to also study the interaction between the two types of residual stress. Preliminary research on the influence of these two types of residual stress has shown deformation caused by bulk residual stress can account for 90% of the total deformation [Huang et al., 2014]. For thin-walled components, however, machining residual stresses may play a major role in distortion [Li and Wang, 2016]. More fundamental research on the relationship and dynamics between bulk and machining induced residual stresses is needed to understand machining distortion and build predictive models.

1.4 Machining Distortion Modeling and Simulations

With such efforts to understand residual stresses, simulation capabilities for prediction of machining distortion are developing. Current industrial solutions to machining distortion include machining incrementally in small symmetrical steps until the part is obtained within tolerances and desired dimensions [Schajer et al., 2013].

Analytical models have been developed to predict the distortion of monolithic aerospace components [Li and Wang, 2016]. A bending moment model for predicting shape deviation has shown useful in simple geometries [Brinksmeier et al., 2009]. Deflection prediction using response surface design (RSD) has shown promise in predicting RS profiles along the cutting direction for multiple cutting parameters [Jiang et al., 2014]. A physics-based materials processing simulation revealed similar results compared to experimental data [Bi et al., 2009]. Similarly, a physics-based machining model incorporating dynamic cutting forces and tool compliance properties has been developed to predict

in-process deflections along computer numeric control (CNC) machining tool paths [Jayanti et al., 2013]. An enhanced analytic elasto-plastic model which uses superposition of thermal and mechanical stresses, followed by relaxation procedures has been developed to predict residual stresses in machining [Lazoglu et al., 2008].

Using advanced FEM/FEA software, prediction tools have been developed to minimize machining distortion [Li and Wang, 2016]. Recent FEM advancements have attributed distortion to the bending moment, of which is a function of the residual stress profile [Zhang et al., 2014]. The FEM technology of “element birth and death” was used to simulate material removal and deformations [Huang et al., 2014]. A 4-point bending model is used to create an FEM model to simulate distortion [Schulze et al., 2013]. Relaxation modeling of residual stresses can be used to study milling experiments for aerospace components [D’Alvise et al., 2015]. Finite element analysis (FEA) models of quenching was explored to simulate machining deformations related to materials processing [Zhang et al., 2012]. Discrete average stress is used to model stress and moment balance for prediction of distortion of multi-frame monolithic components [Guo et al., 2007].

Minimizing distortion based on cross-sectional RS determination has been researched to show machining adaption strategies [Zhang et al., 2014]. FEM tools have been developed to predict the behavior of the workpiece during machining due to changing geometry and fixture parameters [Cerutti et al., 2015]. A model based on through thickness residual stress determination has been explored to predict distortion for high speed machining practices [Richter-Trummer et al., 2013]. A thermal model has been developed to measure and predict deformation of thin-walled workpieces [Loehe et al., 2012]. Machining strategies used as input into FEM models has been investigated to predict shape deviation on machined workpieces [Denkena et al., 2014].

New knowledge about part distortion investigation and characterization are critical in order for the industry to progress. Recent advancements in distortion engineering have led to a design against distortion approach in which engineers attempt to be proactive to prevent costly deformations [Chantzis et al., 2013]. In-process deformation measurements of thin-walled workpieces have also been explored to understand deformations while manufacturing [Loeche et al., 2012]. Based on measured residual stresses in the bulk material, optimized workflow techniques for machinist/technicians at the shop floor level have been researched [Chantzis et al., 2013]. Machining strategies have been investigated such that the material removal steps are able to minimize part distortion based on geometrical symmetries [Zhang et al., 2014]. Analysis of all production steps in the manufacturing of mechanical gears has been studied to minimize shape deviations [Brinksmeier, et al., 2011].

1.5 Machining Distortion Measurement Methods

As shown in the previous section, many researchers are investigating the effects of machining distortion at various levels of the industries. The methodologies for defining distortion however vary from researcher to researcher as seen in Table 1. Currently in the literature, distortion can be measured however the researcher deems fit. Distortion measurements and measurands can be described in many ways including: a single value (i.e. maximum distortion, average distortion), a single curve along a reference surface (usually along the longitudinal direction with maximum deviation noted), a collection of curves along a surface (in both longitudinal and transverse directions with distinct distortion values noted), uniform spaced measurement schemes in both x and y coordinate directions with maximum and minimum values described, etc.

Table 1 Distortion research examples from the literature often show a vague description of the data collection and analysis methods used [Ma et al., 2015], [Zhang et al., 2014], [Jayanti et al., 2013], Huang et al., 2015], [Gulpak et al., 2013], [Bi et al., 2009]

	RESEARCHERS					
	Ma et al., 2015	Zhang et al., 2014	Jayanti et al., 2013	Huang et al., 2015	Gulpak et al., 2013	Bi et al., 2009
Measurement Tool	Taylor Hobson Form Talysurf Scanner	Hexagon Micro HITE 3D CMM	CMM	Mistral 775 3D CMM	CMM	N/A
Measurement Tool Technology	Tactile probe	Tactile probe	N/A	N/A	N/A	N/A
Distortion Data Collection Method	Central line in length direction	Central line in length and width	N/A	3 lines in length equidistant	Measured grid on opposite of machined surface	N/A
Distortion Space	2D	2D	3D	2D	3D	2D
Distortion Data Analysis Method	N/A	N/A	N/A	N/A	N/A	N/A

Some examples of distortion experimental results are described in Figure 6 - Figure 15. Ma et al. described distortion as a single profile measured along the central axis line after machining as seen in Figure 6. Zhang et al. portrayed distortion as multiple line measurements from a CMM as seen in Figure 7. Jayanti et al. provided 3-dimensional measurements via CMM from a machined component as seen in Figure 8. Huang et al. showed distortion as a single line plot measured from a CMM as seen in Figure 9. Gulpak et al. measured distortion using a grid layout on a CMM shown in Figure 10.

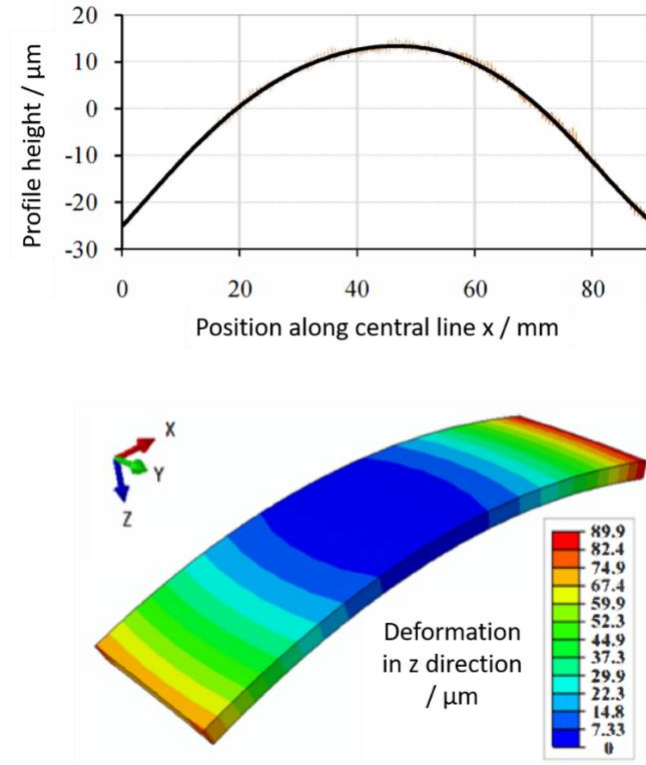


Figure 6 Distortion as a 2D line measurement along the central line [Ma et al., 2015]

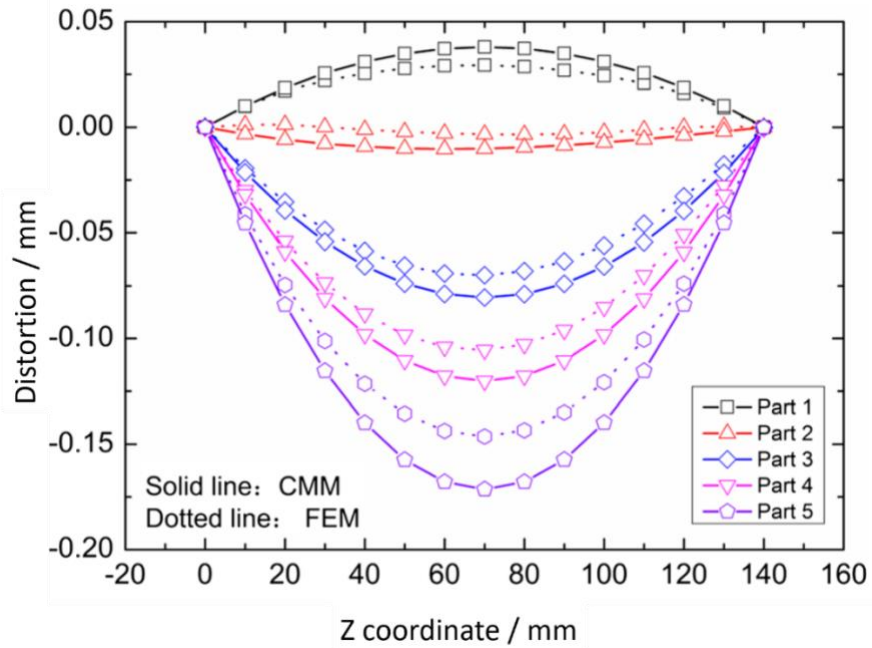


Figure 7 Distortion as multiple line plot measurements [Zhang et al., 2014]

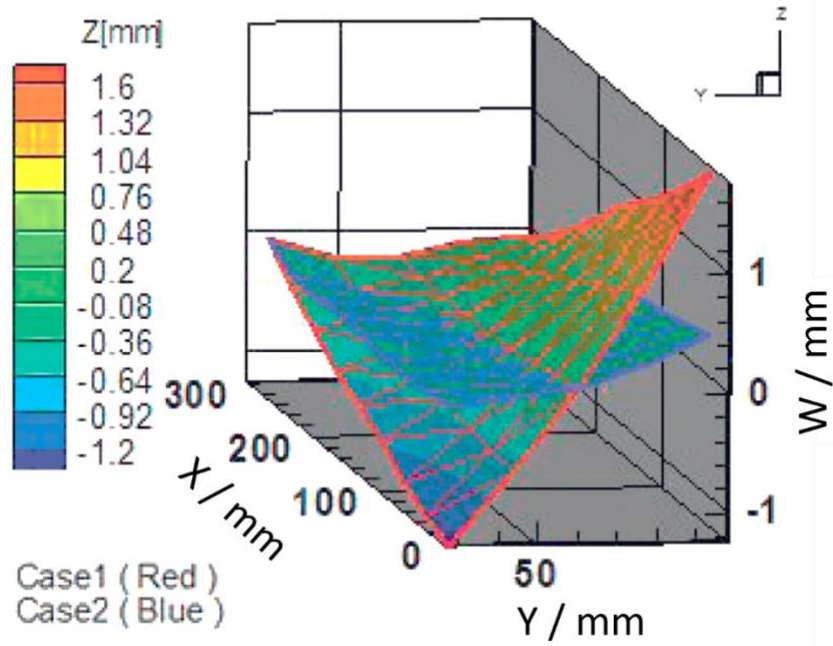


Figure 8 Distortion presented as a 3D measurement [Jayanti et al., 2013]

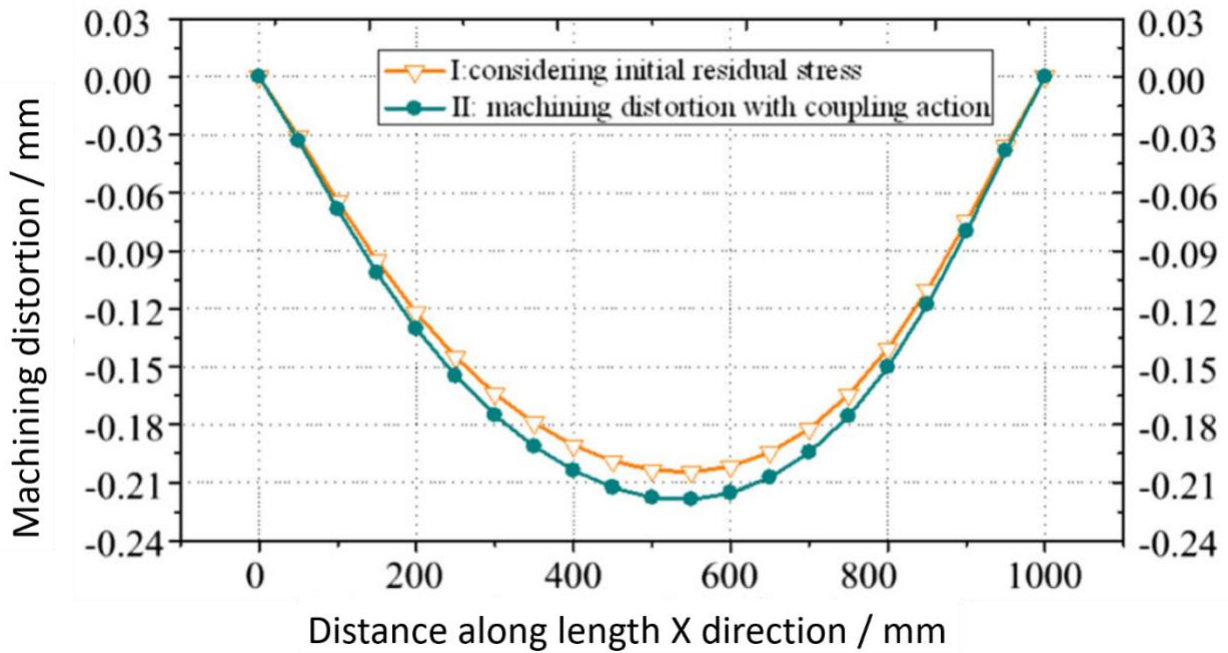


Figure 9 Distortion as a 2D measurement [Huang et al., 2015]

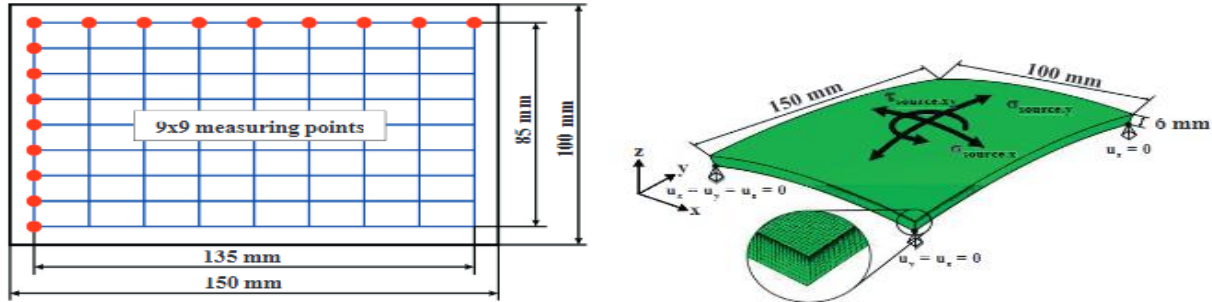


Figure 10 Distortion measured as a grid measurement [Gulpak et al., 2013]

Bi et al. measured distortion as a 2D profile with measurement parameters and equipment unknown as seen in Figure 11. Sim et al. used maximum distortion at varying plate thickness to define part distortion on aerospace structural parts shown in Figure 12. Madariaga et al. defined the final distortions as measured on a Mitutoyo Crysta-Apex S 7106 CMM along the longitudinal axis in the center of the specimen as seen in Figure 13. Yang et al. measured distortion of thin walled parts using a mathematical model used to predict coupled and uncoupled stress distribution. The experimental comparison for measuring the distortion is unclear, see Figure 14. Li et al. measured the top and bottom of a thin walled part using a Global performance 7107 CMM. The measurements scheme used on the bottom and top were arranged uniformly with 5 x 6 points (length x width) and 4 x 5 points (length x width) respectively, see Figure 15.

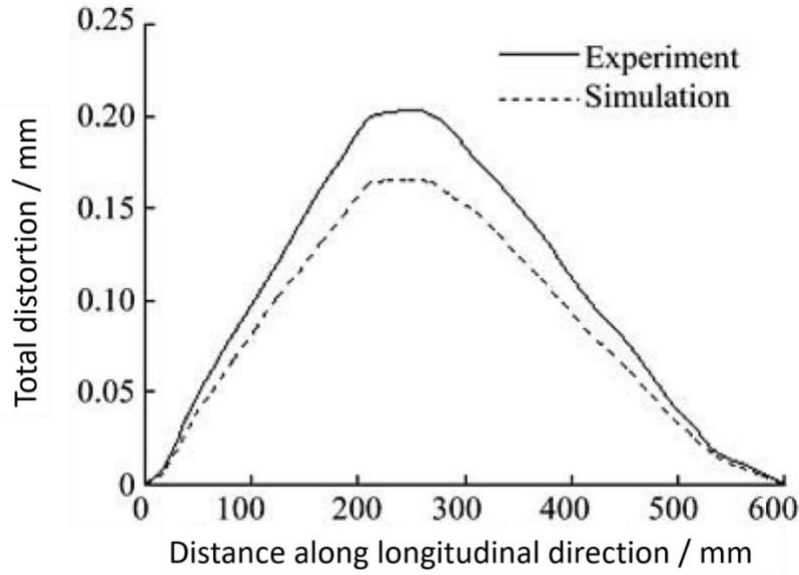


Figure 11 Distortion as a 2D line measurement [Bi et al., 2009]

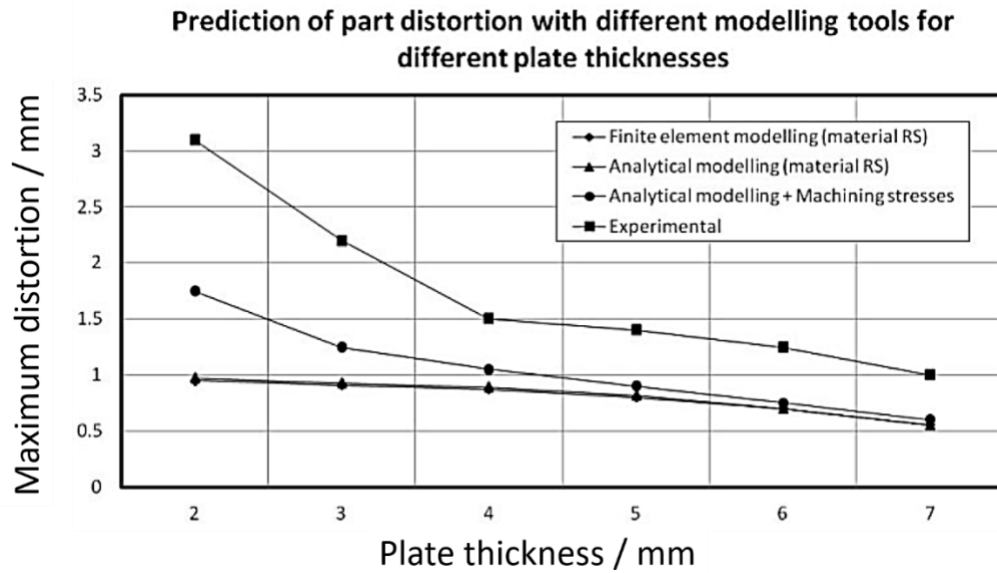


Figure 12 Maximum distortion at varying plate thickness example [Sim et al., 2011]

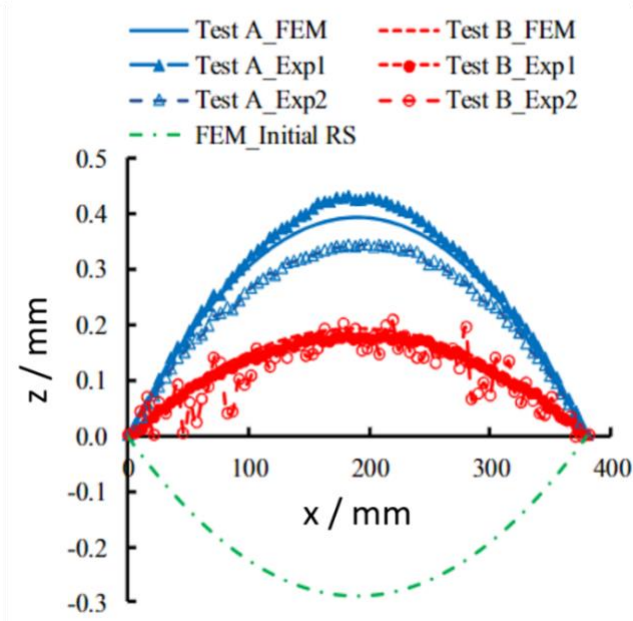
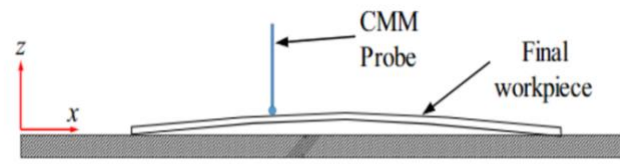


Figure 13 Distortion measured along the longitudinal axis in the center of the specimen [Madariaga et al., 2018]

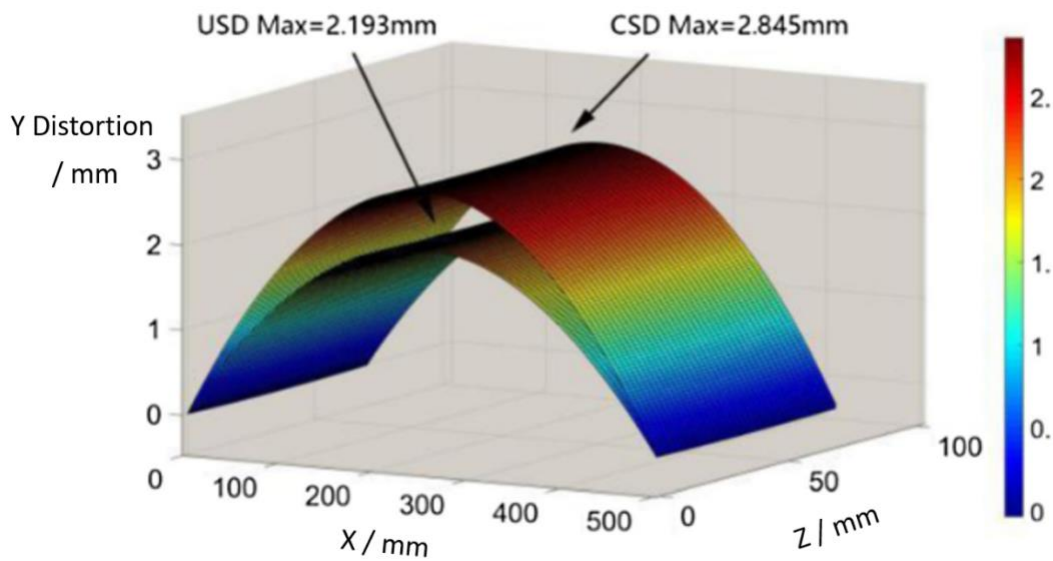


Figure 14 Measured distortion of thin walled part using mathematical model [Yang et al., 2018]

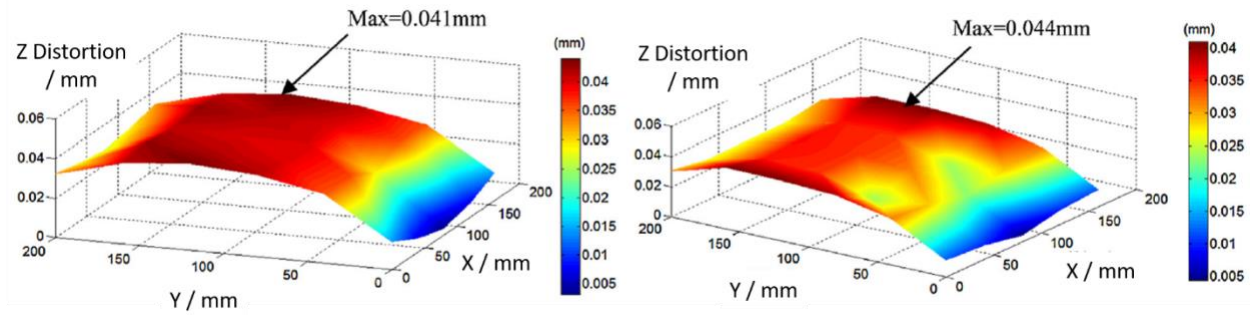


Figure 15 Measured distortion using uniform measurement CMM scheme [Li et al., 2015]

Distortion measurement definitions in the literature are not uniform and each researcher has their own way of establishing this parameter in their research. Although, the basic understanding of distortion, or the deviation from the part from what was intended is somewhat transparent – the transferability of information from researcher to researcher, or model to model is not clear – creating a need for a better relay of information.

Therefore, there is a need to have a standard method for distortion measurements as it will help push for a better solution for transferring research results and homogenizing research on part distortion to improve current manufacturing industry approaches.

1.6 Metrological Advancements

Quality assurance (QA) is a means of providing high quality parts in the production environment and it ensures that processes and products comply with the predetermined quality specifications [Schmitt, 2014], and characteristics – through metrological measurements [Savio et al., 2016]. The introduction of measuring systems in a company or industry is often driven by the need of ensuring a specific level of quality in manufacturing, using metrology for inspection purposes [Savio et al., 2016]. Metrology has the potential to improve the capability of manufacturing processes in a production environment

[Savio et al., 2016]. This research hopes to bring new knowledge about machining distortion as it relates to quality and metrology.

There are many types of measurement methods used in distortion research and metrology. A measurement is obtained from a measurement process, and that process requires measurement variables, hardware and software and human input to carry out the measurement [ASTM E2782-17]. A measurement systems analysis or MSA, is used to characterize the measurement process [ASTM E2782-17]. In understanding machining distortion, a measurement method is selected and used to collect distortion data, but before a method of measuring distortion is determined, the equipment or measuring process is analyzed such that the basic properties of the measurement system are capable. Properties to analyze include repeatability, reproducibility, linearity, bias, stability, consistency, and resolution of the measurement system [ASTM E2782-17]. The results from studying these properties give insight to the capability of the measurement system with respect to the measured item [ASTM E2782-17]. In machining distortion, we use a coordinate system from a coordinate measuring machine (CMM) to describe the deviation in z height. The resolution of the CMM determines the range of distortion it is capable of detecting.

A CMM is a measurement device that uses spatial points on the surface of a workpiece [ISO 10360-1], [Luebke, 2014]. A CMM is equipped with a specific type of probing system – contact 3D, optical 2D, and multi-sensor 2D/3D [Sladek, 2016]. The probing systems can collect data as single points or a series of points by scanning the workpiece inside the measurement field [Luebke, 2014]. Coordinate measuring machines are designed to measure size, form, and position deviations of a workpiece [Luebke, 2014]. Coordinate metrology provides a scientific basis to carry out measurements and 3D geometric object imaging with the use of coordinate measuring systems [Sladek, 2016]. Measurement of 3D objects marks the section of the space with the geometry of the measured object given as a point coordinate in a reference coordinate system [Sladek, 2016].

Commonly research experiments in manufacturing (including machining distortion milling experiments), involve collecting measurements; thus, experimentation and measurements are closely related, but they also are clearly distinct – to which measurements deserve to be viewed independently from the study of experimentation [Mitchell et al., 2017]. The concept of measurement is present in a myriad of fields including many day-to-day human activities to industrial, commercial, scientific, healthcare, safety and environmental industries, etc. [JCGM 2009]. The purpose of measurements is to provide information about a quantity of interest, and when that quantity is measured, the results depend of the measuring system itself [JCGM 2009]. Measurements are not exact, but rather depend on multiple factors including the measurement procedure, the operator skill, the environment, and other effects [Bell et al., 1999]. Measurements have an associated measurement uncertainty that is used in a central role to assess quality and quality standards [JCGM 104:2009].

Metrology, or the study of measurements and its applications [JCGM 2012], can be described as the “hidden infrastructure of the modern world” [Quinn et al., 2017], orienting the complexities of the measurement methods and science. Metrology is focused on design, maintenance, and improvements to technology to create accurate measurements [Mitchell et al., 2017]. For machining distortion, the need to understand measurement techniques, measurability, and measuring practices all come into play.

The measurement results, or the coordinate data from the CMM is further used to characterize the sample. ISO 25178 gives insight into classification methods for measuring surface texture and characterization for roughness, with more work in progress to incorporate metrological characteristics and calibration instrumentation [ISO 25178]. In order to characterize surface measurement features, an understanding of filtering and fitting techniques is evaluated to the data.

The tasks of production metrology include ensuring the function of the workpieces, test equipment, and the product quality [Eifler, 2018]. There are many types of measuring principles [Klocke, 2011] related to production metrology including but not limited to stylus instrument, white-light interferometer, confocal microscope, focus variation microscopy, angular resolved scattering light sensor, pneumatic distance measurement, etc. [Eifler, 2018]. There are advantages and disadvantages for each measuring principle and ultimately the measurement principle is selected based on requirements of the production. Optical probes have advantages of being able to collect data faster than analogue contact tactile probes but are less accurate than industrially available contact probing systems [Flack et al., 2014]. Tactile probing systems have roughness limitations due to the stylus tip size diameter. There are many different techniques available for surface measurement analysis and it is important to understand the sample properties, limitations of each, and analysis required [Conroy et al., 2005].

Recent advancements for surface metrology include a detailed review of current large-scale metrology with the consideration of the entire measurement processes [Schmitt et al., 2016]. In the aerospace industry, airplane structures are metrologically-assisted to detect deformations through robot-based assembly systems [Schmitt et al., 2014]. A software assisted procedure for beacon positioning in large scale metrology applications has been designed to incorporate pre-processing information in a three-dimensional network design [Galletto et al., 2010]. Investigation into surface topography methods and future reference techniques shows that white light interferometry and confocal microscopes are promising optical techniques for future applications, but until then, tactile stylus techniques will be treated as the reference technique and more work is needed for topography characterization [Mathia et al., 2011]. Recent work has suggested the use of combination metrology systems which account for measurement uncertainty in the distance and angular measurement of sensors of different natures [Franceschini et al., 2015]. A new purely optical 3D micro coordinate measurement machine has been

implemented to measure and evaluate micro-injection holes [Zangl et al., 2018]. A structural characterization of measurement has been proposed, being partly empirical and partly theoretical, showing that the structure of the measurement process guarantees the reliability of its results – even after assumptions of measurements are more reliable than opinions and guesses [Mari et al., 2017]. International collaborations, from thirteen different laboratories worldwide, have been employed to compare surface texture parameters using optical instruments for polymer artifacts [Tosello et al., 2016]. New ISO 1101:2017 (the International Organization for Standardization) standards have been created to implement technological developments in tolerancing and metrology, of which have been analyzed for their potential impact on the digitization of manufacturing [Morse et al., 2018]. Information rich metrology (IRM) has been researched for surface metrology applications, as the far from effortless incorporation of additionally available information in the data acquisition and processing pipeline of a measurement process in order to improve the efficiency and quality of the measurement, resulting in expensive value added surface characterization results [Senin et al., 2018]. Of all the recent advancements in metrology, metrology research is pushed in particular by of application changes, evolvement of manufacturing instruments, and new customer specifications related to more accurate and precise parts.

1.7 Conclusion

Many of the current approaches to solving machining distortion provide point-solutions for specific circumstances while relying on empirical trials at excessive costs. In the distortion literature, basic information is missing about how distortion is practically characterized. Examples from the literature show inconsistent methodologies for effectively collecting and analyzing distortion data. Results of experiments or modeling approaches are not easy to transfer. Therefore, a transparent way to quantify

distortion data collection and analysis is needed and will enhance the transferability of experimental and analytical results.

CHAPTER 2 RESEARCH OBJECTIVES

As discussed in Chapter 1, there are critical issues relating to machining distortions (in particular part quality.) that directly relate to sustainability. Minimizing machining distortions and reducing the amount of waste that is a direct result from machining distortions, can lead to more sustainable manufacturing. Sustainable manufacturing requires simultaneous consideration of economic, environmental, and social implications associated with the production and delivery of goods [Haapala et al., 2013]. In the aerospace and manufacturing industries, billions of dollars are credited to the costs from reworking, scrapped materials, remanufacturing, and/or rejecting components that are defective and do not pass quality inspections due to machining distortions [Bowden et al., 2001], [Thoben et al., 2002]. Minimizing machining distortion can positively impact all three pillars of sustainability by saving money, reducing waste, and advance manufacturing technicians and workers machining abilities.

The overall hypothesis of this dissertation is that *a new model for the characterization of machining distortion using three dimensions, provides a larger added value to optimize distortion minimization than the common two-dimensional approaches taken in the manufacturing industry.* One of the main questions to be answered in this research is, *how can we create a robust method or procedure for measuring and analyzing three-dimensional distortion for multiple applications?*

Introductory work gives insight to challenges in characterizing distortion and the different applications distortion research can be applied to. Further work is needed to investigate overall 3D part distortion and proper characterization procedures and techniques – to ultimately reduce and minimize distortions.

The research objectives of this study are divided into three specific aims.

1. Develop a transparent and robust distortion characterization tool for various machining processes and geometries
2. Investigate measurement machine capabilities and measurement methods for collecting machining distortion data
3. Investigate manufacturing applications related to machining distortion including nano-manufacturing and process planning optimization

The first objective is to determine data analysis methods for an optimized distortion data analysis. The research questions to be answered include: How do we create a robust method to analyze coordinate data from part/machining distortion coordinate measurements? What type of data fitting/filtering will be used for the multiple facets of the part geometry? A distortion tool will be created to investigate both 2D and 3D distortion data. Basic fitting models such as least-squares fitting, will be used for the different polynomial and surface data sets, to relate the difference between measured data. Using the knowledge from the data collection and data analysis tasks, further information post analysis can help determine the characterization of distortion such as: curvature, symmetries, and other form features. ISO and ASTM standards will be used to create a standard set of methods/procedures to collect and analyze overall part distortion for further characterization. The geometric form and position characteristics of interest can include straightness, flatness, line shape, and surface shape [ISO:1101]. The geometric position characteristics of interest can include parallelism, perpendicularity, angularity, position, and symmetry [ISO:1101]. There is no current standard method for the characterization of part distortion. Creating a set of instructions for collecting and analyzing distortion data, is likely to reduce the variation in the distortion results from the literature. To fully understand part and machining distortion, a transparent way to quantify distortion data collection and analysis is needed to enhance the transferability of experimental and analytical results.

The second objective is to investigate the capabilities of specific measurement tools used to measure distortion. In this objective, the research questions to be investigated are, how do measurement capabilities differ for several types of CMMs used for distortion data collection? What benefits do different CMMs have as part distortion validation methods? How much information is lost by simplifying part distortion to a two-dimensional problem? How much more information from the data is obtained from different data collection methods? A measurement capability analysis for the coordinate measuring machine systems used for data collection of part/machining distortion will be carried out to create a fingerprint for capability for the different tools available. Distortion data will be restrained to only consider the surface of the part. A correspondence of points will be developed for the original and distorted geometries. A registration will be developed to satisfy the 1:1 correspondence. Distortion measurements as a standardized method will help push for a better solution for understanding part distortion than compared to current manufacturing industry approaches.

The third objective is to investigate various manufacturing applications as they relate to machining distortion including nanofabrication and an optimized process planning chain. This third objective aims to understand machining distortion for specific machining processes and geometries. A schematic of the research objectives can be seen in Figure 16.

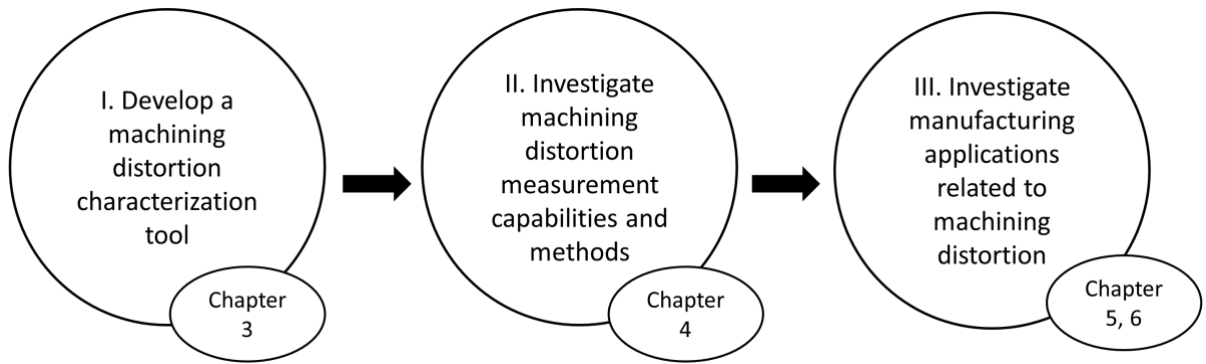


Figure 16 Schematic of the combined research objectives with overall goal of producing a distortion tool used for various manufacturing distortion data

There are an infinite amount of shapes and geometries with numerous functions and capabilities to explore in understanding part distortion. For time and resource limitations, the geometries researched include: U-shape prism, rectangular beam, and complex pockets.

The dissertation at hand will explore a state of the art (Ch. 1), research objectives and motivation (Ch. 2), an initial routine for characterizing machining distortion, which includes data collection and analysis (Ch. 3), an optimized routine for this featuring distortion measurement capabilities and enhanced data analysis with Gaussian surface curvature (Ch. 4), case study I: distortion in a nanomanufacturing application (Ch. 5), a case study II: distortion and part quality in a process planning tool (Ch. 6), conclusion (Ch. 7), appendix, and references.

CHAPTER 3 INITIAL ROUTINE OF MACHINING DISTORTION CHARACTERIZATION

In the distortion literature, basic information is missing about how distortion is practically characterized and therefore the results are not easy to transfer. In the following, an initial routine or method for machining distortion characterization is developed to obtain distortion values in a transparent way. This will enhance transferability of experimental and analytical results.

In order to begin this research, simple models of complex aerospace parts are investigated to understand distortion and its overall behavior. This chapter focuses on the methodology of characterizing and quantifying distortions based on coordinate data sets of pre- and post-machining, which follows routines from the literature. After simple shapes are studied with respect to their distortion, more complex shapes such as pockets and slots will be investigated in the next chapter.

This chapter shows an initial transparent and repeatable method for characterizing distortion for machined parts. The results from the distorted u-shapes indicate similar characteristics from distortion due to bulk residual stresses and machining factors. However, this chapter also describes shortcomings of this initial method, which are tackled in the next chapters.

3.1 Methods

3.1.1 Material and Experimental Setup

Quenched 7050 T74 aluminum is used to investigate material removal with respect to milling machining distortion. The residual stress profile has been obtained in another research work [Olson et al., 2016]. A prismatic u-shape geometry is machined, and distortions are characterized, quantified, and described in detail. Experimental research based on design of experiments (DOE) allows analysis

of how residual stresses affect distortion and the machining process. In the following, experiment setup and distortion characterization are described.

The material used in this case study is a quenched aluminum bar in alloy 7050 T74, which has high residual stresses. The dimensions of the initial quenched bar were 50.8mm x 76.2mm x 609.6mm. The contour method [Hill et al., 2014] was used to measure a two-dimensional map of the residual stress component acting along the bar length (σ_{yy}), as shown in Figure 17. Residual stress was found to range from -150 MPa to +150 MPa. The material was selected as a typical aerospace alloy, with high toughness and corrosion resistance, in a condition of high residual stress that would effectively show machining distortion.

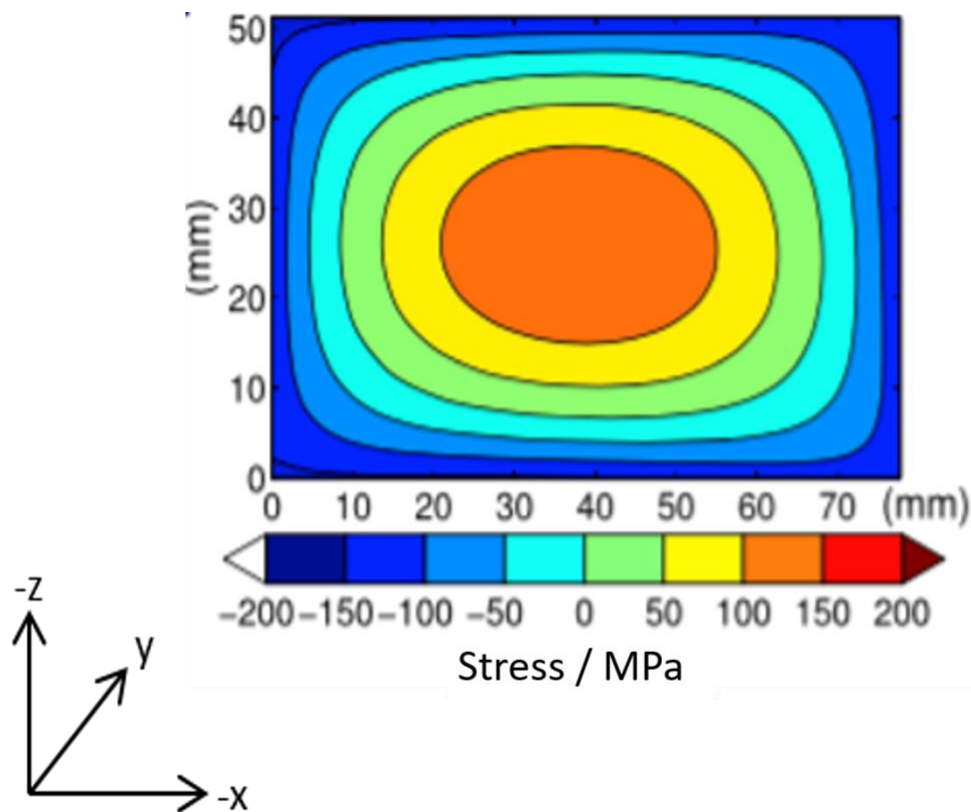


Figure 17 Residual stress profile in the aluminum bar [Hill et al., 2014]

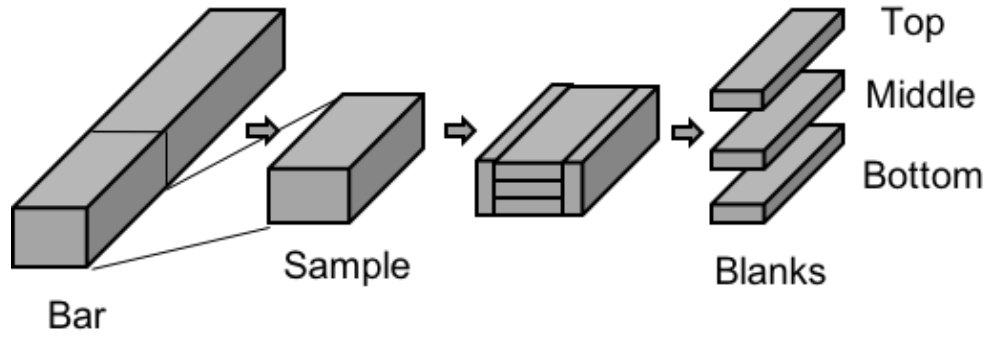


Figure 18 Schematic of the material division

Based on previous research studies on machining distortion due to residual stresses [Zhang et al., 2014], a simple u-shape geometry was designed to assess machining distortion. In order to test for distortion, the original stock material, or bar, was divided into different sections termed samples (Figure 18). Samples were cut to be 50.8 mm x 76.2 mm x 127 mm. Samples were then divided into blanks 8.75 mm x 31.75 mm x 127 mm, each taken from a different region: Top, Middle, Bottom, Left, and Right. In order to keep the setup controlled, each side of the blanks was labelled according to its location and orientation (i.e. top, left, right, bottom, front, back). The stress distribution is position dependent, such that the blank location and orientation are key attributes. The schematic of the material divisions can be seen in Figure 18, where the test blanks were taken from the center (along x) of each initial division of the top, middle and bottom regions.

An issue faced in the experiment setup was the clamping mechanism and understanding how to hold and secure a material with high residual stresses while machining. For safety concerns, a fixture was designed with zero degrees of freedom to prevent distortion while machining (Figure 19). A breadboard fixture was manufactured from a 38mm thick aluminum plate. Threaded holes were milled and tapped into the plate using a CNC milling center. The final fixture including clamps can be seen

in Figure 19. Designing the fixture for the experiments stressed the importance of the impact of clamping on distortion during machining.

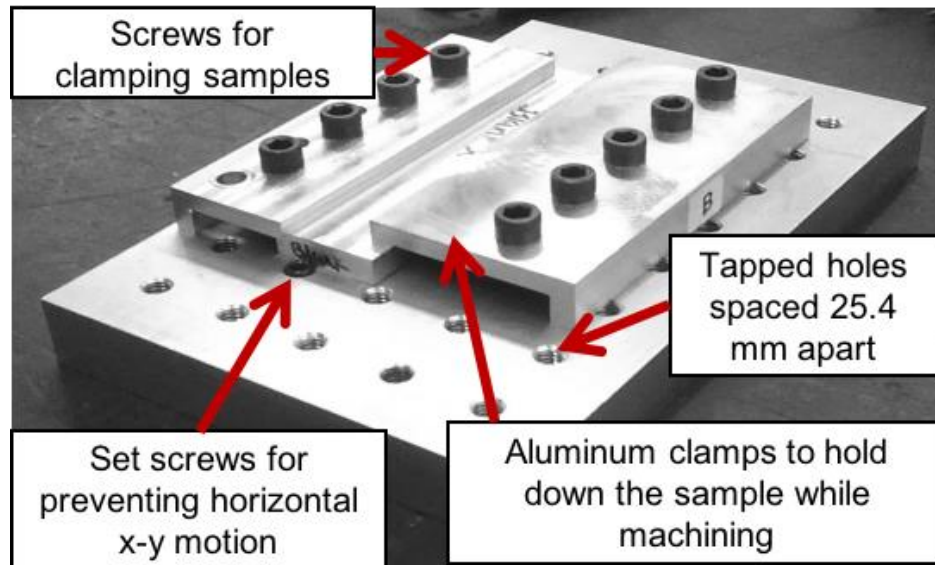


Figure 19 Clamping fixture with labeled components

For the part shape, a prismatic u-shape geometry was chosen to represent a scaled down version of an aerospace monolithic component (Figure 20). The u-shape part provided a geometry of thin walls, and a long length to encourage distortion. The u-shape was created by milling a 25.4 mm wide slot into each blank, removing 64% of the blank material. Milling was performed on a *Bridgeport CNC mill*. The machining parameters for the milling experiment are listed in Table 2. The u-shape part locations in the initial bar cross-section can be seen in Figure 21.

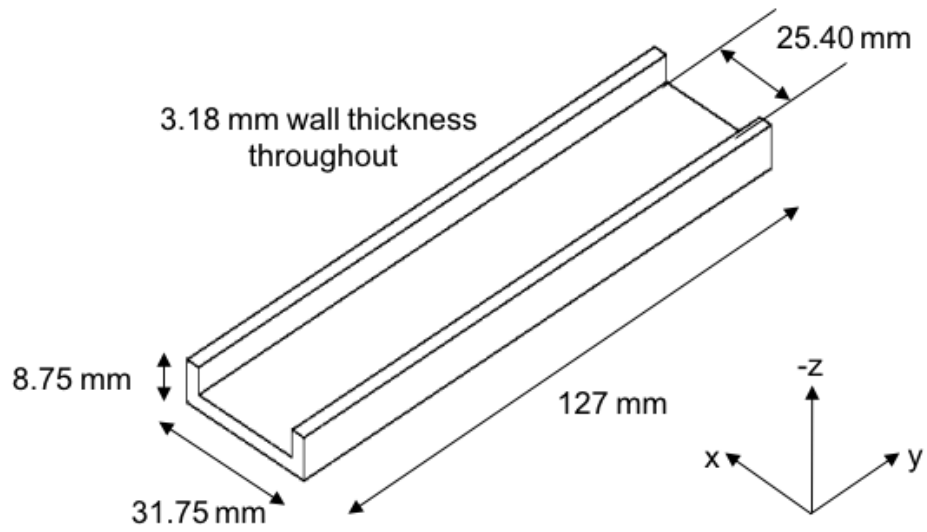


Figure 20 U-shape geometry

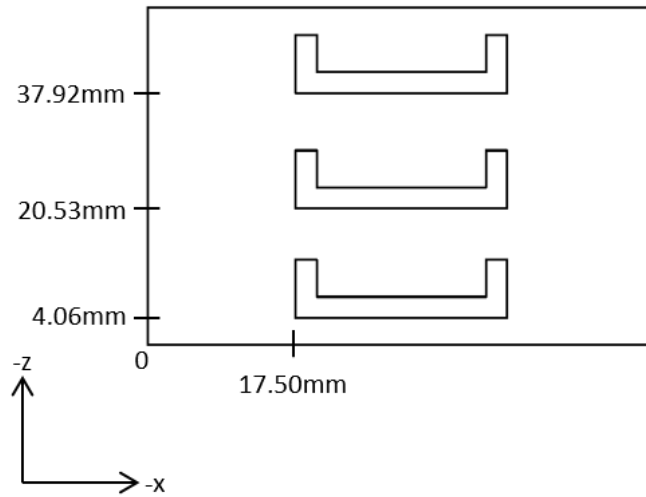


Figure 21 U-shape locations in the initial sample

Table 2 Machining Parameters of distortion sample

Machining Parameters	
Machine Tool	Bridgeport 3.5 axis CNC Milling Center
Cutting Tool	12.7 mm Diameter. TiCN-Coated 3-Flute Carbide End Mill
Spindle Speed	2000 RPM
Feed rate	254 mm/min
Depth of Cut per Pass	0.127 mm
Number of Passes	44

3.1.2 Initial Distortion Characterization Tool

Data collection

In this experiment, data were obtained using a scanning profilometer over a workpiece reference surface before and after machining (pre- and post-machining). Pre- and post- measurement differences were used in this study, as an already established method for determining the overall distortion after being released from the fixture. Since there are many factors influencing distortion including time, temperature, clamping forces, etc., focusing on a distortion timeframe between before and after machining is used to determine the overall distortion from the milling process. Here, the reference surface is the lower surface of each blank, which is intended to be flat. No machining operation was performed on the reference surface when milling the u-slot, which makes it a useful reference. The reference surface profile was measured using a *Taylor Hobson Talyscan 250* profilometer (Figure 22), which uses a laser-based sensor to measure surface height at a specified array of x and y positions. Here, the x locations had 0.1 mm spacing, and the y locations had 0.4 mm spacing, and measurements were made on the entire surface.

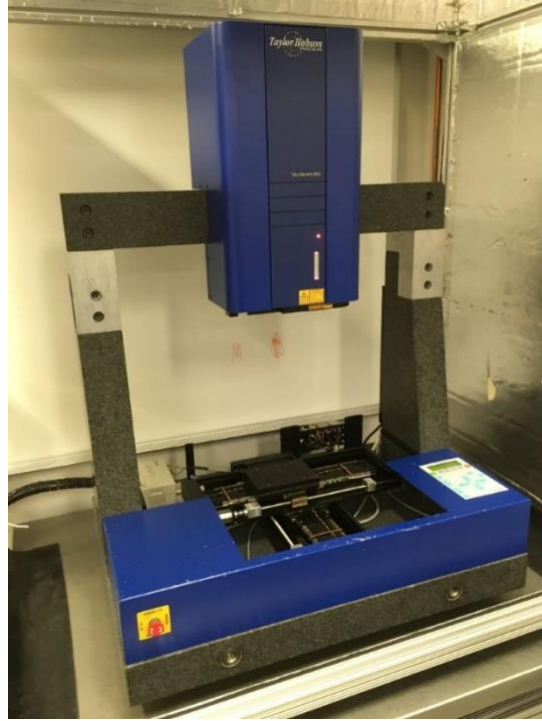


Figure 22 Distortion data was measured using a Taylor Hobson Talyscan 250 CMM at the University of California Davis

Data analysis

In order to quantify the amount of distortion specific to each finished u-shape, the difference between surface profile data pre- and post-machining was calculated using an algorithm created in *Matlab 2014*. The distortion characterization algorithm is illustrated in Figure 23 and Figure 24 from the raw data to the final calculated difference. Surface data are initially filtered (see Equations (1) – (3)) to remove z-coordinate values that are obviously off the surface (typically because a given x-y location is outside the part boundary, or surface reflectivity prevents a signal from the laser sensor). After the initial filter, a planar fit is used to level the data to the x-y plane as seen in the Equation (1).

$$z(x, y) = a + bx + cy \quad (1)$$

The fit residual (data minus fit) provides leveled data for the following step. Outliers in the leveled data are filtered further from the leveled data, where outliers are defined as z values near the extremes (maximum and minimum z values). Defining the z range R as maximum minus minimum (Equation 2), outliers are identified and removed if outside the range of z from the data by Equation (3).

$$R = z_{max} - z_{min} \quad (2)$$

$$z = \begin{cases} > \frac{1.5}{100} R + z_{min} \\ < z_{max} - \frac{1.5}{100} R \end{cases} \quad (3)$$

Repeating the planar fit, leveling, and filtering steps 3 times provides a useful set of data for further steps. The next steps of the algorithm align the pre- and post-machined surfaces, by rotating and translating one relative to the other, linearly interpolate them to a common grid, and take their difference. The final three-dimensional distortion is defined as the pre-machined surface height subtracted from the post-machined surface height.

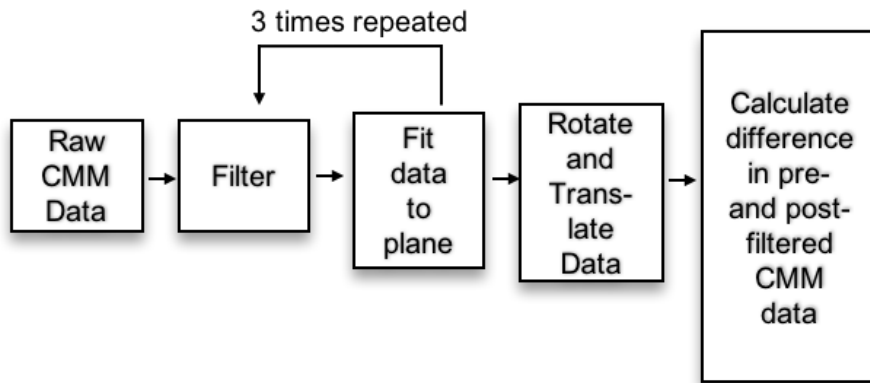


Figure 23 Algorithmic steps in characterizing distortion

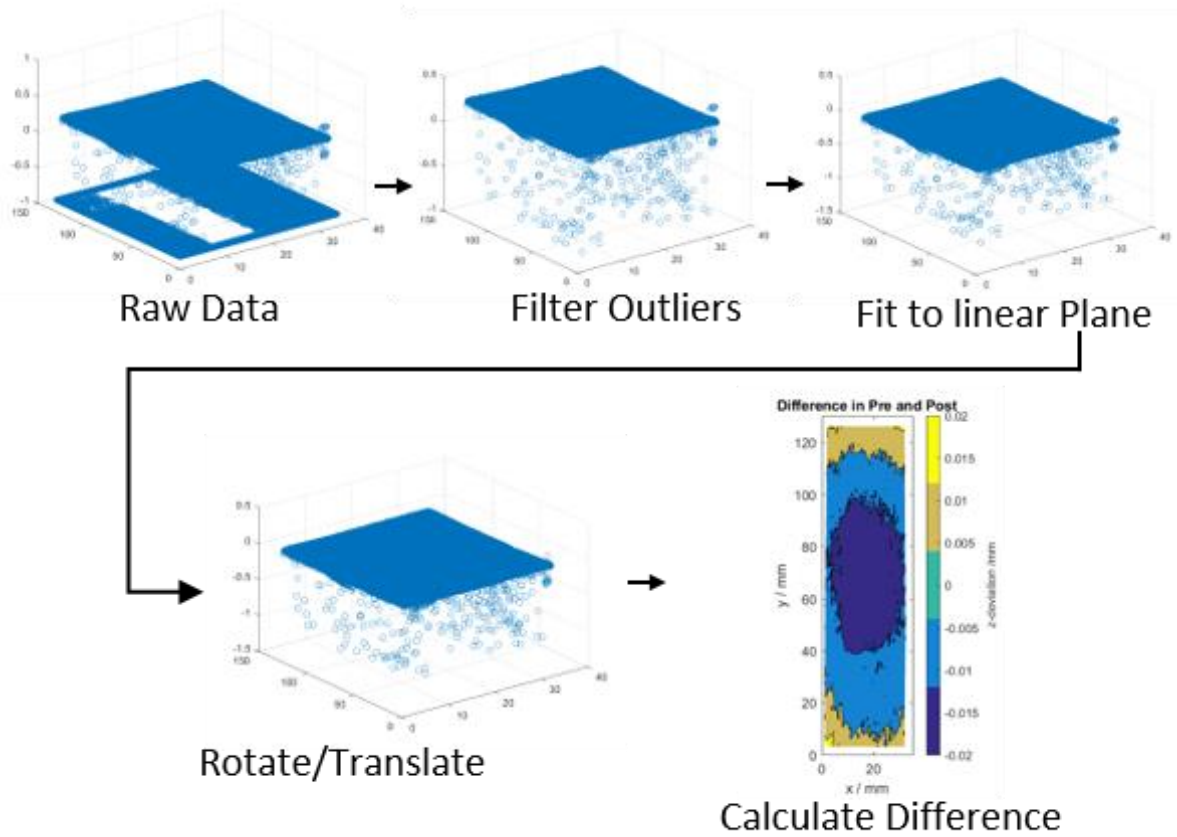


Figure 24 Analysis steps depicted in distortion characterization tool [Garcia et al., 2017]

3.2 Results and Discussion

After carrying out the milling tests, machining distortion was quantified for each of the blanks. Figure 25 shows the results of the z-deviation provided through the distortion characterization tool.

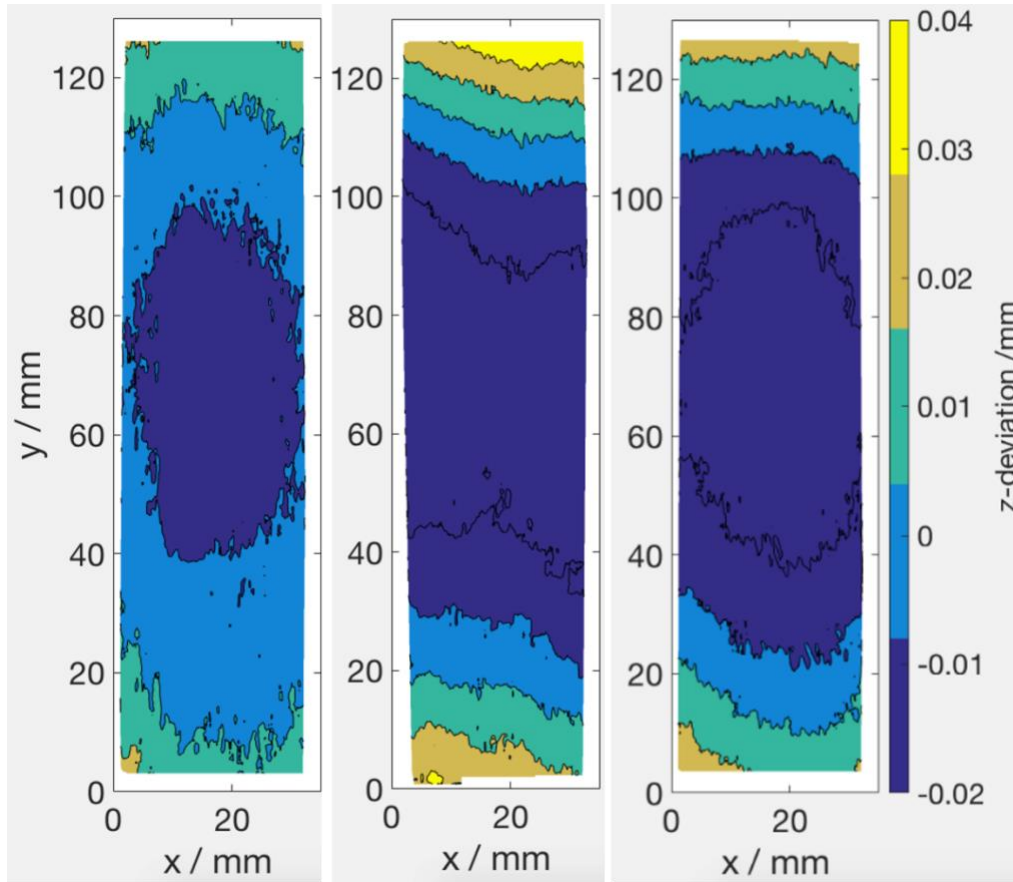


Figure 25 Distortion visualization of z-deviation of top, middle and bottom blank displayed together from left to right respectively

The results show each blank piece experienced similar distortion characteristics. The reference surface of each blank bowed downward at the mid-length and experienced a torsional characteristic on each end as depicted in Figure 26.

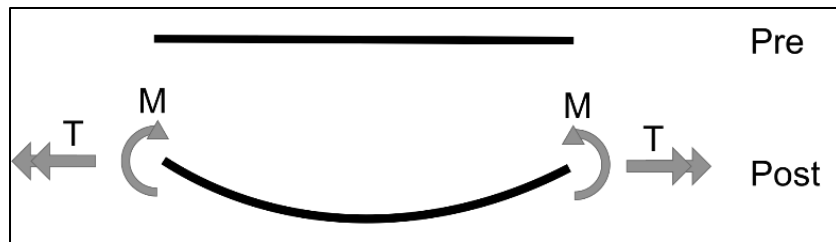


Figure 26 Representation of bending and torsion each blank experience along the y-axis

Each blank piece location (Top, Middle, Bottom) has a unique bulk residual stress distribution from Figure 17, and it was assumed that the distortion would be different for each blank location. But there is a similar distortion pattern in Figure 27 for each location, and this motivates further work, including residual stress modeling and the assessment of additional factors such as the details of machining and clamping.

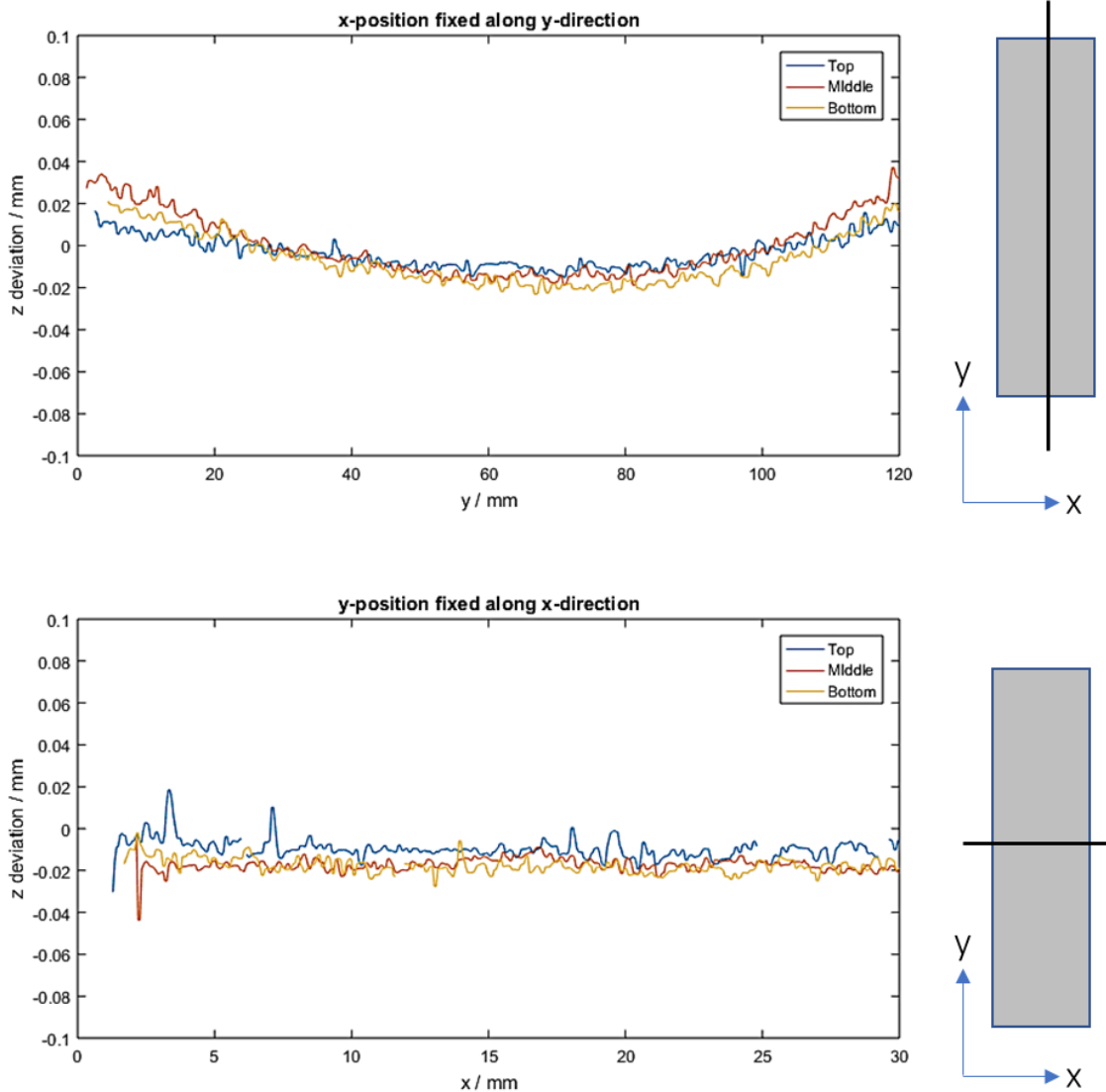


Figure 27 Line plots at the midline of each distortion sample combined together in both x and y directions

Distortion plots for each sample are shown below in Figure 28 – Figure 30. The results show a similar bending characteristic with a maximum z-deviation at the center of the blank.

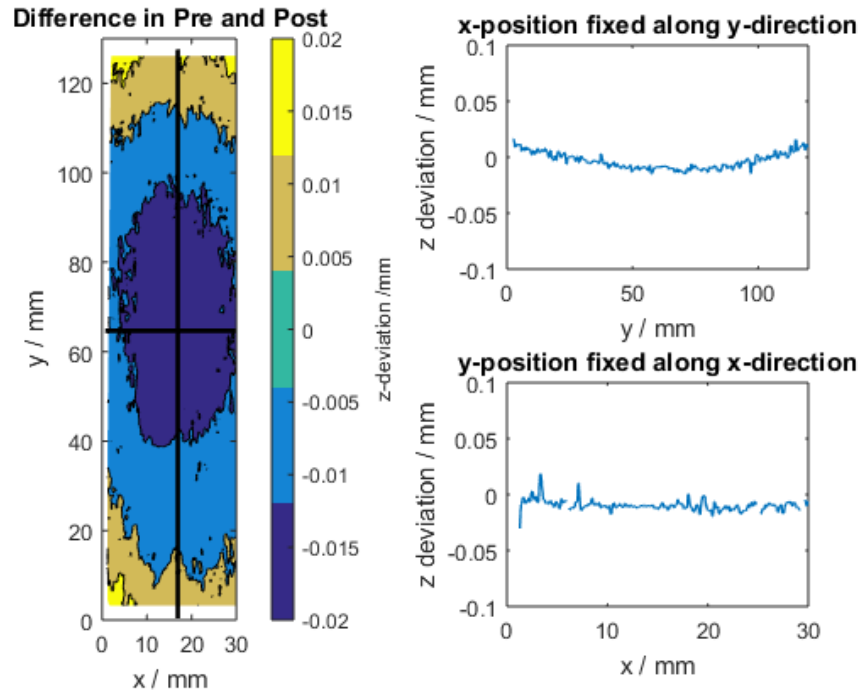


Figure 28 UC Davis top sample distortion presented along with central line plots in both x and y directions

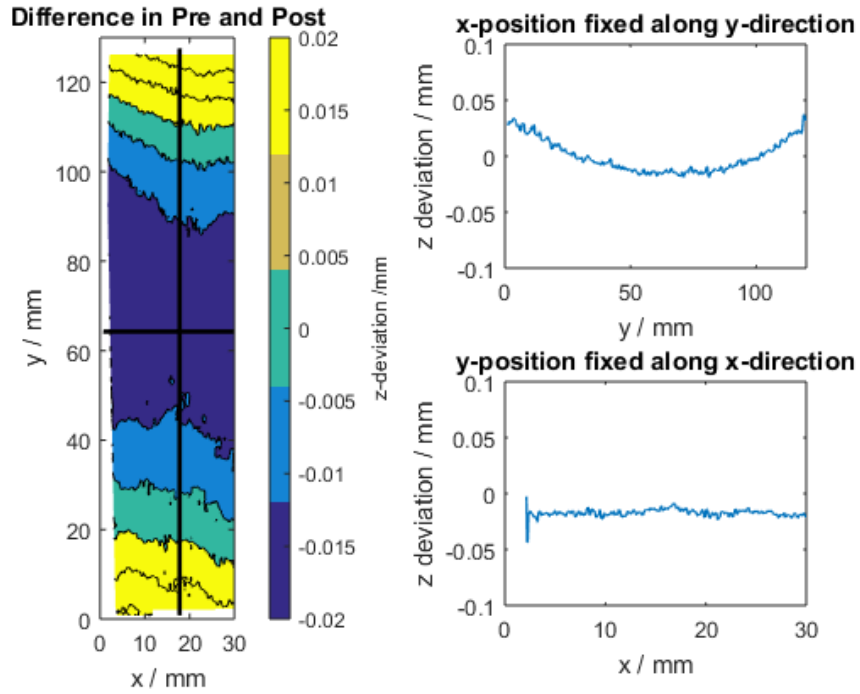


Figure 29 UC Davis middle sample distortion presented along with central line plots in both x and y directions

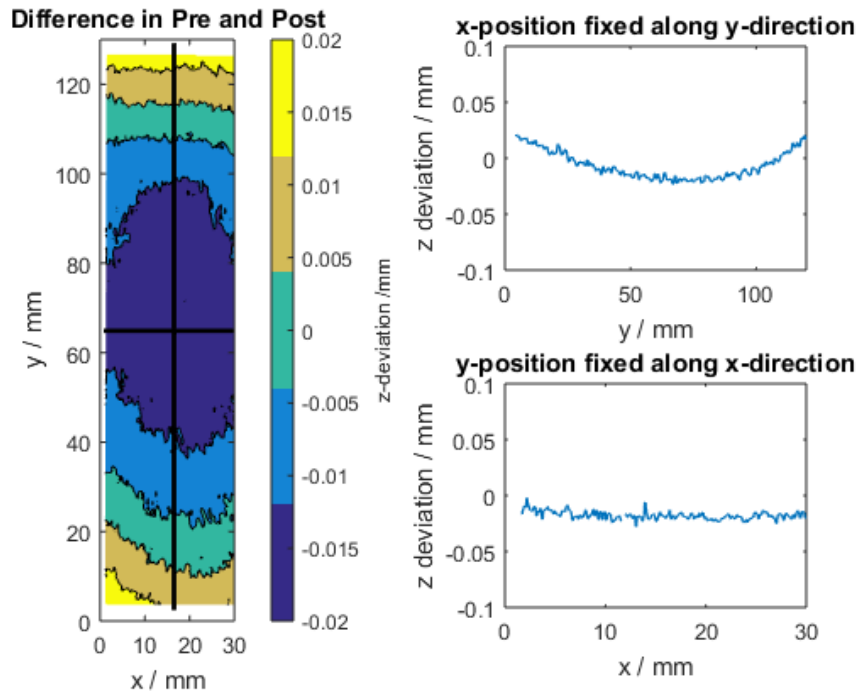


Figure 30 UC Davis bottom sample distortion presented along with central line plots in both x and y directions

Figure 31 shows the line plots shifted to compare to compare the magnitudes of the distortions. The line profiles were extracted around $x = 18\text{mm}$ for each sample, and the initial z -deviation value for each sample was subtracted so all lines begin at 0 on the vertical axis. The maximum z -deviation (maximum minus minimum z value) for each blank is shown in Table 3. This is defined as the maximum distortion. The middle blank experienced the overall maximum distortion. At the center of the bar, the internal residual stress is the highest as seen for the initial log in Figure 17. This suggests that the highest internal residual stress accounts for the largest distortion.

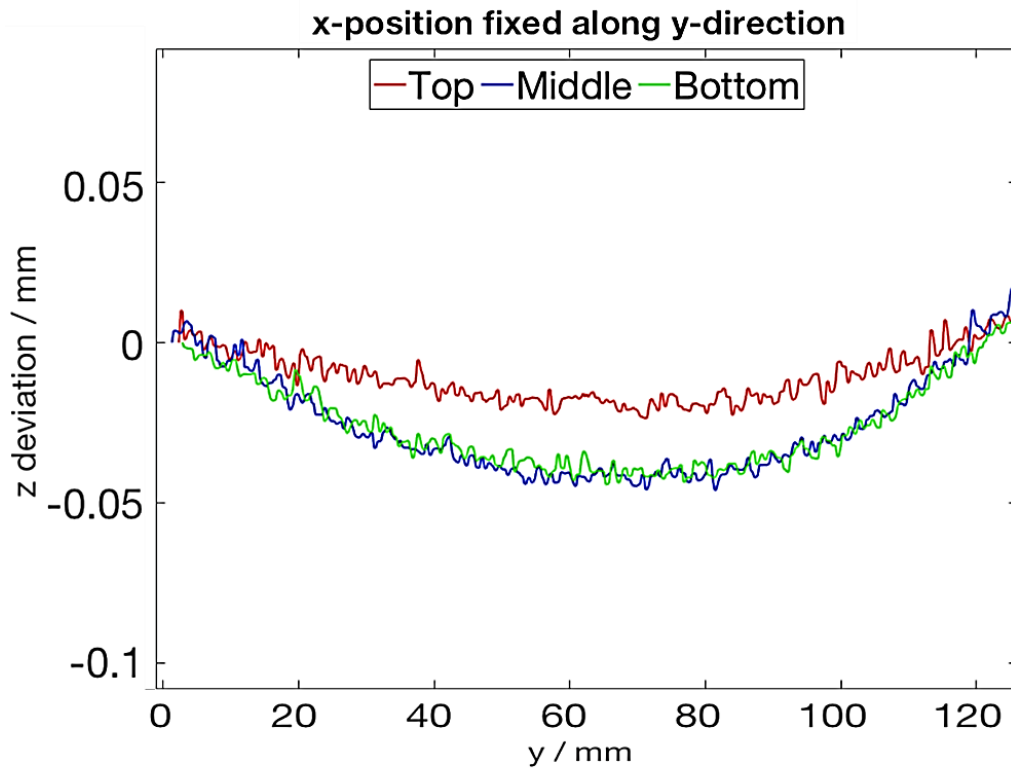


Figure 31 Shifted line plots at midline of each distortion sample

Table 3 Maximum distortion in z-deviation

Blank	Distortion Value in mm
Top	0.024
Middle	0.046
Bottom	0.044

3.2.1 International Collaboration Distortion Data

The distortion experiments presented above were carried out at the University of California Davis and then repeated at the Technical University of Kaiserslautern in the Summer of 2016. Milling experiments were conducted at the FBK institute at TUK using a *DMU 70 eVolution Deckel Maho* 5 axis CNC and distortion measurements were collected using a *Micro-Hite DCC 3D CMM* as seen in Figure 32, with a 1 mm x 1 mm spacing in the x and y directions. The machining parameters were kept constant, using the same machining fixture as seen in Figure 19. The machining setup can be seen in Figure 33.

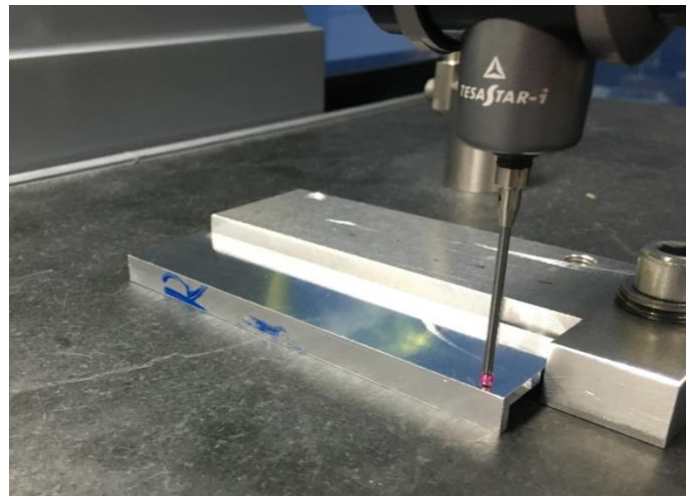


Figure 32 Tactile probe of the Micro-Hite DCC 3D CMM measuring a distortion sample at TUK with measurement fixture for repeat measurements

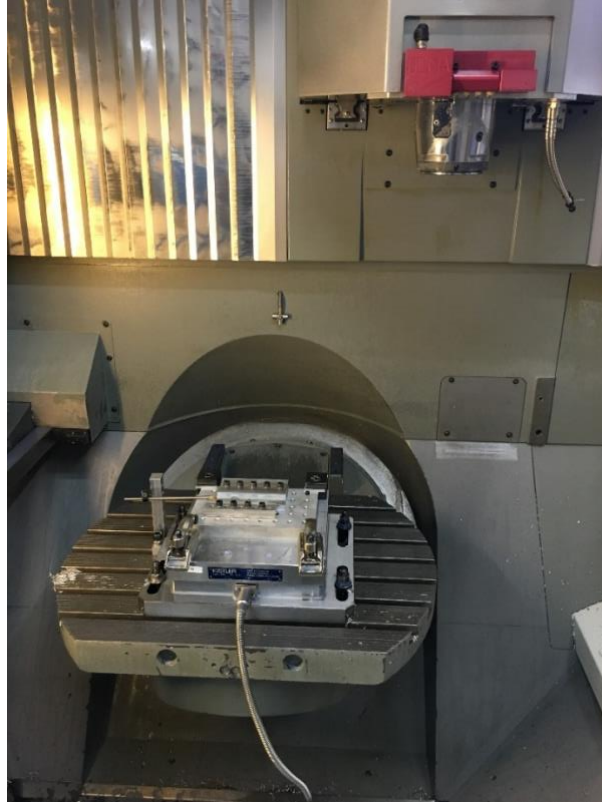


Figure 33 Similar milling experiments were conducted at TUK using a DMU 70 e evolution Deckel Maho advance CNC

Machining distortion results from the TUK milling experiments differed drastically as explained in the following, proving repeatability for exact milling and coordinate measurements more difficult than anticipated. TUK data can be seen in the Figure 34 – Figure 38 below.

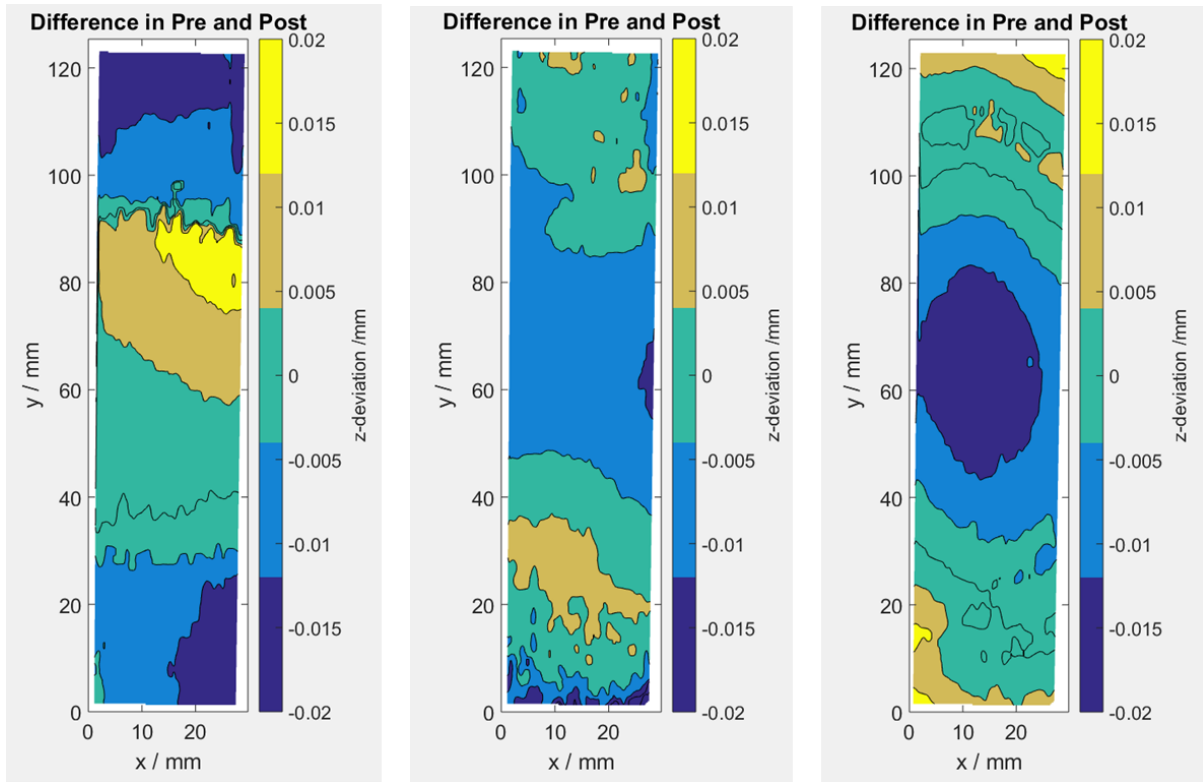


Figure 34 Distortion visualization of z-deviation of top, middle and bottom blanks from TUK displayed together from left to right respectively

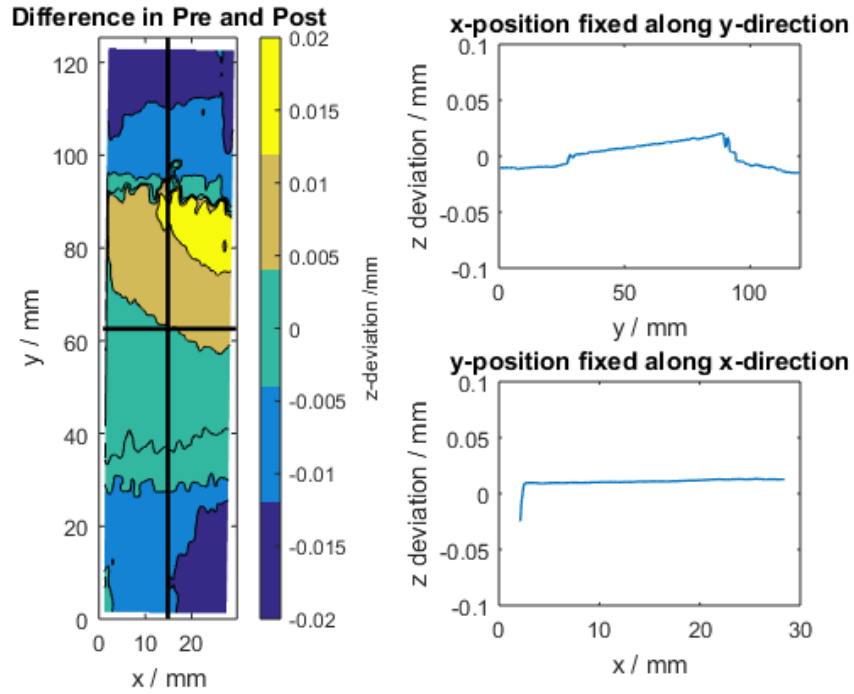


Figure 35 Top sample distortion shown for TUK experiment 1

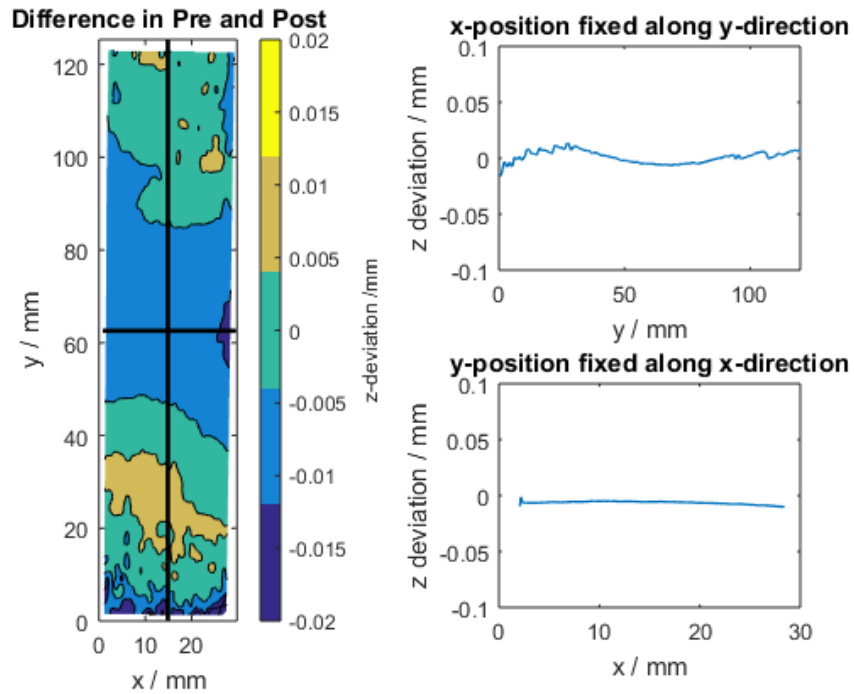


Figure 36 Middle sample distortion shown for TUK experiment 1

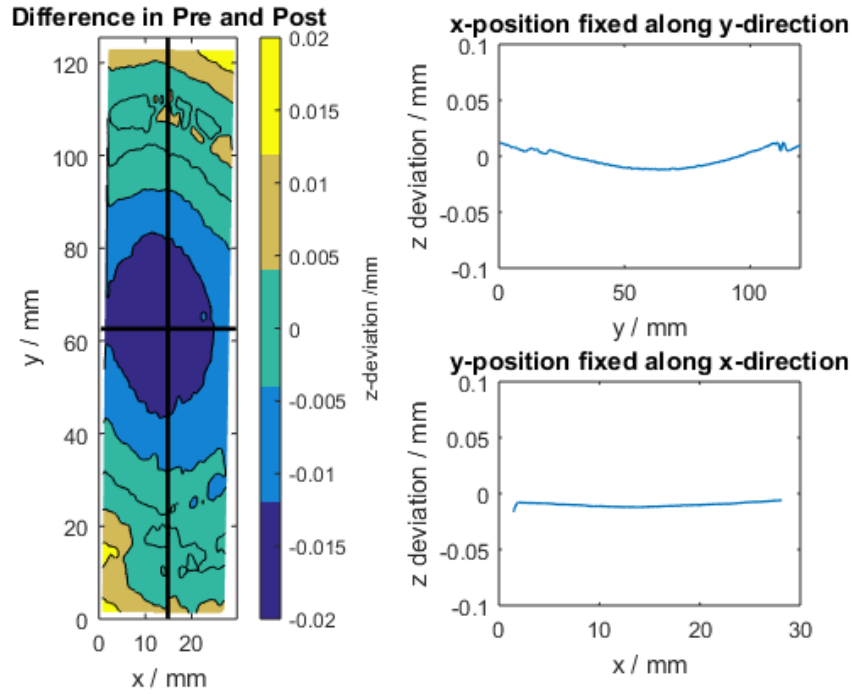


Figure 37 Bottom sample distortion shown for TUK experiment 1

The coordinate data from the TUK experiments had unknown errors causing the data to have step-like discontinuities corrupting the data as seen in the top sample from experiment 1 in Figure 38.

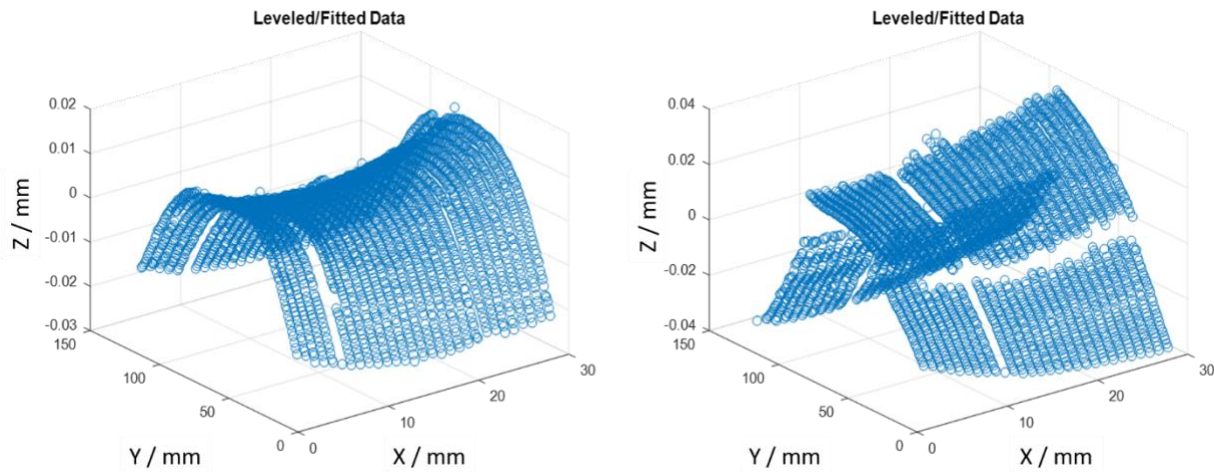


Figure 38 Coordinate data from the Top sample experiment 1 pre (left) and post (right), obtained from the Micro-Hite DCC 3D CMM had poor data quality

Further TUK data also showed poor data quality to create a uniform measurement collection. Distortion data from TUK measured on the Micro-Hite DCC 3D CMM had major differences compared to the Taylor Hobson Talyscan 250 including: tactile probe versus laser optical scanning methods, measurement resolution, sample size space, sample placement, level and orientation in coordinate spacing, etc. Distortion data from TUK helped promote future work into uniform machining distortion data collection and analysis methods (see Appendix I).

3.2.2 Machining Distortion Data collection

Initial work on understanding machining distortion, including creating a methodology to observe distortion from a simple milling experiment, provided unique interpretations on how to define and collect distortion data. Some example distortion data collection methods for a free form feature include but are not limited to: using nominal geometry or pre/post data, measuring flatness, measuring parallel-ness, measuring part thickness at various locations, measuring part thickness in every direction or orientation, measuring the projected light for mapping data, measuring angles for perpendicularity, measuring heights, using a dial gage with runner, using calipers to measure thickness, using a touch probe to measure height, using a “go-no-go” gage, comparing to the CAD model, measuring the straightness of the part, creating a standardized part to compare to, using the negative freeform to measure the distortion, etc. A universal method to measure and collect distortion data is necessary for data transferability and transparency.

3.3 Conclusion

In conclusion, the overall purpose of this chapter is to provide preliminary investigation for characterization of machining distortion of quenched aluminum with high residual stresses. Through this work, one repeatable way of quantifying distortion was described and carried out as a means of

measuring the distortion present in the manufactured blanks. Presenting distortion as the difference between before and after reference datum in addition to displaying the 3D profile with z height deviations and line profiles of critical midline locations on the surface provided more visual information about the overall distortion present in the resulting sample.

Overall the 2D distortion profiles are similar to the distortion literature for simple prismatic shapes. The middle sample experienced the greatest z distortion value. The 2D distortion only shows a curvature of distortion at a fixed location on the blank. Visualizing the 3D distortion provides more visual to the corners and other areas of the blank samples. The results suggest a similar release of residual stresses to obtain the final curved shapes. More work is needed to analyze the effects of the clamping device in relation to the manufacturing steps. In this initial research, information about intermediate residual stress states from initial to final part are absent. For deeper understanding of distortion, the residual stress profiles after each manufacturing step should be analyzed. Another suggestion for further research based on this work is to understand the part deformation after each manufacturing step (i.e. measurements of reference plane distortion after each manufacturing step). The characterization method is cumbersome because pre- and post-measurements have to be made. Furthermore, this method is developed for only one test case (workpiece dimension and CMM). The distortion was defined as a scalar, single value.

Overall, the results give evidence that this distortion characterization algorithm provided an initial robust way to characterize and quantify distortion based on differences of coordinate data. The method described in this paper can easily be reproduced to assess distortion characteristics of different prismatic shapes or other measurement data.

This study reports a transferable analysis method as a basis for a comprehensive DOE for machining distortion. Distortion calculations were achieved by analyzing a subtraction of initial from final

measurements of coordinate data for a reference surface, here being the untouched bottom surface before and after machining. The UC Davis distortion results show a similar bending characteristic for blanks removed from different locations in a quenched bar, suggesting similar residual stress profiles in the intermediate blanks and/or similar machining and clamping effects.

More work is needed to investigate metrological characterization methods and procedures to minimize compromised data and improve repeatability across equipment and technologies. The characterization methods presented in this investigation also must incorporate the way to characterize the overall shape the distortion displays. As seen in the UC Davis distortion results, there are distinct shapes presented in the top, middle and bottom samples. The top and bottom samples are similar but differ in convex magnitude. The UC Davis middle 3D sample result displays a different shape to the top and bottom samples, in which it exhibits a mirror like symmetry about an undefined axis. The following chapter expands the initial method to include different CMM machines, improves data analysis, etc. (for you to fill – needs to show that you found shortcomings in this chapter and try to solve them in the next)

Overall future work is needed to distinguish the effects of different contributing factors to machining distortion individually. Such factors to be further investigated include bulk vs. machining induced residual stresses, work-holding devices and clamping mechanisms, part geometries, scale effects and more. In addition, more work is needed to validate the experimental distortion results, including FEM simulations.

Publications

Garcia DR, Hill MR, Aurich JC, Linke BS. Characterization of Machining Distortion due to Residual Stresses in Quenched Aluminum. ASME. International Manufacturing Science and Engineering Conference, Volume 1: Processes ():V001T02A031. doi:10.1115/MSEC2017-2878.

CHAPTER 4 OPTIMIZED ROUTINE OF MACHINING DISTORTION CHARACTERIZATION FEATURING GAUSSIAN SURFACE CURVATURE

As described in earlier chapters, the literature presents a definition for machining distortion that is loosely defined, but rather an understanding that all changes of part shape are machining distortion. Examples from machining distortion literature show inconsistent methodologies for effectively collecting and analyzing distortion data. Many of the methods used for displaying machining distortion in the literature include a linear or two-dimensional visual representation using either a midline or central line for critical distortion maximum areas. The 2D visual representation often gives a sparse indication of the overall distorted shape. A three-dimensional method for displaying and characterizing machining distortion is necessary for presenting the overall complex shape present in the distorted material [Garcia et al., 2017]. More information about the surface can be extracted from machining distortion data which is collected from a dense three-dimensional surface scan.

Although definitions for the resulting distortion and data collection methods vary, a common denominator for collecting machining distortion data is unique – the use of some form of metrological equipment.

As shown in the previous chapter, data quality and repeatability vary across measurement equipment and technologies. This chapter will therefore explore different metrology equipment in relation to machining distortion such as optical, tactile, and combination CMMs, as well as investigate metrological characterization of machining distortion from coordinate data. The surfaces of the actual distortion, although relatively small in overall z height deviation, have unique complexity in shape. The distorted surface to be characterized has a complex geometry within the small overall z deviation. The machining distortion shape is intricate between positive and negative curvature. Thus, an

approach to characterize machining distortion by Gaussian curvature from control points or datum collected from a parametric surface, created via Bernstein basis functions of a least-squares fit, is demonstrated as a novel means to metrologically characterize distortion.

Machining distortion data presented in earlier research, gave insight to preliminary distortion data collection methods and procedures, and the idea to measure a reference datum before and after machining, or pre- and post-, proved difficult in data quality and consistency [Garcia et al., 2017].

4.1 Methods

4.1.1 Sample Workpiece

Distortion data was collected on the reference surface of an aluminum sample with machined pockets from a PAG quenched aluminum 7050 bar [Olson et al., 2016]. The dimensions of each sample are 76.2 mm x 50.8 mm x 6.35 mm with two equal sized pockets around a stiffener wall at 60 degrees from the sample edge as seen in Figure 39.

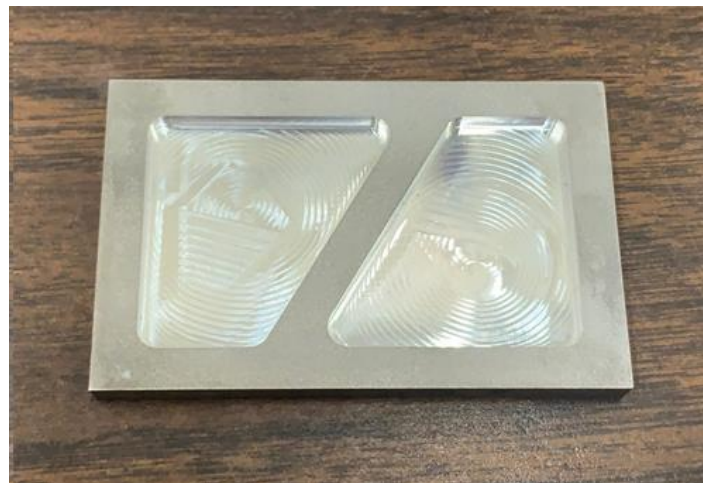


Figure 39 Distortion sample of machined pockets with 60-degree stiffener wall [NSF/DFG Award No. 1663341], [Ribeiro and Hill, 2016]

Data was collected on the bottom surface of each sample, called the reference plane. The data was collected on each sample using each of the three CMMs for comparison. The spacing scheme for the x and y axes on the Mitutoyo Bright BRT 504 CMM, and the Taylor Hobson Talyscan 250 CMM is 1 x 1 mm. The spacing scheme for the Faro Arm Edge CMM is not defined for the optical scanning arm setting from the CMM.

4.1.2 Initial CMM Selection and Parameters

In comparing data collection methods, a coordinate measuring machine (CMM) may be considered the most universal tool for collecting distortion data, such that a CMM is capable of measuring: a point, line, plane, circle, cylinder, cone, sphere, ellipse, step cylinder, slot, circular slot, parabola, paraboloid, torus, parallel planes, curve, surface, etc. For this study, a CMM is used as the means of collecting distortion data. Three CMMs are available at our disposal at the University of California Davis for this study. Initial data collection is carried out on each CMM for investigation of CMM capabilities. The three CMM tools used in the initial preparation for this study are the Mitutoyo Bright BRT 504 CMM, Faro Arm Edge and Scan Arm HD CMM, and the Taylor Hobson Talyscan 250 as seen in Figure 40.

The research questions to be investigated in this chapter include, how do measurement capabilities differ for several types of CMMs used for distortion data collection? What benefits do different CMMs have as part distortion validation methods? How much information is lost by simplifying part distortion to a two-dimensional problem? How much more information from the data is obtained from different data collection methods?



Figure 40 Three coordinate measuring machines are introduced from left to right as the Mitutoyo Bright BRT 504 CMM (left), Faro Arm Edge and Scan Arm HD CMM (middle), and the Taylor Hobson Talyscan 250 CMM (right)

The technical capabilities and specifications of the metrology equipment are presented in Table 4. Note the repeatability data for the Taylor Hobson Talyscan 250 CMM is unavailable from the manufacturer's specification sheet.

Table 4 Specifications for the different CMM machines

Specifications	Mitutoyo Bright BRT504 CMM	FaroArm Edge & Scan Arm HD	Taylor Hobson Talyscan 250
Accuracy	0.0005 mm	0.029 mm	0.001 mm
Repeatability	0.003 mm	0.025 mm	**
Measurement Technology	Tactile Probe	Laser Line/ Tactile Probe	Optical Laser Triangulation
Measuring Capacity	500 mm x 400 mm x 400 mm	1.8 m x 1.8 m x 1.8 m	200 mm x 200 mm x 200 mm

Distortion data was obtained from a single measurement scan from the CMMs, in lieu of nominal geometry scans from a pre and post CMM measurements. Measuring a single surface for the distortion data is sufficient so long as the sample geometry reference initial state (i.e. initial distortion present) is negligible, or flat. In measuring one surface for the distortion, it made it easier for the operator to collect data and compare. Since machining distortion is defined as the deviation of the part shape from

the original intent, one can measure and collect data from a reference surface and compare it to the original CAD dimensions of flatness, etc. Coordinate data will be used to compare surfaces to a flat plane. Distortion visuals for each metrology equipment are shown for the FaroArm, Talyscan, and the Mitutoyo CMM for the 60-degree sample in Figure 41.

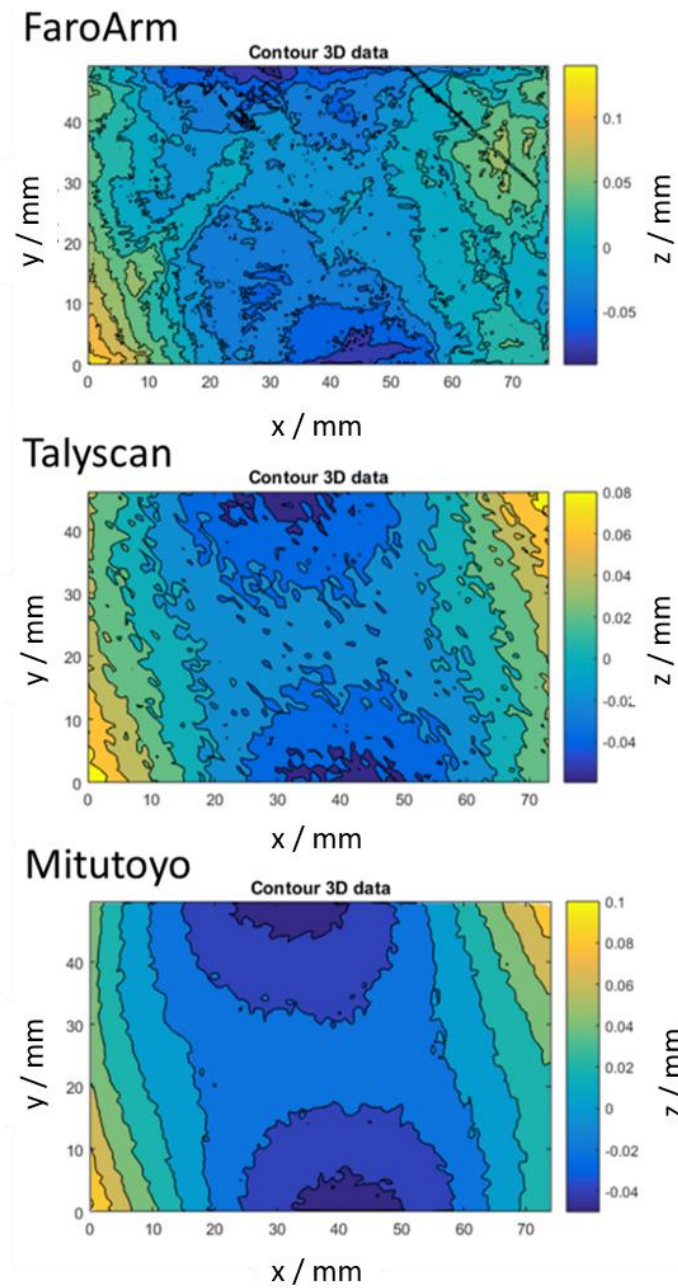


Figure 41 Distortion coordinate data of the same part 60 degree part sample, from 3 different CMMs (FaroArm, Talyscan, and Mitutoyo) are shown

The distortion values (defined as the maximum z-deviations from the intended shape) varied for the different metrology. Note, the scalar distortion values are defined as the maximum distortion value minus the minimum distortion value. The distortion results for the different tools are 0.2438 mm, 0.1504 mm, and 0.1535 mm for the Faro Arm, Talyscan and Mitutoyo respectively. The Faro Arm has a single point accuracy of 0.029 mm and a volumetric accuracy of +/- 0.041 mm which contributes to the noise and difference from the other coordinate measuring machines. The Faro Arm was therefore determined unfit for the distortion measurement tool. The Talyscan exhibited optical difficulty with the reflective metal surface.

Further investigation of the distortion data from the machined pocket samples is conducted on the Mitutoyo BRT Bright 504 CMM due to availability and quality data. The tactile CMM is often still considered the 'golden standard' in metrology as it represents a physical contact on the workpiece and has the longest history of standardization. The final distortion represents the overall shape features, not the minute texture (i.e. surface roughness). Therefore, the coordinate spacing for the Mitutoyo CMM was investigated to provide quality data for the data analysis method. The spacing in the x and y axes were kept uniform. Pitch and increment spacing for the x and y axes respectively were investigated at 5 x 5 mm, 2 x 2 mm, 1 x 1 mm, and 0.5 x 0.5 mm as seen in the following, Figure 42 - Figure 45.

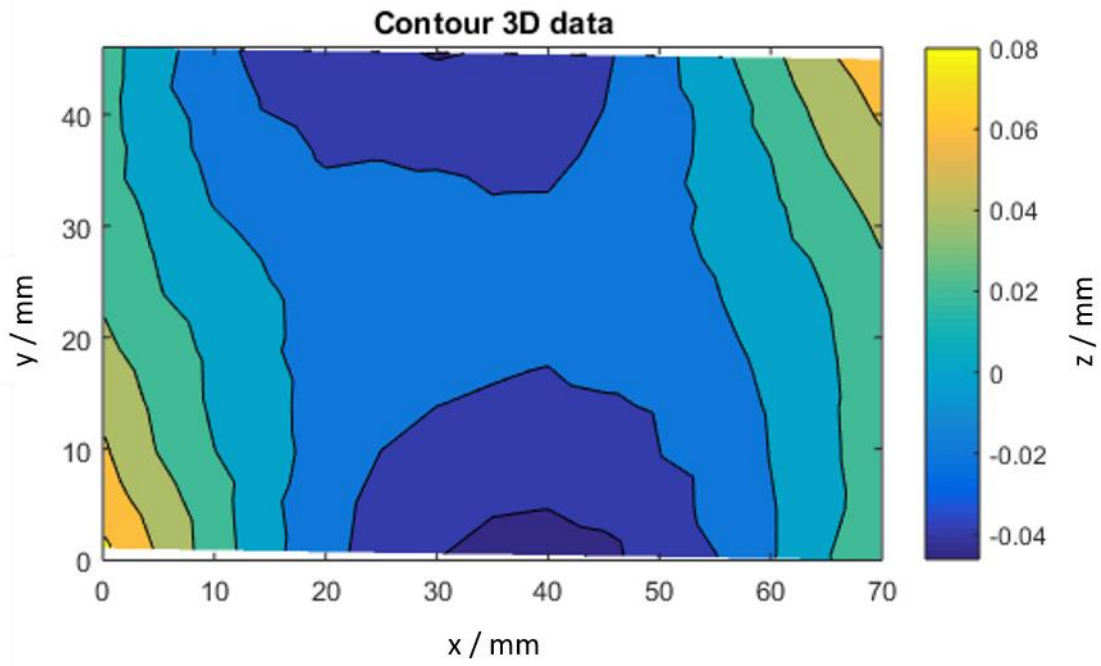


Figure 42 Contour distortion 3D representation using a 5 x 5 mm coordinate spacing scheme

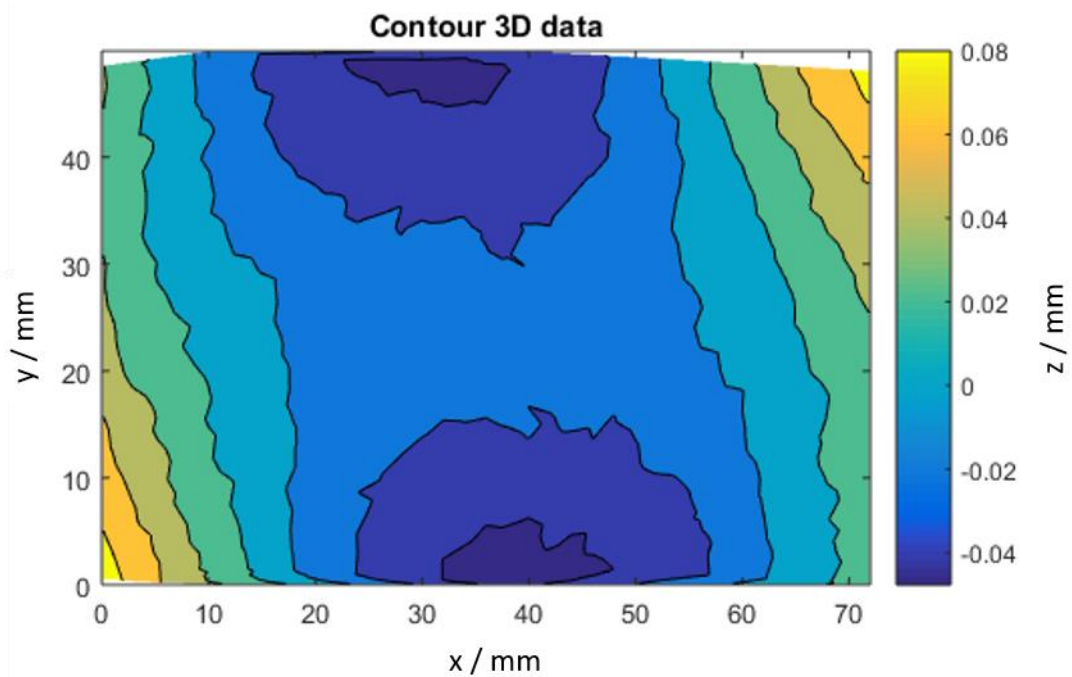


Figure 43 Contour distortion 3D representation using a 2 x 2 mm coordinate spacing scheme

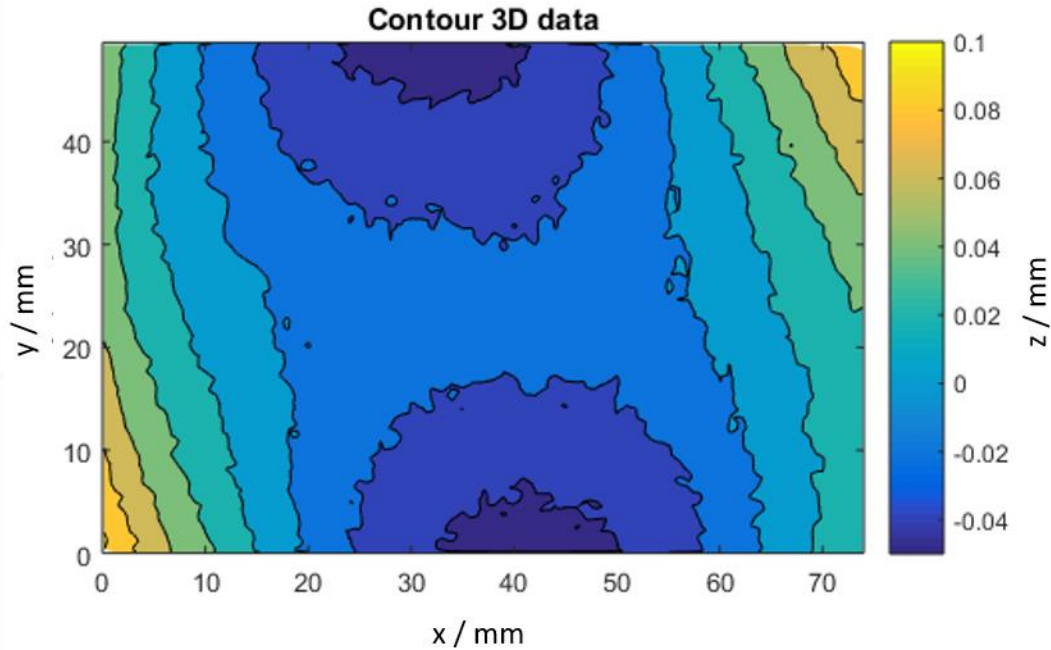


Figure 44 Contour distortion 3D representation using a 1 x 1 mm coordinate spacing scheme

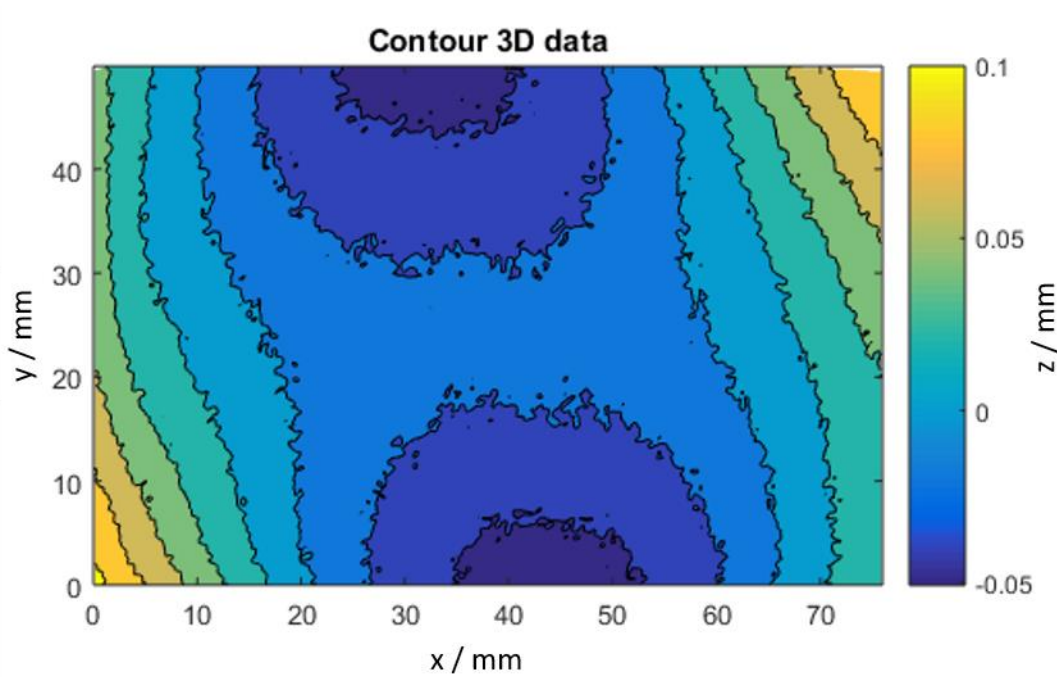


Figure 45 Contour distortion 3D representation using a 0.5 x 0.5 mm coordinate spacing scheme

The spacing is described from coarse to fine for the given x and y increment and spacing schemes, (i.e. coarse from 5 x 5 mm, to fine 0.5 x 0.5 mm spacing, in the x and y directions). The 1 x 1 mm

spacing in both x and y directions provided enough data points and was used for further data analysis.

A list of recommendations for measuring distortion are detailed below.

- Use a tactile CMM
- Use a 1 mm by 1 mm spacing (for parts larger than 100 mm to obtain enough data points)
- Use a large trigger probe ball diameter (to avoid surface roughness interaction)

CMM measurement parameters were determined from the manufacturer's recommendations, sample orientation, and trigger probe size availability at UC Davis. The tactile probe used measures 4 mm in diameter and was selected based on manufacturers recommendations to keep the ruby ball stylus ball as large as possible. Keeping the stylus large had less effect on the surface finish of the part and more flexibility. The scanning parameters used for measuring distortion on the Mitutoyo CMM, or a tactile CMM, are presented in Table 5 below.

Table 5 Mitutoyo BRT Bright 504 distortion measurement parameters

CMM Scanning Parameter	Description	Recommended Parameters
x-spacing	Increment spacing between points in the x direction	1 mm
y-spacing	Pitch spacing between points in the y direction	1 mm
Lace feature	Repeat scan direction uniform or positive/negative direction	off
Scan method	Peck or Drag	Peck
Scan Transversal	x, y or z-axis	y-axis
Pecking axis	x, y, or z-axis	z-axis
Pecking direction	Positive or negative axis (x,y,z) direction	Negative z-axis
No. of T-patches	Length of the part / pitch	25
Retreat axis	x, y or z-axis	z-axis
Probe diameter	Size of the scanning probe ball diameter	4 mm
Probe Compensation	Coordinate datum is compensated using the radius of the scanning probe	On

4.1.3 Leveling Distortion Data

After the data is collected on the reference surface of each sample using each of the three CMMs, the data is then imported into Matlab for further distortion analysis. The raw data from the CMMs are leveled to remove any induced angle from the CMM scanning method. Midlines in both x and y directions are plotted with a z-deviation contour plot. The leveled data is also imported into a least-squares surface fitting function using python. The least-squares surface fit uses Bernstein basis functions to create a uniform grid of distortion data. This new distortion surface is then characterized using Gaussian curvature and is explained in the following chapter.

Coordinate data from the CMMs are imported into Matlab software to be fit, leveled and plotted. A planar fit as seen in Equations (1 – 3), is used to level the raw data to the xy plane. The fit residual (distortion data minus the fitted data) provides leveled data for the following plotting steps. An illustration of the coordinate data leveling analysis and algorithm are shown in Figure 46 and Figure 47 below.

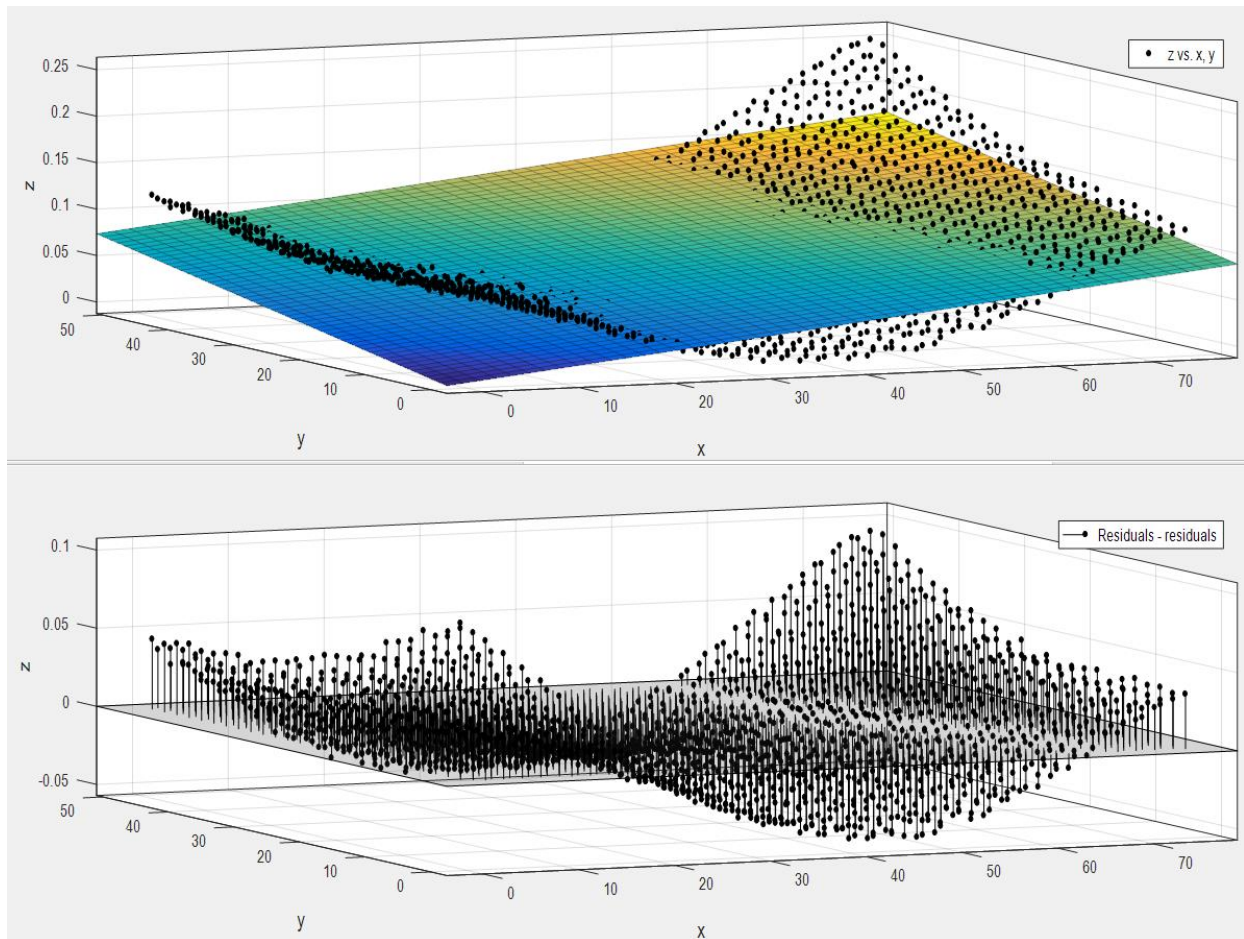


Figure 46 Illustration of the coordinate distortion data leveling analysis with raw data fitted to a plane (top), and the distortion data minus the fitted data (bottom)

A linear plane is fitted to the raw CMM distortion data. The linear fit is then subtracted from the raw data to show the fit residual, or the leveled distortion data. After the data has been leveled, it is reduced to a uniform 500 x 500 2D grid using *meshgrid* and *griddata* in Matlab. The distortion is displayed as a contour plot. After leveling the data in Matlab, a least-squares method is used to remove any noise in the original coordinate data. The idea is to construct a Bezier surface with a grid of control points. The least-squares problem reduces to a linear system that is relatively easy to solve. The height distributions will give an idea about the local distortion shape (convex, saddle, etc.). The algorithmic steps for the optimized routine for characterizing machining distortion is presented below.

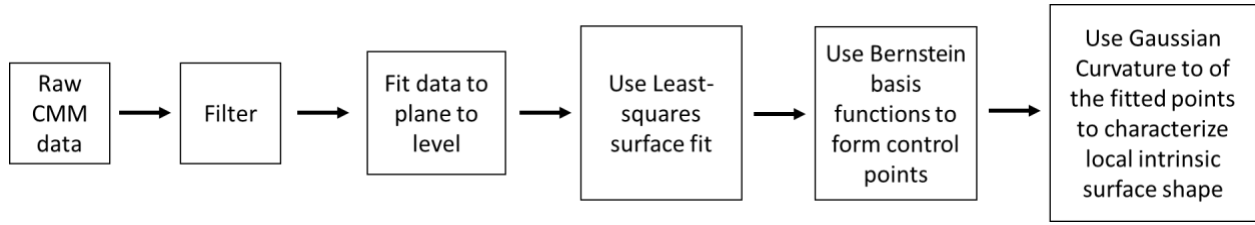


Figure 47 Algorithmic steps in the optimized routine of machining distortion characterization

4.1.3.1 Least-Squares Surface Fit Using the Bernstein Basis Functions

The linear least-squares approximation fitting is a simple form of linear regression. Using the least-squares method, we are able to remove any noise in the original leveled coordinate data. The least-squares method is used to create a best fit for the coordinate data from the CMM. Using the least squares fit is simple and easy to solve. Using the Bernstein basis functions, we are able to solve the least-squares problem to a linear system and create a new surface. This improved distortion characterization method will provide more valuable information than just two-dimensional z-deviation distortion.

The Bernstein basis for polynomials of degree n over the interval $[0, 1]$ is defined as:

$$b_k^n(t) = \binom{n}{k}(1-t)^{n-k}t^k, k = 0, \dots, n \quad (4)$$

This basis is one of the most fundamental algorithms associated with parametric curves and surfaces. Bernstein form properties allow it to be a well-suited candidate for the least-squares surface fit. Properties of the Bernstein polynomial and its coefficients include [Farouki et al., 2008]:

- Unimodality: where $b_k^n(t)$ has a single maximum on $t \in [0,1]$
- Non-negativity: where $b_k^n(t) \geq 0$ on $t \in [0,1]$ for $k = 0, \dots, n$
- Partition of unity: where

$$\sum_{k=0}^n b_k^n(t) \equiv 1 \quad (5)$$

- Lower and upper bounds: $\min_{0 \leq k \leq n} c_k \leq p(t) \leq \max_{0 \leq k \leq n} c_k$ for $t \in [0,1]$
- Variation – diminishing: where the number N of real roots of $p(t)$ on the open interval $t \in [0,1]$ is less than the number $V(c_0, \dots, c_n)$ of sign variations in its Bernstein coefficients by an even amount $N = V(c_0, \dots, c_n) - 2K$
- Derivatives and integrals: where the derivatives and integrals and of $p(t)$ can be expressed as polynomials in Bernstein form of degree $n - 1$ and $n + 1$, respectively, with coefficients that are linear combinations of Bernstein coefficients c_0, \dots, c_n

The steps for the least-squares surface fit for the leveled coordinate, or CMM data, are presented in the following.

We are given measured heights z_i from the coordinate measurement machine at sample points (x_i, y_i) for $1 \leq i \leq N$ on the domain $(x, y) \in [x_{min}, x_{max}] \times [y_{min}, y_{max}]$. The Bernstein basis functions of degree d in x and y on $[x_{min}, x_{max}]$ and $[y_{min}, y_{max}]$ are defined by:

$$b_k^d = \binom{d}{k} \frac{(x_{max}-x)^{d-k}(x-x_{min})^k}{(\Delta x)^d}, k = 0, \dots, d \quad (6)$$

$$b_l^d = \binom{d}{l} \frac{(y_{max}-y)^{d-l}(y-y_{min})^l}{(\Delta y)^d}, l = 0, \dots, d \quad (7)$$

where $\Delta x = x_{max} - x_{min}$, $\Delta y = y_{max} - y_{min}$. We wish to fit a tensor-product surface of degree (d, d) in (x, y) of the form:

$$z = f(x, y) = \sum_{k=0}^d \sum_{l=0}^d c_{kl} b_k^d(x) b_l^d(y) \quad (8)$$

to the given data. The squared error between the fitted surface and the given data is defined as:

$$E = \sum_{i=0}^N [f(x_i, y_i) - z_i]^2 \quad (9)$$

Substituting from Equation (6) and (7) gives:

$$E = \sum_{i=0}^N \left[\sum_{k=0}^d \sum_{l=0}^d c_{kl} b_k^d(x_i) b_l^d(y_i) - z_i \right]^2 \quad (10)$$

The least-squares fit is obtained by minimizing the error E with respect to the coefficients c_{kl} of $f(x, y)$. Setting the derivative of E with respect to the coefficient c_{rs} equal to zero yields the equation:

$$\frac{\partial E}{\partial c_{rs}} = \sum_{i=0}^N 2 \left[\sum_{k=0}^d \sum_{l=0}^d c_{kl} b_k^d(x_i) b_l^d(y_i) - z_i \right] b_r^d(x_i) b_s^d(y_i) = 0 \quad (11)$$

or equivalently,

$$\sum_{k=0}^d \sum_{l=0}^d \left[\sum_{i=0}^N b_k^d(x_i) b_l^d(y_i) b_r^d(x_i) b_s^d(y_i) \right] c_{kl} = \sum_{i=0}^N b_r^d(x_i) b_s^d(y_i) z_i \quad (12)$$

For each pair (r, s) with $0 \leq r, s \leq d$ this defines a system of $(d + 1)^2$ linear equations for the unknown coefficients c_{kl} of the surface (Equation 8).

The linear equations can be solved by standard methods (i.e. Gaussian elimination, etc.). To do this, it is preferable to express the equations in standard matrix form. This is accomplished by assigning:

$$\mu = r(d + 1) + s + 1 \quad (13)$$

$$\nu = k(d + 1) + l + 1 \quad (14)$$

for $0 \leq r, s \leq d$ and $0 \leq k, l \leq d$, so the linear equations can be written as:

$$\sum_{\nu=1}^{(d+1)^2} M_{\mu\nu} \tilde{c}_\nu = r_\mu, \quad \mu = 1, \dots, (d + 1)^2 \quad (15)$$

where the matrix elements, unknowns, and right-hand side values are determined to be:

$$M_{\mu\nu} = \sum_{i=0}^N b_r^d(x_i) b_s^d(y_i) b_k^d(x_i) b_l^d(y_i), \quad 1 \leq \mu, \nu \leq (d + 1)^2 \quad (16)$$

$$\tilde{c}_\nu = c_{kl}, \quad 1 \leq \nu \leq (d + 1)^2 \quad (17)$$

$$r_\mu = \sum_{i=0}^N b_r^d(x_i) b_s^d(y_i) z_i, \quad 1 \leq \mu \leq (d + 1)^2 \quad (18)$$

Once the solution vector \tilde{c}_ν for $\nu = 1, \dots, (d + 1)^2$ has been computed, it can be rearranged as a two-dimensional array c_{kl} with $0 \leq k, l \leq d$ that defines the surface from Equation 8 as:

$$c_{kl} = \tilde{c}_\nu, \text{ where } k = [(\nu - 1)/(d + 1)], \text{ and } l = \nu - k(d + 1) - 1 \quad (19)$$

4.1.3.2 Surface Curvature Analysis

Further analysis of the surface yields characterization of the shape complexities of that surface. This improved distortion characterization tool enhances the distortion characterization by providing more value than just z-deviation distortion. Providing Gaussian curvature allows the distortion to be viewed as a three-dimensional surface characterization. The Gaussian curvature will allow further characterization information to be deduced including distortion symmetries, distortion areal features, etc.

The coefficients of the first fundamental form of a parametric surface, $\mathbf{r}(u, v)$ are defined in terms of the first partial derivative as:

$$E = \mathbf{r}_u \cdot \mathbf{r}_u, \quad F = \mathbf{r}_u \cdot \mathbf{r}_v, \quad G = \mathbf{r}_v \cdot \mathbf{r}_v \quad (20)$$

The second fundamental form has the coefficients given in terms of the surface normal vector, \mathbf{n} , where:

$$\mathbf{n} = \frac{\mathbf{r}_u \times \mathbf{r}_v}{|\mathbf{r}_u \times \mathbf{r}_v|} \quad (21)$$

and the surface second partial derivative is given by:

$$L = \mathbf{n} \cdot \mathbf{r}_{uu}, \quad M = \mathbf{n} \cdot \mathbf{r}_{uv}, \quad N = \mathbf{n} \cdot \mathbf{r}_{vv} \quad (22)$$

The Gaussian curvature is defined in terms of the first and second fundamental form coefficients as:

$$K = \frac{LN - M^2}{EG - F^2} \quad (23)$$

and is a descriptor of the local intrinsic surface shape – where a neighborhood of a point is either bowl shaped, or saddle shaped according to the value of K . If $K > 0$ the shape is bowl-shaped. If $K < 0$ the shape is saddle like. A smooth surface will generally have disjoint regions of positive and negative Gaussian curvatures, separated by parabolic lines, along which $K = 0$.

For the case of a functional surface specified as $z = f(x, y)$ we may take $u = x, v = y$ and the parametrization has the form $\mathbf{r}(x, y) = (x, y, f(x, y))$ with the following properties:

$$\mathbf{r}_x = (1, 0, f_x) \quad (24)$$

$$\mathbf{r}_y = (0, 1, f_y) \quad (25)$$

$$\mathbf{r}_{xx} = (0, 0, f_{xx}) \quad (26)$$

$$\mathbf{r}_{xy} = (0, 0, f_{xy}) \quad (27)$$

$$\mathbf{r}_{yy} = (0, 0, f_{yy}) \quad (28)$$

$$\mathbf{n} = \frac{(-f_x, -f_y, 1)}{\sqrt{f_x^2 + f_y^2 + 1}} \quad (29)$$

$$(E, F, G) = (f_x^2 + 1, f_x f_y, f_y^2 + 1) \quad (30)$$

$$(L, M, N) = \frac{(f_{xx} f_{xy}, f_{xy} f_{yy})}{\sqrt{f_x^2 + f_y^2 + 1}} \quad (31)$$

$$K = \frac{f_{xx} f_{yy} - f_{xy}^2}{(f_x^2 + f_y^2 + 1)^2} \quad (32)$$

Using these properties, positive and negative Gaussian curvature of the fitted surface from Equation 8 are executed and presented in the following.

4.2 Results and Discussion

After successfully implementing the optimized routine for characterizing machining distortion via Gaussian surface curvature the results are displayed below. The leveled data shown in Figure 48 depicts more information in the left contour plot, than in the two midline plots on the right alone. The distortion seen in the 60-degree sample is symmetric and complex – both of which are not able to be extracted from the line plots. As already discussed in chapter 3, having three-dimensional data presented to quantify and visualize the overall experienced distortion results in more information for the user to extract and expand for further analysis.

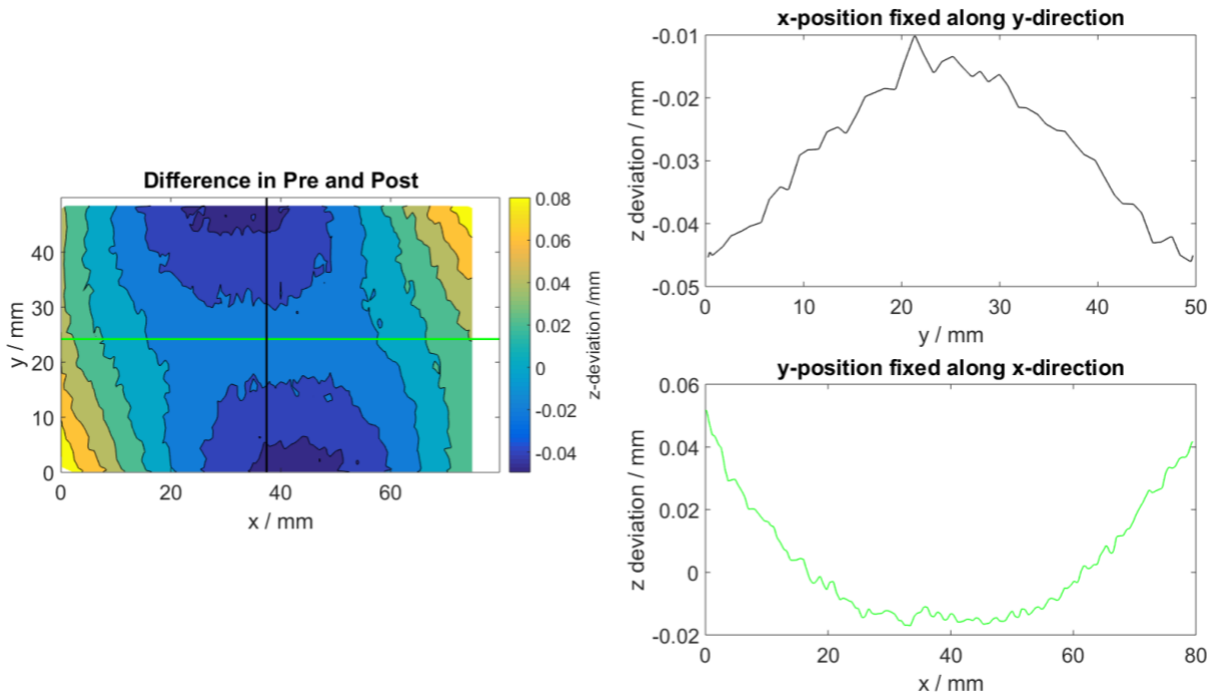


Figure 48 The leveled distortion data for the 60-degree sample with midline plots for both horizontal and vertical directions

The leveled data is further used to execute a least squares surface fit. From the leveled data of $N = 3825$ data points, Gaussian curvature of the fitted surface from Equation 6 is used. After the surface fit is implemented, Gaussian curvature is analyzed for the given distorted sample. The Gaussian

curvature for the 60-degree sample with fitted surface of degree $d = 4, 6,$ and 8 are shown in Figure 49.

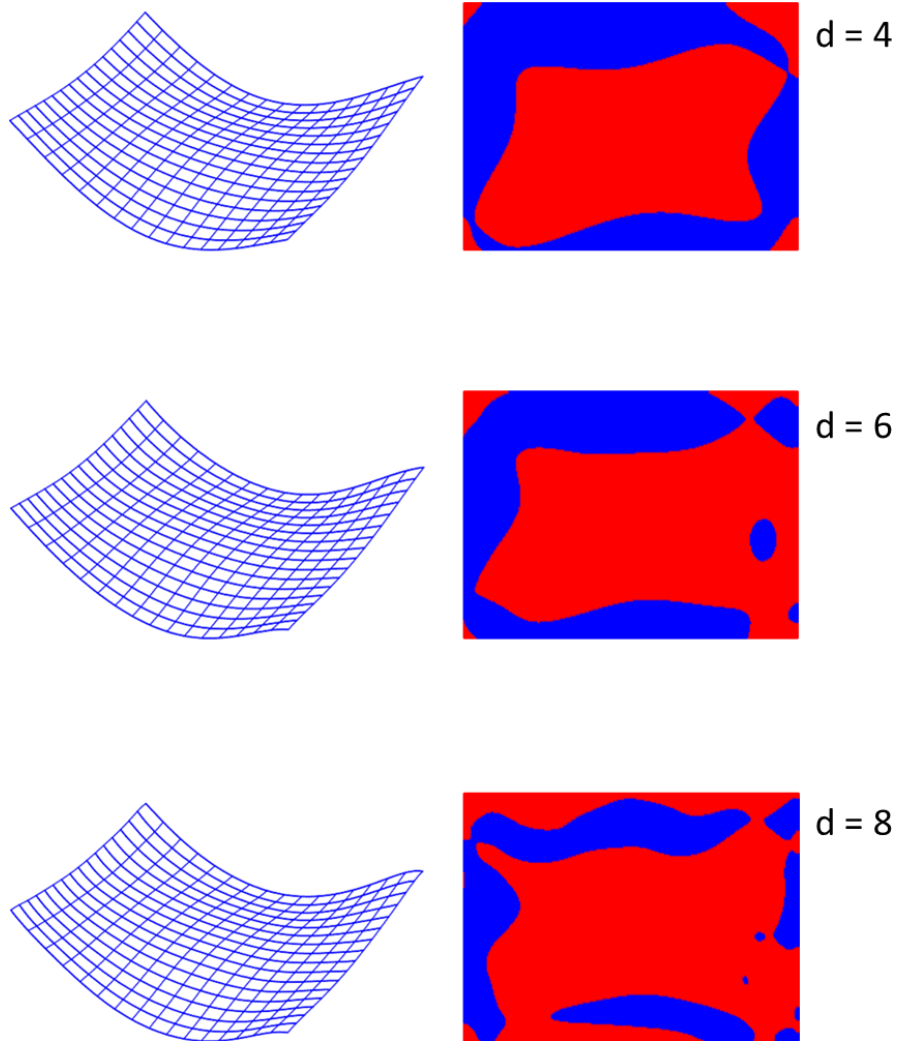


Figure 49 Left: the height variations of the least-squares surface fit (magnified 120x about the mean height) for the surface of degrees, $d = 4$ (top), $d = 6$ (center), and $d = 8$ (bottom). Right: corresponding surface regions that have negative (red) and positive (blue) Gaussian curvature.

An alternative view for the Gaussian Curvature is also shown for the same 60-degree sample but visualized to show regions of low Gaussian curvature magnitudes less than $0.1 z_{rms}^2$, where z_{rms} is the root-mean-square deviation of the z heights as color coded in green in Figure 50. The color coding shows regions in which the Gaussian curvature magnitude, K is greater than z_{rms}^2 , the root mean

square squared deviations of the z heights (red), K values in between ranges of positive and negative z_{rms}^2 , root mean square squared deviation of the z heights (green), and Gaussian magnitudes K less than the negative root mean square squared deviations of the z heights, z_{rms}^2 (blue). This plot is interesting because it shows areas where there is almost no curvature and these sections can be used as critical locations for initial distortion forming.

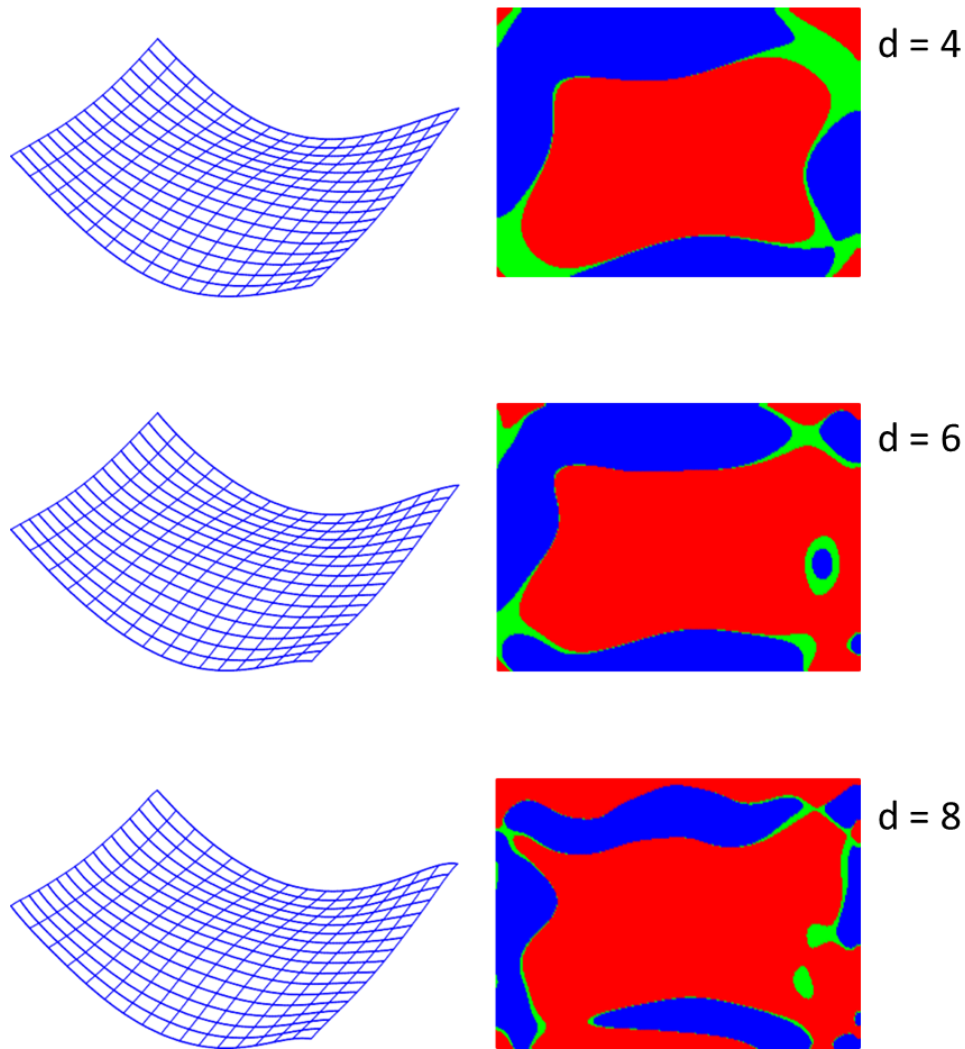


Figure 50 Left: the height variations of the least-squares surface fit (magnified 120x about the mean height) for the surface of degrees, $d = 4$ (top), $d = 6$ (center), and $d = 8$ (bottom). Right: corresponding surface regions that have $K > 0.1 z_{rms}^2$ (red), $-0.1 z_{rms}^2 \leq K \leq 0.1 z_{rms}^2$ (green), and $K < -0.1 z_{rms}^2$ (blue)

The optimized routine for characterizing machining distortion can be seen as a process to investigate the complexities of the unique distorted surface. The overall characterization process as seen in Figure 51, shows the multiple ways with which distortion can be represented. Using multiple representations of distortion in the overall characterization, presents more information about the distortion than just a single line plot or a single 3D image.

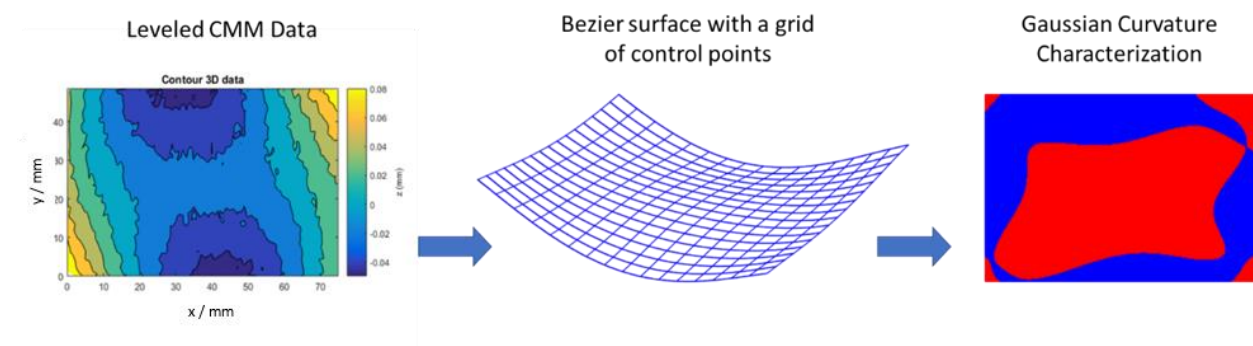


Figure 51 Depiction of the characterization process from leveled data to Gaussian curvature distribution

The lower the degree, d , of the surface in both x and y directions shows to be better for an overall relative shape representation for the surface. As d increases, more features related to surface topography (i.e. surface roughness) are emphasized. The degree of the surface, d , is a smoothing effect variable, such that as $(d + 1)^2$ approaches N (the number of data points) it begins to interpolate every data point creating a Gaussian curvature representation that is noisy with too much information about the surface topography.

4.3 Conclusion

In conclusion, this chapter explains an updated routine for characterizing machining distortion for overall research transferability. Using Gaussian curvature in addition to three-dimensional distortion representation, more information about the overall surface is able to be extracted and used for further

distortion analysis. Distortion data presented as either as a line or curve only exhibits a fraction of the overall experienced distortion on that sample. Two-dimensional data gives a sparse indication of the shape and does not adequately represent the complexity of the distorted shape.

Through this research, it is understood that distortion is a complex shape with regions of the surface between positive and negative Gaussian curvature. A new transparent way to characterize distortion via Gaussian curvature proves to be a simple method to transfer distortion results.

Using the Bernstein basis function as a means for the least-squares surface fit for Gaussian curvature extraction of distorted machined samples, expresses a novel method to characterize machining distortion for the overall complex shape deviation. Expressing machining distortion as a curvature representation can provide general surface features that are easily transferable and repeatable for researchers across technical capabilities and environments. Extracting information from the curvature including symmetries, quantified positive and negative distributions, curvature location with respect to machined geometry, etc., can be useful for further distortion characterization and minimization.

More work is needed using Gaussian curvature characterization to expand the distortion results to show surface curvature symmetries, curvature percentages of both positive and negative curvatures, and distinct characterization Gaussian shapes for different distorted parts. Further work is also necessary in distortion compensation and distortion control. Using the final distorted curvatures can allow for the prediction and manipulation of future machining distortion minimization. Future work is also needed to investigate different milling geometries and dimensions (i.e. complex geometries and pockets).

CHAPTER 5 CASE STUDY: MOLECULAR DYNAMICS SIMULATIONS OF SINGLE GRAIN PURE ALUMINUM IN A VICE FIXTURE FOR NANOMANUFACTURING APPLICATIONS

Current research states that mechanical cutting processes are very important in bridging the gap of macro and nano domains for manufacturing functional components [Chae et al., 2006]. As the advancements of nano-machining stride forward, understanding the machining distortions and deformations related to the nanoscale becomes a vital part of mastering this field. In order to investigate machining distortions, understanding fixture design is a critical aspect. It can be hypothesized that fixturing has a growing influence when the part dimensions get smaller.

This study will investigate distortion at the nanoscale using molecular dynamics simulations to bridge the gap between nano and macro machining.

5.1 Background

5.1.1 Nanomachining

Manufacturing processes at the micro and nanoscales are increasingly in high demand for multiple industries such as electronics, bio-medical engineering, aerospace, etc. The motivation to create smaller devices stems from the need to manufacture workpieces with better performance, less materials, higher efficiencies and being less expensive [Dornfeld et al., 2006]. Nanofabrication techniques include photolithography, chemical etching, laser machining, atomic force lithography, and focused ion beam lithography [Cui et al., 2017].

Manufacturing at the nanoscale includes work areas related to the atomic and material sciences. Such applications in manufacturing have an accuracy of high precision and ultra-precision [Chae et al., 2006]. As the manufacturing scale decreases, challenges arise in accuracy, surface quality, and integrity

of the machined part. Such challenges can emerge from tool edge geometry, grain size, and grain orientation [Dornfeld et al., 2006], even though these factors have little or no effect on the macro-scale. Critical issues associated with understanding the differences between macro and micro/nano machining include the miniaturization of components, tools, and manufacturing processes [Chae et al., 2006].

Advancements in the nano-manufacturing research include nano-mechanical machining to make complex shapes by plowing techniques of semiconductor structures [Kunze et al., 2002]. Molecular dynamics simulations of nanometric cutting mechanisms of amorphous alloys were investigated to study the effects of nano machining [Zhu et al., 2014]. Atomic scale deformations in silicon monocrystals were studied using molecular dynamics under two and three body contact sliding [Zhang et al., 1998]. Molecular dynamic simulations on monocrystalline copper revealed groove forming characteristics and mechanisms in nano-milling [Cui et al., 2017].

5.1.2 Machining Fixtures

To initially understand the relation of machining distortions to both macro and nano-manufacturing, the fixture or work-holding device is an important feature to investigate. In both macro and nano fabrication, the fixture is the primary means of securing the workpiece in place while performing the manufacturing operations.

The primary tasks of the fixture during machining is to: define the position and orientation of the workpiece in the machine tool, maintain defined workpiece location throughout machining forces, and to guide the machining forces of the machine structure [Fleischer et al., 2007], [Hesse et al., 2012], [Mohring et al., 2016]. During machining, the workpiece experiences minor deformations due to the clamping forces. Fixture layout and clamping forces are two main aspects that influence machining deformation [Chen et al., 2007]. Contact forces between workpiece and fixture influence the

workpiece during machining [Asante et al., 2008]. The forces acting in the contact region during clamping are important for understanding workpiece deformation [Asante et al., 2008].

Fixtures can include step clamps, quick release clamps, plain style precision clamps, vice jaw systems, table plate, CNC fixture, etc. [Krar et al., 2011]. Fixtures are an essential element of the machining system related to both the process and machine tool [Mohring et al., 2016]. Machining distortions directly relate to the fixture as the fixture releases the workpiece and the deformations occur during part re-equilibrations [Chantzis et al., 2013].

Advancements in understanding fixture design include computer aided fixture design (CAFD) with respect to information support such as geometry, location, material properties, machining information, applied forces, tolerance requirements, and displacements [Pehlivan et al., 2008]. Intelligent fixtures for deformation compensation of high-performance machining parts have been studied to reduce machining distortions [Mohring et al., 2016]. The optimal clamping forces for multiple clamp fixtures subjected to quasi-static machining forces were determined by Li [Li et al., 2001]. FEM was used to control machining deformation through fixture layout design and clamping force optimization [Chen et al., 2007].

Current approaches for supporting fixture design via CAFD suggest more research in cohesive fixture design support and supporting the detailed design of a fixture's physical structure [Boyle et al., 2011]. Flexible fixture design and automation have been investigated to determine current issues and future directions [Bi et al., 2001].

FEM combined with contact elasticity models shows that it is possible to calculate contact load and pressure for a frictional workpiece fixture system to further investigate workpiece deformation [Asante et al., 2008]. Intelligent fixture optimization has been investigated to determine the optimal positions of locating and clamping elements during machining [Tadic et al., 2014], [Papastathis et al., 2012].

Machining fixtures are an essential tool of machining systems to accurately remove material [Mohring et al., 2016].

This study aims to use molecular dynamics (MD) as a means to study fixtures directly related to machining distortions for nano applications of single grain pure aluminum in a vice fixture for nano-manufacturing applications.

5.2 Methods

In order to study the effects of a vice fixture with respect to nano-manufacturing of pure Aluminum, a molecular dynamics simulation is conducted with different workpiece shapes mounted in the fixture including: a bar, a U-shape prism and a L-shape prism, using the LAMMPS Molecular Dynamics Simulator [Plimpton, 1995]. Aluminum was used to represent the aerospace aluminum materials used in the distortion research aerospace areas. The molecular dynamics simulation volume is set up as a box with a size of 80.99 nm x 40.50 nm and 60.74 nm in xyz coordinate axes. The model contains approximately 12,040,000 atoms. The workpiece consists of a single crystal of Al; this material crystallizes in the face-centered-cubic (FCC) structure with a lattice spacing of 4.032 Å. The crystal $\langle 100 \rangle$ axes are aligned with the edges of the workpiece, such that all workpiece surfaces have $\{100\}$ orientation. The interactions between the Al atoms in this system are described by a potential of the embedded-atom-model (EAM) class originally developed by Daw and Baskes [Daw and Baskes, 1983]; the actual potential used here for Al [Mendeleev et al., 2008] has been optimized to describe, among others, elastic properties and defect energetics correctly. The vice is assumed to be of diamond, because of its high hardness, or resistance to indent; it is considered rigid in this study. The Al-diamond interaction is modeled by a purely repulsive potential; this potential is obtained from a Lennard–Jones potential by prescribing a cut-off distance equal to 4.2 Å at its minimum and then shifting it such that the energy and force are continuous at the cut-off radius [Alhafez et al., 2017].

Before starting the MD simulation, the system is relaxed, such that all components of the stress tensor reach values less than 3 MPa, and the temperature is stabilized at 300K (± 1 K). Each of the two vices is composed of 239,410 carbon atoms arranged in a rigid diamond lattice structure. The vice structures are represented as plate shapes with a thickness of 1.4 nm and a height of 34 nm. The molecular-dynamics simulations are performed in an isothermal-isobaric (NPT) ensemble during relaxation and in the microcanonical (NVE) ensemble during fixture. As thermostat we employ a velocity-scaling algorithm.

As shown in Figure 52, these two vices clamp the bottom half of aluminum bar while the speed of each vice closing is 10 m/s. This velocity, while being too large for fixture applications, has been selected for computational convenience reducing time and modeling computing; such a value is standard in molecular dynamics studies of machining applications [Ruestes et al., 2017]. The Al bar is fixed when each vice moves into it by 2 nm. The vice fixture is modeled to have an infinitely long depth in y direction by using periodic boundary conditions.

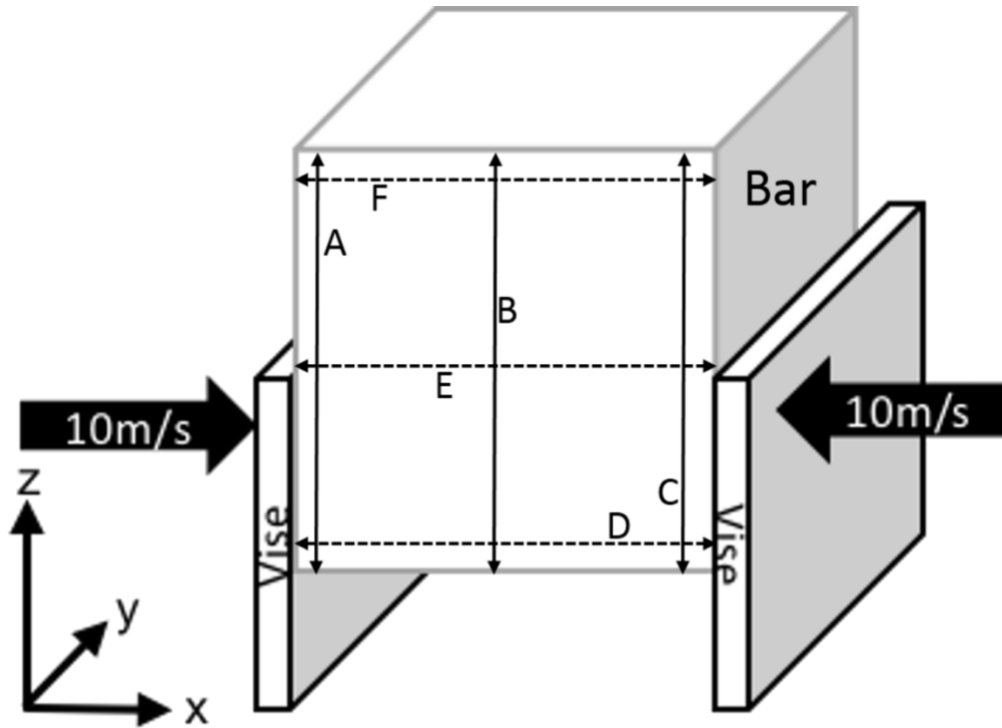


Figure 52 The two vices clamp the bottom half of the aluminum bar. Heights (A, B, C) and lengths (D, E, F) are shown for result references [García et al., 2018]

The simulation setup is created such that the vice plates hold onto the bottom half of the workpiece, with a closing velocity of 10m/s. The height (solid lines A, B and C) and the length (dashed lines D, E and F) of the workpiece are evaluated as a measure of the distortion. For the U-shape, the referenced height, B is half of the original height. For the L-shape, the reference height, C, and length, F, are half of the original height and length, respectively.

The aluminum bar is held in position of the two vice plates for 2×10^{-10} seconds. The processing steps for the MD simulation after the bar is held in the vice fixture are as follows and shown in Figure 53.

- A. The vice plates are moved away at 10 m/s from the Al workpiece.
- B. One fourth (top right section) of Al bar atoms are deleted to construct an L-shape. The fixed vice plates hold the leftover atoms (L-shape) for 2×10^{-10} s and then release at 10 m/s.
- C. The center of the top half atoms with a width of 10 nm are deleted to construct a U-shape. The U-shape formed is subjected to the same processing as the L-shape in which the vice holds and releases the workpiece.

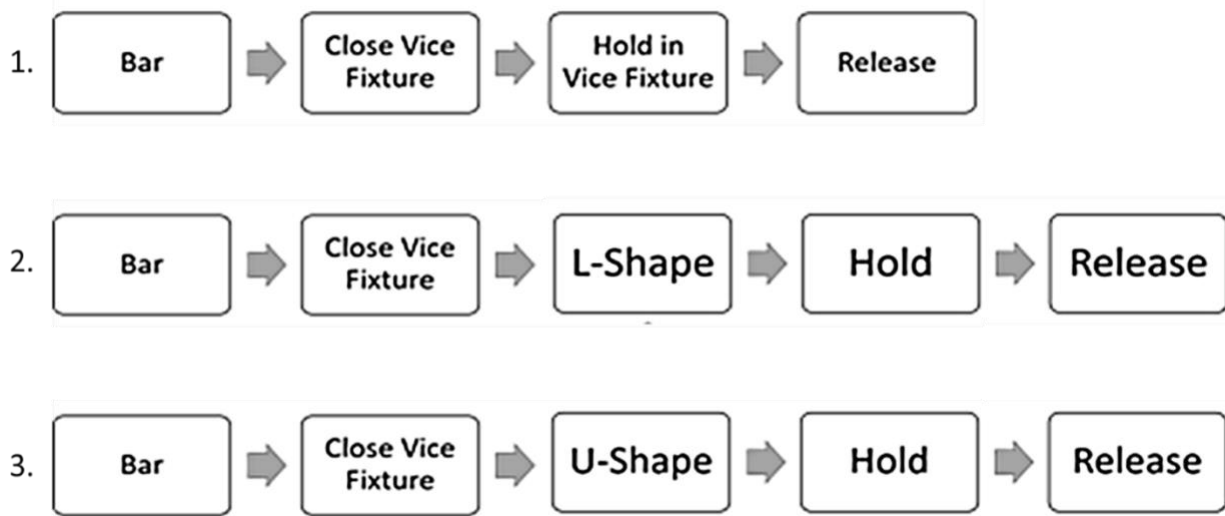


Figure 53 The initial bar undergoes three simple setups in the simulation: 1. Bar, clamp, hold, release. 2. Bar, clamp, hold, L-shape, hold, release. 3. Bar, clamp, hold, U-shape, hold, release.

The simulations were performed by a collaborator from the Technical University of Kaiserslautern and took a computation time of around 4 days on a 128-core machine for relaxation and 8 days for the fixture simulation. In view of this computational cost, we performed only a single simulation for each workpiece geometry in the presented work.

For visualization and rendering of the figures, we used the free software tool OVITO [Stukowski, 2010]. The hydrostatic stress was calculated locally using the LAMMPS software. To this end, the forces acting on the atoms were evaluated to calculate the atomic virial, which – together with the local kinetic energy density – make up the local stress [Frenkel et al., 1996]. In the figures below, stresses are averaged over a region of 4 nm.

5.3 Results and Discussion

After each of the processing steps was completed, the results of the atomic stresses were obtained. The stress distributions in the bar are shown after the vice was closed (Figure 54) and after the vice was held for 2×10^{-10} seconds (Figure 55). After the sample is fixed (Figure 55), a nearly symmetrical distribution of compressive stress builds up in the region compressed by the fixtures. The stress also reaches the upper part of the workpiece in an arch-bridge shape. The stress changes remarkably after holding for 2×10^{-10} seconds (Figure 55). The left-right symmetry is lost; this is due to the formation of plasticity, which occurs in the atomistic simulation in a strongly localized way, for instance at the upper edge of the left fixture. Since the generation of plasticity requires the nucleation of dislocations, and this is a stochastic process subject to local stress and temperature fluctuations, plasticity is not generated homogeneously in the workpiece. Figure 55 exemplifies the plasticity generated by displaying atomistically a stacking fault ribbon of a dislocation formed in Al; similar features can be observed at other spots on the workpiece. The bottom of Figure 55 zooms into the rectangle area of the top figure, where the green line is a $1/6[112]$ dislocation and red atoms are stacking faults.

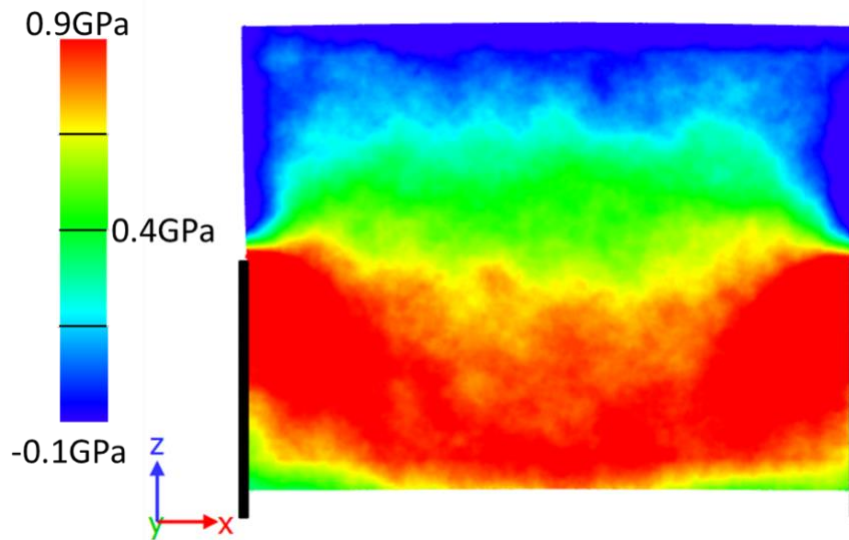


Figure 54 The stress distribution (in the frontal x-z plane) of the bar sample after each vice moved into the bar by 2 nm.

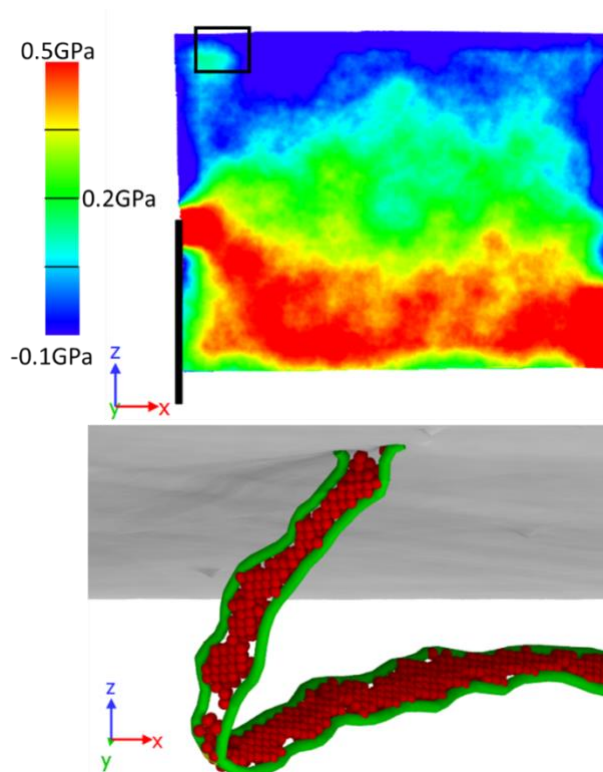


Figure 55 The stress distribution of the bar sample after being held in the vice for 2×10^{-10} second. The bottom image describes the dislocation found in the top left corner box.

Figure 56 shows the stress distribution in the mid-plane of the bar sample, in between the vice fixtures. The stress is very homogeneous in the y direction. The lower half of the section is in compression while the upper half is in tension.

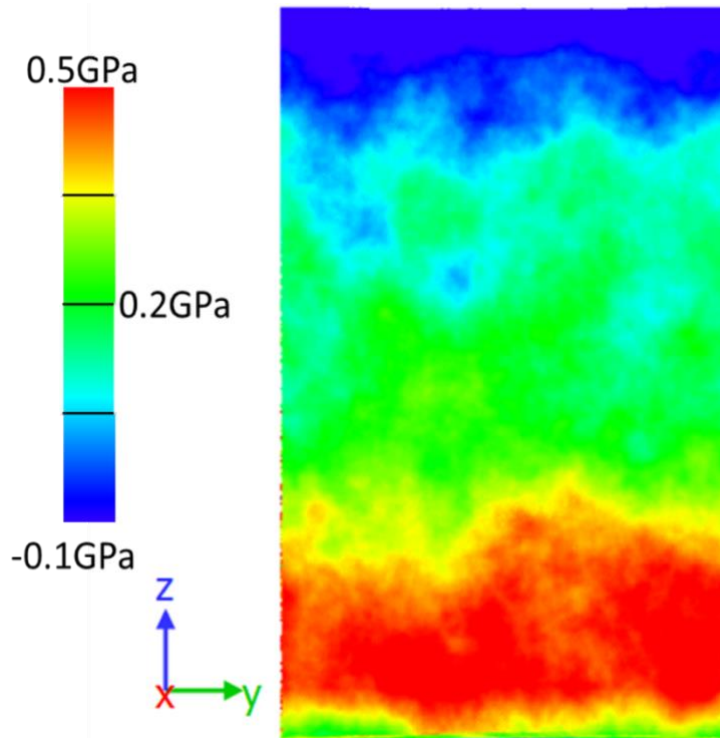


Figure 56 The stress distribution in the mid-plane cross section (y-z plane) after the bar sample was held in the vice for 2×10^{-10} second.

Figure 57 shows the stress distribution in the bar after being released from the fixture. The stress takes considerably smaller values than while being held in the fixtures; it takes values in the range of up to 100 MPa. The stress is dominantly compressive; stress maxima are concentrated on the left-hand side due to the generation of plasticity discussed above. The stress shown here is the residual stress as calculated in our atomistic simulation.

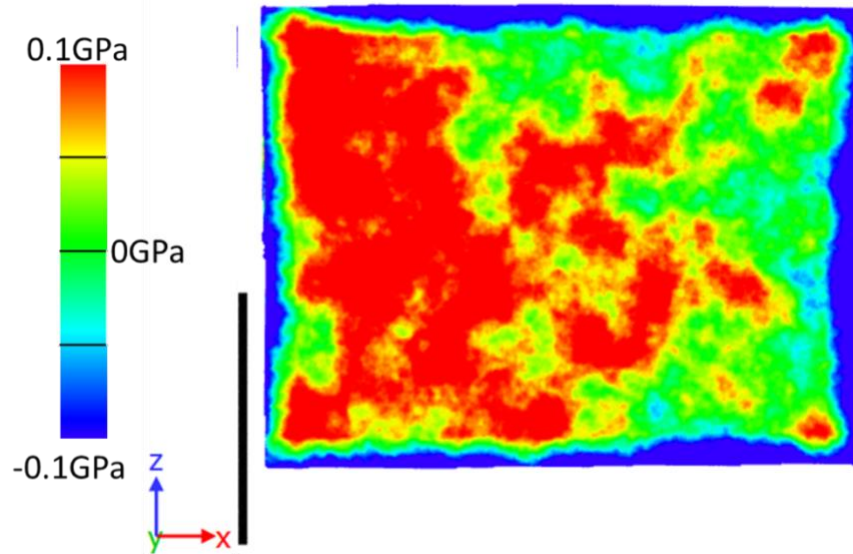


Figure 57 The stress distribution of the bar sample after being released from the vice fixture.

The resulting bar, L-shape, and U-shape distortions are assembled in Figure 58, which provides the data in fractional changes which are useful to relate our results to actual measurements. The workpiece grew in height, while it narrowed in the length dimension. Note that the changes are not uniform. The height increase is concentrated on the left-hand side and the middle part, corresponding to the plasticity generated there. Length changes are most pronounced at the bottom part, where the fixtures were applied.

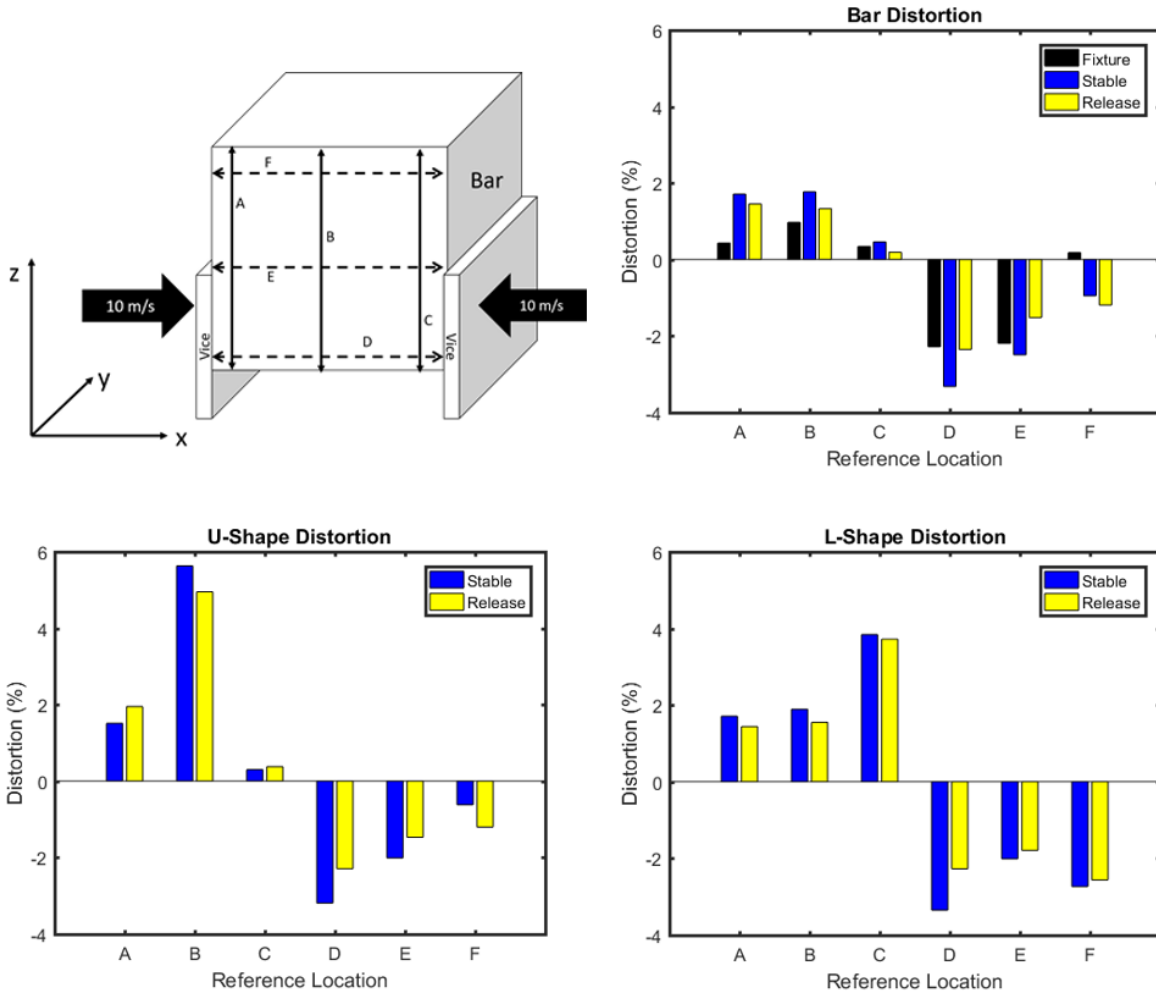


Figure 58 The distortion as percentages (%) for each sample (Bar, U-shape, and L-shape) and their respective locations (A, B, C, D, E, and F) are plotted.

The stress distribution in the U-shaped sample is shown in Figure 59 after holding the sample in the fixtures. Again, the stress is mainly concentrated between the fixtures, in the lower part of the workpiece, and the strong left-right asymmetry is caused by the nucleation of dislocations in the right-hand side, close to the fixtures. The corners of the U-shaped groove are under tensile stress. The height distortion, in particular along the line B (Figure 52), is now considerably larger than for the bar. The reason is that the lower part of the workpiece has more freedom of being pushed up in the U groove than for a solid bar. Length changes are of a similar size, but somewhat smaller than for the bar shape.

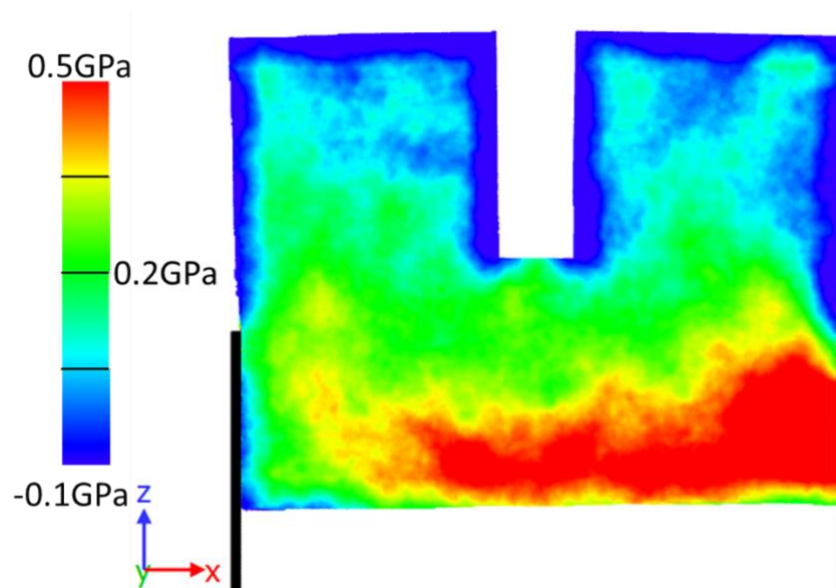


Figure 59 The stress distribution (in the frontal plane) of the U-shaped sample in the fixture after being held in the vice for 2×10^{-10} second.

After release of the fixtures, the stress in the U-shaped sample is very inhomogeneous as seen in Figure 60. In the left-hand side corner of the U groove, tensile stress has been kept and expanded, while compressive stress is generated in the right-hand side part. This example demonstrates the occurrence of strongly inhomogeneous residual stress distributions caused by the local generation of plasticity. The strong distortions that were established during the holding phase survive after removing the fixtures, see Figure 58.

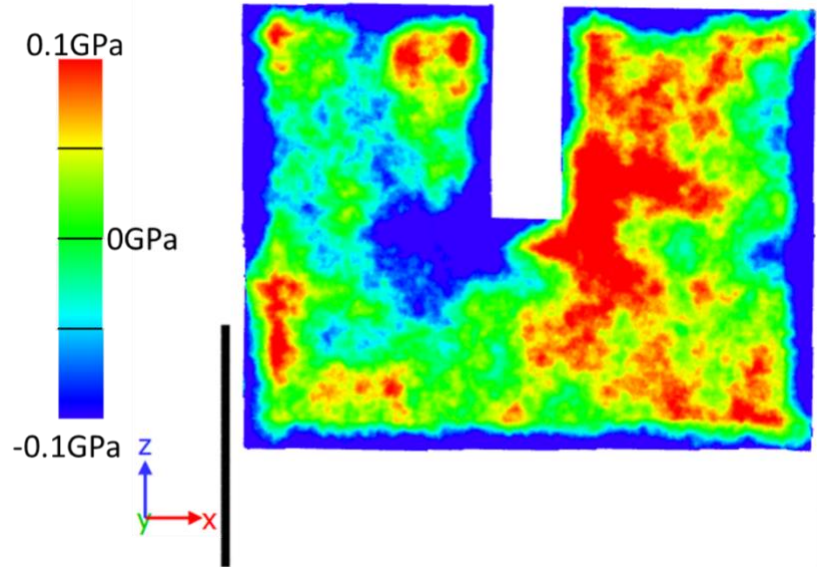


Figure 60 The stress distribution (in the frontal plane) of the U-shape sample after it was released from the vice fixture.

Furthermore, Figure 61 shows the stress distribution in the L-shaped workpiece after holding it in the vice. Compressive stress is concentrated in the right-hand side; the material above the fixtures on the left-hand side helps alleviate the pressure in the left-hand side. Height distortions are now particularly large in the middle of the workpiece, along line B (Figure 52), see Figure 58.

After the L-shape is released from the fixture, the entire sample is under compressive stresses, as seen in Figure 62. Note that the L-shaped sample is rotated during releasing due to the asymmetric shape.

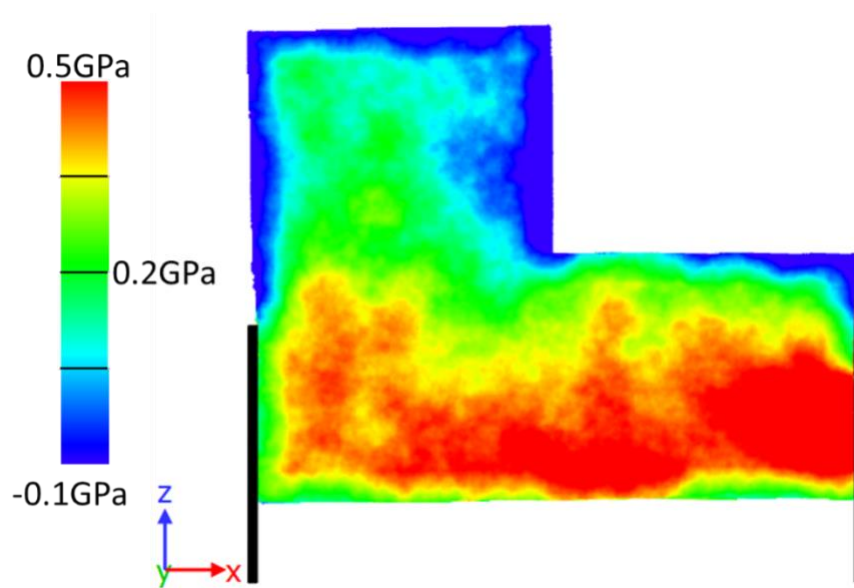


Figure 61 The stress distribution (in the frontal plane) of the L-shaped sample in the fixture after being held in the vice for 2×10^{-10} second.

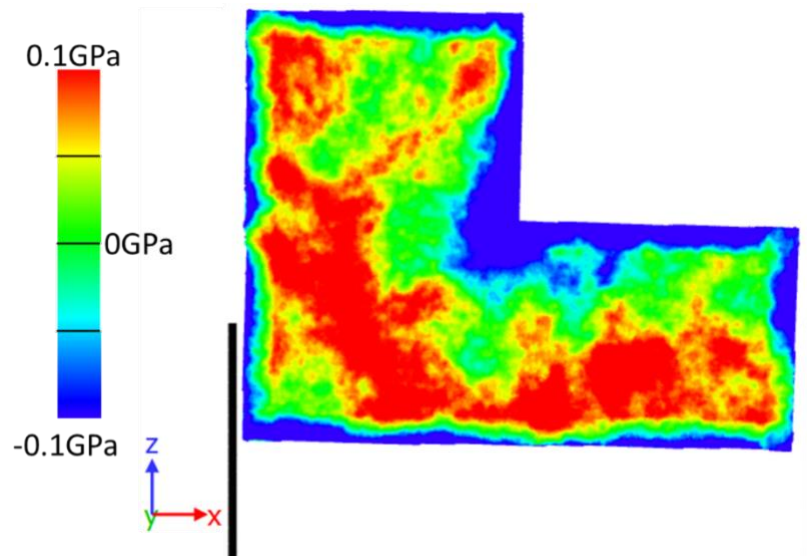


Figure 62 The stress distribution of the L-shape sample after it was released from the vice fixture.

These results provide information about the critical locations in which the workpiece may be affected by the fixture contact. The results show that the vice fixture deformed the single grain pure Al sample

both elastically and plastically to cause overall part distortion shown in the bottom edge of the release figure of each case being deformed from its original position. It has to be noted that we performed only a single simulation for each workpiece. While, due to thermal fluctuations, the exact position of the plastic material failure is subject to statistics, it is not the aim of the present work to calculate averages over these thermal fluctuations, but rather to help understand where these fluctuations occur and how they contribute to distortions. The analysis of statistical fluctuations should be more important in future work, where crystal defects in the workpiece should be considered.

Overall, the results give insight to how nano-manufacturing components deform due to fixture parameters while in the vice. At the nano scale, holding a part in a fixture with a 10 m/s closing velocity experiences distortion. The effect of fixtures and work holding devices at a smaller level could have potentially larger effects than that of the macro scale. In addition, understanding how a workpiece deforms while in the fixture suggests further research at both the macro and nano scale to understand machining distortions due to fixture stresses. More work is needed to analyze the effects of clamping in relation to manufacturing for both macro and nano processes.

5.4 Conclusion

In conclusion, the overall purpose of this case study was to investigate distortion from fixturing in nano machining. Through simulations of nano scale geometries with molecular dynamics, machining distortions and critical stress concentrations directly related to the fixture were revealed.

A major result of this work is that the residual stresses formed could be related to the local generation of plasticity. In addition, it was shown that the local plasticity leads to strongly inhomogeneous residual stress distributions, which do not follow the symmetries of the workpiece.

Although the distortion presented from this simulation in Figure 58 is a two-dimensional characterization, the shape change for each simulation (bar, L-shape, and U-shape) had distortion effects from the fixture location. The bar had maximum distortions experienced near the center of the vice contact. The L-shape had the maximum distortions experienced near the right edge of the L-shape. The U-shape experienced the maximum distortion at the center of the U. The distortions are dependent on the initial shape (bar, U, L, etc.).

Future work is needed to further investigate the applicability of using nano-machining simulations to understand macro machining. An important step that needs to be taken is the inclusion of pre-existing defects in the workpiece, in particular grain boundaries and dislocations; also, the effect of rough surfaces needs to be investigated. For such future investigations, this case study can serve as a reference, as it details the effects in an ideal – i.e., single-crystalline and defect-free workpiece. More research towards fixture related distortion and deformation is needed to fully digest the relation between the two machining scales. All in all, the results from the simulations provide an insight to the behavior of workpieces while in a fixture for manufacturing applications. The results showed an importance of the clamping forces for nano-manufacturing.

Publications

Garcia, D. R., Zhang, Z., Linke, B. S., and Urbassek, H. M. (2018). “Molecular dynamics simulations of single grain pure aluminum in a vice fixture for nanomanufacturing applications.” *CIRP Journal of Manufacturing Science and Technology*.

CHAPTER 6 CASE STUDY: PROCESS PLANNING TOOL FOR SUSTAINABILITY RESEARCH AND TEACHING WITH EMPHASIS ON SCRAP REDUCTION

6.1 Introduction

Sustainable manufacturing includes economic, environmental and social dimensions and is of increasing importance to a variety of manufacturing companies [Haapala et al., 2013], [Duflou et al., 2012]. Common metrics for higher sustainability in manufacturing are energy and material efficiency, emissions, waste, costs, productivity, investment, impacts on society, safety, health, etc. [Sarkar et al., 2011]. Process planning details how products are manufactured in terms of processes and parameters. The manufacturing engineer must choose the manufacturing processes, decide which process steps are in-house or outsourced, and scale up production to the market demand. In concurrent engineering, these decisions are preferably shared by designers and manufacturing engineers, which allows to find optimized product and process design for highest sustainability.

In process planning the following questions are answered [Linke et al., 2016]:

- How many products are made in total and in which frequency and batch size?
- Which manufacturing processes are used?
- What are the parameters, machines, tools, and auxiliary materials for each process?

Process planning is an optimization problem to find the optimal process sequence with the associated optimal process parameters with minimum cost [Deshpande and Cagan, 2004]. This offers great potential for sustainability improvements. For a comprehensive analysis, both value-adding and non-value adding steps should be considered [Linke et al., 2016]. In particular, the non-value adding operations, including metrology, can lead to great cost-savings, even though they first consume time and labor [Savio et al., 2016]. Metrology steps, such as intermediate quality checks, can improve the overall outcome and quality of the manufactured part. Machining distortion has shown to be a large

contributor of economic waste due to scrapped or re-worked parts related to the distortion industries. Reducing the amount of total scrapped parts through the use of a process planning tool can help in the global efforts of the machining distortion minimization methods. This chapter will discuss a process planning tool for sustainability that can be transferred to distortion minimization techniques and approaches. The framework demonstrates metrics for different scenarios to enable sustainable process management or improve engineering education.

Computer-based tools have proven to be effective for teaching engineering science. An example of an existing tool to enhance the educational experience and outcomes of production engineering students, is the incorporation of a computer-based simulation tool in manufacturing for a production engineering course at Robert Morris University [Manohar et al., 2014]. The framework is validated with a case study. This case study fosters researchers to understand manufacturing from a sustainability standpoint.

6.1.1 Process Planning

Process planning defines which unit processes are used to manufacture the part. The same part can be made with many different unit processes and process sequences. For example, a tube can be cast or sintered near-net-shape, extruded from semi-finished parts, or bent and welded from sheet metal [Abele et al., 2005]. Each single unit process has unique advantages and disadvantages, as well as inputs and outputs. Each unit process output can become a unit process input, making the optimization problem non-trivial. It is often difficult to decompose the planning process into smaller steps, because most steps are influencing all other steps [Bourne et al., 2011]. The evaluation criteria in process planning are plentiful: processing time, quality, availability, costs, energy, etc. [Kreitlein et al., 2015]. Also, most unit manufacturing processes lack physical models that can be used to compute fast and accurate solutions, so human expertise is needed in process planning [Bourne et al., 2011]. Efforts on

unit process life cycle inventories try to help to bring more data and models [Kellens et al., 2012], [Kellens et al., 2012]. Additional challenges come from the new cloud-based manufacturing environment, in which decisions on process planning might become web-based, distributed and collaborative [Lu et al., 2015].

The value-adding unit manufacturing processes can be differentiated into: primary shaping, forming, separating, coating, property changing, and joining [DIN 8580:2003-09]. These unit processes build a process chain where each process subjects the part to discrete changes (Figure 63). We define process chain as a sequence of value-adding and non-value adding processes. For environmental assessments, unit processes can be characterized through theoretic calculations and/or measurements of energy and material consumption, as described by the Unit Process Life Cycle Inventory (UPLCI) method and the Cooperative Effort on Process Emissions in Manufacturing (CO2PE) method [Duflou et al., 2011]. The new ASTM E3012-16 standard defines a method to describe a unit manufacturing process (UMP) through an input-output system and with formal language such as XML, UML or SysML [ASTM E3012-16] (Figure 64 left). The product and process information include key performance indicators (KPIs), which are quantifiable measures to gauge or compare performance with regard to company goals. This guide uses KPIs for sustainability using the ASTM E3096 - 18 [ASTM E3096-18]. A more generic description of manufacturing as an input-output-system with enablers is shown in Figure 64 right. Assembly energy efficiency has been studied for joining processes [Feng et al., 2014].

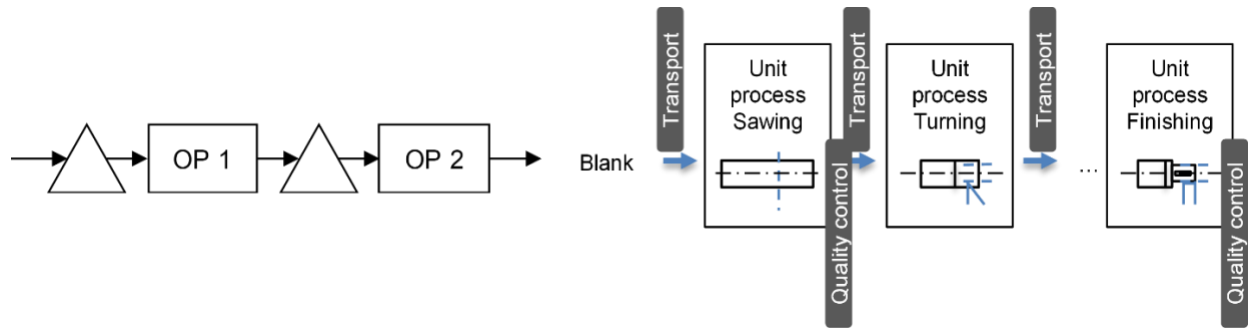


Figure 63 Visualizing process chains including unit processes and non-value adding steps (left: process map with triangles representing inventory [Anderson et al., 2013], right: example from [Linke et al., 2016])

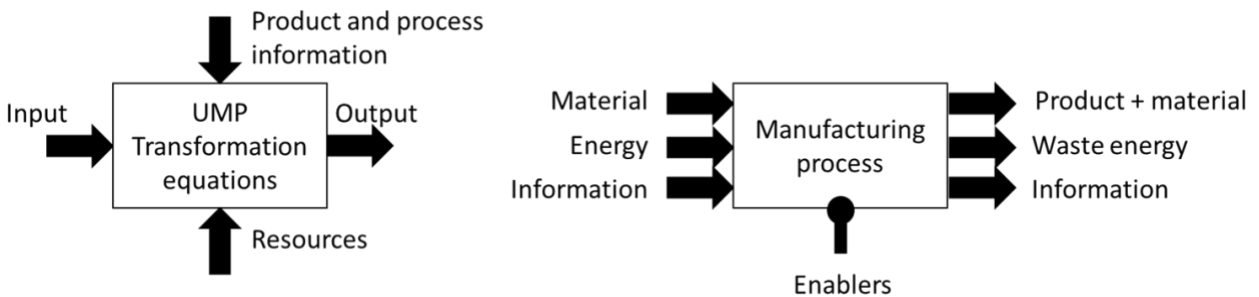


Figure 64 Visualizing unit processes (left: UMP method [ASTM E3012-16], right: generic description)

To evaluate the overall sustainability of a process chain, however, we need to also consider non-value adding unit processes such as transport, part loading/unloading, and quality control, because they can add considerable time, energy, and costs [Linke et al., 2016].

The choice of unit manufacturing processes and non-value adding unit processes depends on the available blank material, machines available and machine times as well as company expertise. Certain processes might need to be outsourced, which can add costs, time, handling, and transport. The process planner needs to satisfy multiple interfering criteria, traditionally production time, costs, and quality. From a sustainability standpoint, additional criteria might become important, such as energy

use, material efficiency, waste, emissions, worker training, and more. These broader criteria are chosen as sustainability indicators in the following. This study aims to teach engineering students to investigate sustainable manufacturing for various metrics and indicators to expand traditional thinking.

6.1.2 Process Chain Model

In the following, a process planning model is developed as a simple and transparent tool for students, researchers, and industrial users to evaluate process planning for sustainability. It is a gate-to-gate model inside one or multiple factories. It starts with the raw material into the factory and ends at the factory gate, where the product is handed off to another company or the user. The model allows users for example to assess optimum batch size, process sequence, or number of quality assurance steps. It transparently shows which unit process contributes and specifically how much, to the environmental or economic impacts.

Process chains need to include value adding unit processes, UMPs, and non-value adding unit processes, APs. There is an extensive number of potential sustainability indicators as collected by the NIST Sustainable Manufacturing Indicators Repository (SMIR) [NIST SMIR]. This repository uses five categories: environmental stewardship, economic growth, social well-being, technological advancement, and performance management [Joung et al., 2012]. Metrics and indicators related to sustainable manufacturing can include cost, energy, waste minimization, safety, environmental impact, personal health, productivity, quality, etc. In this study, scrap, costs, time and energy of different scenarios are used as metrics for process management and engineering education.

Due to their high industrial relevance, we use the following sustainability indicators as a minimum, yet workable number of indicators for this study:

- **Production time** (time consumed by value and non-value adding unit processes)
- **Costs** (costs to produce a part or batch; here consisting of material acquisition costs, energy costs, tooling costs, labor costs, and machine costs [Linke et al., 2013])

- **Energy consumption** (energy used for value and non-value adding unit processes; an alternative indicator is energy intensity, e.g. energy divided by volume of final part)
- **Amount of scrap parts** (number of faulty, or defective parts that cannot be reworked)

6.1.3 Engineering Education

As technology is advancing, so is the way we teach our engineering students to keep up with the ever-changing problem-solving skills needed to advance. New methodologies are aimed at transforming the teaching act in engineering such as it allows the development of creativity, innovation in technological areas, and enhancements of individual accountability [Cristina, 2016]. Basic computer programming skills have become an important fundamental aspect of engineering education. Learning basic coding skills is vital for engineering students during their academic career. Institutions are encouraging improvements in programming skills in engineering education through problem-based software and games for motivation among students [Topalli et al., 2018].

Teaching undergraduate students, the fundamentals of sustainability metrics and indicators, through basic coding skills, has not been presented adequately in current engineering education related to manufacturing. Undergraduate engineering students often struggle with concepts related to sustainability including cost, energy, waste minimization, safety, environmental impacts, and more, because the metrics cannot be compared directly and have different units or importance. Using a basic programming language such as Matlab encourages students to learn basic coding fundamentals as well as it fosters understanding a software tool for process planning that is easily accessible and transparent.

6.1.4 Educational Water Table Study

At the University of California Davis, a new course on integrated STEM education in aerospace design and manufacturing was developed, funded by the NSF IUSE (Improving Undergraduate STEM Education) program [Linke et al., 2017 NAMRC 45], [Linke et al., 2017 Procedia Manufacturing],

[Linke et al., 2017 ASEE Conference]. This course teaches undergraduate students with simple mathematics what makes airplanes fly, while also showing how computer simulations, manufacturing, and experimental validation are integrated in the modern engineering world. The airflow around airfoils needs to be optimized to minimize sonic booms and drag, therefore increasing efficiency. To visualize the airflow around airfoils or in rocket nozzles, a water table experiment is used to show shock waves around models [Hafez et al., 2017]. The hydraulic analogy states that for transonic flows the change in air pressure is equivalent to the change in water height [Orlin et al., 1947]. The students are challenged to predict wave patterns around different model shapes, fabricate the models, conduct water table experiments, and compare computational and experimental results. Design iterations and model surface adjustments are inquired to improve the wave pattern.

The two main quality criteria for the water table models are surface roughness and dimensional tolerance. The model surfaces need to be smooth to avoid turbulences. The dimensional accuracy is critical for the comparison between the computational simulation and the water table experiments. The students will need to produce the models during the course duration while considering the relevant and timely topic of sustainability in manufacturing. The described model for process planning is a simple way to compare different process chains. The following sample values are considering a diamond airfoil shape as shown in [Linke et al., 2017 Procedia Manufacturing].

6.2 Process Chain Steps

The following steps are carried out for the process chain model:

Step 1: Obtain part-specific data

Part-specific data will be defined by the application, the material choice, and initial and final part dimensions.

Here, the following data is collected:

- Material costs C_{material} in \$/kg
- Material density ρ in g/cm³
- Material volume of the raw part V_{w_raw} in mm³
- Material volume of the finished part V_w in mm³

Step 2: Obtain site-specific data

Site-specific data depends on the company and/or location of production. For the model discussed here, it includes the following:

- Electricity cost rate $C_{\text{electricity}}$ in \$/kWh – This cost rate describes the cost of the electricity consumed by machines and devices.
- Scrap costs C_{scrap} in \$/part – The scrap costs per part are specific to the process chain operations and the costs associated with each, including: the final part material, machining cost, worker cost, tool cost, and the energy cost.

Step 3: Obtain unit process data

Each unit manufacturing process UMP_i and unit auxiliary process AP_i , here consisting of transport and quality control processes, is modelled by a set of relevant parameters [Overcash et al., 2009], [Linke et al., 2012]:

- Set-up time $t_{\text{setup},i}$ in min – This time describes the initial machine set-up for the next processing operation including tool or fixture change. The machine is usually in basic power mode. Set-up occurs once per batch.
- Idle time $t_{\text{idle},i}$ in min – This time occurs per part during tool air travel and part loading if the spindles and motors are running. (Figure 65)
- Processing time $t_{\text{process},i}$ in min – This time describes the value-adding steps per part in an UMP or the operating time in an AP. In milling and sawing, processing time is calculated from the feed rate v_f , length to be cut l_c , and number of passes N_t . In measurement operations, processing time is the measurement time.

$$t_{\text{process},i} = l_c \times N_t / v_f \quad (33)$$

- Basic power $P_{basic,i}$ in W – This power is continuous over the cycle time and typically includes machine controls, unloaded motors, oil pumps, and more.
- Idle power $P_{idle,i}$ in W – This power is needed in addition to the basic power when there is relative movement of the tool and the workpiece without processing, for example during air travel, part loading or tool change.
- Process power $P_{process,i}$ in W – This power is needed in addition to the basic and idle power when the workpiece is processed. Since the process power in machining depends on the machining load, it can be measured or estimated from specific process energies.

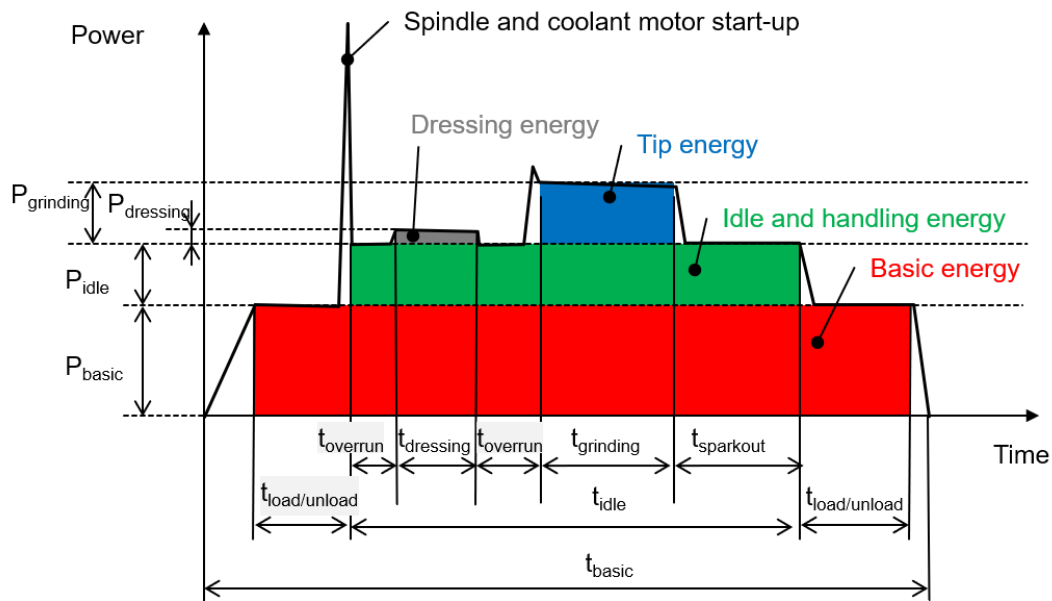


Figure 65 An example of a generic electric power and time profile for a grinding process [Linke and Overcash, 2017]

- Machine costs per hour $C_{machine,i}$ in \$/h – The machine costs are an hourly rate and include the machine investment and overhead costs. Electricity costs are calculated separately in this example.
- Worker costs per hour $C_{labor,i}$ in \$/h – The worker costs are an hourly rate and depend on the skill set and training of the worker.
- Material volume removed $V_{w_removal,i}$ in mm^3 – Equation 34 gives an example equation for material removal in surface milling, calculated from width of cut, a_p , depth of cut, a_e , length of cut, l_c , and number of passes, N_t .

$$V_{w_removal} = a_p \times a_e \times l_c \times N_t \quad (34)$$

- Tool costs per part, i in \$ – The investment costs of the tool have to be divided by the number of total parts.
- Scrap rate S_i in % scrap – The scrap rate indicates process reliability and can represent faulty parts with large distortions . The scrap rate is the percentage of faulty or defective parts. Defective parts accrue additional labor and material expenses. For any items that must be scrapped, all the labor, material, and resource expenses of producing them is wasted [Nicholas, 2010]. For quality assurance processes, we assume they set the scrap rate as $S_i = 0$. This will make sure that the following process step has no faulty parts as input. Scrap is used as a metric to mimic negative distortion outcomes resulting in scrapped and reworked parts that are costly and wasteful.
- Auxiliary material waste per part $m_{aux,i}$ in kg – This metric includes any auxiliary material that is wasted per part excluding tool wear. For example, a small amount of cooling lubricant is carried out from the machine by the part rather than being reused or a certain amount of grease is consumed by the machine guideways when they move to produce a part.

Step 4: Choose number of parts per batch and process chain

The operator then chooses a number of parts per batch, N , and selects a process chain from the available UMPs and APs. To produce a certain part, generic unit processes can be added to a chain (e.g. sawing separates a part from a blank, turning produces outer surface, milling produces a slot, etc.). The selected unit process variants however cannot be added arbitrarily because the output quality of one-unit process variant might not qualify as input for another unit process variant. This needs to be pointed out but will not be the focus of this study. The users build alternative process chains first from generic unit processes (Figure 66), then detailing the unit process variants. The users need to critically consider the finishing processes with regard to part quality, such as surface quality, edge roundness, form errors, time, effort, and user skills required.

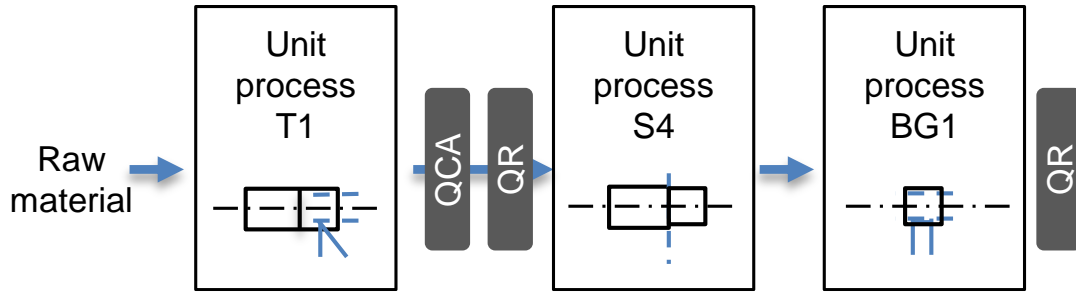


Figure 66 Process chain with specific UMPs and non-value adding steps (auxiliary processes) [Linke et al., 2016]

Step 5: Calculate process chain sustainability indicators

From the information above, several metrics to evaluate sustainability can be calculated. Here production time, energy consumption, costs, and scrapped parts per batch and per part are defined.

Time

The total time per batch per process is calculated from setup time plus idle time and process time multiplied with parts per batch, N (Equation 35). Adding all total times per batch per process for the process chain and dividing by the number of parts per batch, gives the total time per part for the complete process chain (Equation 36).

$$\text{Total time per batch per process } i, t_{total_batch_i} = t_{setup,i} + (t_{idle,i} + t_{process,i}) * N \quad (35)$$

$$\text{Total time per part for the complete process chain, } t_{total_part} = \frac{\sum_{i=0}^n t_{total_batch_i}}{N} \quad (36)$$

Energy

Total energy per batch per process comes from the sum of all powers multiplied with the respective times (idle, batch and process) (Equation 37). Again, adding all those energies per batch per process for the process chain and dividing by number of parts per batch, gives total energy per part for the complete process chain (Equation 38) [Linke and Overcash, 2017].

Total energy per batch per process i , $E_{total_batch,i} = P_{basic,i} * t_{setup,i} + (P_{basic,i} + P_{idle,i}) * t_{idle,i} * N + (P_{basic,i} + P_{idle,i} + P_{process,i}) * t_{process,i} * N$ (37)

Total energy per part for the complete process chain,

$$E_{total_part} = \frac{\sum_{i=0}^n E_{total_batch,i}}{N} \quad (38)$$

Scrap

It is assumed that each unit process i , has a specific scrap rate S_i per its process conditions. This could for example include parts with a machining distortion exceeding a threshold value. The total scrap rate $Scrap_rate_i$ is calculated from the process scrap rates S_i from all previous steps. Here, a worst case is assumed that each process destroys parts that are not defect from previous steps. A more realistic case is if the process would destroy defect and non-defect parts similarly lowering the scrap. If a preceding unit process $j-1$ has a scrap rate S_{j-1} greater than zero, the scrap rate accumulates to $Scrap_rate_i = S_j + S_{j-1}$ (Equation 39). If a quality assurance step happens in the process chain, the scrap from the quality assurance process is zero and the number of parts in the batch reduces by the removed parts.

$$\text{If } S_{j-1} > 0: \quad Scrap_rate_j = S_j + Scrap_rate_{j-1} \quad (39)$$

$$\text{If } S_{j-1} = 0: \quad Scrap_rate_j = Scrap_rate_{j-2} + (1 - Scrap_rate_{j-2}) * S_j \quad (40)$$

$$\text{Scrap parts for the complete chain, } S_{scrap_batch} = N * \sum_{i=0}^n (Scrap_rate_i) \quad (41)$$

For the scrap material mass, it is assumed that the complete raw material mass of the scrap parts is counted as wasted mass. The scrap material mass for the complete chain per part is calculated from the number of scrap parts for the complete chain (Equation 41), the part mass (Equation 43), and the number of parts per batch, N .

$$\text{Scrap material mass for the complete chain, } m_{scrap_part} = S_{scrap_batch} * m_{w_raw} \quad (42)$$

$$\text{With part mass } m_{w_raw} = V_{w_raw} * \rho \quad (43)$$

Cost

The costs per batch and part are calculated from electricity, machine, labor and raw material costs. From the previously calculated energy per batch, we can calculate the electricity costs per batch (Equation 44). Here, we define production costs per batch as sum of electricity costs, machine and labor costs times total time per batch per process and tool costs (Equation 45). The total costs for the complete process chain per part include these production costs and divide them by the number of parts per batch plus raw material costs and scrap costs (Equation 46).

$$\text{Electricity costs per batch for process } i, C_{\text{electricity_batch}, i} = C_{\text{electricity}} * E_{\text{total_batch}, i} \quad (44)$$

$$\text{Production costs per batch for process } i, C_{\text{total_batch}, i} = C_{\text{electricity_batch}, i} + (C_{\text{machine}} + C_{\text{labor}}) * t_{\text{total_batch}, i} + N * C_{\text{tool}} \quad (45)$$

$$\text{Total costs for the complete process chain per part, } C_{\text{total_part}} = \frac{\sum_{i=0}^n C_{\text{total_batch}, i}}{N} + V_{\text{w_raw}} * \rho * C_{\text{material}} + (S_{\text{scrap_batch}} * C_{\text{rework}}) / N \quad (46)$$

$$\text{where, } V_{\text{w_raw}} = V_{\text{w}} + V_{\text{w_removed}} \quad (47) \text{ [Linke et al., 2013]}$$

Step 6: Give weight factors to each sustainability indicator

The operator needs to decide on weight factors WF_i for the selected sustainability indicators, here production time $t_{\text{total_part}}$, energy $E_{\text{total_part}}$, scrap $S_{\text{scrap_part}}$, and costs $C_{\text{total_part}}$ for the complete process chain per part. The weight factors need to sum up to 100%.

Step 7: Calculate overall sustainability indicator

The values for the production time $t_{\text{total_part}}$, energy $E_{\text{total_part}}$, scrap $S_{\text{scrap_part}}$, and costs $C_{\text{total_part}}$ for the complete process chain per part are entered into the scoring tool [see Table 6]. The scoring model is described in reference [Linke et al., 2013]. The user has to find the optimum value for each indicator. For example, for energy consumption, there is a theoretical minimum resulting from processing energy and machine idle energy. All waste or water and air releases intensities would equal 0 in the best case

[Linke et al., 2013]. For the model described in this case study, the optimum value of each sustainability indicator is simplified in that way that it is just the minimum value. For other indicators, e.g. energy efficiency, renewable materials content, the optimum value would be the maximum value of the compared alternatives.

The degrees of fulfilment (DF) range from 1 (poor, low sustainability) to 10 (optimum value). The degree of fulfilment for each sustainability indicator and process chain (DF_{xi}) are then calculated (for example with Equation 48). The degrees of fulfilment can be displayed as radar charts or columns and give a fingerprint of the process chain.

Table 6 Scoring Tool, after [Linke et al., 2013]

Sustainability metrics	Optimum value (DF = 10)	Weight factors	Chain or process 1			Chain or process 2			Chain or process n			
			Value	DF	U	Value	DF	U	Value	DF	U	
time t_{total_part}	Min. of ($t_1 ; t_n$)	WF _t	t ₁	DF _{t1}	WF _t *DF _{t1}	t ₂	DF _{t2}	WF _t *DF _{t2}	t _n	DF _{tn}	WF _t *DF _{tn}	
energy E_{total_part}	Min. of ($E_1 ; E_n$)	WF _E	E ₁	DF _{E1}	WF _E *DF _{E1}	E ₂	DF _{E2}	WF _E *DF _{E2}	E _n	DF _{En}	WF _E *DF _{En}	
scrap S_{scrap_part}	Min. of ($S_1 ; S_n$)	WF _S	S ₁	DF _{S1}	WF _S *DF _{S1}	
costs C_{total_part}	Min. of ($C_1 ; C_n$)	WF _C	C ₁	DF _{C1}	WF _C *DF _{C1}	
		$\sum WF = 100\%$			$\sum U_1 = SI_1$			$\sum U_2 = SI_2$			$\sum U_n = SI_n$	= SI

$$DF_{xi} = 10 - \left(integer \left(\frac{x_i - \min(x_1; x_n)}{\max(x_1; x_n) - \min(x_1; x_n)} \cdot 9 \right) \right) \quad (48)$$

The weight factors, WF, are multiplied with the degrees of fulfilment, DF, to (sub-) utility values, U. The utility values, U, are summed into one overall score called the total sustainability indicator, SI. This allows to consider multiple metrics while having transparency on the largest contributing factors.

Step 8: Analyze result sensitivity and find biggest impact factors

The sensitivity of the results with regard to the input parameters should be checked. For example, the input values of the single unit processes can be changed by +5% or -5%. Then the modified results are compared to the original results. The largest deviations point to a high sensitivity and the input values should be confirmed. The same sensitivity of the results with regard to the weight factors should be evaluated. An example is given in [Linke et al., 2013].

6.3 Case study

6.3.1 Part-Specific and Site-Specific Data

The raw material is assumed as an easy-to-machine polypropylene (PP) rectangular bar (50.8 mm x 101.6 mm x infinite length (2 in. x 4 in. x 3 feet)) seen in Figure 67. Values for the part-specific and site-specific data are described in Table 7.

Table 7 Part-specific and site-specific data

Part-Specific data	Description
Material costs per kg C_{material} in \$/kg	2.2
Material Density ρ in g/cm ³	0.9
Material Volume of the raw part V_{w_raw} in mm ³	Dependent on V_w and $V_{w_removed}$
Material Volume of the finished part V_w in mm ³	617250
Site-specific data	
	Description
Electricity Costs $C_{\text{electricity}}$ in \$/kWh	0.13
Scrap costs C_{scrap} in \$/part	Dependent upon V_w , C_{machine_i} , C_{labor_i} , C_{Tool_i} , and $C_{\text{electricity}}$. It is assumed to be C_{part}

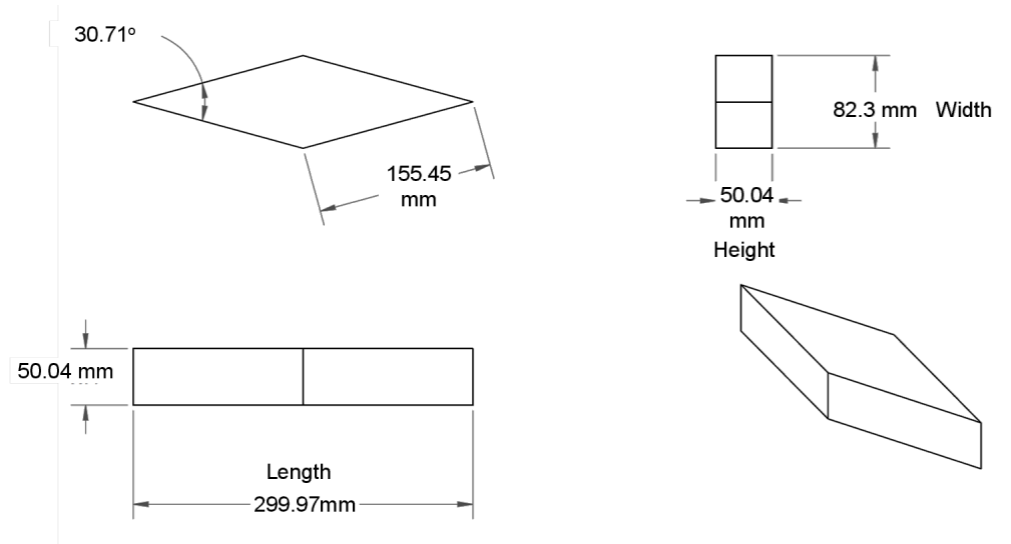


Figure 67 Diamond model of the milled and water jetted models [Linke et al., 2017 NAMRC 45]

6.3.2 Unit Manufacturing Process (UMP) Data and Unit Auxiliary Process (AP) Data

Process data and site-specific data is presented to the users, e.g. students or researchers, as prepopulated data that is imported into a simple Matlab process planning tool. The users can view and edit the data for further case analysis. Further data collection on both additive and subtractive manufacturing processes can advance understanding and research.

In a course environment, the students could be encouraged to record as much data as possible, e.g. when manufacturing the models for the water table experiment. In the case study discussed here, reasonable data is provided via manufacturing datasheets, and machine specification sheets. All data is displayed in text files that are easily imported into the chosen coding environment, Matlab. The manufacturing processes presented include milling, sawing, drilling, water jet cutting, and manual grinding with sandpaper. We assume 20 seconds part loading and unloading time for each automated process and 10 seconds for manual grinding.

The non-value adding unit processes include slow, medium, and fast transport between processes, as well as quality assurance steps. It is assumed that a worker moves the complete batch from one machine to the next with the selected speed.

Quality assurance is a means of providing high quality parts in the production environment and ensures that processes and products comply with the predetermined quality specifications [Schmitt et al., 2014]. Here, quality assurance, or a distortion check is done via manually measuring the external dimensions of the part with calipers. Tradeoff decisions must be made between increasing quality and lowering costs, for example with the Cost of Quality [Farooq et al., 2017]. The costs of conformance (prevention) and non-conformance (appraisal + failure) have opposing trends with process quality but lead to an economic sweet spot. In this case study, quality control steps will lower the outgoing scrap rate for the next operation as discussed in Equation 39. Values for UMP and AP data are presented in Table 8.

The assumptions for the data provided in Table 8 include using

- machines that are used in a workshop-type setting,
- machines that are older and used for teaching purposes,
- machines that use manual and semi-automatic manufacturing, and
- negligible power data for the sandpaper grinding process; however, human power can be considered in future work.

Table 8 UMP and AP data for the case study

	Process Specification Operation	Set-up time per batch in min	Idle time per part in min	Process time per part in min	Basic power in W	Idle power in W	Process power in W	Machine costs in \$/h	Worker costs in \$/h	Tool costs per part in \$	Scrap rate in %	Removed material in mm ³
UMP	Rough Milling	9	0.33	7	920	1450	2400	80	50	0.12	0.08	641553.2
	Fine Milling	9	0.33	10	920	1450	2000	80	50	0.10	0.02	641553.2
	Rough Sawing	0.5	0.33	2	300	400	370	40	50	0.06	0.08	15483.8
	Fine Sawing	0.5	0.33	3.5	300	400	250	40	50	0.05	0.02	15483.8
	Rough Drilling	1	0.33	2	300	400	350	35	50	0.08	0.08	11490.7
	Fine Drilling	1	0.33	3.5	300	400	250	35	50	0.075	0.02	11490.7
	Rough Sandpaper Grinding	0.05	0.17	1	0	0	0	0	50	0.02	0.01	631.75
	Fine Sandpaper Grinding	0.05	0.17	2	0	0	0	0	50	0.02	0.01	631.75
	Rough Water Jet Cutting	5	0.33	5.6	2000	2000	30000	120	50	0.12	0	128310.6
AP	Caliper Measurement	0	0.17	1	0	0	100	50	50	0	0	0
	Fast Transport Method	0	0	0.1	0	0	0	0	50	0	0.08	0
	Medium Transport Method	0	0	0.5	0	0	0	0	50	0	0.05	0
	Slow Transport Method	0	0	1	0	0	0	0	50	0	0.01	0

6.3.3 Generation of Alternative Process Chains

Using Matlab, a process chain tool is pre-established for the users, e.g. engineering students, to explore a specific case scenario. For the various process planning cases, the users are then able to compare different process chains with various manufacturing operations, material selection, number of steps, batch sizes, etc., by changing and manipulating various sections of the code. An example of a generic

process chain is shown in Figure 68, where the initial operation is a saw cut, followed by a material removal step, then a drill operation, grinding, and ending with a quality assurance step with a caliper measurement. The users will create the overall process chain that creates the final diamond model. The diamond model can be manufactured in various ways with a variety of chosen UMPs and APs.

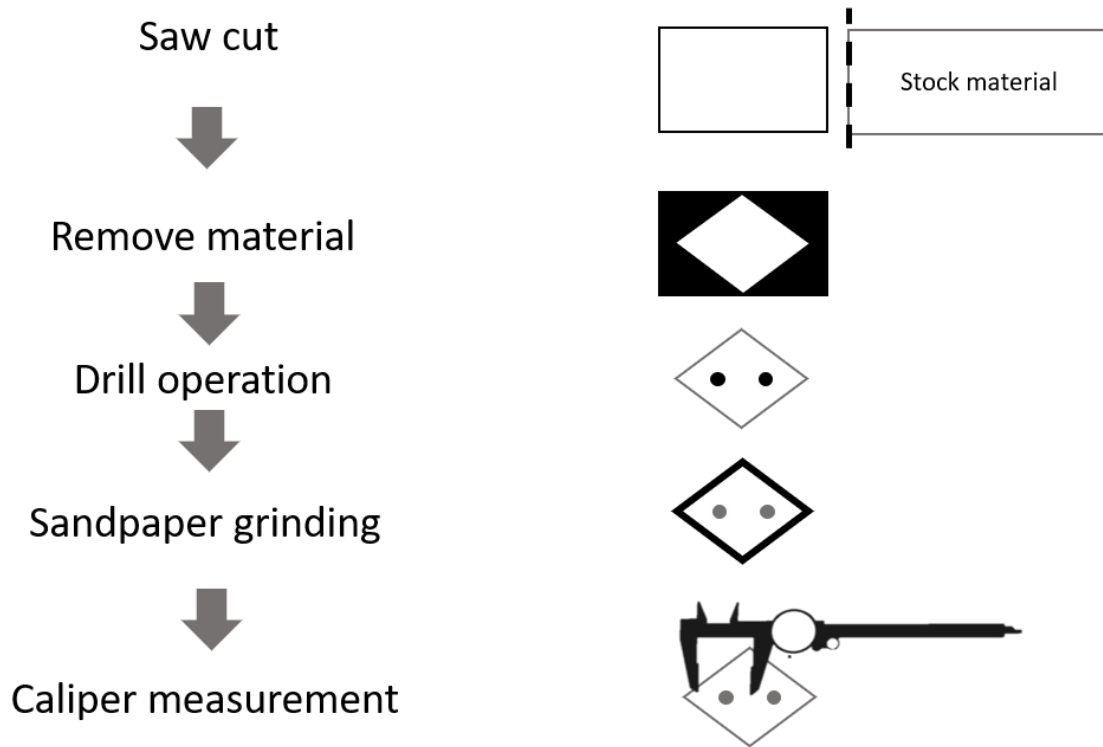


Figure 68 A generic process chain is shown for the diamond model

The specific case scenario essentially provides a skeleton code for the user to inspect, change, and edit for further analysis and for specific outcomes, such as information requested by the instructor, or independent learning from the student. The basic procedure of the process chain Matlab model is presented as a flowchart in Figure 69.

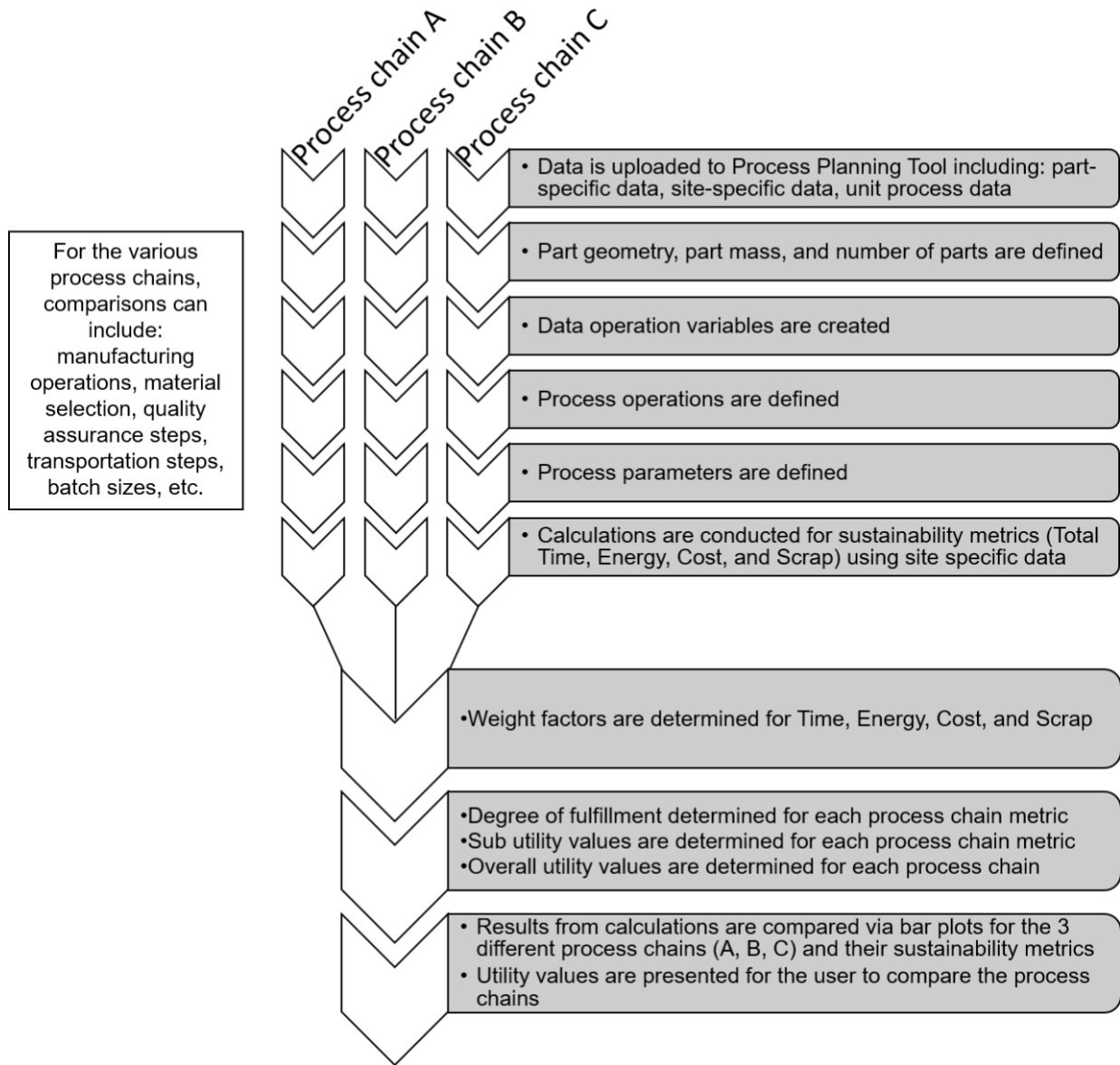


Figure 69 Matlab process chain model presented as a flowchart

6.4 Results and Discussion

A *Process Planning Matlab Tool* allows the user to choose the UMP and AP steps for each of the three different process chains A, B, and C. The user is then able to modify the code to answer questions about sustainability and metrics related to costs, energy, time, and scrap. The different process chains

can involve a variety of steps including milling, drilling, sawing, sand paper grinding, quality assurance (caliper measurement) of part dimensions, and transportation steps (Figure 70).

This example case study compares three different process chains of batch sizes, $N = 100$. The complete steps of each process chain A, B and C are detailed in the matlab code as:

- A = [Rough_Sawing_Data; Caliper_Data; Rough_Drilling_Data; Caliper_Data; Rough_Milling_Data; Caliper_Data; Rough_SandPaper_Data; Caliper_Data];
- B = [Rough_Sawing_Data; Rough_Drilling_Data; Rough_Milling_Data; Rough_SandPaper_Data; Caliper_Data];
- C = [Fine_Sawing_Data; Fine_Drilling_Data; Fine_Milling_Data; Fine_SandPaper_Data; Caliper_Data];

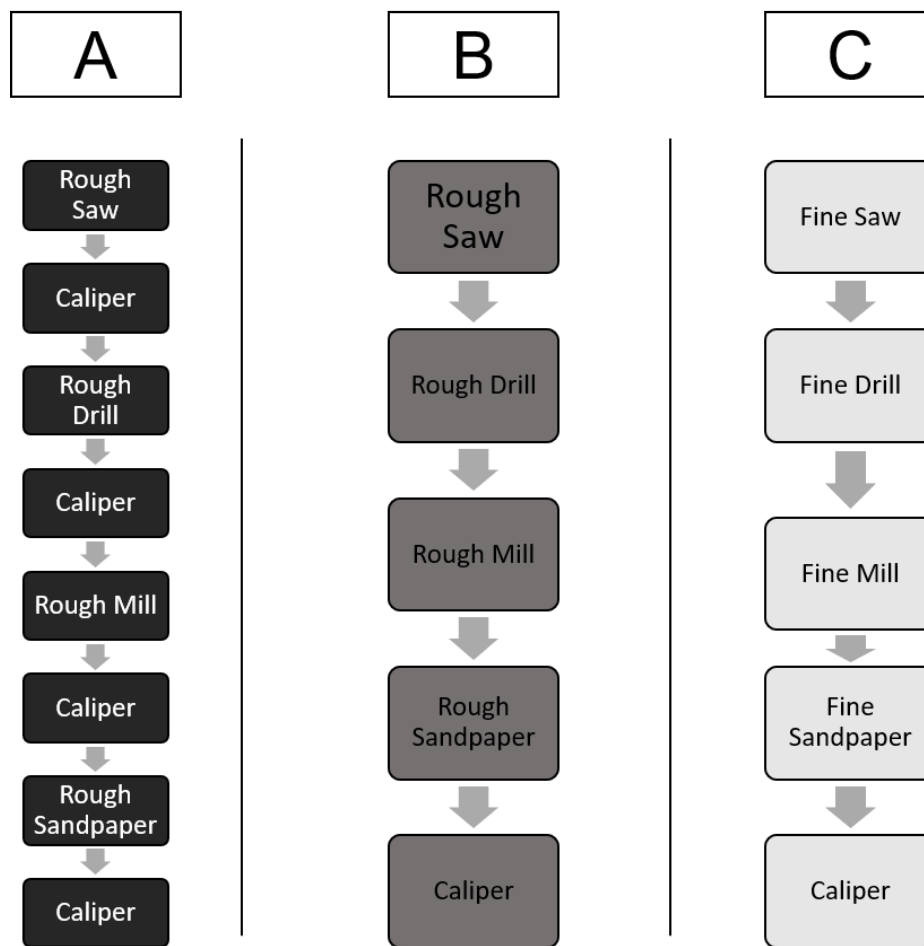


Figure 70 The complete steps of each process chains A, B and C

The process chains (A, B and C) can be compared to each other to show the similarities and differences (Figure 70). Process chains A and B are similar sequences, however, process chain A contains intermediate quality assurance (QA) steps between the UMP operations. Process chains B and C are also similar, but they differ between rough and fine settings for the UMPs selected. The weight factors, WF, for the given sustainability metrics (t, E,S, C) are defined as:

- Weight factor for time = 5 %; $WF_t = 5$; %Time weight factor percentage
- Weight factor for energy = 5 %; $WF_E = 5$; %Energy weight factor percentage
- Weight factor for scrap = 85 %; $WF_S = 85$; %Scrap weight factor percentage
- Weight factor for costs = 5 %; $WF_C = 5$; %Cost weight factor percentage

For teaching and learning purposes, the users are able to investigate the alternative process chains and compare sustainability metrics and key indicators. Time, energy, scrap, and costs are used as metrics to determine which process chain is optimal with the given weight factors and input criteria. In this case study, the highest weight factor is placed on the ‘scrap’ metric, meaning the scrap holds the highest level of importance when investigating the sustainability indicators. We can change the weight factors (weight factors must sum to 100%) to place the highest rank on whichever metric we are curious about studying.

Once the process planning tool is executed, it generates six figures for the user:

1. An overall metric comparison (Figure 71)
2. Production time comparison (Figure 72)
3. Energy comparison (Figure 73)
4. Scrap comparison (Figure 74)
5. Cost comparison (Figure 75)
6. Different sustainability indicator results (Figure 76).

The overall comparison for the complete process chain, for this example (Figure 71 and Table 9), shows that process chain B has the lowest time, energy, and cost but the highest scrap compared to process chains A and C. Results from the three different process chains are presented in Table 9.

Process chain B manufactured the diamond model with fast processes such as rough saw, rough drill, rough mill, rough sandpaper, and a caliper measurement. Process chain A (rough saw, caliper measurement, rough drill, caliper measurement, rough mill, caliper measurement, rough sandpaper, and a caliper measurement) was very similar to process chain B, but had more caliper measurements between the manufacturing processes. The quality control measurement steps from process chain A resulted in fewer total percentage scrapped pieces but a higher overall time, energy, and cost per part.

Process chain C manufactured the diamond model with slower processes such as fine saw, fine drill, fine mill, fine sandpaper, and a caliper measurement. This process chain was different from process chains A and B such that it used fine manufacturing processes to fabricate the diamond model. This sequence of precision processes produced the highest time, energy, and cost, but resulted in the lowest total percentage scrap per part. These results suggest that having fine machining processes results in a lower total scrap percentage, because the scrap rates for fine machining operations are lower than that of the rough machining operations. We assumed that the rough machining operations use aggressive cutting methods that produce more user errors and scrapped pieces, e.g. from machining distortion.

Most fine machining processes require a level of precision which include slower feedrates, longer machining times, greater user expertise, which result in a better surface finish and quality. These factors increase machining time, worker time, machining costs, worker costs, energy costs, etc. Although fine machining processes produce better parts and less scrap, it is more expensive overall with relation to cost, energy and time. The higher product quality can lead to leveraging benefits with a more efficient product life [Helu et al., 2011].

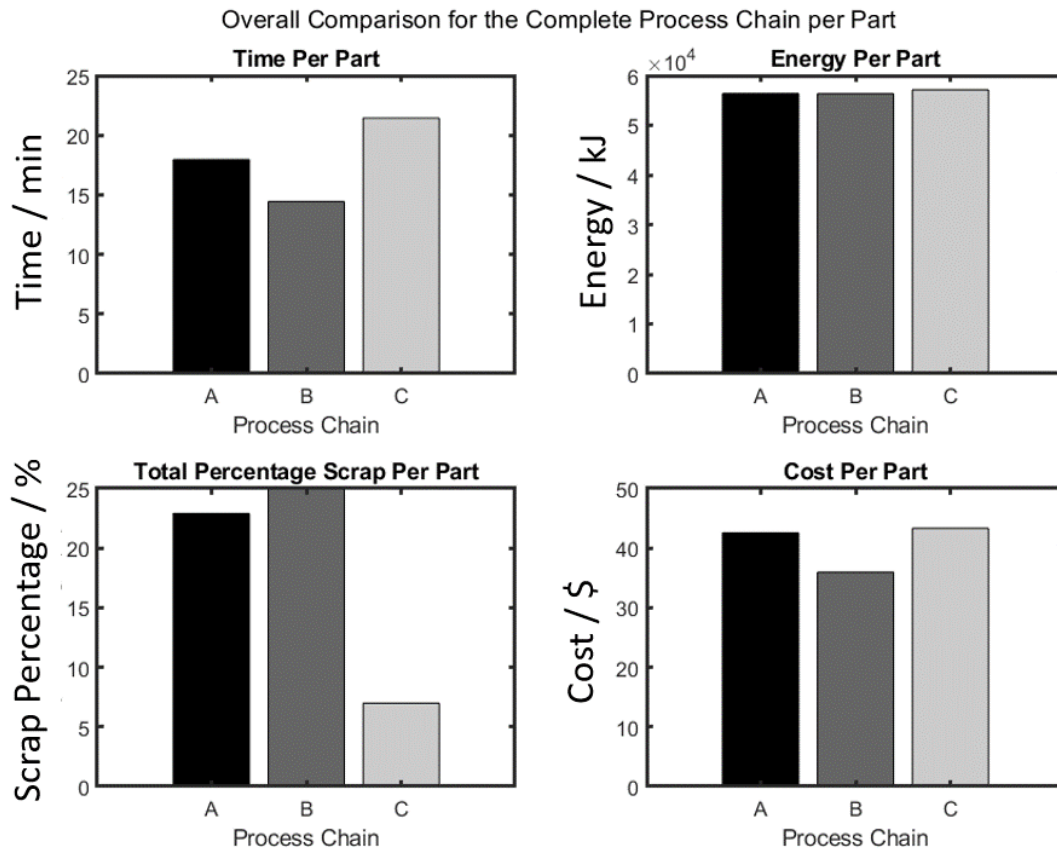


Figure 71 The overall metric comparison including time, energy, scrap and cost for the complete process chains A, B and C

Table 9 Results from process chains A, B and C

Process Plan	Time (Min)	Energy (kJ)	Scrap (%)	Cost (\$)	Sustainability Indicator (SI)
A	17.95	56388.1	22.9	42.56	2.55
B	14.44	56370.1	25.0	35.97	2.35
C	21.44	57133.3	7.0	43.31	8.65

It must be determined which process chain is best suited for the manufacturing needs based on the sustainability indicators selected. From the results of this case study, process chain C proves to be the best suited process chain for a weight factor associated with scrap to be 85% (the highest importance is placed on the scrap (see Table 9, last column)). The process chain that yields the least amount of

scrap percentage is therefore the best option between the alternatives. Although process chain C has the highest production time, highest energy and highest cost – it has the least amount of scrap percentage.

The results from Figure 72 - Figure 75, show the time, energy, scrap percentage, and cost for each process chain A, B and C with the accompanying operations. Through these figures, we can determine which operations are time consuming, energy consuming, scrap producing, and costly. From Figure 72, users can deduce that the milling process uses the most processing time, with fine milling the highest. From Figure 73, the total embodied energy per part, for each process chain, is the same (based on the same batch size, $N = 100$) as 52,774.9 kJ. The total energy per part shown in Figure 73, shows that milling also uses the most energy, with fine milling being the maximum energy producer. Caliper measurements produce 0 scrap percentage, whereas each other machining process produces some nonzero value of scrapped parts (Figure 74). From Figure 75, the highest associated costs with the process chains A, B and C are from the milling processes, with fine milling producing the largest costs. Note, that the material embodied energy is the largest contributor to the total energy.

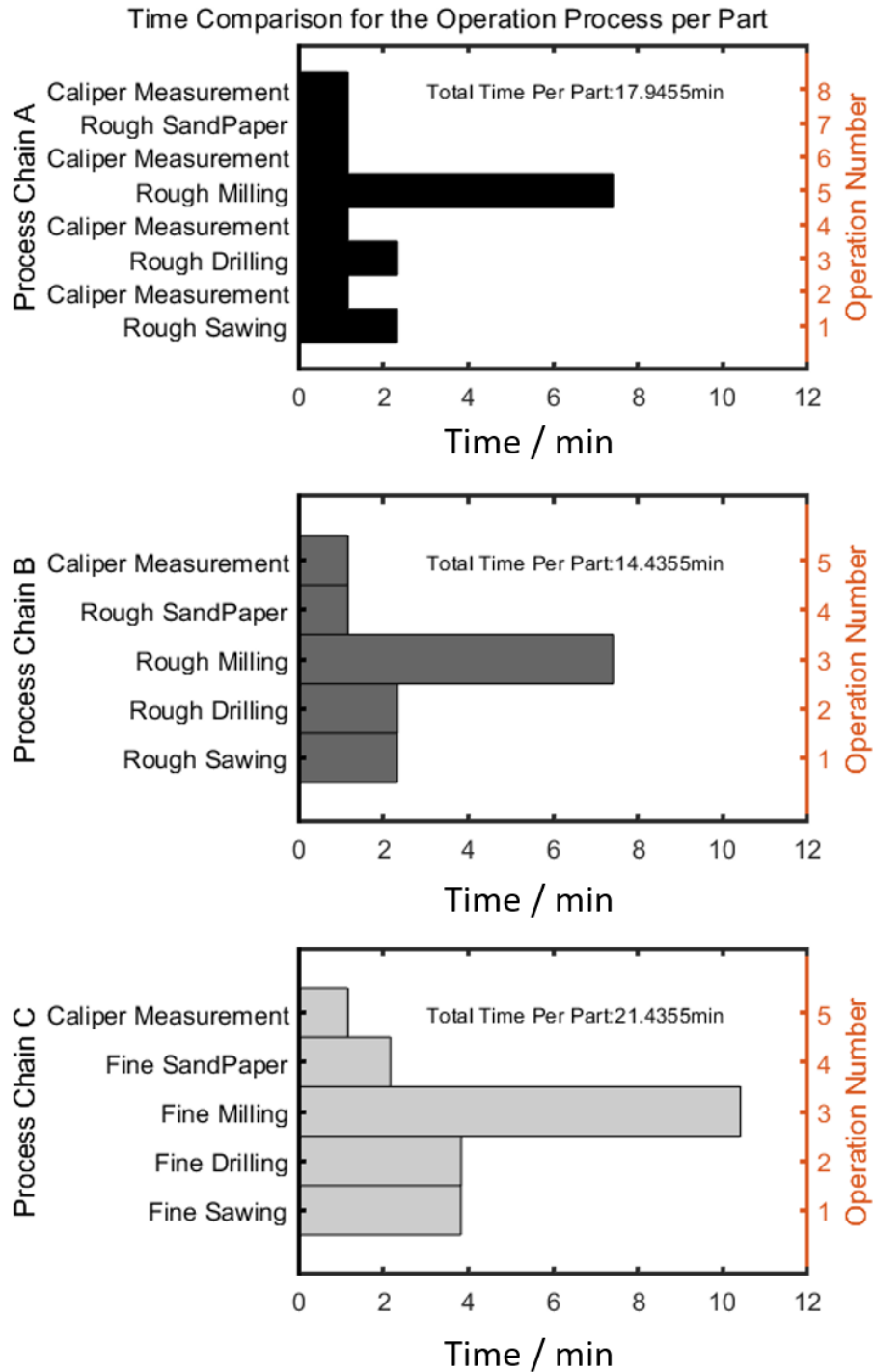


Figure 72 Times for process chains A, B, and C

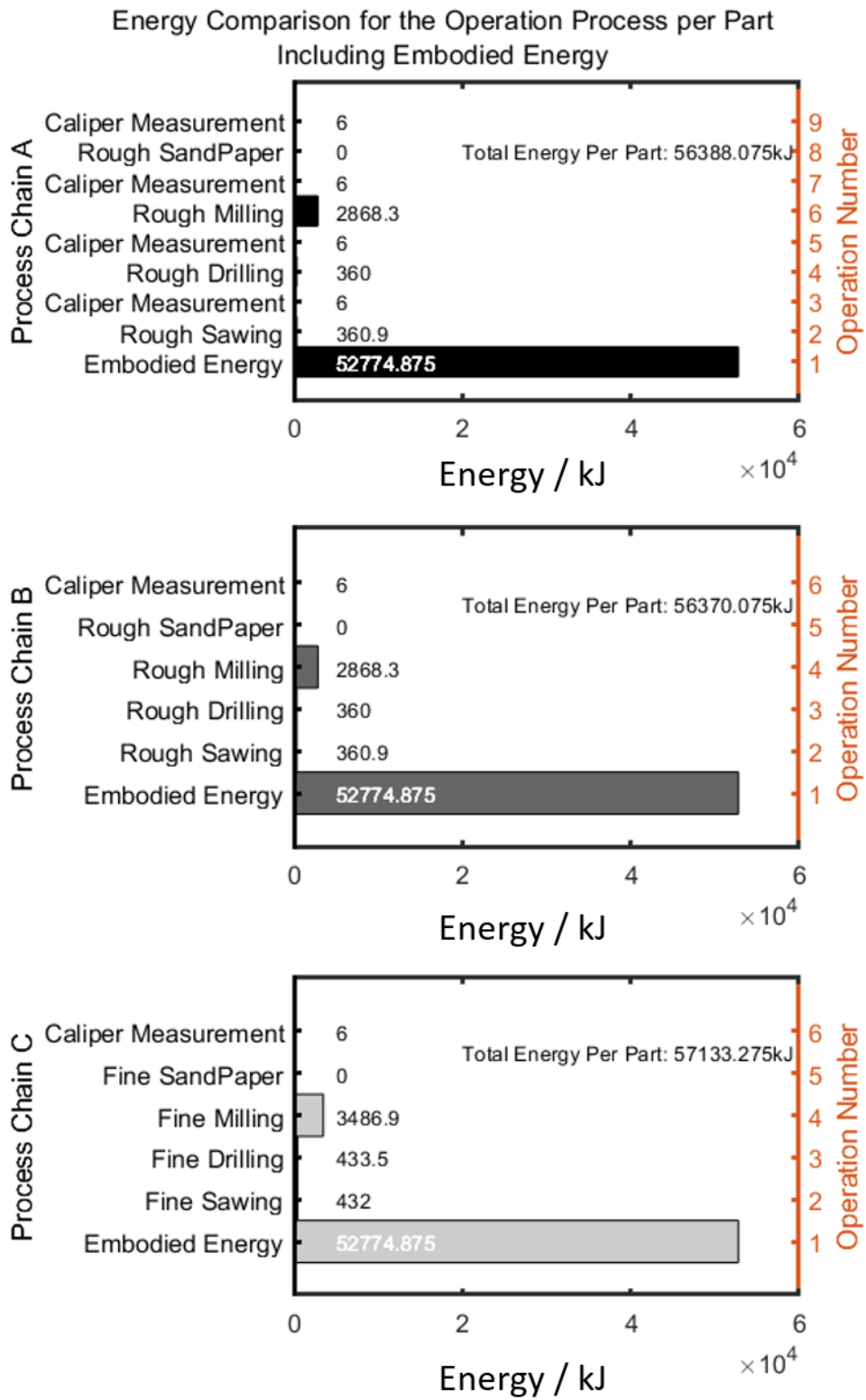


Figure 73 Energy for process chains A, B, and C

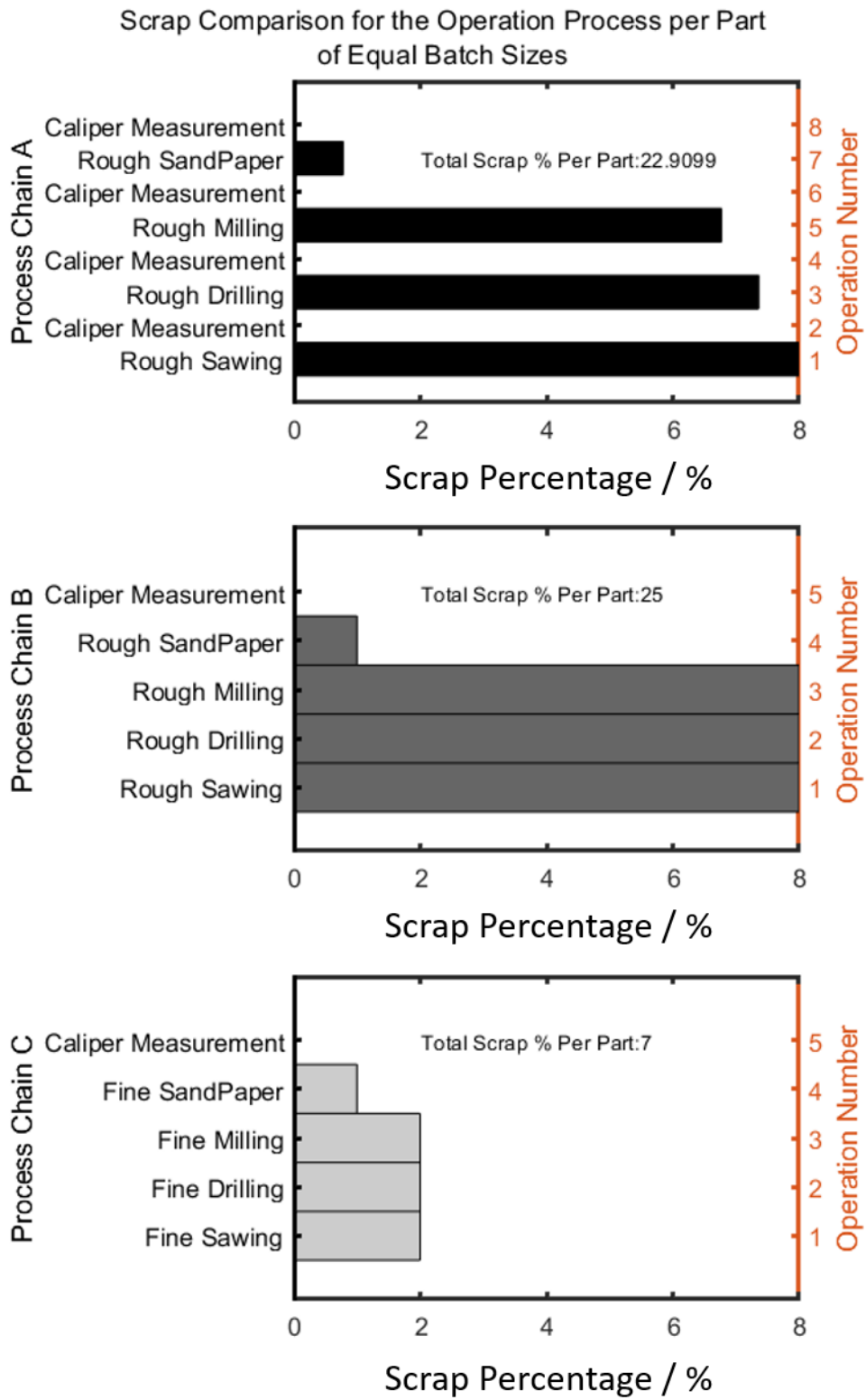


Figure 74 Scrap percentage for process chains A, B, and C

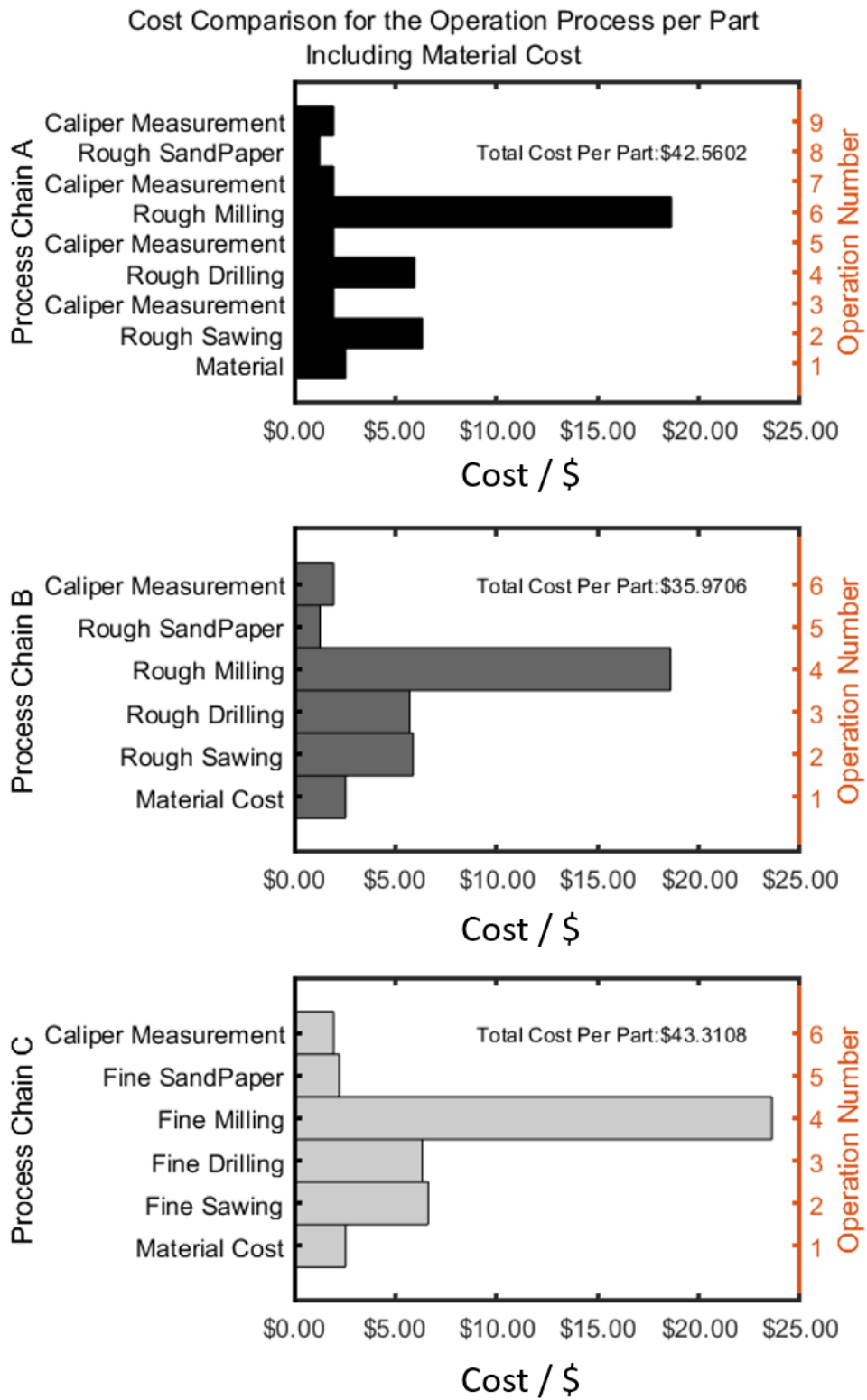


Figure 75 Costs for process chains A, B and C

Adjusting the weight factors for the overall sustainability yields different results (Figure 76 and Table 10). Recall from earlier sections, the total sustainability indicator allows the user to consider multiple metrics while having transparency on the largest contributing factors. In this first case example, the largest weight factor was assigned to the scrap percentage. Therefore, the best total SI value (with 0 - worst, 10 - best) of the different process chains was for chain C, which produced the least total scrap percentage. Adjusting the WFs to different indicators (time, energy, costs) will yield different results for the total SI.

When the largest influence of the weight factor is distributed equally between all four indicators, the highest total SI is achieved by process chain B as seen in Figure 76. Placing the highest WF on time, shows that process chain B is the best option. Placing the highest WF on energy still shows process chain B as the best, but with process chain A following very closely behind. Placing the highest WF on the cost yields process chain B as the best option. Users can continue to change the WF of each contributing indicator (as long as the total WF sums to 100%) to deduce which process chain is best. Based on the WF schemes 1 to 5 presented in Figure 76, process chain B shows promise as the best process chain except for scheme 4, in which the scrap is heavily weighted (WF for scrap = 85%). Total SI data from Figure 76 is represented in Table 10, where the optimum process chain is highlighted and comments on the WF schemes are noted.

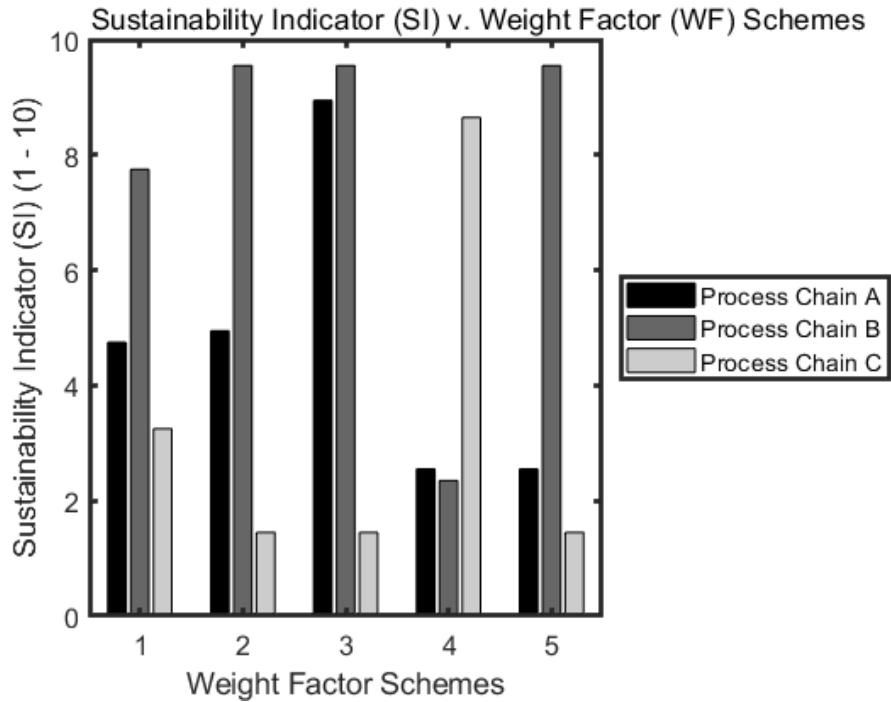


Figure 76 The total Sustainability Indicator versus weight factors for process chains A, B, and C, see schemes in table 5

Table 10 Total SI values for different weighing schemes

Weight Scheme	Weight Factors	Total Sustainability Indicator Value		
		Process chain A	Process chain B	Process chain C
1	All weight factors are 25%	4.75	7.75	3.25
2	High (85%) WF on time, each other indicator is 5%	4.95	9.55	1.45
3	High (85%) WF on energy, each other indicator is 5%	8.95	9.55	1.45
4	High (85%) WF on scrap, each other indicator is 5%	2.55	2.35	8.65
5	High (85%) WF on cost, each other indicator is 5%	2.55	9.55	1.45

Further analysis can include sensitivity analysis of WF or DF, change of process chain design, change of batch size, etc. This process planning tool has been explored by some undergraduates as a pilot test for user interaction and usability. The users were given the case study with each weight factor assigned

at 25%. After running the initial process planning tool the users are then able to implement different case scenarios and comment on their understanding of the overall process planning tool development. Users were prompted to decide which metric they considered the most important - time, energy, scrap, cost - and to reassign the weight factors accordingly. Allowing students to explore the different process chains and sustainability metrics and indicators can provide more insight for students to make confident manufacturing decisions.

6.5 Conclusion

Although sustainability has become an almost everyday term, engineering education for undergraduate students needs to be improved such that basic concepts from sustainability, such as process planning, quality, metrics, optimization, etc. are better transferred into the curriculum. This study proposes an easily accessible and transparent process planning framework, implemented as an easy Matlab tool for students to learn about sustainability indicators, and different process planning optimizations for sustainability. This study chooses to focus on scrap reduction, as an example of the need for distortion reduction and characterization, as a means of improving sustainability. As we reduce the amount of scrap through process optimization and process planning, we can help the overall minimization of machining distortion and material waste. In addition to the students learning about sustainability concepts, they will also gain better insight into basic coding skills for future engineering problem solving.

The data presented in this case study is an initial validation for the process planning tool. Moreover, this case study only presented three process chains in which the process planning tool was used. There are other interesting cases to investigate such as: high vs. low volume batch sizes, varying numbers of operations, traditional vs. nontraditional manufacturing operations, etc. This framework can also be

improved upon, and more data can be added such as: more site-specific manufacturing operations, additional experimental data, and differently generated plots to provide more information.

For expanding the process planning model, we propose to consider intensity indicators on part quality, for example the resources spent are divided by the quality improvement gained, (i.e. energy per difference in average surface roughness Ra [Linke et al., 2014]). Social sustainability indicators should be implemented and can for example cover the duration of manual labor or the minimum expertise level needed to perform the tasks. Future work will consider identifying different sustainable approaches to get to the significant value, for comparing processes and determining the superior sustainable process [Doran et al., 2016]. Future work on analyzing manufactured samples related to various industries including aerospace, digital technologies, automotive, etc. for machining distortion research. Future work can include incorporating the process chain for the machined sample in Chapter 4, the 60-degree aerospace sample. The distortion sample process chain steps will include rough sawing, wire electrical discharge machining (WEDM), rough milling, fine milling, fine grinding, caliper measurements. More work is needed collecting unit manufacturing process (UMP) data for WEDM processes [Gamage et al., 2017].

Future work should focus on the process planning tool on residuals. This includes workpiece mass removed, for example in the form of chips, scrap parts, auxiliary materials such as coolants, lubricants and tool material consumed, direct and indirect process emissions (e.g. CO₂ from electricity, gas directly produced from the process, etc.). The metric CO₂ emission ratio of local electricity generation CO₂ electricity [g/kWh] is specific to the energy source mix for the local electricity generation. For example, electricity generation from wind or solar power has almost negligible CO₂ emissions per kilowatt hour compared with electricity generation from natural gas or coal, which adds valuable insight into manufacturing location and environmental impact. The tool cost calculation can be a

bigger focus, involving available tool volume, tool wear, tool type, tool dependence on process parameters, etc.

In conclusion, the process planning tool is a way for users such as students or researchers to engage in sustainability through coding and visualization and it is useful for sustainability research and engineering education. It is flexible and open enough to satisfy many settings and uses.

Publications

Linke B., Garcia D., Process Planning Tool for Sustainability Research and Teaching, “In preparation for journal submission”.

CHAPTER 7 CONCLUSION AND FUTURE WORK

Machining distortion has been an inevitable manufacturing phenomenon that can have costly and lengthy outcomes and demands preventative measures. This dissertation provides a thorough research investigation of the metrological aspects of machining distortion with relation to quality, manufacturing, metrology, nanomachining, process planning, and overall transparent characterization and representation. An initial routine of three-dimensional machining distortion characterization is presented with a refined and optimized routine incorporating three-dimensional representation and Gaussian curvature to classify distortion for an example aerospace sample. Two case studies are presented to illustrate machining distortion in different research settings including nanomachining and process planning.

7.1 Overall Summary of Contributions

Many of the current approaches to solving machining distortion minimization and control provide point solutions for specific circumstances while relying on expensive empirical trials. In the distortion literature, basic information about the distortion data collection and analysis methods are missing. Examples from the literature show inconsistent methods for analyzing distortion data. Results of the experiments or modeling approaches related to machining distortion are not easily transferred from researcher to researcher. This dissertation provides a transparent way to quantify distortion data collection and analysis for enhanced transferability of experimental and analytical results. A schematic of the research flow can be seen in the figure below.

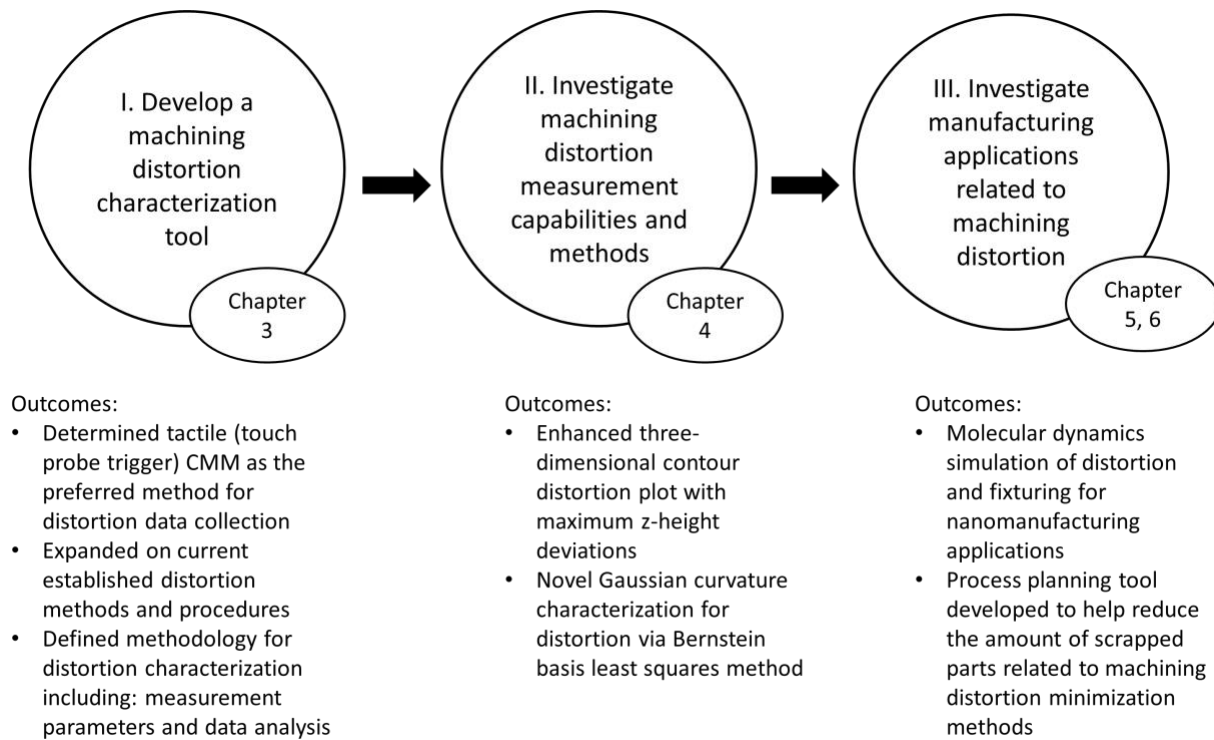


Figure 77 Schematic of dissertation objectives and outcomes

The first initial routine for characterizing machining distortion, presented in Chapter 3, provided preliminary research into the distortion characterization domain including data collection methods and procedures. An experimental design was carried out to investigate machining distortion of aerospace sample blanks taken from the same quenched material bar but extracted from different sections of the bulk material – top, middle, and bottom. The distortion method used to characterize the distortion present in the 3 samples showed that the top and bottom blanks (extracted with a similar RS profile) exhibited similar deformations. The middle sample, extracted from the center of the block, displayed dissimilar distortions compared to the other samples. This initial work relied on information that distortion is heavily, and almost entirely, influenced from bulk residual stresses present in the initial material. Presenting the distortion as a clearly defined method of z height deviations from a pre and post difference in surface data collection helped project future distortion collection methods to a three-dimensional method. Displaying the 3D profiles of the distortion in addition to the midlines in

both x and y directions, provided more information about the overall complex distortion present in the samples.

Expanding on the initial machining distortion characterization routine, an updated and optimized method for characterizing distortion involving Gaussian surface curvature is implemented in Chapter 4. Distortion literature vaguely defines distortion as the deviation of the shape change from the original intent, after being released from a fixture. This definition leaves the researcher to calculate the shape change deviation under open and loose terms. Distortion has been described in many ways including a single max scalar value, a single curve, collection of curves along the mid-length of the sample, 3-dimensional uniform spaced coordinate data, etc. From initial investigation of characterizing machining distortion, it is observed that distortion is a complex feature. Therefore, using three-dimensional transferable methods to characterize machining distortion is needed and presented in Chapter 4. Using the Bernstein basis function as a means for solving a least-squares problem to create a grid of control points to further assess Gaussian curvature is shown as a novel way to characterize overall complex shape deviation and distortion. The degree of the surface, d , is kept small for extracting the overall relative surface shape. A detailed study in which the degree of the surface is investigated for various complex distorted surfaces is needed. Furthermore, using this method of metrological characterization of machining distortion using Gaussian surface curvature as input data information for simulation prediction and control methods can prove useful in controlling and minimizing overall distortion in various industries.

This dissertation includes two case studies in which distortion was further investigated including nanoscale machining distortion (Chapter 5) and more broadly related to process planning and scrap minimization (Chapter 6). Through the work of researching nanomachining related to work holding devices, simulations gave insight into critical stress concentrations being directly related to the fixture

at such small scales. In addition, the molecular dynamics (MD) simulations of single grain pure aluminum in a vice fixture for Nano manufacturing applications showed that residual stresses formed could be related to the local generation of plasticity in the material. The local plasticity that resulted from this study led to inhomogeneous residual stress distributions on a symmetrical workpiece. The MD simulation gave insight into machining distortion at the nano scale.

The process planning tool case study from Chapter 6, provided an opportunity to investigate process chains and specific sustainability indicators for manufacturing optimization. Traditionally, process planning decisions are mainly based on manufacturing costs and product quality. This chapter developed a tool to compare different process chains with regard to selected sustainability indicators, such as energy or waste from scrapped parts. Non-value adding steps such as quality control and different transportation methods are included. The process planning tool is explained with a case study in which different sustainability indicators are implemented. Common manufacturing processes are chosen such as milling, sawing, drilling, and sanding, with a distortion/shape error measurement with a caliper instrument as a quality control/distortion check. A simple Matlab code allows engineering students and researchers to determine scrap, costs, time and energy for the different case scenarios for process management or engineering education. This case study fosters students and researchers to understand manufacturing from a sustainability standpoint comparing cost, time, energy and scrap.

7.2 Future Research

Although these research contributions for machining distortion can be used to help in the minimization and control work of deformation, machining distortion research is still a large and ongoing effort. More research into materials characterization techniques for machining distortion samples can be explored.

This research explored specific cases of machining distortion with specific methodologies from the experimental design. More work is needed to investigate the complex shapes and residual stress distributions for both experimental and analytical results. Prismatic shapes were studied for their simplicity and representation of aerospace components. Future work is needed to study other complex parts and geometries for distortion. In addition, there are numerous external factors to directly relate to distortion efforts including thermal effects, scaling effects, bulk v. machining induced RS, clamping mechanics, machining factors, materials factors, tool path optimization, etc. Future work on expanding and refining the overall characterization process is also needed as the field of mechanical engineering is ever changing – as are manufacturing demands and needs. More work is also needed on using the parameters from the curvature analysis for characterization and input for distortion minimization. Future work is needed using Gaussian curvature characterization to expand the distortion results to show surface curvature symmetries, curvature percentages of both positive and negative curvatures, and distinct characterization Gaussian shapes for different distorted parts.

More work is needed in the area of distortion at the nanoscale. Scaling effects can be investigated to help both the macro distortion and nano distortion domains. Future MD simulations incorporating material defects, grain boundaries, multiple grains, dislocations, etc. are needed to understand the applicability of using nanomachining simulations to understand macro machining. More work related to clamping mechanisms at the nanoscale are needed to understand the critical effects contact has at small scale geometries. Distortion at the nanoscale can provide key insight into macro deformations and distortions caused by residual stresses. Nanomanufacturing and MEMS applications have high impacts of warpage and deformation, and more research into machining distortion at these levels are useful for overall distortion research.

The process chain presented can be further reformed to investigate other sustainability indicators and areas such as worker quality, manual labor, residuals of machined parts, batch sizes, manufacturing processes, various industries, number of operations, tradition v. nontraditional manufacturing operations, etc. For expanding the process chain model, more data on both UMP and AP are needed to examine further process chains and their interactions on sustainability indicators.

A standard method of machining distortion characterization should be created for universal and uniform research actions. A robust and transparent way to fully characterize machining distortions is necessary to advance this area of manufacturing. Machining distortion minimization through experimental and analytical results are an enduring effort globally. Through this work, and the proposed future work for this research, machining distortion can one day be controlled – in place of being minimized, reworked, or scrapped.

Appendix

I. TUK Distortion Data – Technical University of Kaiserslautern

The following figures (Figure 78 – Figure 92) show in distortion results from experiments conducted at the Technical University of Kaiserslautern, Germany.

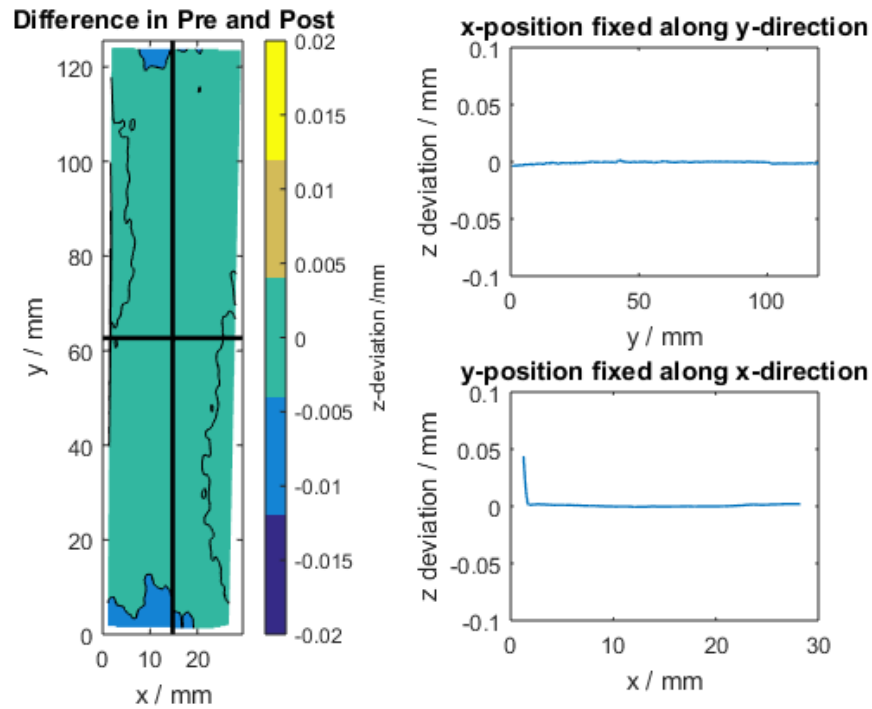


Figure 78 Top sample distortion shown for TUK experiment 2

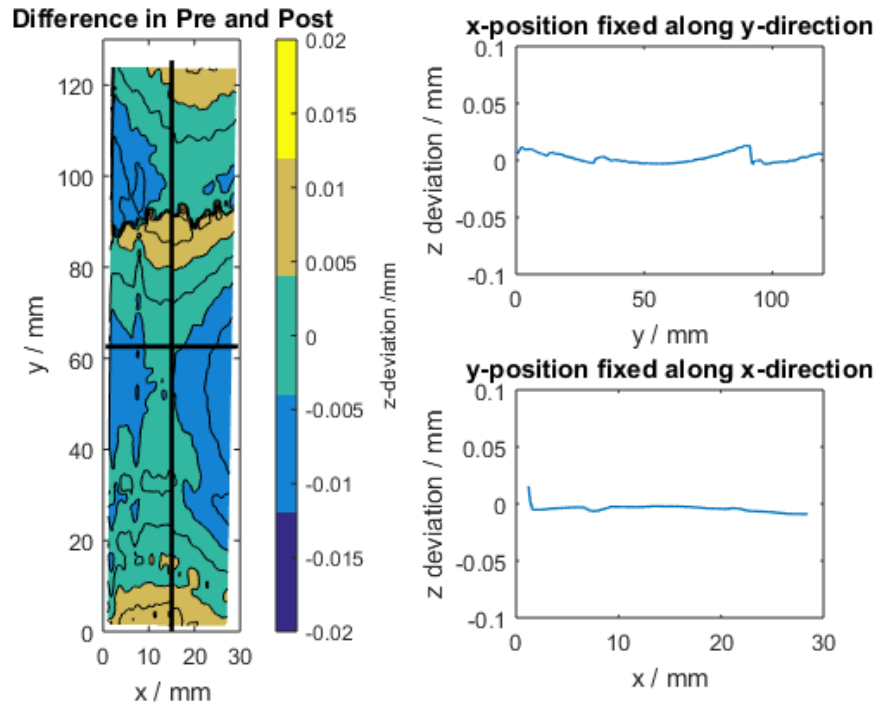


Figure 79 Middle sample distortion shown for TUK experiment 2

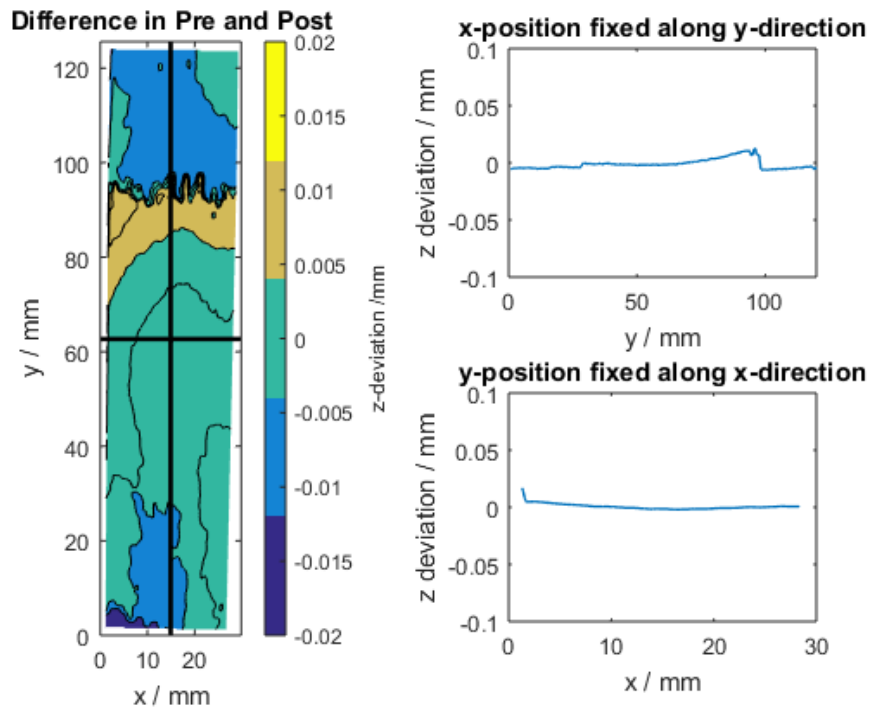


Figure 80 Bottom sample distortion shown for TUK experiment 2

Efforts to re-scan the data using other qualified measurement CMM have not been investigated. Future work to rescan these samples is needed. TUK data was investigated for both pre and post data and the results are presented below. These results instead reflected CMM metrology tool capabilities and methodologies.

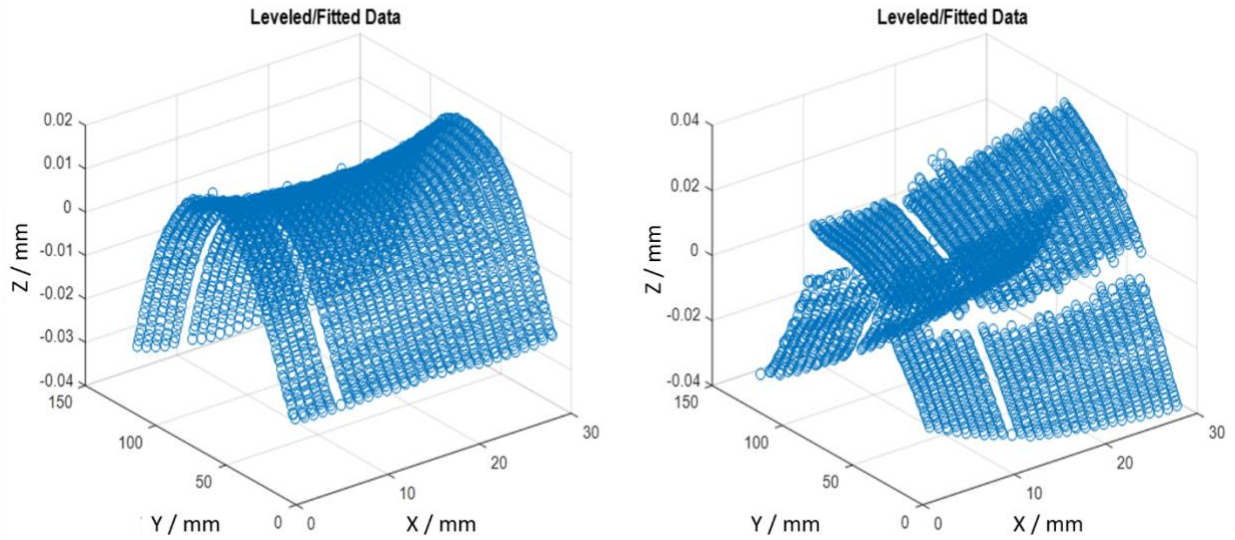


Figure 81 Reference surface datum from the pre (left) and post (right) for the top sample of TUK experiment 1

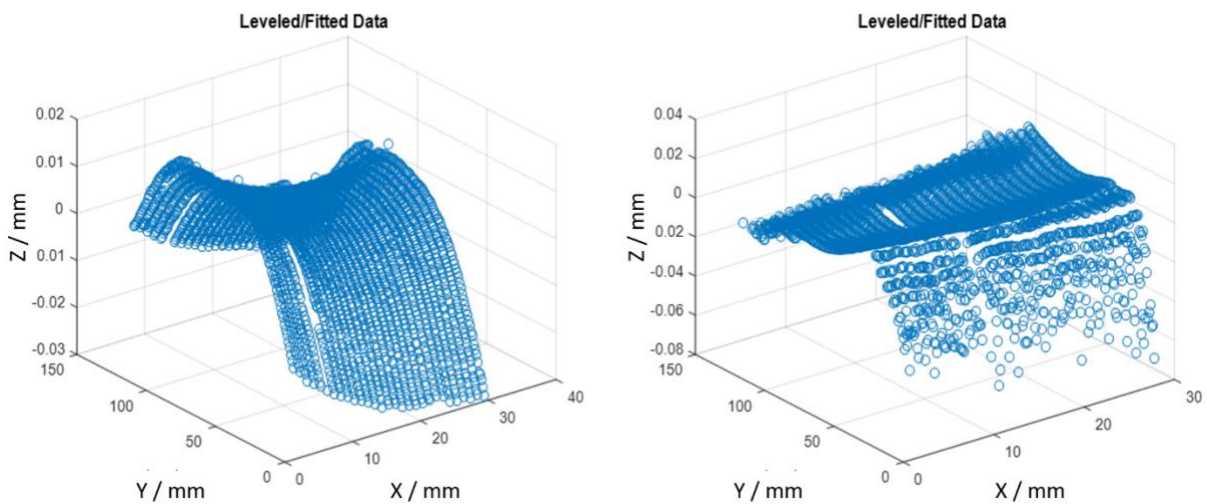


Figure 82 Reference surface datum from the pre (left) and post (right) for the middle sample of TUK experiment 1

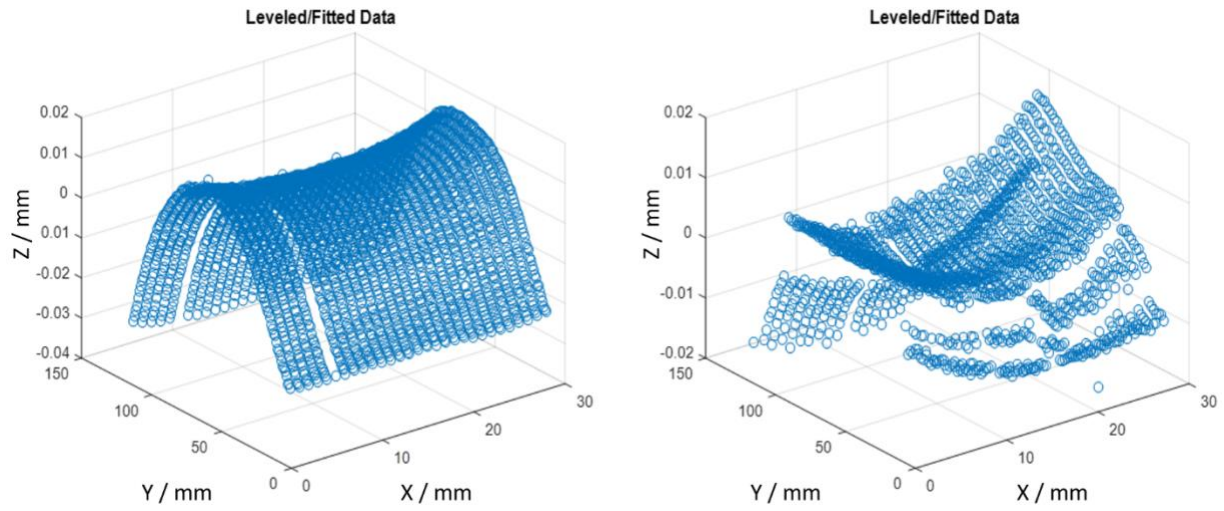


Figure 83 Reference surface datum from the pre (left) and post (right) for the bottom sample of TUK experiment 1

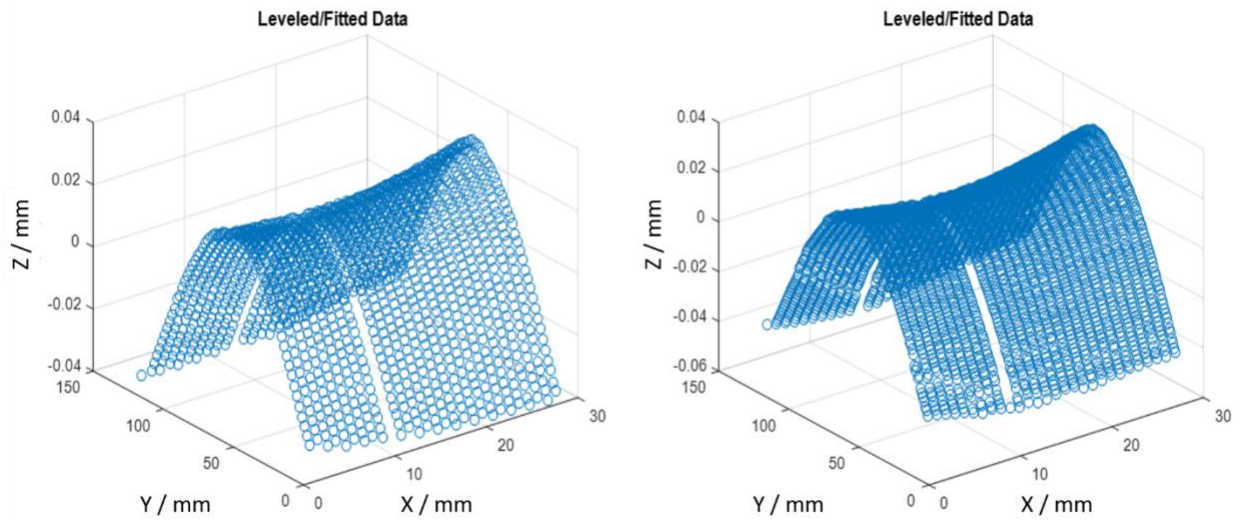


Figure 84 Reference surface datum from the pre (left) and post (right) for the top sample of TUK experiment 2

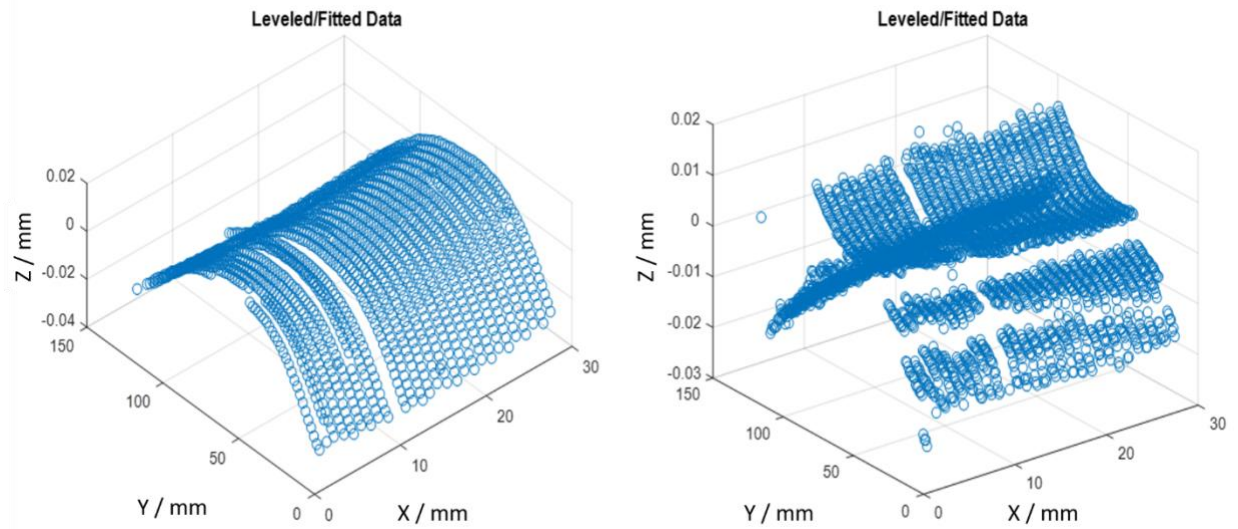


Figure 85 Reference surface datum from the pre (left) and post (right) for the middle sample of TUK experiment 2

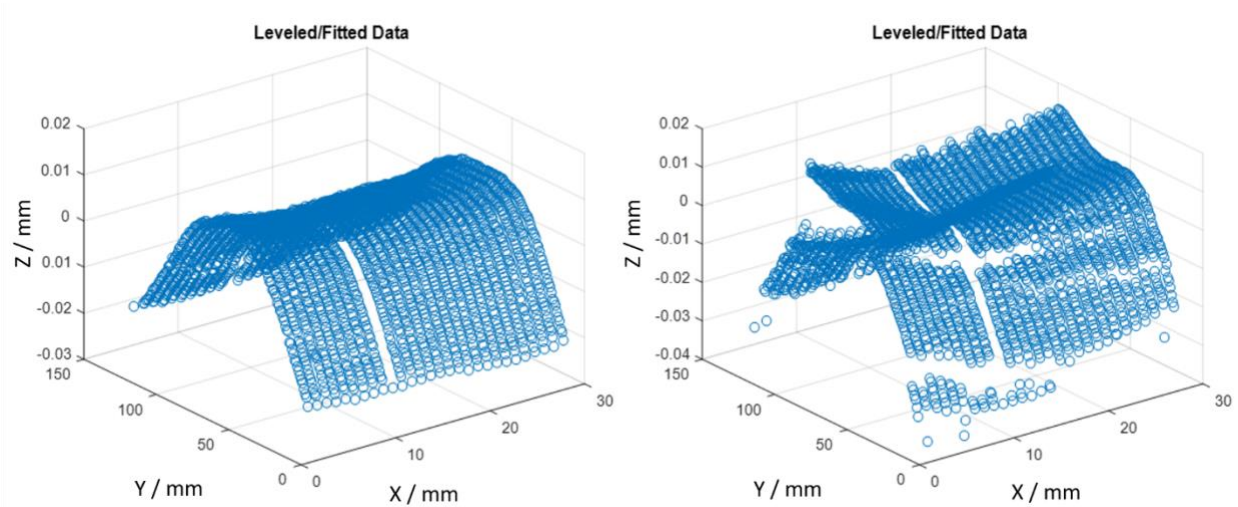


Figure 86 Reference surface datum from the pre (left) and post (right) for the bottom sample of TUK experiment 2

The post results for all the TUK samples, excluding the post top sample from TUK experiment 2, had data that was compromised during the scanning process using the Micro-Hite DCC 3D CMM. Possible scanning errors for the Micro-Hite DCC 3D CMM post measurements include the sample not being properly secured, resulting in movement during the probe engagement. While the exact

determination for the compromised data is unknown, the post results give insight into metrological equipment, setup, and their technical capabilities.

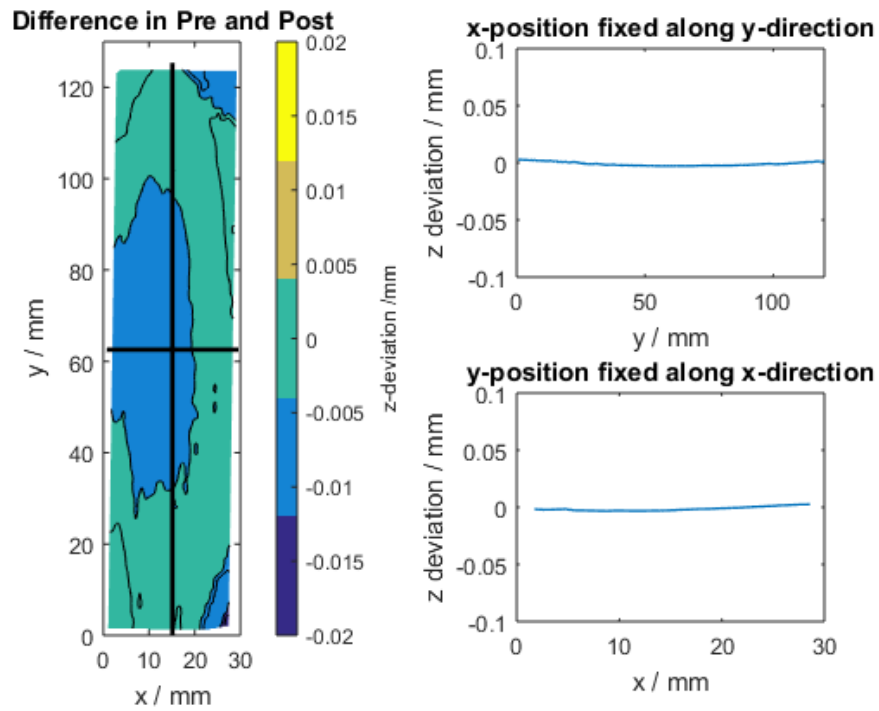


Figure 87 TUK Experiment 3 top sample distortion results

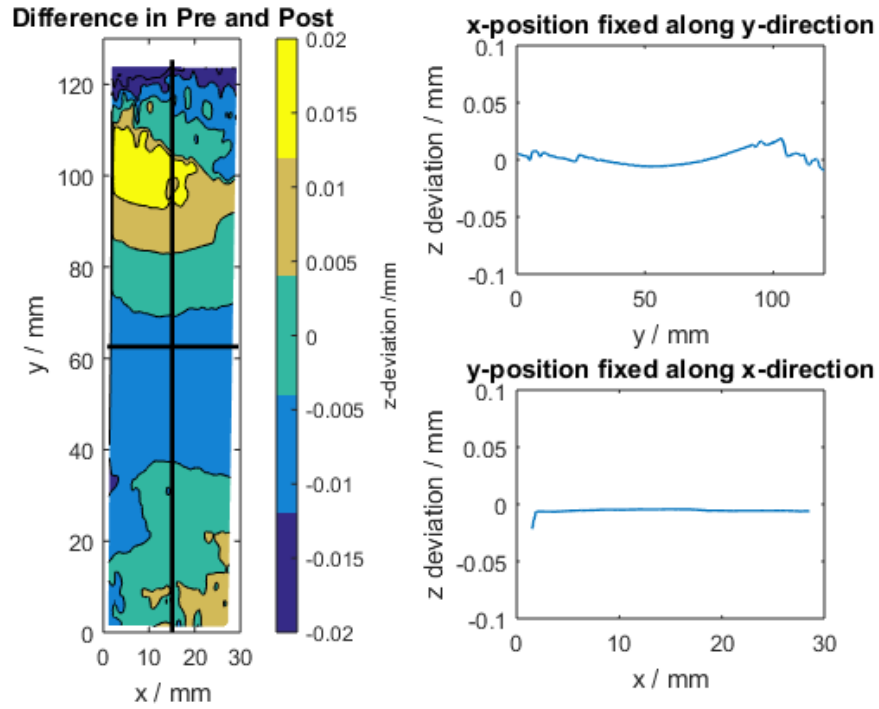


Figure 88 TUK Experiment 3 middle sample distortion results

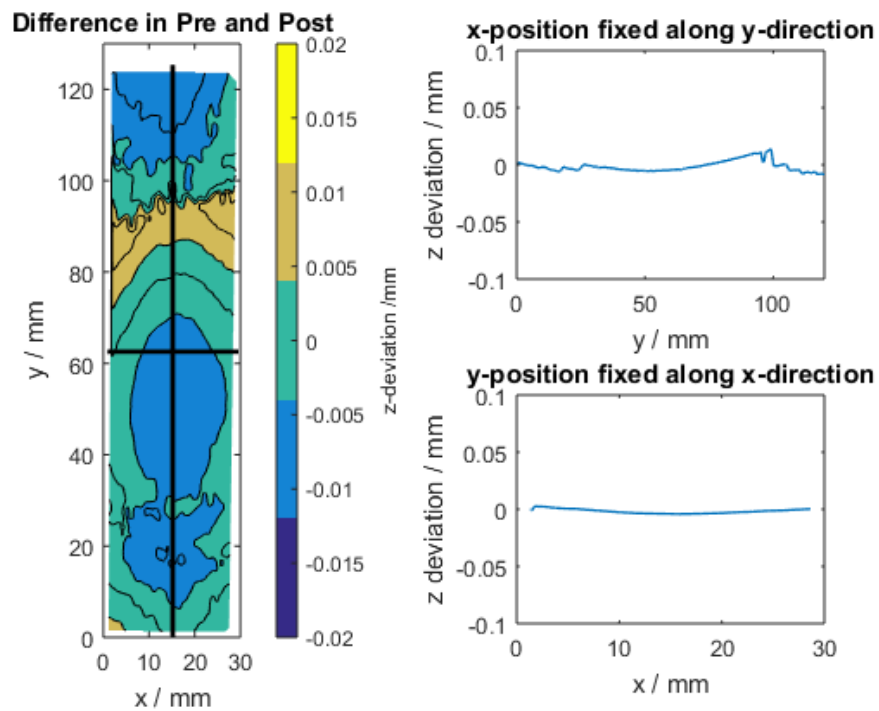


Figure 89 TUK Experiment 3 middle sample distortion results

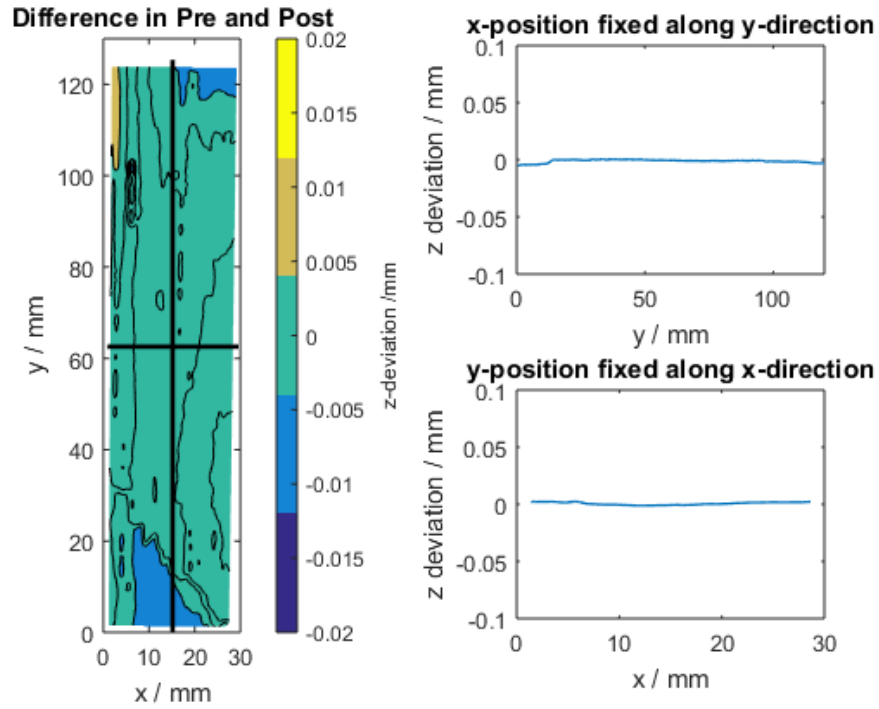


Figure 90 TUK Experiment 4 top sample distortion results

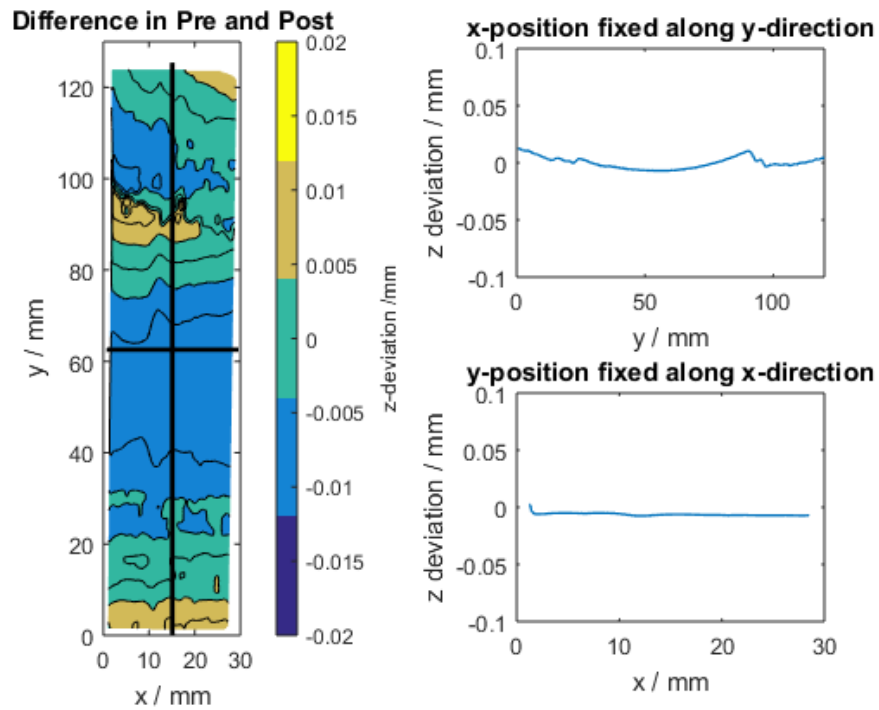


Figure 91 TUK Experiment 4 middle sample distortion results

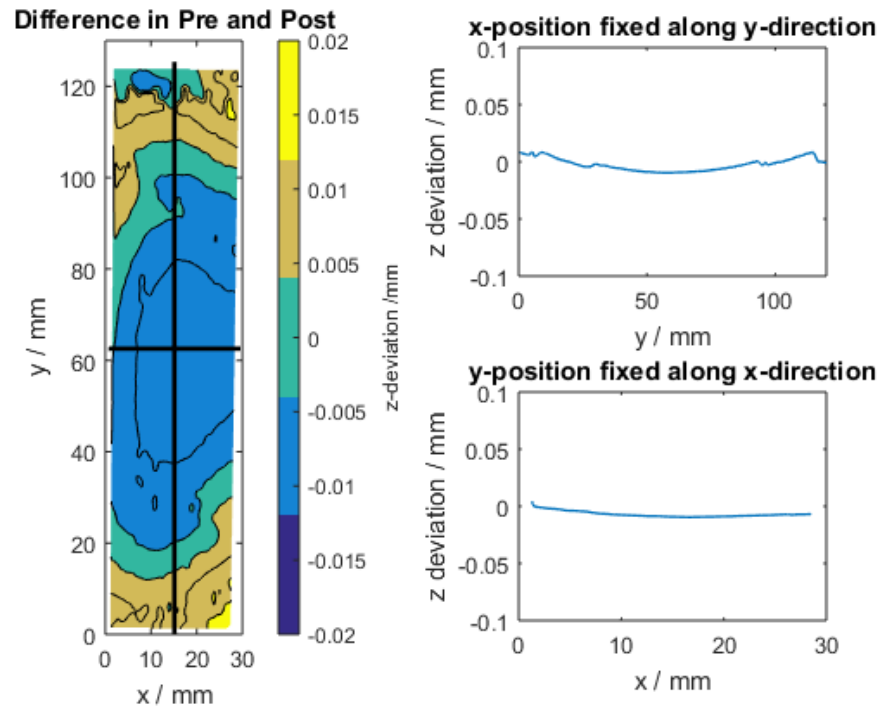


Figure 92 TUK Experiment 4 bottom sample distortion results

II. Preliminary Distortion Data Collection Methods

Preliminary research provided several means of collecting distortion data including distortion analysis via dial indicator in between cutting passes of the milling process and using a Faro Arm Edge CMM to measure the deviation of a sample from the scanned plane to the CAD plane. Another method for collecting distortion data was purposely distorting aerospace material in an attempt to measure surface structures that resembled bent and twisted beam samples. While these methods seemed straightforward, they created more work in extracting the final overall distortion of the sample pieces.

A. Dial Indicator Deflections

Initial distortion data is presented as a difference in pre and post datum as seen in Chapter 3. After TUK experiments, this method introduced subtraction complications from inconsistent quality data. A method of collecting distortion data in-line using a dial indicator for aerospace samples was implemented as seen in Figure 93.



Figure 93 A dial indicator is used to measure deflection of thin walled aerospace workpieces in between milling passes at designated constant incremental locations



Figure 94 A front view of a dial indicator is used to measure deflection of thin walled aerospace workpieces

Distortion, or deflection from using the dial indicator was extremely time consuming and tedious. The results show changing deflections with each pass, as seen in the Figures below.

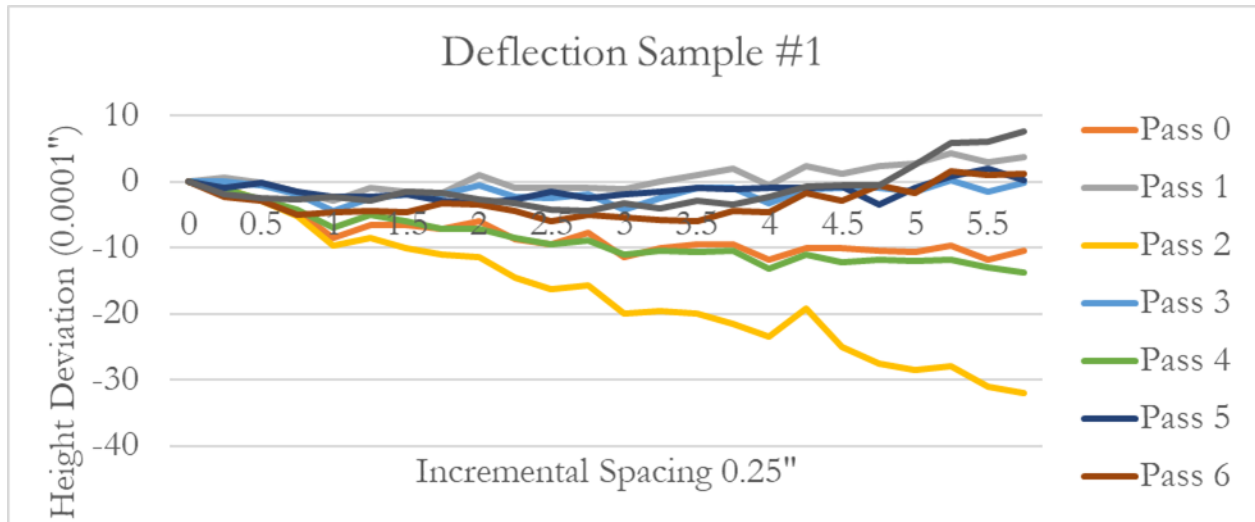


Figure 95 Height deviation collected via dial indicator for sample #9

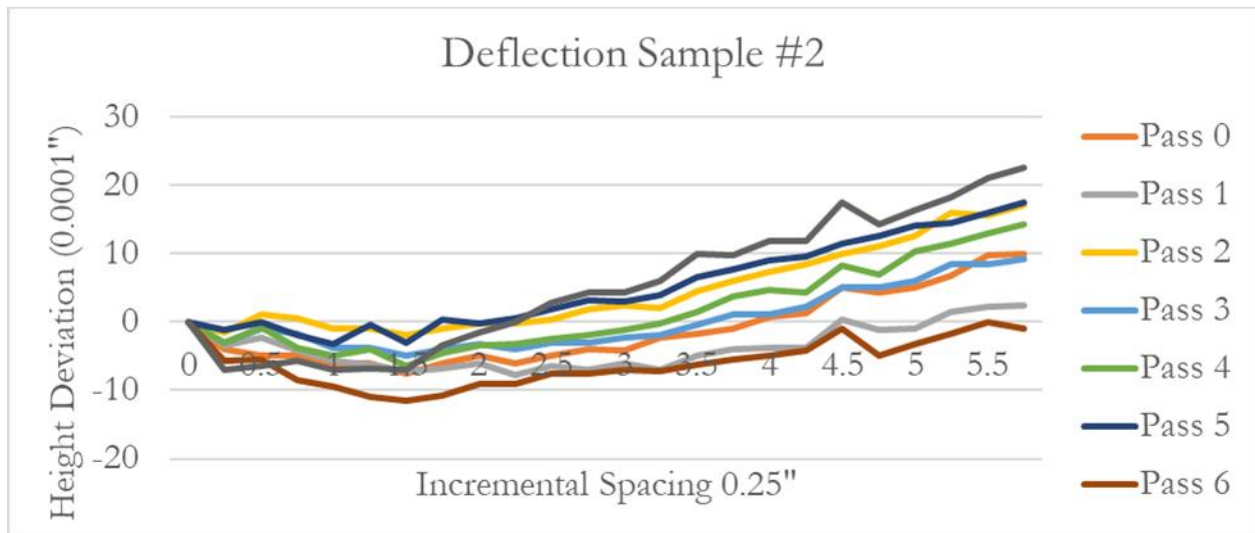


Figure 96 Height deviation collected via dial indicator for sample #24

The deflection results show initial deflection in the samples as well as changing deflections after each pass. The distortion potential changes after each pass, and comparing incremental passes resulted in deflections varying in both directions compared to the initial pass 0.

B. Dial Indicator Central Lines

Another method for collecting distortion was 3 central lines along the bottom edge of a milled sample before and after each cutting pass starting at 0: no machining and ending at 7: last pass. This method also demonstrated to be tedious and extremely time consuming and distortion data was complicated to extract easily. The legend on the plots refer to lines 1, 2 and 3 respectively.

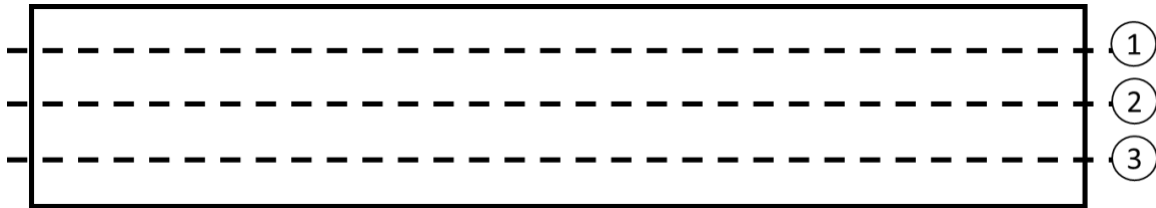


Figure 97 Distortion data collected at 3 different midline locations (lines 1, 2, and 3)

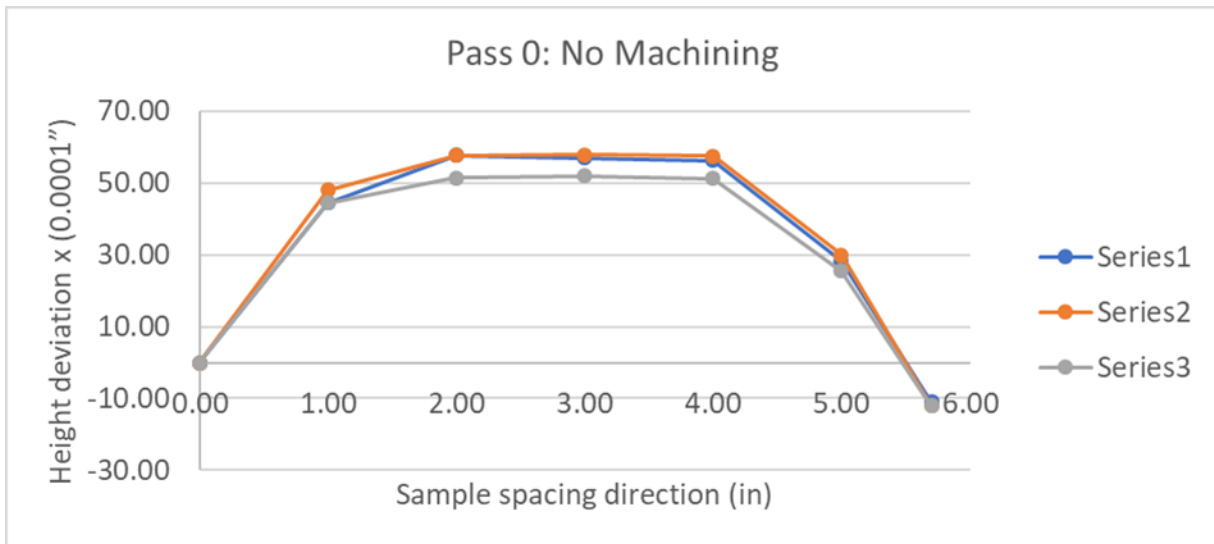


Figure 98 Three central distortion lines taken along the length of the sample for pass 0

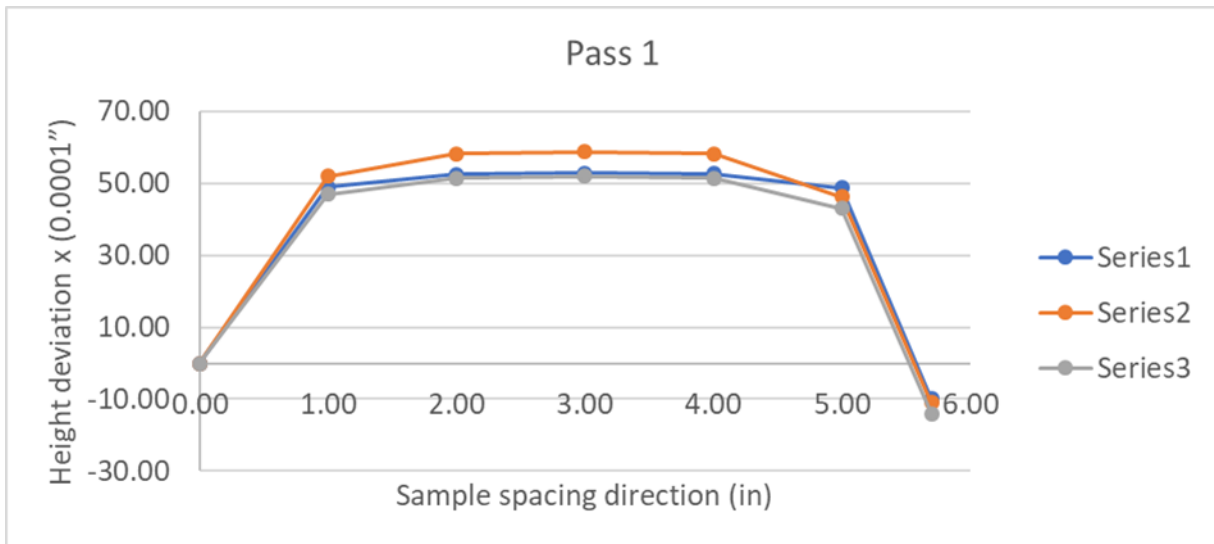


Figure 99 Three central distortion lines taken along the length of the sample for pass 1

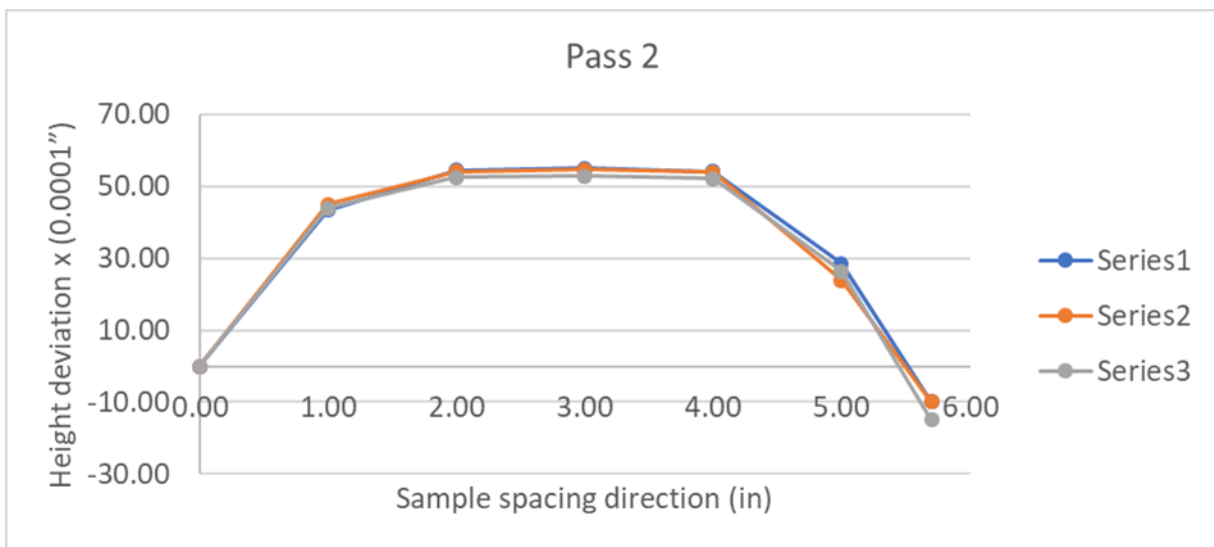


Figure 100 Three central distortion lines taken along the length of the sample for pass 2

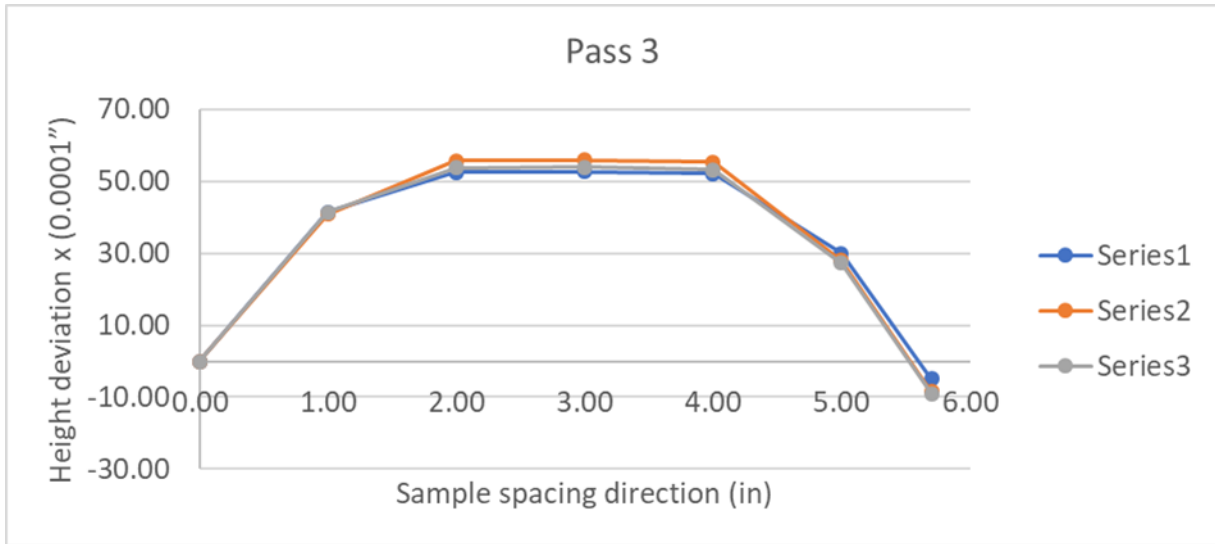


Figure 101 Three central distortion lines taken along the length of the sample for pass 3

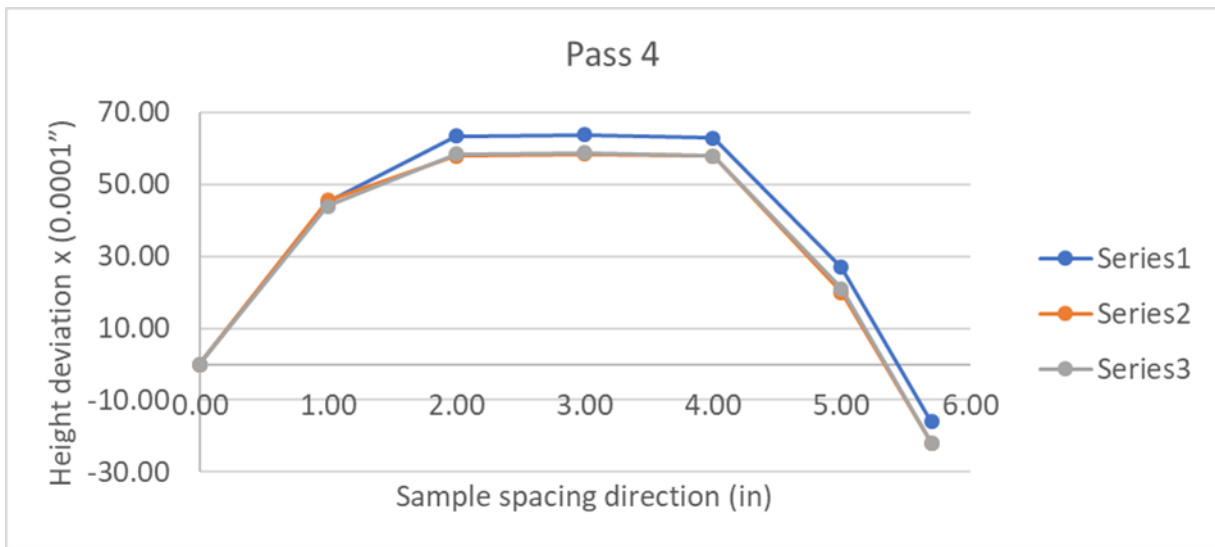


Figure 102 Three central distortion lines taken along the length of the sample for pass 4

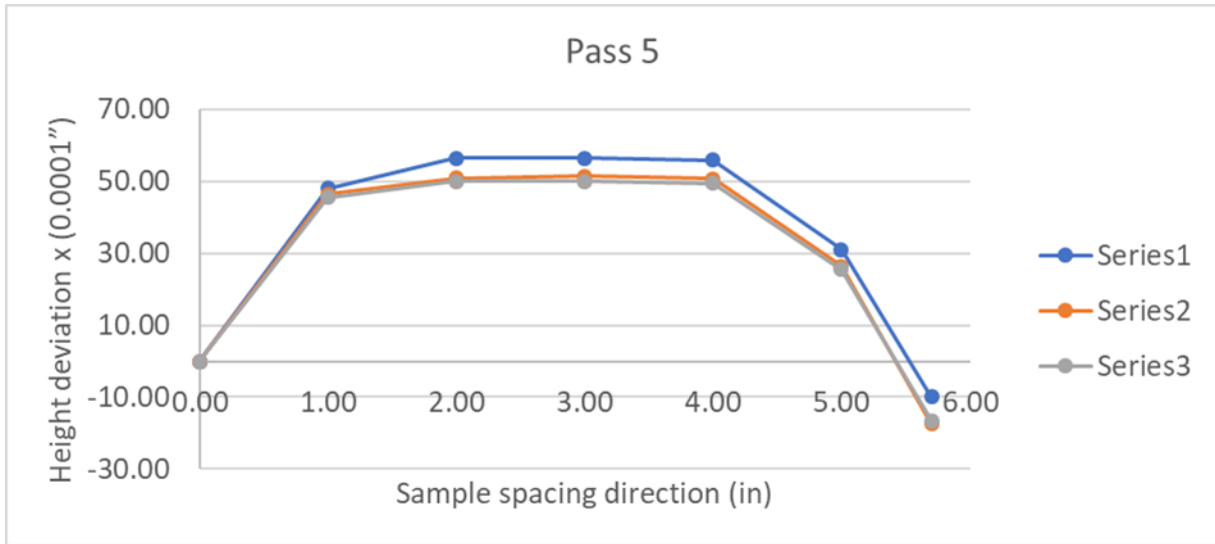


Figure 103 Three central distortion lines taken along the length of the sample for pass 5

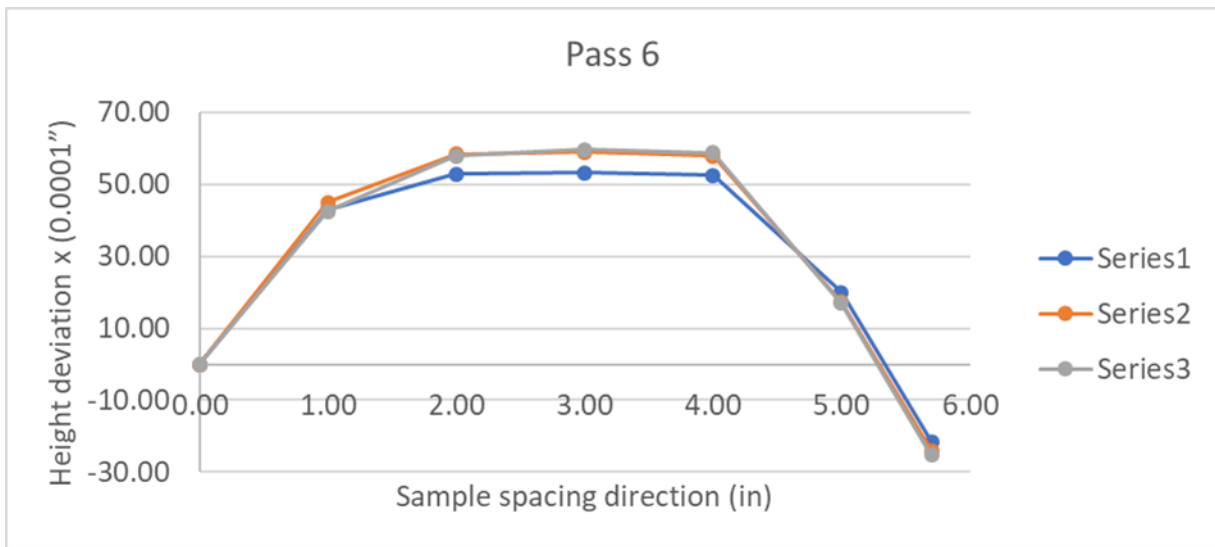


Figure 104 Three central distortion lines taken along the length of the sample for pass 6

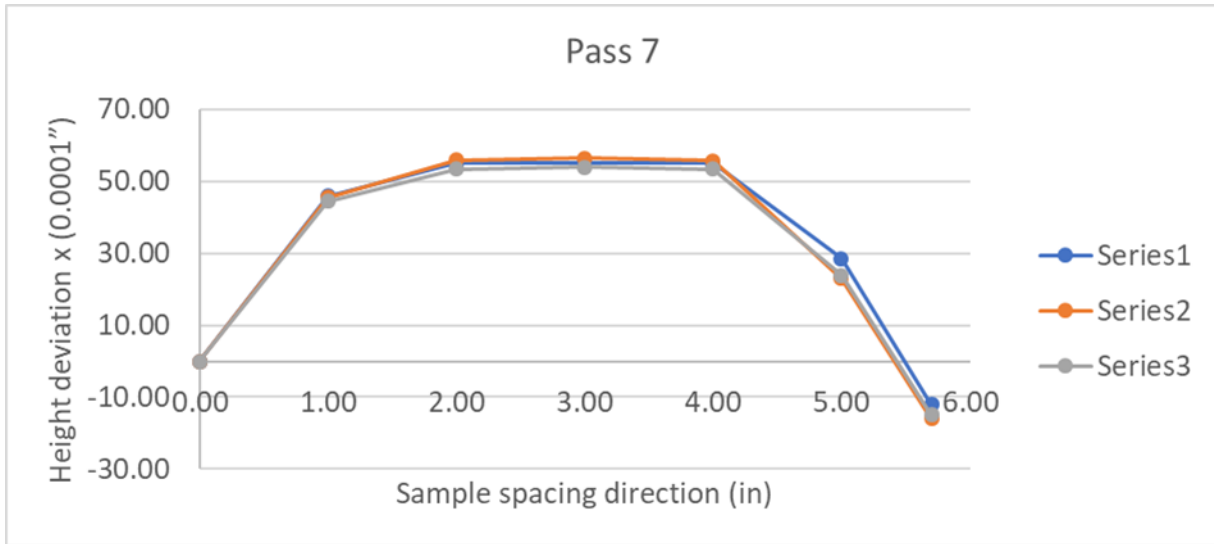


Figure 105 Three central distortion lines taken along the length of the sample for pass 7

The data from these 7 passes show consistent deflections at each location on the bar. This method was tedious and time costly. A more robust method to collect distortion at precise locations is needed.

C. Calculating Distortion Using a Faro Arm Edge CMM

Another method implemented for assessing the distortion was using a Faro Arm Edge optical and tactile combination CMM at the Engineering Student Design Center (ESDC) at the University of California Davis. The Faro Arm was able to probe the sample surface and calculate the deviation between the actual part CAD model and the scanned plane, as seen in Figure 106 and Figure 107.

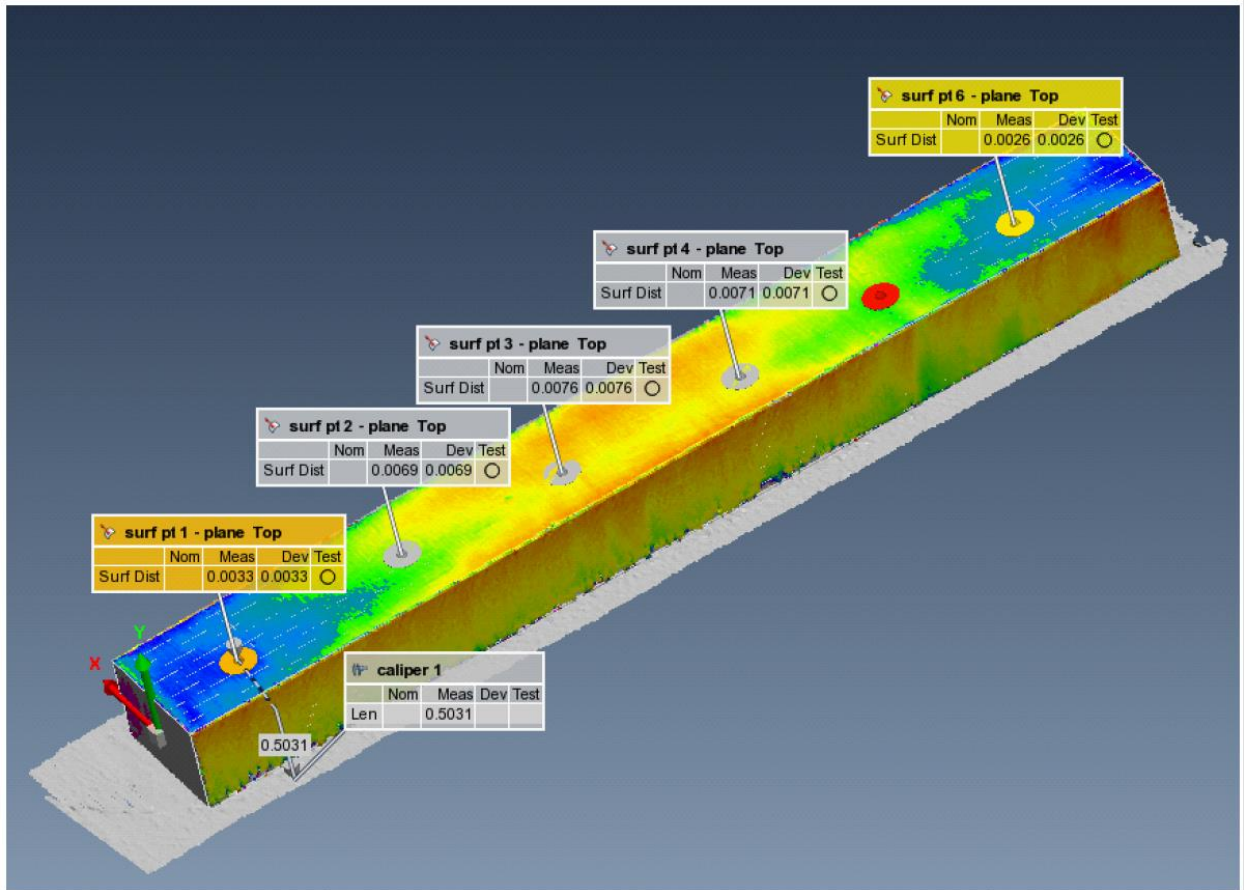


Figure 106 Probe feature from the Faro Arm Edge calculated the deviation between scan and CAD

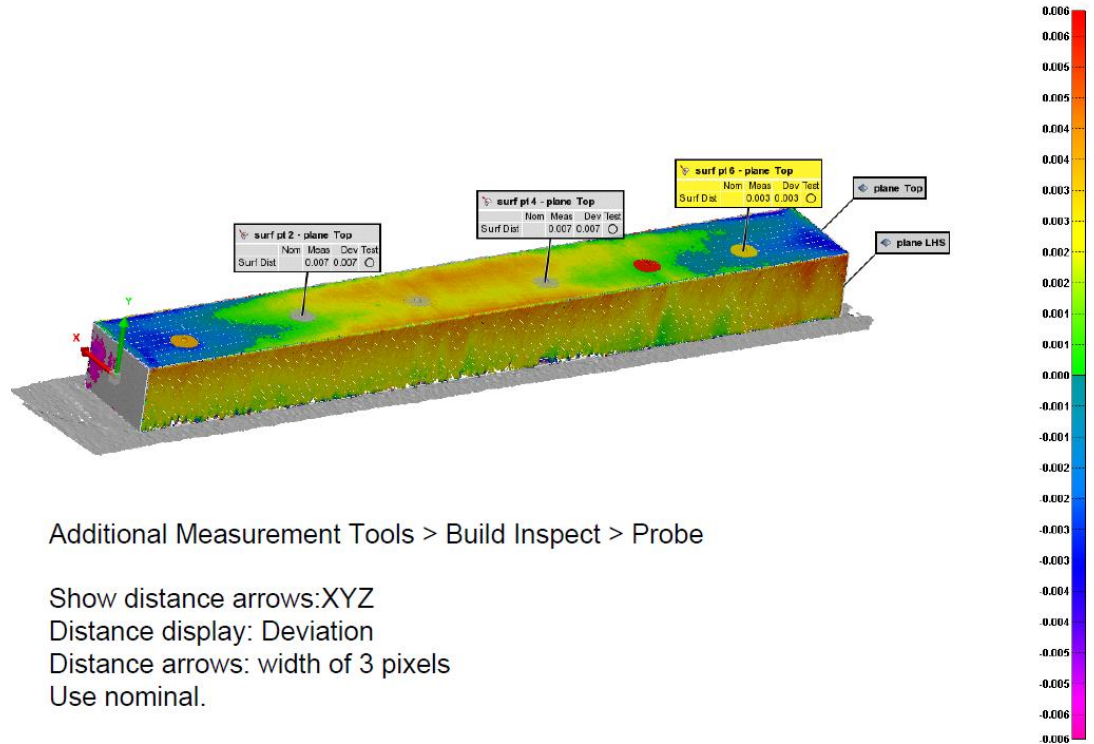


Figure 107 Probe features from the Faro Arm Edge display the deviation from scanned surface and CAD model

Another measurement method from the Faro Arm CMM allowed the user to create standard calipers to measure points along the surface of the part and also the reference scanning precision table. The caliper method was complicated in that the program could not find a nominal value, or a measurement to compare the caliper measurement to, which ultimately disabled the ability to use the table as a reference. Another issue with this method was manual probing to the sample to create a straight line proved imperfect.

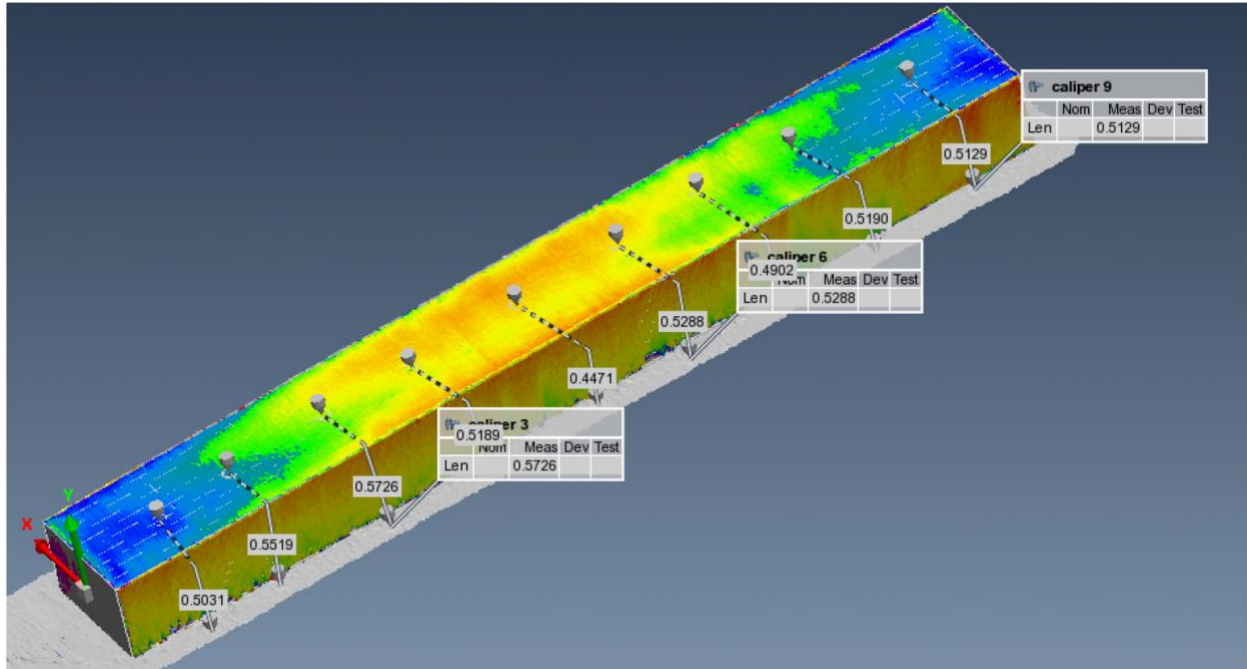


Figure 108 Standard Caliper tool features from the Faro Arm Edge provided displacement values of the surface to the CMM table

Another tool from the Faro Arm Edge was the Surface Comparison Points feature in which the method measures the deviations of the scan from the CAD planes and aligns the plane and plane measurements to compare.

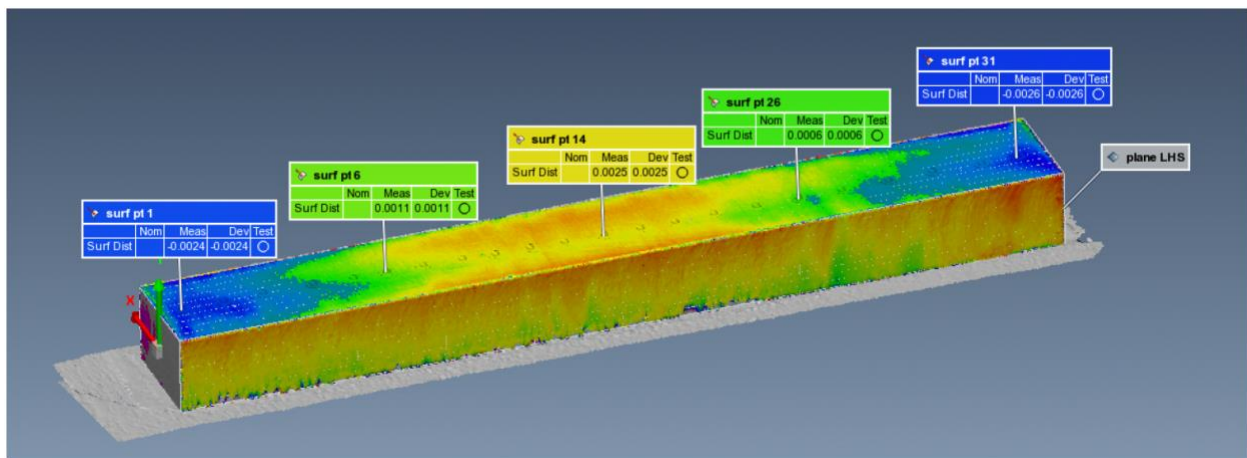


Figure 109 Distortion values from the CMM table plane are calculated using Create Surface Comparison Points on the Faro Arm Edge CMM

The last method investigated using the Faro Arm Edge was the Surface Comparison Points using a sample grid. This method measures, in regular intervals, the deviation of the scanned surface to the CAD plane. This method was relatively easy to implement, and the information extracted for distortion was interesting as seen in Figure 110 and Figure 111. The downside of this method was collecting the surface deviation values from the software, as it printed a PDF with the table, instead of a user-friendly file download.

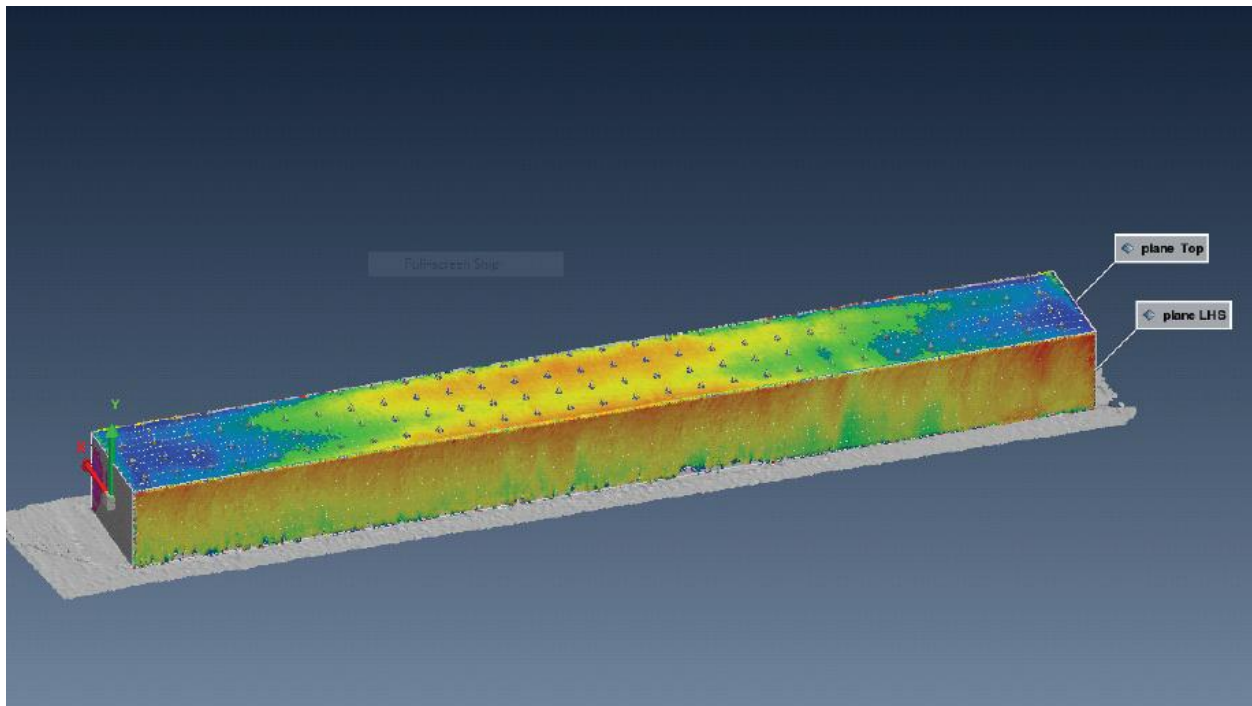


Figure 110 Display of the sample grid used to measure deviations from the CAD surface

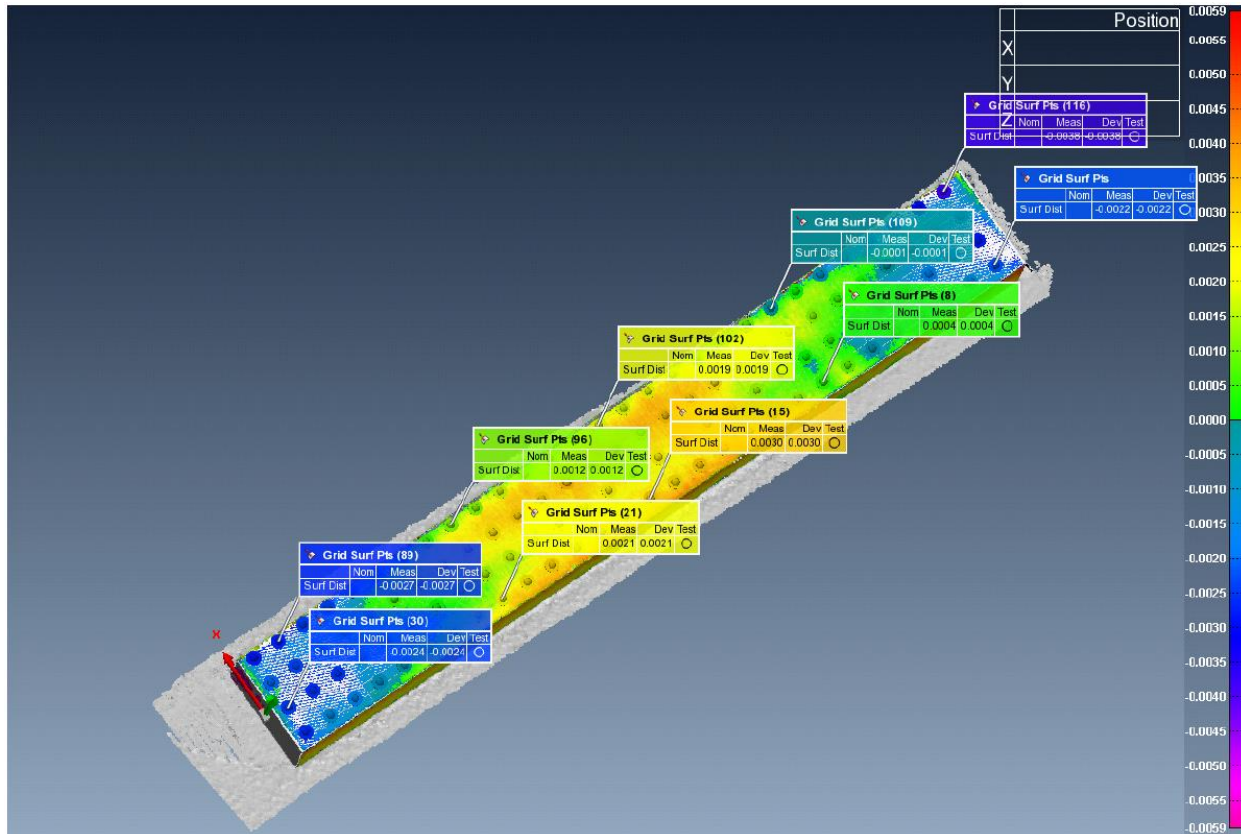


Figure 111 Selected points and their respective deviation value from the CAD model using a Faro Arm Edge CMM Software

Another complication of this method was the data extracted from the PDF with the comparison table only provided the spatial points as point numbers instead of coordinate values (x, y, and z) as seen in Figure 112.

Comparison Point Table

Units Inches
Coordinate System world
Data Alignments best-fit to ref 5
Linked Objects Original Sample.IGS

















Name	Control	Nom	Meas
 Grid Surf Pts	Surface Distance		-0.0022
 Grid Surf Pts (2)	Surface Distance		-0.0012
 Grid Surf Pts (3)	Surface Distance		-0.0010
 Grid Surf Pts (4)	Surface Distance		-0.0007
 Grid Surf Pts (5)	Surface Distance		-0.0002
 Grid Surf Pts (6)	Surface Distance		-0.0005
 Grid Surf Pts (7)	Surface Distance		0.0009
 Grid Surf Pts (8)	Surface Distance		0.0004
 Grid Surf Pts (9)	Surface Distance		0.0013
 Grid Surf Pts (10)	Surface Distance		0.0014
 Grid Surf Pts (11)	Surface Distance		0.0023
 Grid Surf Pts (12)	Surface Distance		0.0028
 Grid Surf Pts (13)	Surface Distance		0.0030
 Grid Surf Pts (14)	Surface Distance		0.0027
 Grid Surf Pts (15)	Surface Distance		0.0030
 Grid Surf Pts (16)	Surface Distance		0.0027

Figure 112 A screenshot of the comparison point table created from the Faro Arm Edge software

D. Calculating Distortion from Purposely Induced Distorted Aerospace Samples

This distortion data collection method involved a methodology including procedures employed to induce bending and torsional distortions to three different identical aluminum 7050 grade samples. Of the three samples, one was purposely bent, one purposely twisted, and the third purposely bend and twisted altogether. The three samples can be seen in Figure 113.



Figure 113 Al 7050 samples with induced bending, twisting, and combined bending and twisting distortions

The approximate forces used for each sample is displayed in Table 11. The distortion was purposely induced using the facilities of the Engineering Student Design Center at the University of California Davis. A Dake Hydraulic press was used to induce bending into samples 14 and 22 Al 7050 samples as seen in Figure 114. Torsion was exerted on samples 10 and 22 using a vice and a Craftsman WF 1335 beam-style torque wrench as seen in Figure 115.

Table 11 Purposely induced distortion sample summary

Sample	Distortion	Forces Used
10	Torsion	135-foot pounds
14	Bending	0.149 tons
22	Bending and Torsion	135-foot pounds and 0.149 tons



Figure 114 A Dake Hydraulic Press is displayed exerting force on a distortion sample



Figure 115 A craftsman torque wrench is displayed exerting torsion onto a distortion sample

The results from this study display induced distortion into aerospace parts representing bending, twisting, and a combination of bending and twisting. The resulting samples suggest bending the samples is easier to implement than twisting. Nonetheless, all three samples were purposely distorted, and the qualitative results are seen in Figure 116. All in all, the method for inducing distortion to Al 7050 samples was successful. One comment for future investigation is to determine a twisting mechanism that exaggerates the distortion and does not damage the width of the part as seen in samples 10 and 22 in Figure 116.



Figure 116 All three samples are displayed after applying bending and torsion forces with top, middle, and bottom samples as 14, 10, and 22 respectively

The overall distortion results for the three samples was determined using a Mitutoyo Bright BRT 504 CMM with a 1 x 1 mm spacing scheme. The data was imported into Matlab and the distortion was calculated as the max z deviation – min z deviation of the resulting leveled surface plot. The results are displayed in the table below.

Table 12 Induced distortion results

Sample	Distortion	Maximum z-height deviation in mm
10	Torsion	0.2146
14	Bending	1.8691
22	Bending and Torsion	2.5200

E. Visuals for Purposely Induced Distortion using Matlab

Using a Mitutoyo Bright BRT 504 CMM, the distortion data is collected from the top plane of the purposely induced distortion sample using a 1 x 1 mm spacing in the x and y directions. The data from the CMM is imported into Matlab, where the data is fit to a linear plane and residual data (data minus fit) are displayed as contour and surface overall distortion plots. Further expansion to the distortion tool is presented in Chapter 4.

The distortion analysis for each purposely distorted sample via Matlab are presented below.

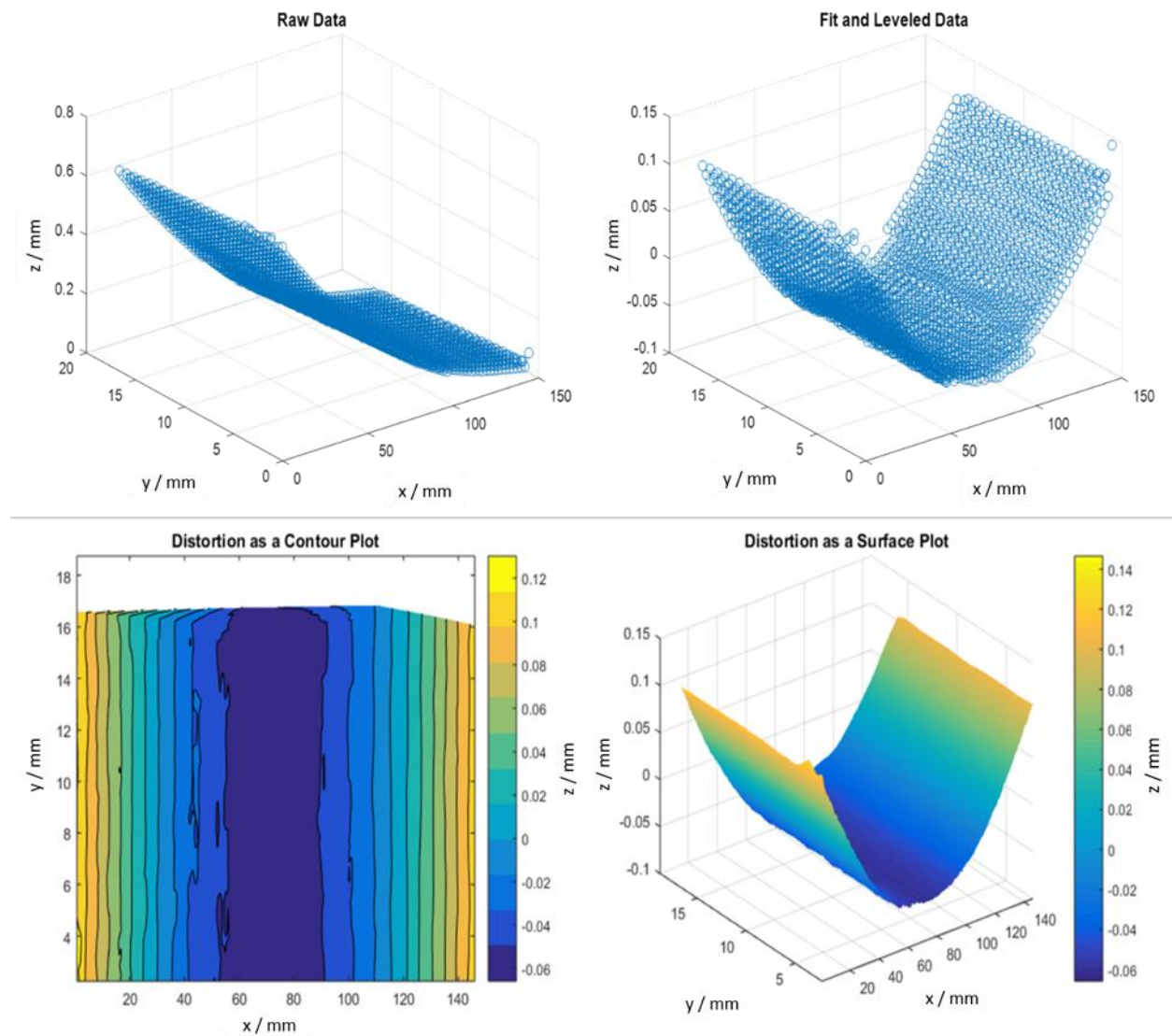


Figure 117 Distortion analysis and visuals for sample 10 torsion

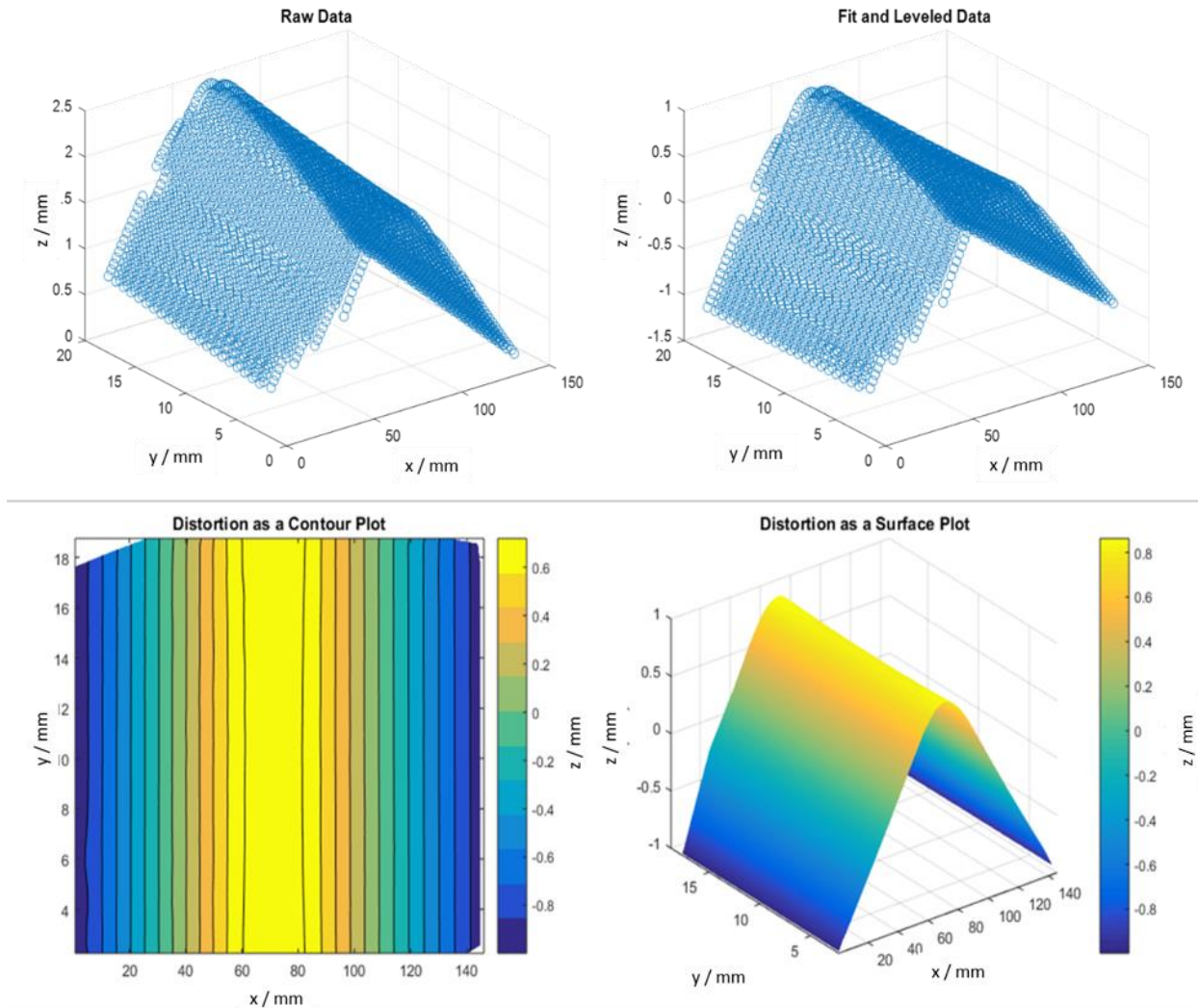


Figure 118 Distortion analysis and visuals for sample 14 bending

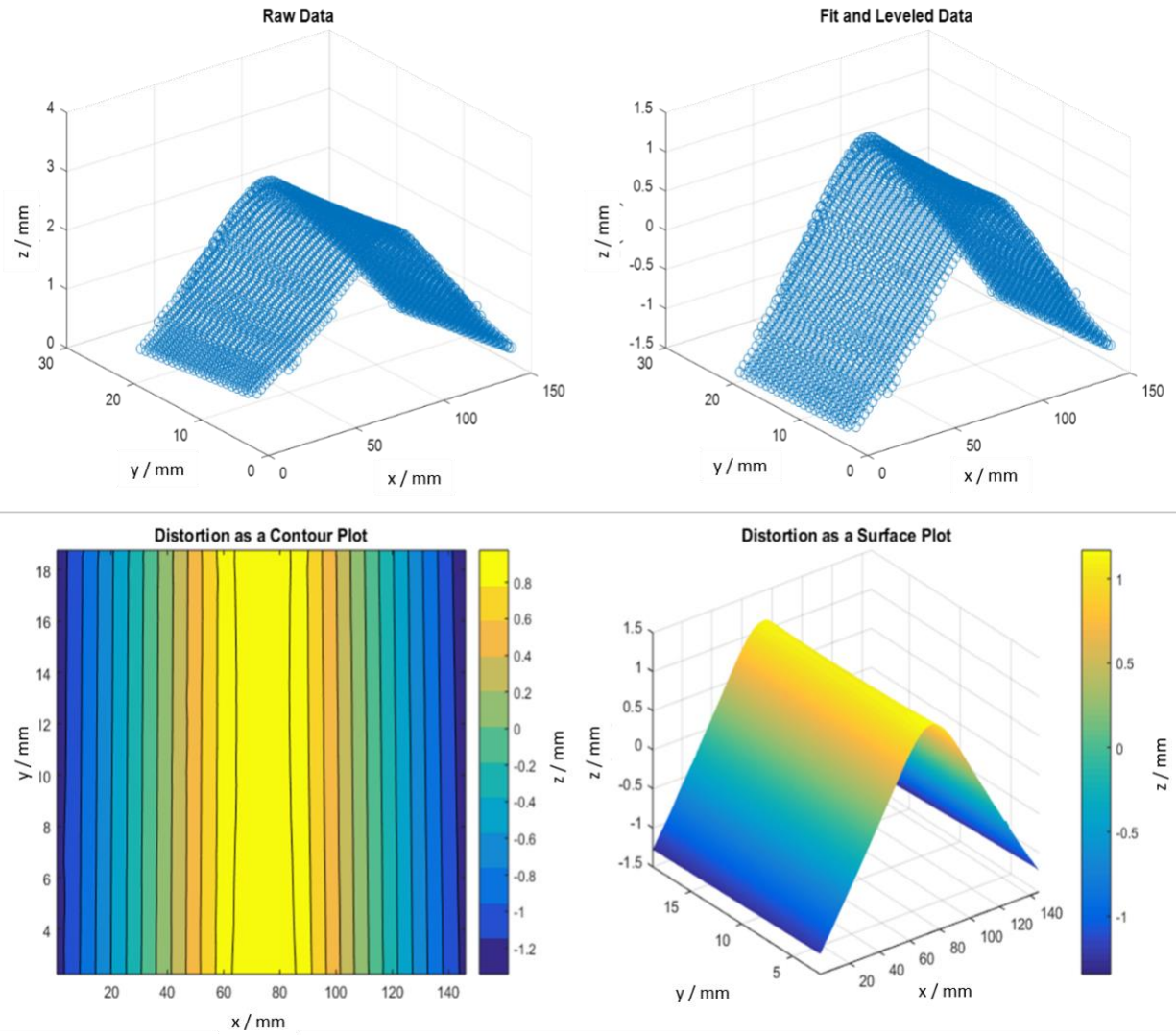


Figure 119 Distortion analysis and visuals for sample 22 combined bending and torsion

III. Distortion Collection Survey

A distortion measurement survey was shared and conducted in the research lab setting among 5 lab members and visitors (MASTeR Lab UC Davis). The distortion survey can be seen in the figure below.

Distortion measurement Pre-Survey

Name: _____

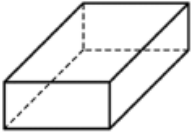
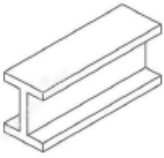
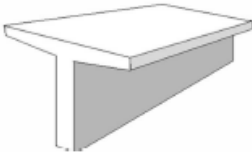
	Part	Description	How would you measure features of distortion?
1		Rectangular prism (EX: structural package)	EX: <ul style="list-style-type: none"> • Use a nominal geometry (one plane or multiple) to measure before and after • Flatness + Parallelism
2		I-beam (EX: structural support)	
3		T-beam (EX: structural support)	
4			

Figure 120 The distortion measurement survey collected individual responses of how they would measure a feature for distortion or deviations

For all three parts, many measurement methods were shared, including:

- Using nominal geometry or pre/post data
- Measuring flatness
- Measuring parallel-ness
- Measuring part thickness at various locations
- Measuring part thickness in every direction or orientation
- Measure the projected light for mapping data
- Measure angles fir perpendicularity
- Measure heights
- Use a dial gage with runner
- Use calipers to measure thickness
- Use a touch probe to measure height
- Use a “go-no-go” gage
- Compare to the CAD model
- Measure the straightness of the part
- Create a standardized part to compare to
- Use the negative freeform to measure the distortion

For part 4 of the survey, the lab member would think of his/her own part to determine distortion data. Some examples are included in the table below.

Table 13 Distortion survey collection for perceived distortion data collection methods for various parts

User Defined Part	Measurement Method
Any freeform shape	Negative free form Make a standard part Create a functional measurement vs. a geometrical measurement
A hip cup	Measure circularity Measure perpendicularity Measure the symmetry Measure the cup volume Measure the wall thickness at various locations
A hollow sphere	Use x-ray to measure distortion Measure magnetism
A hook	Use interferometry to measure deviation Create a CAD model to compare Measure concentricity of the hook
A knife or blade	Measure flatness

IV. Environmental Aspects of Coordinate Metrology

Environmental aspects with technical capabilities have not been discussed adequately for quality assurance. This study establishes a first unit manufacturing process (UMP) model for a selected quality assurance step – coordinate measuring machine (CMM).

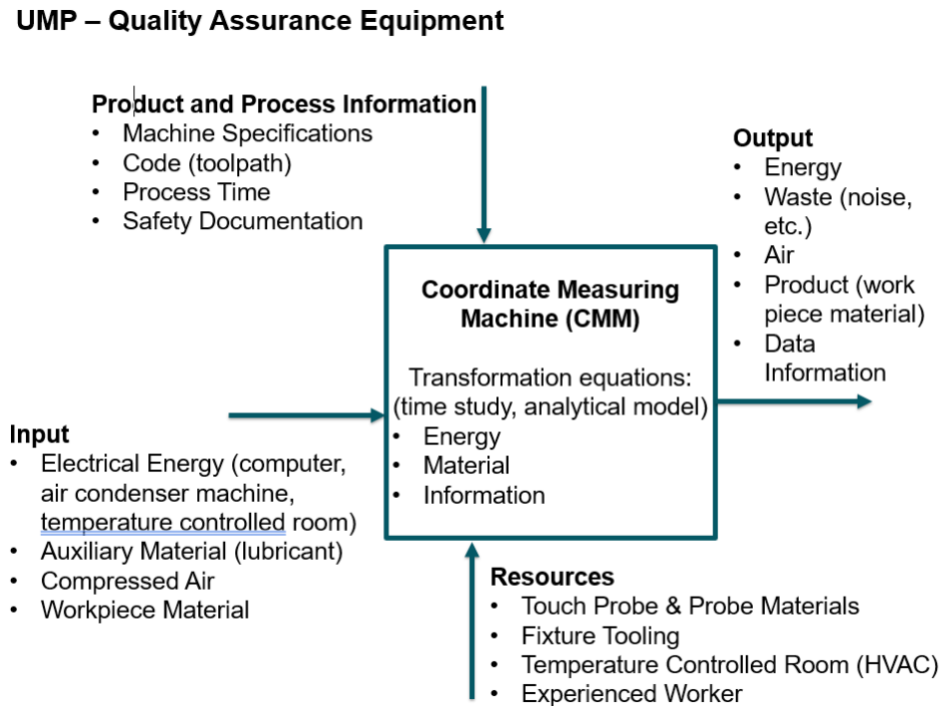


Figure 121 UMP for a quality assurance step – a coordinate measuring machine (CMM)

V. Faro Arm Edge Accuracy Measurements

Accuracy measurements were conducted on the Faro Arm Edge CMM using a 0.1” gauge block. The results are displayed below in Table 14. A total of 20 measurements were taken for the accuracy test using the preset standard data setting and another 20 times using the fine data setting.

Table 14 Accuracy measurements (20 measurements) from the Faro Arm Edge CMM

Accuracy Test Data	Fine Data Setting in inches	Standard Data Setting in inches
1	0.1013	0.1017
2	0.1013	0.1011
3	0.101	0.101
4	0.1009	0.1012
5	0.1015	0.1011
6	0.1012	0.1009
7	0.1008	0.101
8	0.1009	0.1013
9	0.1008	0.1012
10	0.1011	0.1011
11	0.1012	0.101
12	0.1002	0.1012
13	0.1006	0.1011
14	0.1011	0.1013
15	0.1007	0.1012
16	0.1012	0.1011
17	0.1014	0.101
18	0.1009	0.1014
19	0.101	0.1012
20	0.1006	0.1009
Average	0.100985	0.10115
Variance	9.924E-08	3.42105E-08
Standard Deviation	0.000315	0.000184961

VI. Distortion Data for 0 And 90-Degree Samples

Distortion was collected on 0, 60, and 90-degree samples as discussed in Chapter 4.

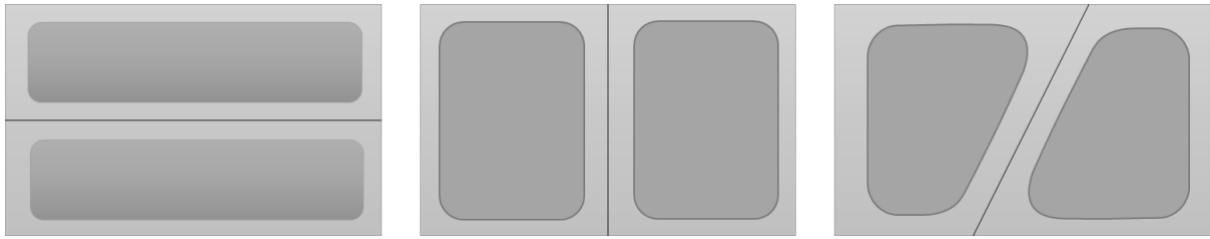


Figure 122 The distortion sample machined geometry (0, 90, and 60-degree)

The distortion profiles and curvature analysis are presented in Chapter 4. The distortion profiles for the 0 and 90-degree sample are presented below (Figure 123 - Figure 128).

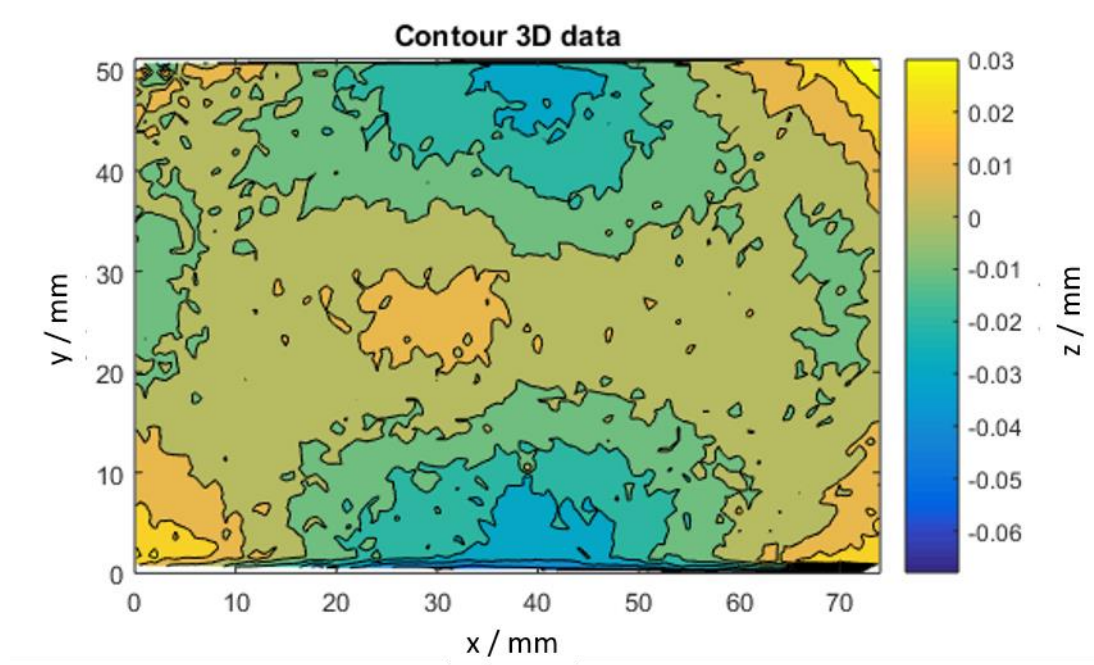


Figure 123 0-degree sample measured on the Mitutoyo CMM

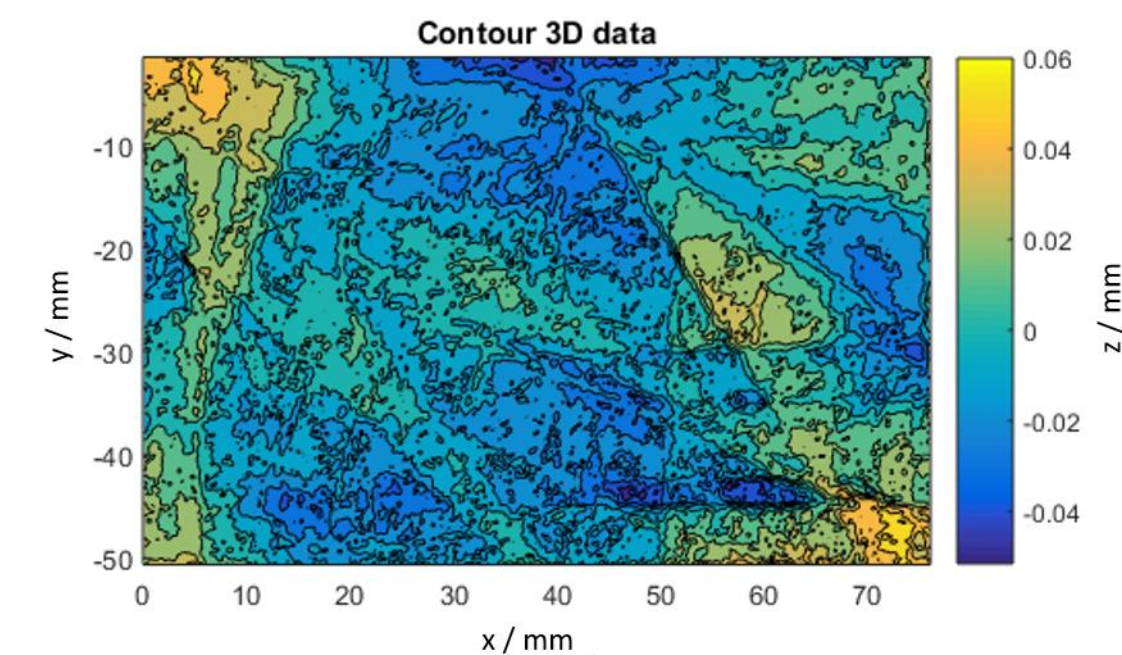


Figure 124 0-degree sample measured on the FaroArm CMM

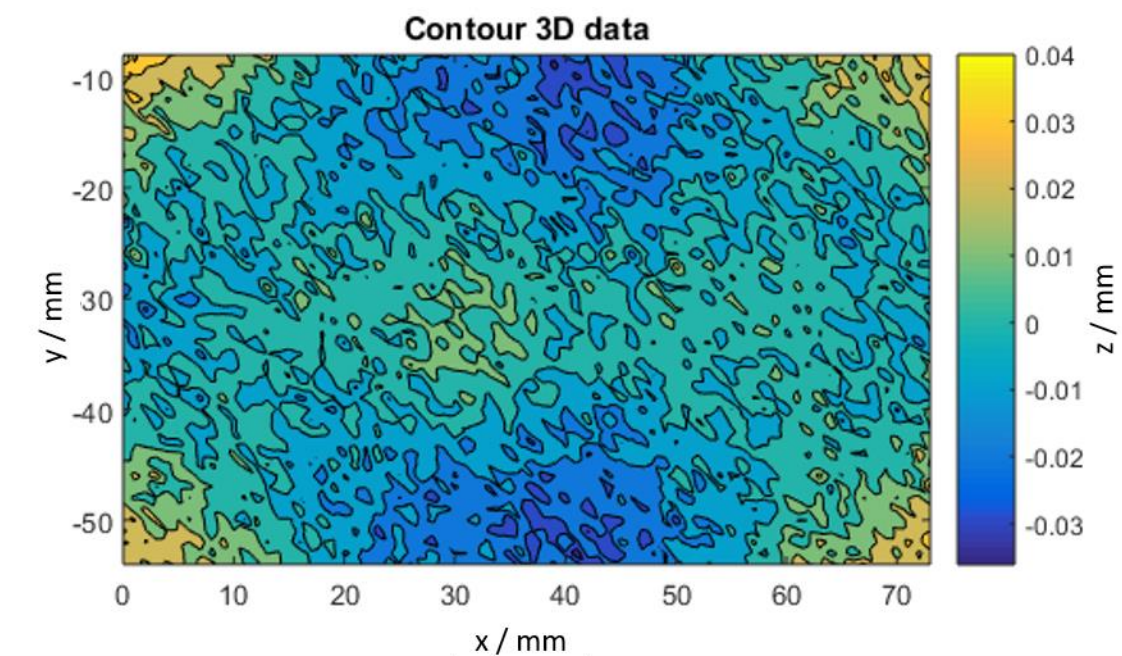


Figure 125 0-degree sample measured on the Talyscan CMM

The distortion profiles for the 90-degree sample are presented below.

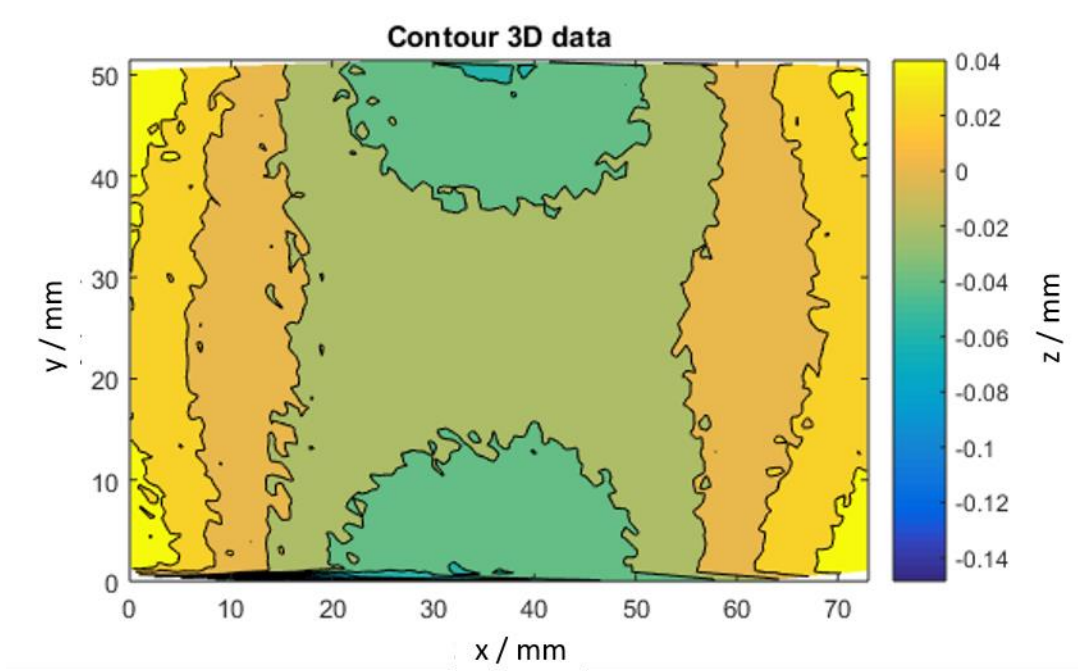


Figure 126 90-degree sample measured on the Mitutoyo CMM

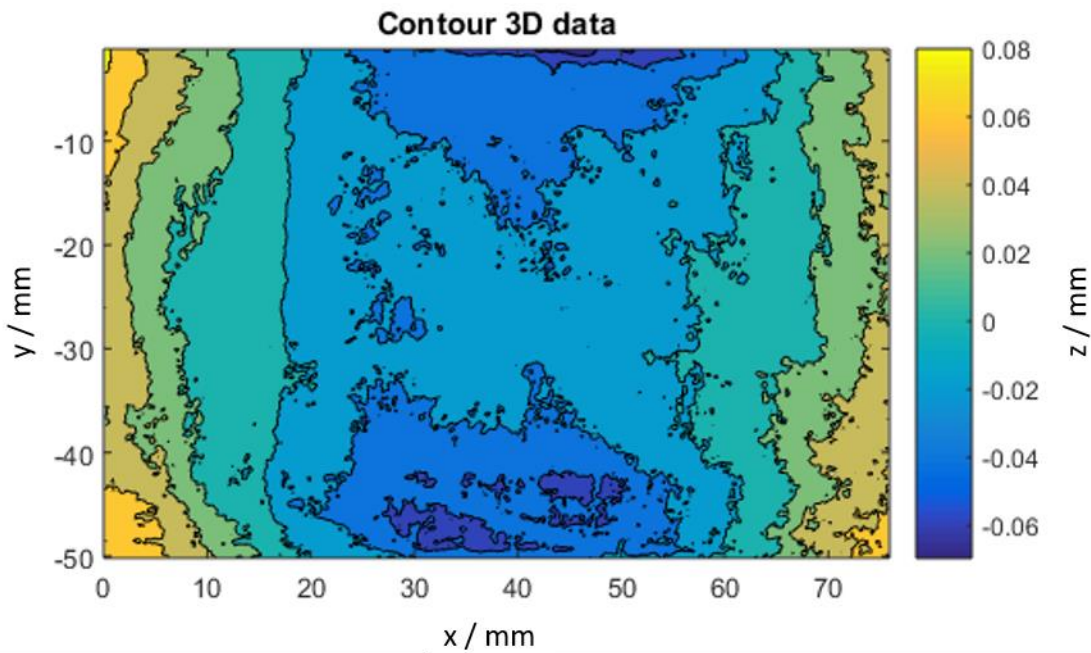


Figure 127 90-degree sample measured on the FaroArm CMM

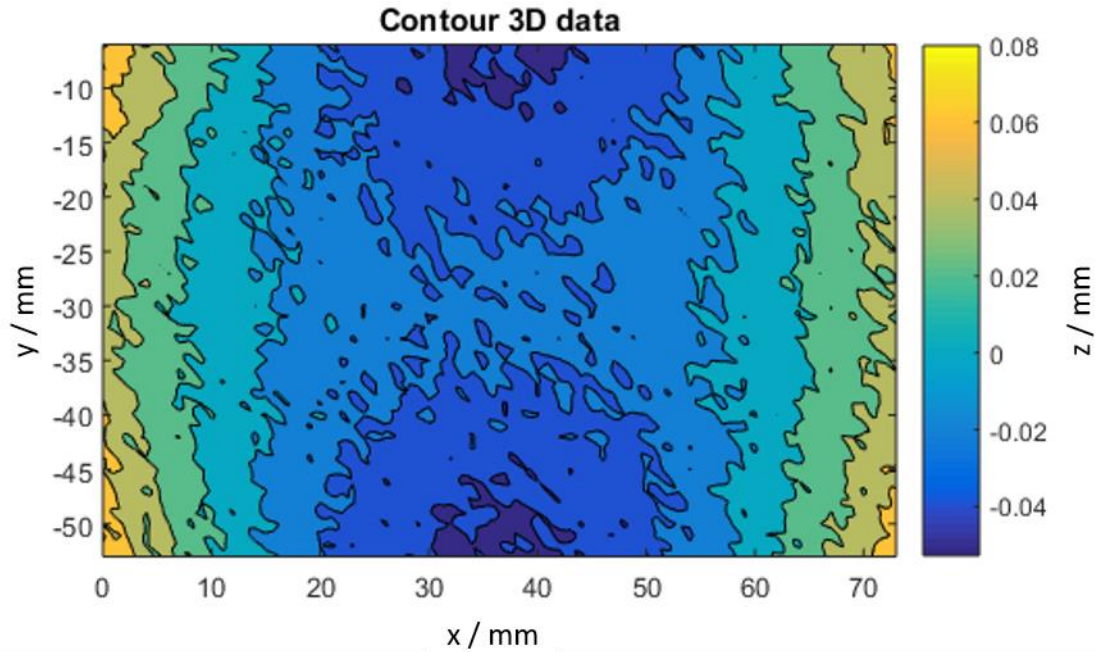


Figure 128 90-degree sample measured on the Talyscan CMM

The distortions are unique for each of the samples. The complexities of distorted surfaces are shown. Gaussian Curvature analysis for the 0, and 90-degree stiffener sample are shown in Figure 129 with degree 4 for analysis. Future work is needed to analyze the symmetries and direct comparison to the physical part samples from the least squared Bernstein basis fit and the Gaussian curvature analysis.

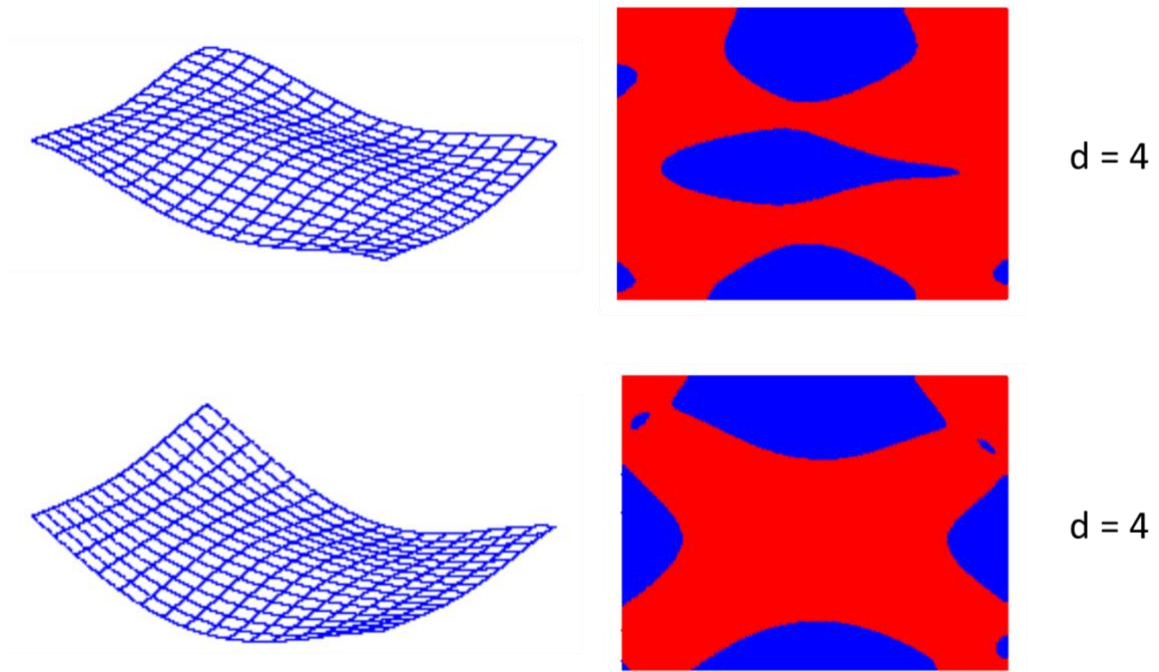


Figure 129 Gaussian curvature analysis for the 0 (top) and 90-degree (bottom) stiffener samples

PUBLICATIONS

List of Publications and Submitted Manuscripts during the PhD studies

Linke B., Garcia D., Process Planning Tool for Sustainability Research and Teaching, “In preparation”

Linke, B. S., Garcia, D. R., Kamath, A., and Garretson, I. C. (2019). “Data-driven Sustainability in Manufacturing: Selected Examples.” *Procedia Manufacturing*, 33, 602–609.

Garcia, D., Zhang, Z., Linke, B. S., and Urbassek, H. M. (2018). “Molecular dynamics simulations of single grain pure aluminum in a vice fixture for nanomanufacturing applications.” *CIRP Journal of Manufacturing Science and Technology*. <https://doi.org/10.1016/j.cirpj.2018.07.005>

Garcia D, Hill M, Aurich J, Linke B. Characterization of Machining Distortion due to Residual Stresses in Quenched Aluminum. ASME. International Manufacturing Science and Engineering Conference, Volume 1: Processes doi:10.1115/MSEC2017-2878.

Linke B, Garcia D, Kaur G, Ghadamli F. Sustainable Process Planning for Subtractive and Additive Manufacturing Unit Processes. ASME. International Manufacturing Science and Engineering Conference, Volume 3: Joint MSEC-NAMRC Symposia doi:10.1115/MSEC2016-8517.

VanderGheynst J, Lee A, Anderson E, Claypool J, Garcia D, Harold D, Hestmark K, Jabusch L, Kessler J, Kon A, Langel C, Pace S, Palermo A, Richards N, Smith T, Tu T, “Elementary School Engineering Design Field Day - Unit.” www.teachengineering.org, NSF Sponsored, 20 July 2017, www.teachengineering.org/curricularunits/view/ucd_fieldday_unit.

REFERENCES

"Distortion." Merriam-Webster.com. Merriam-Webster, n.d. Web. 8 Nov. 2017

"Quality." Merriam-Webster.com. Merriam-Webster, n.d. Web. 8 Nov. 2017.

Abele E. , Anderl R., and Birkhofer H., "The Product Life Cycle," Environmentally-Friendly Product Development, E. Abele, R. Anderl, and H. Birkhofer, eds., Springer London, pp. 35-126. 2005

Anderson, M. A., Anderson, E., and Parker, G., 2013, Operations Management for Dummies, John Wiley & Sons, Inc., Hoboken, New Jersey.

Asante, J.N. Int J Adv Manuf Technol (2008) 39: 578. doi:10.1007/s00170-007-1187-5

ASTM International. ASTM E2782-17 Standard Guide for Measurement Systems Analysis (MSA). West Conshohocken, PA; ASTM International, 2017. doi: <https://doi.org/10.1520/E2782-17>

ASTM, 2016, "E3012-16 - Standard Guide for Characterizing Environmental Aspects of Manufacturing Processes," ASTM International, West Conshohocken, PA.

ASTM, 2018, "E3096-18 - Standard Guide for Definition, Selection, and Organization of Key Performance Indicators for Environmental Aspects of Manufacturing Processes, ASTM International, West Conshohocken, PA, www.astm.org

Bell, S. Measurement Good Practice Guide No. 11. A Beginner's Guide to Uncertainty of Measurement. Tech. rep., National Physical Laboratory, 1999. 3.2

Bi Y., Cheng Q., Dong H., and Ke Y., "Machining distortion prediction of aerospace monolithic components," J. Zhejiang Univ. Sci. A, vol. 10, no. 5, pp. 661–668, 2009.

Bi Z. M. and Zhang W. J., "Flexible fixture design and automation: Review, issues and future directions," Int. J. Prod. Res., vol. 39, no. 13, pp. 2867–2894, Jan. 2001.

Bourne, D., Corney, J., and Gupta, S. K., 2011, "Recent Advances and Future Challenges in Automated Manufacturing Planning," Journal of Computing and Information Science in Engineering, 11(2), pp. 021006-021006.

Bowden, D.M., Halley, J.E., Aluminum reliability improvement program final report 60606. Chicago, IL, USA: The Boeing Company, 2001.

Boyle, Y. M. Rong, and D. C. Brown, "A review and analysis of current computer-aided fixture design approaches," Robot. Comput. Integr. Manuf., vol. 27, no. 1, pp. 1–12, Feb. 2011.

Brinksmeier, E., Cammett, J. T., Koenig, W., Leskovar, P., Peters, J., Toenshoff, H. K., Residual Stresses - Measurement and Causes in Machining Processes, CIRP Annals - Manufacturing Technology., vol. 31, no. 2, p. 491–510, 1982.

Brinksmeier, E., Lübben T., Fritsching U., Cui C., Rentsch R., Sölter, J., Distortion minimization of disks for gear manufacture, Int. J. Mach. Tools Manuf., vol. 51, no. 4, p. 331–338, 2011.

Brinksmeier, E., Sölter, J., Prediction of shape deviations in machining, CIRP Annals - Manufacturing Technology., vol. 58, no. 1, p. 507–510, 2009.

Budynas, Richard G, J K. Nisbett, and Joseph E. Shigley. Shigley's Mechanical Engineering Design. New York: McGraw-Hill, 2011. Print.

Cerutti, X., Arsene, S., Mocellin, K., Prediction of machining quality due to the initial residual stress redistribution of aerospace structural parts made of low-density aluminium alloy rolled plates, Int. J. Mater. Form., p. 1–14, 2015.

Chae J., Park S. S., and Freiheit T., “Investigation of micro-cutting operations,” Int. J. Mach. Tools Manuf., vol. 46, no. 3–4, pp. 313–332, Mar. 2006.

Chantzis, D., Van-der-Veen, S., Zettler, J., Sim, W.M., An Industrial Workflow to Minimise Part Distortion for Machining of Large Monolithic Components in Aerospace Industry, Procedia CIRP, Volume 8, p. 281-286, ISSN 2212-827, 2013.

Chen W., Ni L., and Xue J., “Deformation control through fixture layout design and clamping force optimization,” Int. J. Adv. Manuf. Technol., vol. 38, no. 9, p. 860, 2007.

Conroy, M., and Armstrong, J. (2005). “A comparison of surface metrology techniques.” Journal of Physics: Conference Series, IOP Publishing, 13, 458–465.

Cristina, M. D., 2016, "Promoting Technological Entrepreneurship through Sustainable Engineering Education," Procedia Technology, 22, pp. 1129-1134.

Cui D., Zhang L., Mylvaganam K., Liu W., and Xu W., “Nano-milling on monocrystalline copper: A molecular dynamics simulation,” Mach. Sci. Technol., vol. 21, no. 1, pp. 67–85, 2017.

D’Alvise, L., Chantzis, D., Schoinochoritis, B., Salonitis, K., Modelling of Part Distortion Due to Residual Stresses Relaxation: An aeronautical Case Study, Procedia CIRP, vol. 31, p. 447–452, 2015.

Daw, M. S.; Baskes, M. I. Semiempirical, Quantum Mechanical Calculation of Hydrogen Embrittlement in Metals. Physical Review Letters, 1983, 50, 1285-1288

Denkena, B., Dreier, S., Simulation of Residual Stress Related Part Distortion BT - New Production Technologies in Aerospace Industry: Proceedings of the 4th Machining Innovations Conference, Hannover, September 2013, B. Denkena, Ed. Cham: Springer International Publishing, p. 105–113, 2014.

Denkena, B., Dreier, S., Simulation of Residual Stress Related Part Distortion, Lecture Notes in Production Engineering New Production Technologies in Aerospace Industry, 105-13, 2013.

Deshpande, S., and Cagan, J., 2004, "An Agent Based Optimization Approach to Manufacturing Process Planning," Journal of Mechanical Design, 126(1), pp. 46-55.

DeWald, A.T., Hill, M.R., Eigenstrain-based model for prediction of laser peening residual stresses in arbitrary three-dimensional bodies Part 2: Model verification, *J. Strain Anal. Eng. Des.*, vol. 44, no. 1, p. 13–27, 2009.

DIN, 2003, "DIN 8580:2003-09 Title (german) Fertigungsverfahren - Begriffe, Einteilung, Title (english): Manufacturing processes - Terms and definitions, division," DIN Deutsches Institut für Normung e. V., Beuth.

Doran, M. P., Smullin, M. M., and Haapala, K. R. (2016). "An Approach to Compare Sustainability Performance of Additive and Subtractive Manufacturing During Process Planning." doi:10.1115/detc2016-60209.

Dornfeld D., Min S., and Takeuchi Y, "Recent Advances in Mechanical Micromachining," *CIRP Ann. - Manuf. Technol.*, vol. 55, no. 2, pp. 745–768, 2006.

Duflou, J. R., Kellens, K., and Dewulf, W., 2011, "Unit process impact assessment for discrete part manufacturing: A state of the art," *CIRP Journal of Manufacturing Science and Technology*, 4(2), pp. 129-135.

Duflou, J. R., Sutherland, J. W., Dornfeld, D., Herrmann, C., Jeswiet, J., Kara, S., Hauschild, M., and Kellens, K., 2012, "Towards energy and resource efficient manufacturing: A processes and systems approach," *CIRP Annals - Manufacturing Technology*, 61(2), pp. 587-609.

Eifler, Matthias. "Mini-Course Fundamentals of Surface Topography Measurement." 4 part Series. Part 0: Introduction, Davis, UC Davis. October 2018

Farooq, M. A., Kirchain, R., Novoa, H., and Araujo, A., 2017, "Cost of quality: Evaluating cost-quality trade-offs for inspection strategies of manufacturing processes," *International Journal of Production Economics*, 188, pp. 156-166.

Farouki, R. T. (2008). *Pythagorean-Hodograph Curves: Algebra and Geometry Inseparable*. Springer, Berlin.

Feng, S. C., Senthilkumaran, K., Brown, C. U., and Kulvatunyou, B., 2014, "Energy metrics for product assembly equipment and processes," *Journal of Cleaner Production*, 65, pp. 142-151.

Flack, D., Claverley, J., and Leach, R. (2014). "Chapter 9 - Coordinate Metrology." *Micro and Nano Technologies*, R. B. T.-F. P. of E. N. (Second E. Leach, ed., William Andrew Publishing, Oxford, 295–325.

Fleischer J. and Kotschenreuther J., "The manufacturing of micro molds by conventional and energy-assisted processes," *Int. J. Adv. Manuf. Technol.*, vol. 33, no. 1–2, pp. 75–85, 2007.

Franceschini, F., Galetto, M., Maisano, D., and Mastrogiacomo, L. (2016). "Combining multiple Large Volume Metrology systems: Competitive versus cooperative data fusion." *Precision Engineering*, 43, 514–524.

Frenkel, D.; Smit, B. Understanding molecular simulations: From algorithms to applications. Academic, 1996.

Galetto, M., and Pralio, B. (2010). "Optimal sensor positioning for large scale metrology applications." *Precision Engineering*, 34(3), 563–577.

Gamage, J. R., DeSilva, A. K. M., Chantzis, D., and Antar, M. (2017). "Sustainable machining: Process energy optimisation of wire electrodischarge machining of Inconel and titanium superalloys." *Journal of Cleaner Production*.

Gulpak M., Sölter J., and Brinksmeier E., "Prediction of Shape Deviations in Face Milling of Steel," *Procedia CIRP*, vol. 8, pp. 15–20, 2013.

Guo, H., Zuo, D. W., Wu, H. B., Xu, F., Tong, G. Q., Prediction on milling distortion for aero-multi-frame parts, *Mater. Sci. Eng. A*, vol. 499, no. 1–2, p. 230–233, 2009.

Haapala K.R. et al., "A Review of Engineering Research in Sustainable Manufacturing," *J. Manuf. Sci. Eng.*, vol. 135, no. 4, pp. 41013–41016, Jul. 2013.

Haapala, K. R., Zhao, F., Camelio, J., Sutherland, J. W., Skerlos, S. J., Dornfeld, D. A., Jawahir, I. S., Clarens, A. F., and Rickli, J. L., 2013, "A Review of Engineering Research in Sustainable Manufacturing," *Journal of Manufacturing Science and Engineering*, 135(4), pp. 041013-041013.

Hafez, M., Jan, F., Linke, B., and Garretson, I., 2017, "Hydraulic analogy and visualization of two-dimensional compressible fluid flows. Part II: Water table experiments," *International Journal of Aerodynamics*, in press.

Han, R.D., *Metal cutting theory and cutting tools*. Harbin Institute of Technology press, Harbin, 2007.

Helu M, Vijayaraghavan A, Dornfeld D (2011) Evaluating the Relationship Between Use Phase Environmental Impacts and Manufacturing Process Precision. *CIRP Annals – Manufacturing Technology* 60 (1): 49 – 52 <https://www.sciencedirect.com/science/article/pii/S0007850611000217>

Hesse, S., Krahn, H., Eh, D.: *Betriebsmittel Vorrichtung*. Carl Hanser Verlag München, 2012

Hill, M.R., Olson, M.D., Repeatability of the Contour Method for Residual Stress Measurement. *Exp Mech* 54:1269–77. doi:10.1007/s11340-014-9867-1, 2014.

Huang, X., Sun, J., Li, J., Finite element simulation and experimental investigation on the residual stress-related monolithic component deformation, *International Journal of Advanced Manufacturing Technology*, Volume 77, Issue 5, pp 1035–1041 doi:10.1007/s00170-014-6533-9, 2015.

Husson, R., Dantan, J.Y., Baudouin, C., Silvani, S., Scheer, T., Bigot, R., Evaluation of process causes and influences of residual stress on gear distortion. *CIRP Annals - Manufacturing Technology* 61, p. 551-554, 2012.

International Organisation of Standardization. (2010). "ISO 25178." *Geometric Product Specifications (GPS) – Surface texture: areal*.

International Organization for Standardization 1101 (2004) Geometrical product specifications (GPS): geometrical tolerancing: tolerances of form, orientation, location and run-out. Deutsches Institut für Normung e. V., Berlin

International Organization for Standardization. (1992). ISO 9000: International standards for quality management. Genève, Switzerland: International Organization for Standardization.

Iyad Alabd Alhafez, Yu Gao and Herbert M. Urbassek, Nanocutting: A Comparative Molecular-Dynamics Study of Fcc, Bcc, and Hcp Metals, Current Nanoscience, volume 13, issue 1, pages 40-47, year 2017, issn 1573-4137/1875-6786, doi 10.2174/1573413712666160530123834

Jawahir, I. S., Brinksmeier, E., M'Saoubi, R., Aspinwall, D. K., Outeiro, J. C., Meyer, D., Umbrello, D., Jayal, A. D., Surface integrity in material removal processes: Recent advances, CIRP Annals - Manufacturing Technology, vol. 60, no. 2, p. 603–626, 2011.

Jayanti, S., Ren, D., Erickson, E., Usui, S., Marusich, T., Marusich, K., Elanvogan, H., Predictive modeling for tool deflection and part distortion of large machined components, Procedia CIRP, vol. 12, p. 37–42, 2013.

JCGM (Joint Committee for Guides in Metrology). (2009). 104:2009. Evaluation of measurement data – An introduction to the "Guide to the expression of uncertainty in measurement" and related documents.

JCGM (Joint Committee for Guides in Metrology). (2012). International Vocabulary of Metrology—basic and general concepts and associated terms (VIM), 3rd edition with minor corrections. Sèvres: JCGM <http://www.bipm.org/en/publications/guides/vim.html>

Jiang, Z., Liu, Y., Li, L., Shao, W., A novel prediction model for thin plate deflections considering milling residual stresses, Int. J. Adv. Manuf. Technol., vol. 74, no. 1, p. 37–45, 2014.

Joung, C. B., Carrell, J., Sarkar, P., and Feng, S. C., 2012, "Categorization of indicators for sustainable manufacturing," Ecological Indicators(24), pp. 148–157.

Kellens, K., Dewulf, W., Overcash, M., Hauschild, M., and Duflou, J., 2012, "Methodology for systematic analysis and improvement of manufacturing unit process life-cycle inventory (UPLCI)—CO2PE! initiative (cooperative effort on process emissions in manufacturing). Part 1: Methodology description," Int J Life Cycle Assess, 17(1), pp. 69-78.

Klocke, F., (2011), Manufacturing Processes 1: Cutting, Rwthedition, Springer, Berlin.

Krar, Stephen F., Arthur Gill, and Peter Smid. Technology of Machine Tools. New York: McGraw Hill, 2011. Print.

Kreitlein, S., Schwender, S., Rackow, T., and Franke, J., 2015, "E|Benchmark - A Pioneering Method for Energy Efficient Process Planning and Assessment Along the Life Cycle Process," Procedia CIRP, 29, pp. 56-61.

Kunze U., "Invited Review Nanoscale devices fabricated by dynamic ploughing with an atomic force microscope," *Superlattices Microstruct.*, vol. 31, no. 1, pp. 3–17, 2002.

Lazoglu, I., Ulutan, D., Alaca, B.E., Engin, S. Kaftanoglu, B., An enhanced analytical model for residual stress prediction in machining, *CIRP Annals - Manufacturing Technology.*, vol. 57, no. 1, p. 81–84, 2008.

Li B. and Melkote S. N., "Fixture Clamping Force Optimisation and its Impact on Workpiece Location Accuracy," *Int. J. Adv. Manuf. Technol.*, vol. 17, no. 2, pp. 104–113, 2001.

Li, J., Wang, S., Distortion caused by residual stresses in machining aeronautical aluminum alloy parts: recent advances. *The International Journal of Advanced Manufacturing Technology*, 1–16. article. <http://doi.org/10.1007/s00170-016-9066-6>, 2016.

Linke, B. & Overcash, M. *Prod. Eng. Res. Devel.* (2017) 11: 643. <https://doi.org/10.1007/s11740-017-0768-x>

Linke, B. S., Corman, G. J., Dornfeld, D. A., and Tönissen, S., 2013, "Sustainability indicators for discrete manufacturing processes applied to grinding technology," *Journal of Manufacturing Systems*, 32(4), pp. 556-563.

Linke, B., and Overcash, M., 2012, "Life Cycle Analysis of Grinding," *Leveraging Technology for a Sustainable World*, D. A. Dornfeld, and B. S. Linke, eds., Springer Berlin Heidelberg, pp. 293–298.

Linke, B., Das, J., Lam, M., and Ly, C., 2014, "Sustainability Indicators for Finishing Operations based on Process Performance and Part Quality," *Procedia CIRP*, 14, pp. 564-569.

Linke, B., Garcia, D., Kaur, G., and Ghadamli, F., "Sustainable Process Planning for Subtractive and Additive Manufacturing Unit Processes," *Proc. ASME 2016 11th International Manufacturing Science and Engineering Conference*.

Linke, B., Garretson, I., Jan, F., and Hafez, M., 2017, "Integrated Design, Manufacturing and Analysis of Airfoil and Nozzle Shapes in an Undergraduate Course," *Procedia Manufacturing*, 10, pp. 1077-1086.

Linke, B., Garretson, I., Jan, F., and Hafez, M., 2017, "Manufacturing and Analysis of Airfoil and Nozzle Shapes in an Undergraduate Course," *North American Manufacturing Research Conference (NAMRC 45)*, SME, Los Angeles, CA, pp. 1077-1086.

Linke, B., Garretson, I., Jan, F., Hafez, M., Martin, L., Design and Manufacturing of Nozzles and Airfoil Shapes for Compressible Flow Visualizations in a new Engineering course, *Proceedings of the 124th American Society for Engineering Education (ASEE) Annual Conference*, June 25-28, 2017 in Columbus, OH, USA

Linke, B., Huang, Y.-C., Dornfeld, D., Establishing Greener Products and Manufacturing Processes, *Int. Journal of Precision Engineering and Manufacturing*, July, Vol. 13, Issue 7, p. 1029 – 1036, 2012.

Linke, B., Overcash, M., Life Cycle Analysis of Grinding, Proceedings of the 19th CIRP Conference on Life Cycle Engineering, Berkeley, CA, USA, May 23 – 25, 2012, p. 293 ff, 2012.

Loeche, J., Zaeh, M. F., Roesch, O., In-process deformation measurement of thin-walled workpieces, *Procedia CIRP*, vol. 1, no. 1, p. 546–551, 2012.

Lu, J., and S. for E. M. (U.S.), *Handbook of Measurement of Residual Stresses*. Fairmont Press, 1996.

Lu, Y., and Xu, X., "Process and Production Planning in a Cloud Manufacturing Environment," *Proc. ASME 2015 International Manufacturing Science and Engineering Conference*.

Luebke, K. (2014). "Coordinate Measuring Machine." *CIRP Encyclopedia of Production Engineering*, L. Laperrière and G. Reinhart, eds., Springer Berlin Heidelberg, Berlin, Heidelberg, 285–289.

Ma, N. & Huang, H. J. of *Material Eng and Perform* (2017) 26: 5206. <https://doi.org/10.1007/s11665-017-3000-4>

Ma, Y., Liu, S., Feng, P. F., Yu, D. W., Finite element analysis of residual stresses and thin plate distortion after face milling, 12th International Bhurban Conference on Applied Sciences and Technology (IBCAST), Islamabad, 2015, p. 67-71. doi: 10.1109/IBCAST.2015.7058481, 2015.

Madariaga, A., Perez, I., Arrazola, P. J., Sanchez, R., Ruiz, J. J., and Rubio, F. J. (2018). "Reduction of distortions in large aluminium parts by controlling machining-induced residual stresses." *International Journal of Advanced Manufacturing Technology*.

Manohar Priyadarshan, A., Acharya, Sushil, Wu, Peter: Enhancing manufacturing process education via computer simulation and visualization. *J. Edu. Learn.* 3(3), 172–182 (2014)

Mari, L., Carbone, P., Giordani, A., and Petri, D. (2017). "A structural interpretation of measurement and some related epistemological issues." *Studies in History and Philosophy of Science Part A*, 65–66, 46–56.

Masoudi, S., Amini, S., Saeidi, E., Eslami-Chalander, H., Effect of machining-induced residual stress on the distortion of thin-walled parts, *Int. J. Adv. Manuf. Technol.*, vol. 76, no. 1–4, p. 597–608, 2014.

Mathia, T. G., Pawlus, P., and Wiczorowski, M. (2011). "Recent trends in surface metrology." *Wear*, 271(3), 494–508.

Mendelev, M. I.; Kramer, M. J.; Becker, C. A.; Asta, M. Analysis of semi-empirical interatomic potentials appropriate for simulation of crystalline and liquid Al and Cu. *Philosophical Magazine*, 2008, 88, 1723-1750.

Mitchell, D. J., Tal, E., and Chang, H. (2017). "The making of measurement: Editors' introduction." *Studies in History and Philosophy of Science Part A*, 65–66, 1–7.

Möhring H.-C. and Wiederkehr P., "Intelligent Fixtures for High Performance Machining," *Procedia CIRP*, vol. 46, pp. 383–390, 2016.

Morse, E. P., Shakarji, C. M., and Srinivasan, V. (2018). "A Brief Analysis of Recent ISO Tolerancing Standards and Their Potential Impact on Digitization of Manufacturing." *Procedia CIRP*, 75, 11–18.

Navalho, D., Deus, A.M., Infante, V., Residual stress due to quenching in aluminum forging parts for aerospace applications: finite element analysis and contour method measurement. *Proceedings of the 6th International Quenching and Control of Distortion Conference, Chicago, Illinois, USA*, pp 281–293, 2012.

Nicholas, J. (2010). *Lean Production for Competitive Advantage*. New York: Productivity Press.

Olson, M.D, Robinson, J. S., Wimpory, R.C., Hill, M.R., Characterisation of residual stresses in heat treated, high strength aluminium alloy extrusions, *Materials Science and Technology*, doi:10.1080/02670836.2016.1164973, 2016.

Orlin, W. J., Linder, N. J., and Bitterly, J. G., 1947, "Application of the Analogy Between Water Flow with a Free Surface and Two-Dimensional Compressible Gas Flow."

Overcash, M., Twomey, J., and Kalla, D., 2009, "Unit Process Life Cycle Inventory for Product Manufacturing Operations," (43611), pp. 49-55.

Papastathis T., Bakker O., Ratchev S., and Popov A., "Design Methodology for Mechatronic Active Fixtures with Movable Clamps," *Procedia CIRP*, vol. 3, pp. 323–328, 2012.

Pehlivan S. and Summers J. D., "A review of computer-aided fixture design with respect to information support requirements," *Int. J. Prod. Res.*, vol. 46, no. 4, pp. 929–947, Feb. 2008.

Plimpton S., Fast Parallel Algorithms for Short-Range Molecular Dynamics, *J Comp Phys*, 117, 1-19 (1995). <http://lammps.sandia.gov>.

Prime, M.B., Hill, M.R., Residual stress, stress relief, and inhomogeneity in aluminum plate. *Scripta Materialia*, 46(1), p.77-82, 2002.

PZ Z., Qiu C., FZ F., DD Y., and XC S., "Molecular dynamics simulations of nanometric cutting mechanisms of amorphous alloy," *Appl. Surf. Sci.*, vol. 317, pp. 432–442, 2014.

Quinn, T. (2017). From artefacts to atoms - A new SI for 2018 to be based on fundamental constants. *Studies in History and Philosophy of Modern Physics*, 65-66, 8-20.

Rao, B., Shin, Y.C., Analysis on high-speed face-milling of 7075-T6 aluminum using carbide and diamond cutters, *Int. J. Mach. Tools Manuf.*, vol. 41, no. 12, p. 1763–1781, 2001.

Ribeiro R.L., Hill M.R., A benchmark fracture mechanics solution for a two-dimensional eigenstrain problem considering residual stress, the stress intensity factor, and superposition. *Eng Fract Mech* doi:10.1016/j.engfracmech. 2016.06.007, 2016.

Richter-Trummer, V., Koch, D., Witte, A., dos Santos, J. F., de Castro, P. M. S. T., Methodology for prediction of distortion of workpieces manufactured by high speed machining based on an accurate through-the-thickness residual stress determination, *Int. J. Adv. Manuf. Technol.*, vol. 68, no. 9, p. 2271–2281, 2013.

Ruestes, C. J.; Bringa, E. M.; Gao, Y.; Urbassek, H. M. "Molecular dynamics modeling of nanoindentation", in *Applied nanoindentation in advanced materials*, edited by A. Tiwari and S. Natarajan (Wiley, Chichester, UK, 2017) Chap. 14, pp. 313-345.

Santana, A., Lino Alves J., and da Costa Sabino Netto A., "A study of parametric calibration for low cost 3D printing: Seeking improvement in dimensional quality," *Mater. Des.*, vol. 135, pp. 159–172, 2017.

Sarkar, P., Joung, C. B., Carrell, J., and Feng, S. C., "Sustainable Manufacturing Indicator Repository," *Proc. ASME 2011 International Design Engineering Technical Conferences and Computers and Information in Engineering Conference*, August 28–31, 2011, pp. 943-950.

Savio, E., De Chiffre, L., Carmignato, S., and Meinertz, J., 2016, "Economic benefits of metrology in manufacturing," *CIRP Annals - Manufacturing Technology*, 65(1), pp. 495-498.

Schajer, G. S., Prime, M. B., Use of Inverse Solutions for Residual Stress Measurements, *J. Eng. Mater. Technol.*, vol. 128, no. 3, p. 375, 2006.

Schajer, G. S., Residual Stresses: Measurement by Destructive Testing. *Encyclopedia of Materials: Science and Technology*, Elsevier, p.8152-8158, 2001.

Schajer, G. S., Ruud, C. O., Overview of Residual Stresses and Their Measurement, *Practical Residual Stress Measurement Methods*, John Wiley & Sons, Ltd, p. 1–27, 2013.

Schmitt, R. H., Peterrek, M., Morse, E., Knapp, W., Galetto, M., Härtig, F., Goch, G., Hughes, B., Forbes, A., and Estler, W. T. (2016). "Advances in Large-Scale Metrology – Review and future trends." *CIRP Annals*, 65(2), 643–665.

Schmitt, R., 2014, "Quality Assurance," *CIRP Encyclopedia of Production Engineering*, L. Laperrière, and G. Reinhart, eds., Springer Berlin Heidelberg, Berlin, Heidelberg, pp. 1021-1024.

Schmitt, R., Witte, A., Janßen, M., and Bertelsmeier, F. (2014). "Metrology Assisted Assembly of Airplane Structure Elements." *Procedia CIRP*, 23, 116–121.

Schulze, V., Arrazola, P., Zanger, F., Osterried, J., Simulation of distortion due to machining of thin-walled components, *Procedia CIRP*, vol. 8, p. 45–50, 2013.

Senin, N., and Leach, R. (2018). "Information-rich surface metrology." *Procedia CIRP*, 75, 19–26.

Serruys, W., Van Houtte, P., Aernoudt, E., Peters, J., Why Are X-Ray Measurements of Residual Stresses Different from Mechanical Residual Stress Measurements?, *CIRP Annals - Manufacturing Technology.*, vol. 37, no. 1, p. 527–530, 1988.

Shet, C., Deng, X., Residual stresses and strains in orthogonal metal cutting, *Int. J. Mach. Tools Manuf.*, vol. 43, no. 6, p. 573–587, May 2003.

Shigeo Sato, Kazuaki Wagatsuma, Shigeru Suzuki, Masayoshi Kumagai, Muneyuki Imafuku, Hitoshi Tashiro, Kentaro Kajiwara, Takahiasa Shobu, Relationship between dislocations and residual stresses in cold-drawn pearlitic steel analyzed by energy-dispersive X-ray diffraction, *Materials Characterization*, Volume 83, September 2013, Pages 152-160, ISSN 1044-5803, <http://dx.doi.org/10.1016/j.matchar.2013.06.017>

Sim, W., Challenges of residual stress and part distortion in the civil airframe industry. *International Journal of Microstructure and Materials Properties*, 5(4-5), 446-455, 2010.

Sim, W., Residual Stress Engineering in Manufacture of Aerospace Structural Parts, in *International Conference of distortions engineering*, p. 187–194, 2011.

Sladek, J. (2016). *Coordinate metrology : Accuracy of systems and measurements / (Springer Tracts in Mechanical Engineering)*. Heidelberg :: Springer.

Stukowski A., Visualization and analysis of atomistic simulation data with OVITO – the Open Visualization Tool. *Model. Simul. Mater. Sci. Eng.* 18 (2010) 015012. <http://www.ovito.org/>

Tadic B., Vukelic D., Miljanic D., Bogdanovic B., Macuzic I., Budak I., and Todorovic P., “Model testing of fixture–workpiece interface compliance in dynamic conditions,” *J. Manuf. Syst.*, vol. 33, no. 1, pp. 76–83, Jan. 2014.

Tansel N., Arkan T. T., Bao W. Y. , Mahendrakar N., Shisler B., Smith D., and McCool M., “Tool wear estimation in micro-machining. Part I: Tool usage-cutting force relationship,” *Int. J. Mach. Tools Manuf.*, vol. 40, no. 4, pp. 599–608, 2000.

Technology), N. N. I. o. S. a., 2011, "Sustainable Manufacturing Indicators Repository," <http://www.mel.nist.gov/msid/SMIR/>.

Teng, T.-L., Chang, P.-H., Tseng, W.-C., Effect of welding sequences on residual stresses, *Comput. Struct.* vol. 81, no. 5, p. 273–286, Mar. 2003.

Thoben, K.-D., Lubbn, Th., Clae, B., Schulz A., Rentsch, R., Kusmierz, R., Nowag, L., Surm, H., Freichs, F., Hunkel, M., Klein, D., Mary, P., Distortion engineering: eine systemorientierte Betrachtung des Bauteilverzugs, *HTM 574*, pp 276 – 282, 2002.

Topalli, D., and Cagiltay, N. E., 2018, "Improving programming skills in engineering education through problem-based game projects with Scratch," *Computers & Education*, 120, pp. 64-74.

Tosello, G., Haitjema, H., Leach, R. K., Quagliotti, D., Gasparin, S., and Hansen, H. N. (2016). “An international comparison of surface texture parameters quantification on polymer artefacts using optical instruments.” *CIRP Annals*, 65(1), 529–532.

Totten, G., Howes, M., Inoue, T., *Handbook of Residual Stress and Deformation of Steel*. ASM International, Materials Park, OH, 2002.

Wang, Z., Chen, W., Zhang, Y., Chen, Z., Liu, Q., Study on the Machining Distortion of Thin-walled Part Caused by Redistribution of Residual Stress, Chinese J. Aeronaut., vol. 18, no. 2, p. 175–179, 2005.

Wyatt, J. E., Berry, J. T., A new technique for the determination of superficial residual stresses associated with machining and other manufacturing processes, J. Mater. Process. Technol., vol. 171, no. 1, p. 132–140, 2006.

Yang, Y., Li, M., Establishment of Mathematical Relation Model between Dislocation Motion and Machining Deformation of Titanium Alloy Monolithic Component, Advanced Materials Research, Vol. 820, p. 212-215, 2013.

Yang, Y., Li, M., Li, K. R., Comparison and analysis of main effect elements of machining distortion for aluminum alloy and titanium alloy aircraft monolithic component, Int. J. Adv. Manuf. Technol., vol. 70, no. 9, p. 1803–1811, 2014.

Yang, Y., Xia, L., Zhao, G., Meng, L., and He, N. (2018). “Investigation of the coupled distribution of initial and machining-induced residual stress on the surface of thin-walled parts.” The International Journal of Advanced Manufacturing Technology, 98(1), 213–222.

Zangl, K., Danzl, R., Helml, F., and Prantl, M. (2018). “Highly accurate optical μ CMM for measurement of micro holes.” Procedia CIRP, 75, 397–402.

Zhang L., and Tanaka H., “Atomic scale deformation in silicon monocrystals induced by two-body and three-body contact sliding,” Tribol. Int., vol. 31, no. 8, pp. 425–433, 1998.

Zhang, L., Feng, X., Li, Z., Liu, C., FEM simulation and experimental study on the quenching residual stress of aluminum alloy 2024, Proc. Inst. Mech. Eng. Part B J. Eng. Manuf., May 2013.

Zhang, Z., Li, L., Yang, Y., He, N., Zhao, W., Machining distortion minimization for the manufacturing of aeronautical structure, Int. J. Adv. Manuf. Technol., vol. 73, no. 9, p. 1765–1773, 2014.